Centro Regionale di Competenza (CRdC)
Analisi e Monitoraggio del Rischio Ambientale (AMRA)

The Many Facets of Seismic Risk

Edited by
Marisa Pecce
Gaetano Manfredi
Aldo Zollo

Centro Regionale di Competenza (CRdC)
Analisi e Monitoraggio del Rischio Ambientale (AMRA)

The Many Facets of Seismic Risk

Proceedings of the Workshop on Multidisciplinary Approach to Seismic Risk Problem

Abbazia del Goleto
Contrada San Guglielmo
Sant'Angelo dei Lombardi (AV)

22 September 2003

Edited by

Marisa Pecce
Dipartimento di Ingegneria, Università degli Studi del Sannio

Gaetano Manfredi
Dipartimento di Analisi e Progettazione Strutturale, Università degli Studi di Napoli "Federico II"

Aldo Zollo
Dipartimento di Scienze Fisiche, Università degli Studi di Napoli "Federico II"

Centro Regionale di Competenza
Analisi e Monitoraggio del Rischio Ambientale
Polo delle Scienze e delle Tecnologie
Dipartimento di Scienze Fisiche
C/o Facoltà di Ingegneria – Via Nuova Agnano, 11 – III° Piano
80125 – Napoli – Italy
www.amra.unina.it
ambiente@na.infn.it
Telefono +39 081 76-85125/124/115
Fax. +39 081 76-85144

Coordinamento editoriale
doppiavoce
www.doppiavoce.it

Contents

Seismic engineering

Diagnostic and monitoring of structures by innovative methods

Management of urban systems in sesmic areas

The background of this book

The year 2002 was a crucial one for research on Environmental Risk in the Campania region of Southern Italy. The Regional Government of Campania decided in fact to finalise a EU-ESRD financial support to launch a Project aiming at creating a Regional Center of Competence on Analysis and Monitoring of the Environmental Risk (CRdC AMRA).
The Project's (hence the Center's) objectives are:

- to increase the capability of different research groups existing in Campania to approach effectively environmental risk problems (this aim being pursued both acquiring new high tech instrumentation and creating a synergy among the best expertise existing in the Universities and Research Organizations in the territory);
- to foster the formation of an interface for efficient transfer of innovation technologies and know how from the academic world to private enterprises and public stakeholders;
- to approach the problem of environmental risks in a comprehensive and quantitative way, giving public authorities comparative estimates of different typologies of risk in different areas as a basis for mitigation actions, land use or urban plans;
- to offer Civil Defence and other public organization of emergency management new high tech solutions to improve prevention and crisis management capabilities.

The ultimate goal of the Project is to transform AMRA into a public enterprise geared towards high tech transfer in favour local systems. AMRA is meant to fill a position intermediate among the vocations of the Universities and Research Organizations, of the enterprise system and of the land and catastrophic event management agencies.
Finally AMRA wishes to be a structure where the fragmentation due to hyper specialization of the present research on environmental risk can be accommodated favouring the integration of different know-how (although each maintaining the needed depth) turned towards a global approach to complex problems. From this point of view AMRA can propose itself as a regional knot of an European network of Research and Technology Centers.
Tectonic earthquakes are a major source of hazard in Regione Campania. A considerable fraction of the AMRA effort is dedicated to the implementation

of a system of high tech instrumentation (seismic-accelerometric digital network, a-synchronous shaking tables, etc) allowing to approach seismic risk reduction in an integrated way. Furthermore AMRA wants to foster training courses to introduce in the Campania productive system intellectual resources capable to increase the competitiveness of the system.
An agreement was signed among AMRA, Regione Campania and the municipality of Sant'Angelo dei Lombardi, one of the most damaged towns from the destructive tectonic earthquake striking the Campania Appenninic range in November 1980. The agreement established Sant'Angelo dei Lombardi as the preferred site of AMRA for formation courses, workshops, etc.
The event which inaugurated this activities was a one day international workshop on seismic risk which was convened on September 2003 by the Editors of this volume.

Paolo Gasparini
Scientific Coordinator of CRdC AMRA
Professor of Geophysics
Università degli Studi di Napoli "Federico II"

Preface

Introduction

Earthquakes and their catastrophic consequences caused to social communities are studied nowadays by several researchers world-wide. The efforts of such researchers have given rise to many remarkable achievements. Notwithstanding, when new seismic events occur and cause extensive damage, it seems that the results achieved are inadequate and/or unreliable. Traditional methods used in the past should be revised and further reseach stimulated.

The evaluation and the mitigation of the seismic risk is a complex problem. It requires continuous sinergic exchanges between researchers with different background and expertises. The collaborative work between experts of various disciplines is, in fact, essential to joint the elements of the puzzle of seismic risk research. In so doing, reliable results can be achieved and utilized to protect our cities and communities.

The papers included in these Proceedings are high quality contributions in the area of seismic risk and stress the importance of the meeting held in Sant'Angelo dei Lombardi on September, 2003. An innovative strategy for the assessment of seismic risk has been suggested which is based on a multi-disciplinary approach. The latter is essential to optimize and merge the results of all related disciplines. The research team involved, which is apparently eterogeneous because of their background, is adequately integrated and in close cooperation. The village of Sant'Angelo dei Lombardi was selected as the location of the meeting because it is a symbol of the destructive consequences of the Irpinia earthquake in 1980.

The papers presented in this meeting illustrate the recent advances and state-of-the-art in seismic risk assessment; they merge seismology, earthquake engineering, social science, urban planning, remote sensing and non-destructive testing. Traditionally, the assessment of seismic risk has included (i) the analysis of fault mechanism, (ii) the propagation of waves in deep soil strata, (iii) local effects due to local soil conditions, (iv) earthquake response of structures employing different lateral resisting systems, (v) the economic and social impacts of earthquake damage. Nevertheless, modern methods and technologies should also be employed for seismic risk assessment. These may include technologies for testing and monitoring of buildings, the use of IT for the urban management, e.g. via GIS, innovative systems for early warning to detect rapidly the earthquake occurrence.

The merging of the above disciplines, methods and technologies is of paramount importance to achieve adeguate results. In so doing, the Center of Competence of the Campania Region AMRA is the permanent institution in which the seismic risk is assessed through a multi-disciplinary approach.
The mitigation of seismic risk is difficult and onerous, but it is essential to ensure that local social communities may live safely in their environment. The aim of the centre AMRA to provide support for research, either theorethical or applied, continuing education, and develop technologies and methodologies that can implemented in the industry and/or used by consultancy agencies.

The Editors

Seismology and geophysics

Rapid magnitude determination for earthquake early warning

R.M. Allen

Department of Geology and Geophysics, University of Wisconsin-Madison, Madison, WI, USA

Introduction

The goal of an earthquake early warning system is to provide notification of ground shaking hazard before significant ground motion is felt. An operational system requires four components: (1) seismic network infrastructure, (2) rapid event characterization, (3) spatial hazard prediction, and (4) a notification system to warn of hazard. Here I present an overview of such an early warning system designed for use with a dense seismic network in the earthquake source region. Emphasis is placed on components (2) and (3) as they are common to implementation of the system in any region. The particular example described is for southern California; however, the same methodology could be utilized in the Irpinia region of Italy.

In many earthquake prone regions, including California, Japan, Taiwan, Italy, and Turkey, population centers are collocated with the earthquake source region. In such a case, hazard must be determined using the low amplitude P-wave which can be detected seconds before significant ground motion begins. The earthquake early warning methodology described here, named ElarmS, uses the P-wave arrival to estimate hazard and therefore has the potential to issue warning before damaging ground shaking begins, even at the epicenter of an earthquake.

Seismic network infrastructure

The network infrastructure required consists of seismometers and a rapid telemetry system. Fig. 1 shows the seismic network in southern California, TriNet [1, 2]. Station density is greatest where population (yellow regions, Fig. 1) coincides with earthquake source regions represented by known faults (black lines) and earthquake epicenters (red dots). In these regions the typical stations spacing is ~25 km. Such dense coverage is important as the accuracy of the magnitude estimate increases with the number of stations recording the P-wave arrival. Rapid telemetry is also central to an effective warning system, since any delay in transmittal of information from seismic station to the cen-

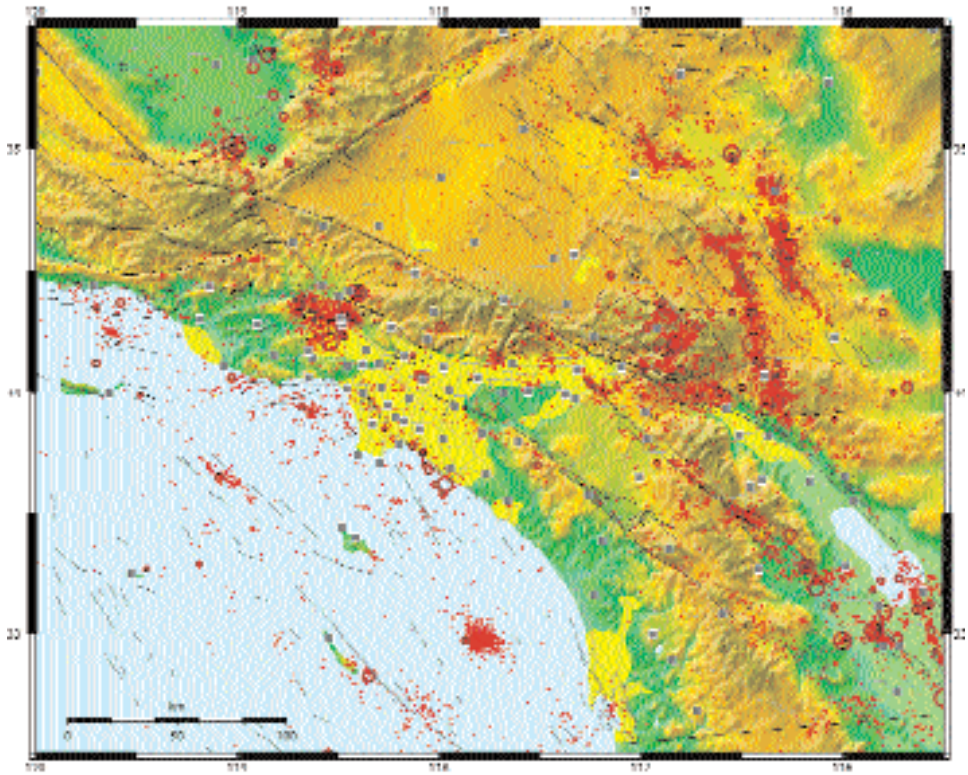

Fig. 1. Map of southern California showing the collocation of known faults (black lines), past earthquake epicenters (red dots for magnitude < 5 and black circles for mag > 5) and population centers (bright yellow). The seismic stations belonging to TriNet and capable of onsite data processing are shown as grey squares. Station density is greatest in at-risk populated areas where the typical station spacing is ~25 km.

tral processing site is a delay in the issuance of a warning. Communication delay can be minimized by processing waveforms at the seismic stations and transmitting only parameter information to the central processing site.

Event characterization: magnitude

To predict the hazard posed by an earthquake two event parameters are needed: location and magnitude. Earthquake location can be determined using a similar approach to normal network operation based on P-wave arrival times. Initially, an event is located at the site of the first station to trigger, then between the first two, and then first three stations. Once arrival times at four stations are known, the event can be accurately located using normal techniques. Local earthquake magnitude is usually determined using peak ground motion

observations, i.e. it is not available in time to issue a warning. An alternative approach to magnitude determination must therefore be developed using the P-wave arrival.

ElarmS rapidly determines magnitude based on the frequency content of the P-wave. Small earthquakes rupture small fault patches generating a high frequency signal, while large events rupture large faults generating a lower frequency signal. The frequency content is characterized using the predominant period, T^p, which is determined in realtime from the vertical component of a velocity sensor [3, 4]. Fig. 2 shows the relationship between the T^p and magnitude determined using 53 earthquakes in southern California ranging in magnitude from 3.0 to 7.3. The relation for low-magnitude events (mag < 5, Fig. 2A) is determined using the maximum predominant period, T^p_{max}, within 2 seconds of the P-wave trigger having low-passed the data at 10 Hz. For larger

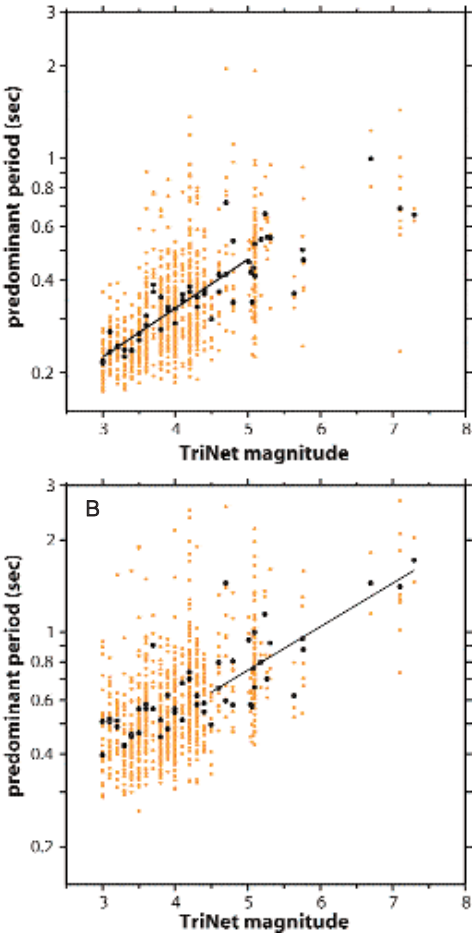

Fig. 2. Relation between predominant period and magnitude. Predominant period measured on the vertical component of a broadband velocity sensor. A. Maximum predominant period observed within 2 seconds of the P-wave arrival low-pass filtered at 10 Hz versus TriNet magnitude for individual stations (gray dots) and event averages (black dots) for all 53 events. The black line is the best fit (least absolute deviation of event averages) for data from magnitude 3.0 to 5.0 events. B. as A except maximum predominant period within 4 seconds of the P-arrival on the same data stream low-pass filtered at 3 Hz. The black line is the best fit to event averages for earthquakes with magnitude between 5.0 and 7.3. Observations of predominant period at single stations show significant scatter (gray dots), but once several stations are averaged the scatter is reduced significantly (black dots).

magnitude events (Fig. 2B) better magnitude estimates require 4 seconds of data and a low-pass filter of 3 Hz. Earthquake magnitude can therefore be determined using the following relations:

$$m_l = 6.3log(T^p_{max}) + 7.1; \quad m_h = 7.0log(T^p_{max}) + 5.9$$

where m_l and m_h are the magnitude estimates for low-magnitude and high-magnitude events respectively [4]. Waveform datasets from other regions including the Pacific Northwest of the U.S. and Japan show similar magnitude period relations [5].

ElarmS uses a realtime approach to magnitude determination. Fig. 3 shows the progression of the magnitude determination using the predominant frequency ($f^p = 1/T^p$) trace calculated from the vertical velocity recorded at a station 50 km from the epicenter of a magnitude 3.9 earthquake. After the P-wave trigger, the first 0.5 sec of f^p is ignored as it contains transients between the frequency content of background noise and the P-wave arrival. The first magnitude estimate is available 1 sec after the trigger. It is calculated from the minimum f^p between 0.5 and 1 sec using the magnitude-period relation shown in

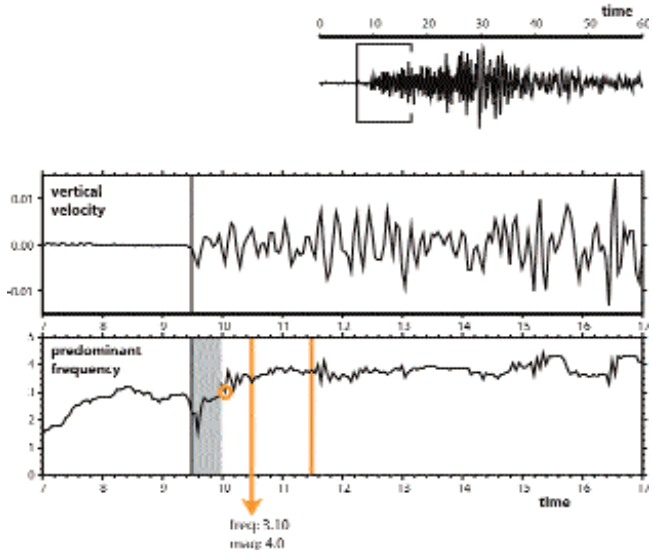

Fig. 3. Example magnitude estimation using the single station PDR 50 km from the epicenter of the January 29, 2002, magnitude 3.9, Simi Valley earthquake. The top trace shows the full vertical velocity waveform of which a 10 sec window is shown on the middle trace with the trigger time indicated by a vertical line. The bottom trace is the predominant frequency, f^p, calculated from the vertical velocity after low-passing the waveform at 10 Hz. Magnitude estimation proceeds as follows: (1) The first 0.5 sec of f^p is ignored as it contains transients. (2) The minimum f^p within 1 sec of the trigger, 3.10 Hz, is reported and converted to a magnitude of 4.0. (3) If a lower f^p is recorded within the 2nd second, it is reported and the magnitude estimate is updated to this larger magnitude (this does not occur in this example). Only 2 sec of data are used for small-magnitude events.

Fig. 2A. In the example shown in Fig. 3 the minimum f^p is 3.10 Hz providing a magnitude estimate of 4.0. ElarmS then continues to monitor f^p for the 2nd second. If f^p should drop lower than what was observed during the 1st second, it would represent a new T^p_{max} and would be used to generate a new magnitude estimate that would be greater than the initial estimate. This does not occur in the example shown in Fig. 3; the best magnitude estimate in this case is available within 1 sec of the P-wave arrival and has an error of 0.1 magnitude units.

In a larger magnitude event both the low- and high-magnitude estimates are used as ElarmS updates the magnitude estimate. The example shown in Fig. 4 uses the vertical velocity trace from a station 82 km from the epicenter of the

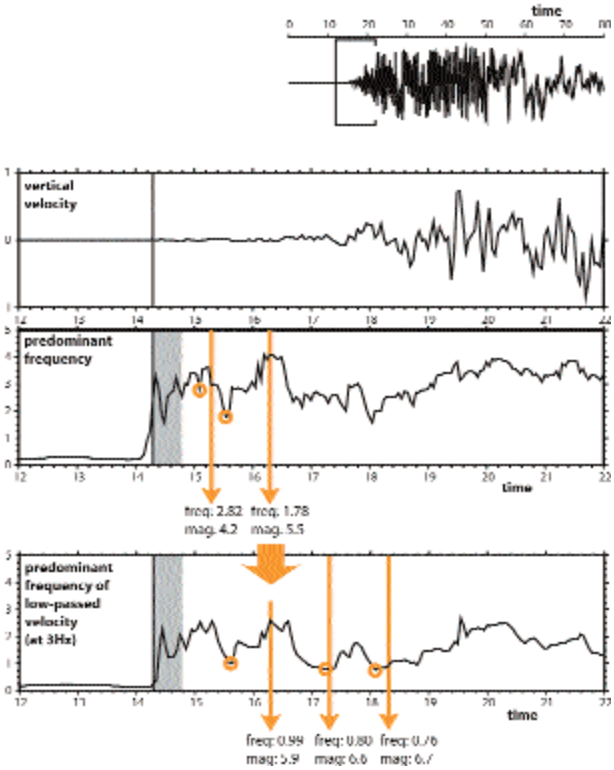

Fig. 4. Example magnitude estimation using the single station DAN 82 km from the epicenter of the October 16, 1999, magnitude 7.1, Hector Mine earthquake. The top three traces are the same as Fig. 3. Magnitude estimation proceeds as follows: (1) The first 0.5 sec of f^p is ignored as it contains transients. (2) The minimum f^p within 1 sec of the trigger, 2.82 Hz, is reported and converted to a magnitude of 4.2. (3) The minimum f^p within 2 sec of the trigger is lower, 1.78 Hz, corresponding to an updated magnitude of 5.5. This classifies the event as a large-magnitude earthquake. Therefore f^p is recalculated having low-passed the data at 3 Hz and will be monitored for 4 sec. The new minimum f^p within 2 sec is 0.99 Hz corresponding to a magnitude of 5.9 using the high-magnitude relation. (4) Within 3 sec the minimum f^p drops to 0.80 Hz and the magnitude is updated to 6.6. (5) Within 4 sec the minimum f^p drops again to 0.76 Hz providing a final magnitude estimate of 6.7.

magnitude 7.1 Hector Mine earthquake. Initially the event is treated as a small-magnitude event: within the 1st second the minimum f^p observation is 2.82 Hz, corresponding to a magnitude of 4.2; in the 2nd second f^p drops to 1.78 Hz, providing a magnitude estimate of 5.5. A magnitude greater than 4.5 classifies the earthquake as a large-magnitude event causing the system to switch to using m_{fj}. The minimum f^p (having low-passed the data at 3 Hz, Fig. 4) after 2, 3 and 4 sec is 0.99, 0.80 and 0.76 Hz corresponding to magnitude estimates of 5.9, 6.6 and 6.7 respectively. The final error in the magnitude estimate using this single station is 0.4.

The use of a dense seismic network in the earthquake source region provides for rapid event detection, location, and also multiple observations of T^p_{max} and corresponding magnitude estimates. The error in the event-magnitude estimate is rapidly reduced when multiple station-magnitude estimates are averaged. Tab. 1 shows the average absolute magnitude estimate for the dataset of 53 earthquakes in southern California. When only the closest station is used to estimate magnitude the average error is 0.7, when the closest 5 stations are averaged the error drops to 0.45, and with 10 stations the error is 0.35. For the purpose of early warning it is the speed with which accurate magnitude estimates are available that is important. To estimate how quickly magnitude estimates could be available in southern California a subset of 28 events is used. These are the events which occur within the dense portion of the seismic network (Fig. 1) and are also the events for which the most rapid hazard estimates would be needed. Tab. 2 shows the proportion of events for which a magnitude estimate would be available and the average error with respect to

Tab. 1. The average absolute error in the event magnitude is reduced as more stations provide individual magnitude estimates that can be averaged.

Number of stations	Average magnitude error (magnitude units)
1	0.7
5	0.45
10	0.35

Tab. 2. Case study showing the timing and accuracy of event magnitude estimates in southern California. The timing of magnitude estimates is reported relative to the S-wave arrival at the epicenter which represents the earliest possible timing of peak ground shaking at the surface.

Time after S-arrival at the epicenter (sec)	Proportion of events for which a magnitude estimate is available	Average magnitude error (magnitude units)
0	43%	0.52
2	82%	0.41
4	96%	0.29

the time of the S-wave arrival at the epicenter. The S-wave arrival at the epicenter is chosen as the reference time as it represents the earliest time of peak ground motion at the Earth's surface. It is also a conservative estimate as in larger magnitude events (the ones for which a warning would be needed) peak ground motion usually occurs several seconds after the S-wave arrival. In the case of southern California magnitude estimates could be available for 43% of events at the arrival time of the S-wave at the epicenter with an average error of 0.52. Magnitudes are available for 82% of events 2 sec later and the average error is 0.41.

HAZARD PREDICTOR: ATTENUATION RELATIONS

Given the location and magnitude of an earthquake the spatial distribution of predicted peak ground motion can be estimated using attenuation relations. Many different functional forms have been used for different types of earthquakes in different regions (e.g. [6-13]), however most are based on the functional form

$$A = A_0 r^n e^{-kr}$$

where A is the peak ground acceleration (PGA) at a distance r, and A_0, n and k are constants to be determined. This functional form has a term for geometric spreading, r^n, and one for intrinsic attenuation, e^{-kr}. Previously determined attenuation relations for southern California used only PGA observations for earthquakes with magnitudes greater than 5.5. Therefore, ElarmS uses its own attenuation relations that have been developed using observations from earthquakes ranging in magnitude from 3.0 to 7.3. It was found that the effect of intrinsic attenuation was not significant within 200 km of an event so k was set to zero to reduce the unknowns in the regression. n was determined as a function of magnitude by grouping PGA observations by magnitude and calculating the best fitting n. Having determined n, A_0 was calculated for each event and the best fitting linear relation between A_0 and magnitude was obtained. Fig. 5 shows how A_0 and n vary as a function magnitude.

ElarmS uses the attenuation relations in a two-stage process. One second after the first P-wave trigger the first estimate of magnitude is available. Given the magnitude, A_0 and n are determined from the relations shown in Fig. 5, and estimated PGA is calculated as a function of distance. As time progresses during the event sequence, the stations closest to the epicenter measure their PGA. Once this information is available from a few stations it is used to adjust the attenuation relation by keeping n fixed but allowing A_0 to change in order to best-fit the attenuation relation to PGA observations. Fig. 6 shows examples of the attenuation relations for magnitude 5.1, 6.1 and 7.1 earthquakes. Note the discrepancy between the observations and predictions

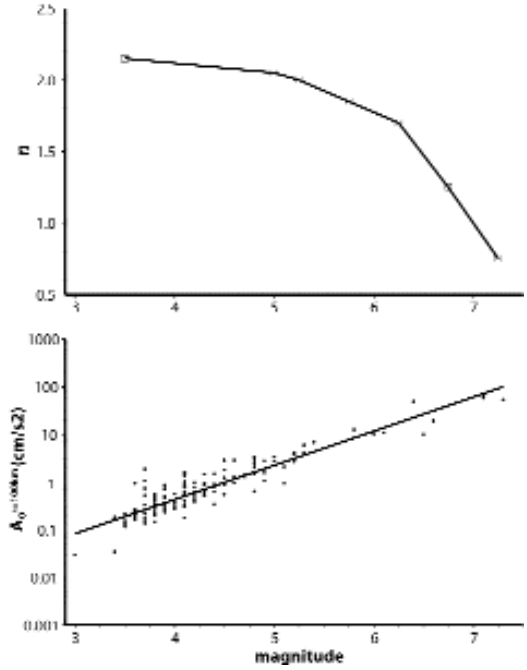

Fig. 5. Empirically determined values of n and A_0 as a function of earthquake magnitude. PGA observations were initially grouped by magnitude and n determined for each group by regression. Having determined n, the best fitting A_0 (defined as the amplitude at r = 100 km) was calculated for each event. Linear regression provides A_0 as a function of magnitude.

of the [13] attenuation relations. This discrepancy is a common problem when using attenuation relations determined from larger-magnitude events only. The attenuation relations described here do not account for near-surface amplification effects, such as rock versus soil, which are responsible for much of the scatter in the acceleration observations shown in Fig. 6. Although site corrections are not currently part of ElarmS they can easily be included when known (e.g. [14, 15]).

Notification system

The methodology presented above has the potential to provide zero to a few seconds of warning of forthcoming ground shaking at the epicenter. The warning time increases with distance from the epicenter: at 30 km approximately 10 sec of warning is possible; ~20 sec is available at 60 km. ElarmS is designed to provide a prediction of hazard as quickly as possible and then to update the prediction every second. The initial prediction is based on limited data and has the most uncertainty. As time proceeds, the initial stations provide more information and additional stations trigger, reducing the uncertainty in the hazard prediction along with the amount of warning time. The notification system should therefore allow users to decide on their tolerance for

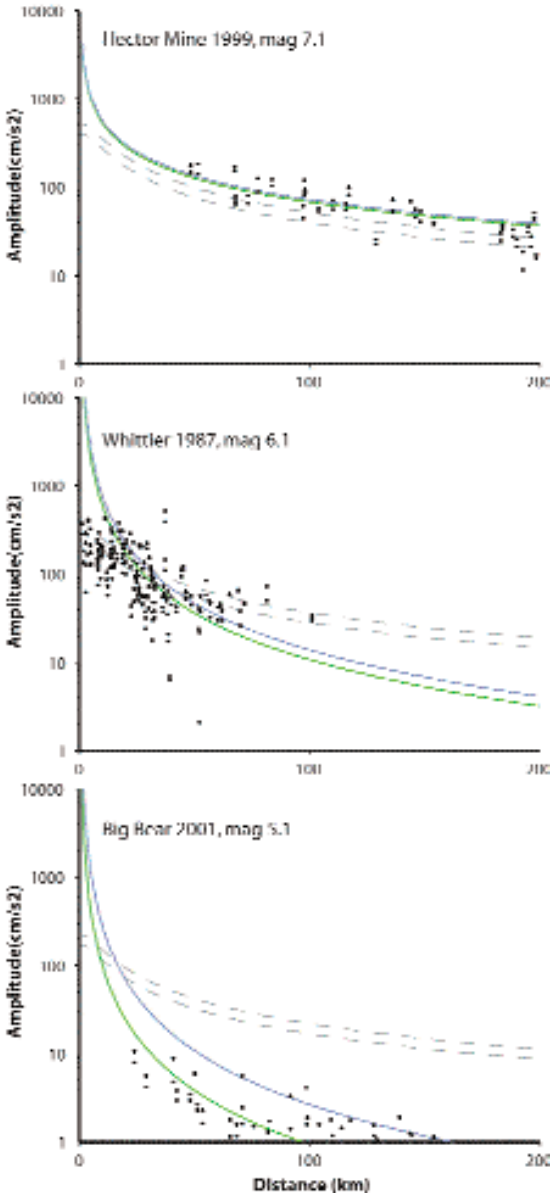

Fig. 6. Examples of attenuation relations (lines) and PGA observation (dots). (Top) The 1999, magnitude 7.1, Hector Mine earthquake. (Middle) The 1987, magnitude 6.1, Whittier earthquake. (Bottom) The 2001, magnitude 5.1, Big Bear earthquake. The grey lines show the ElarmS attenuation relations determined given just earthquake magnitude and the green lines are the result of adjusting the relation based on PGA observations. Dashed lines show the [13] attenuation relations for rock and soil for comparison.

false alarms. For example, a school may decide to use the earliest warning possible because one or two false alarms per year can be considered as drills with little cost. However, an industrial user wishing to shut down a production line may decide that it would rather have less warning time but be more certain before a costly shut-down.

References

1. Kanamori H, Hauksson E, Heaton T. Real-time seismology and earthquake hazard mitigation. *Nature* 390(6659):461-4, 1997.
2. Hauksson E, Small P, Hafner K, Busby R, Clayton R, Goltz J, Heaton T, Hutton K, Kanamori H, Polet J, Given D, Jones LM, Wald D. Southern California Seismic Network: Caltech/USGS Element of TriNet 1997-2001. *Seis. Res. Lett.* 72(6):690-704, 2001.
3. Nakamura Y. On the Urgent Earthquake Detection and Alarm System (UrEDAS). *Proceedings of Ninth World Conference on Earthquake Engineering*, VII:673-8, 1988.
4. Allen RM, Kanamori H. The Potential for Earthquake Early Warning in Southern California. *Science* 300(5620):786-9, 2003.
5. Lockman A, Allen RM. *Rapid magnitude determination for earthquakes in Japan and the Pacific Northwest*. In preparation.
6. Campbell KW. Near-source attenuation of peak horizontal acceleration. *Bulletin of the Seismological Society of America* 71(6):2039-70, 1981.
7. Joyner WB, Boore DM. Peak horizontal acceleration and velocity from strong-motion records including records from the 1979 Imperial Valley, California, earthquake. *Bulletin of the Seismological Society of America* 71(6):2011-38, 1981.
8. Fukushima Y, Irikura K. Attenuation characteristics of peak ground motions in the 1995 Hyogo-ken. *J. Phys. Earth* 45:135-46, 1982.
9. Abrahamson NA, Silva WJ. Empirical response spectral attenuation relations for shallow crustal earthquakes. *Seismological Research Letters* 68(1):94-127, 1997.
10. Boore DM, Joyner WB, Fumal TE. Equations for estimating horizontal response spectra and peak acceleration from western North American earthquakes; a summary of recent work. *Seismological Research Letters* 68(1):128-53, 1997.
11. Campbell KW. Empirical near-source attenuation relationships for horizontal and vertical components of peak ground acceleration, peak ground velocity, and pseudo-absolute acceleration response spectra. *Seismological Research Letters* 68(1):154-79, 1997.
12. Sadigh K, Chang CY, Egan JA, Makdisi F, Youngs RR. Attenuation relationships for shallow crustal earthquakes based on California strong motion data. *Seismological Research Letters* 68(1):180-9, 1997.
13. Field EH. A modified ground-motion attenuation relationship for southern California that accounts for detailed site classification and a basin-depth effect. *Bulletin of the Seismological Society of America* 90(6):S209-21, 2000.
14. Wald DJ, Quitoriano V, Heaton TH, Kanamori H. Relationships between peak ground acceleration, peak ground velocity, and Modified Mercalli Intensity in California. *Earthquake Spectra* 15(3):557-64, 1999.
15. Wald DJ, Quitoriano V, Heaton TH, Kanamori H, Scrivner CW, Worden CB. TriNet "ShakeMaps": Rapid generation of peak ground motion and intensity maps for earthquakes in southern California. *Earthquake Spectra* 15(3):537-55, 1999.

Detecting and understanding slow crustal transients: a clue for the modeling of earthquake triggering

P. Bernard, S. Bourouis, F. Boudin
Institut de Physique du Globe de Paris, Paris, France

Introduction

The occurrence of any earthquake is well known to significantly increase the likelihood of a next earthquake in its vicinity, an effect which decays with time t as 1/t, following the Omori law, generalizing the concept of aftershocks (e.g., [1]). This leads naturally to the observation of the "inverse" Omori law, which is that, statistically, the seismicity rate before any earthquake at time t_o increases as $1/(t_o-t)$ [2, 3]. However, it is yet not clear what is the respective contribution of the static stress change and of the shaking itself in this triggering (see, e.g., [4]). The picture is further complicated by the fact that earthquakes are not the only instabilities which can rapidly change stresses in the crust and trigger earthquakes: transient aseismic slip on faults at seismogenic depths are also documented, as well as fluid instabilities like natural hydro-fracturation, and can last minutes to days [5-7]. The cross-coupling between slow and fast (seismic) instabilities may lead to a generalized self-organized criticality (SOC) model which remains compatible with earthquake short term predictability [8, 9]. In this framework, earthquake precursors are those transients, slow or fast, which succeeded in triggering large earthquakes. In the present short note, we describe two experiments related to the search of cross-triggering between seismic and non seismic slip on faults.

Creep and seismic slip during a deep hydrofracturation experiment

The cross-coupling between fluid instability, slow creep, and microseismicity can be illustrated by the case of Soultz-sous-Forêt, in Alsace (France), where 45,000 m^3 of water have been injected during 14 days in 1993 at 3 km in depth, within granite. Some 12,000 induced micro-earthquakes were located with 4 deephole seismometers, and form a cloud with an ellipsoidal shape 1.5 km high, 1.5 km long and 0.4 km wide (e.g., [10]). More than 40% of this acti-

vity consists of multiplets, i.e., sequences of ruptures generating almost identical waveforms at all stations, and hence being assumed to involve faulting with nearly the same location and focal mechanisms. Some of these multiplets count up to 60 similar events. A repeated logging of the injection well after the experiment reveals that several faults crossing it have slipped by a few millimetres up to a few centimetres during the injection.

About 30 multiplets coincident with the fault plane presenting the largest slip through the borehole (4.2 cm) have been selected [11]. The mean distance between events in a single multiplet is accurately calculated by cross-correlation, with an uncertainty smaller than one meter. This distance is usually less than 5 m, smaller than their rupture dimension, typically 5 to 20 m, estimated from their corner frequency. Each multiplet is thus the repeated rupture of a single asperity. Consequently, the cumulative slip of each of these asperities can be estimated by the sum of the individual mean slip of each subevent.

The time sequence of each multiplet shows that the successive ruptures of the asperity are concentrated at early times after the first event, resulting in a lowering of the mean slip rate on the asperity with time (Fig. 1). The final slip of each asperity ranges between 0.5 to 4 cm, thus compatible with the local measure of slip within the borehole. Groups of multiplets, quite distant from each other, are observed to start nearly at the same time, and the whole sequences of multiplets appears as a sequences of such phases.

We interpret this space-time seismic activity as asperities repeatedly loaded and ruptured by the aseismic slip of fault surfaces around them, a slip which is itself triggered by the pore pressure increase of the water injection. Thus, the multiplet seismicity would just be a weak, but easily detectable by-product of a much more important, slow stress release: asperities have a typical size of 10 m wit ha slip ranging from 0.1 to 1 mm, and a typical seismic moment of about 10^{10} Nm, whereas the 1 cm mean slip on the 100 x 300 m^2 fault has a mostly non-seismic moment of about 10^{13} Nm, corresponding to a magnitude 2.5-3.0 earthquake. The clustering of the starting times of multiplets shows that the selected fault plane is segmented, each segment slipping as a whole, one after the other, and triggering multiplets. The average decay in time of the seismicity of each multiplet, similar to an Omori law, shows that the fault segment slip rate decreases with time. Thus, the time decay of the multiplet seismic activity is due to a slip deceleration of the fault after its destabilisation. This necessarily involves slip or velocity strengthening property of the fault surface [12]. This is at odds with the standard aftershock model proposed by Dieterich [13], where the Omori law results from the delayed rupture of asperities which have an unstable, accelerating slip, requesting slip or velocity weakening properties.

These results suggest that a significant part of natural aftershock sequences or swarm activity may be related to non-seismic slip at a large scale, possibly involving also natural hydro-fracturation processes. The analysis of multiplet sequence could help to quantify otherwise hidden, large slow slip on active

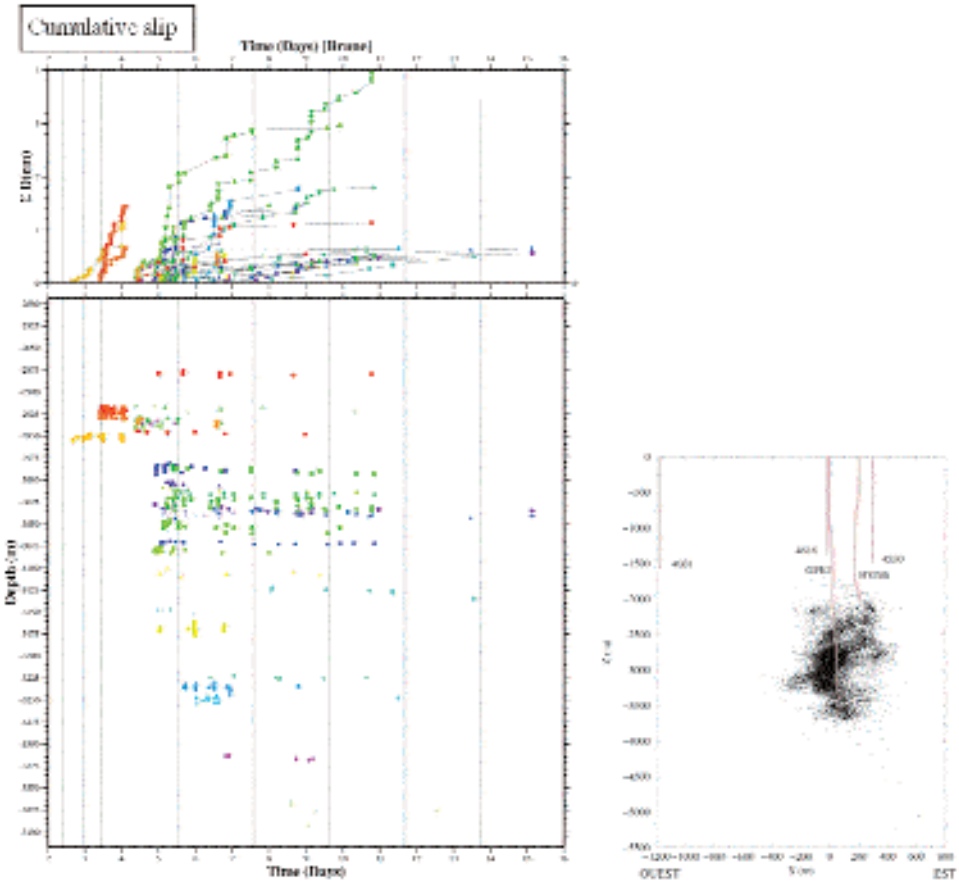

Fig. 1. Time characteristics of selected multiplets in Soultz. Left: Cumulative slip (top) and depth distribution (bottom) of multiplets with time. The multiplets correspond to the largest activated fault plane. Each multiplet has a given color. Right: vertical cross-section of the induced seismicity.

faults. The independent detection of these slow motions, through high resolution strain or tilt measurements, appears necessary for a better quantification of these models.

High resolution strain measurements in the Corinth rift Laboratory

High resolution strainmeters and tiltmeters have been recently installed near the western end of the rift of Corinth, Greece, as part of a European effort to monitor the tectonic and seismic activity of the area, one of the most active in the Euro-Mediterranean (see [14, 15]). These instruments complement

the Corinth Rift Laboratory (CRL) seismic and the continuous GPS arrays. Within the E.C project CORSEIS, and thanks to the active collaboration of the Carnegie Institution of Washington, a *Sacks-Evertson* borehole dilatometer [16] was installed and cemented at 150 m in depth, in the Trizonia island, in November 2002 (red dot in Fig. 2A). Its continuous recordings show a clear semi-diurnal signal, resulting from the combination of earth and sea tide. It also records local, regional, and teleseismic earthquakes, providing a strain signal proportional, to the first order, to the ground velocity. The M = 8, Hokkaido earthquake of 25 September 2003 was used for the first reliable *in situ* calibration of the instrument.

In one year, from its installation to the end of 2003, it produced only one significant, anomalous signal, which lasted about an hour, and was unrelated to external loading (air pressure, rain, sea level) (Fig. 2). This signal started the

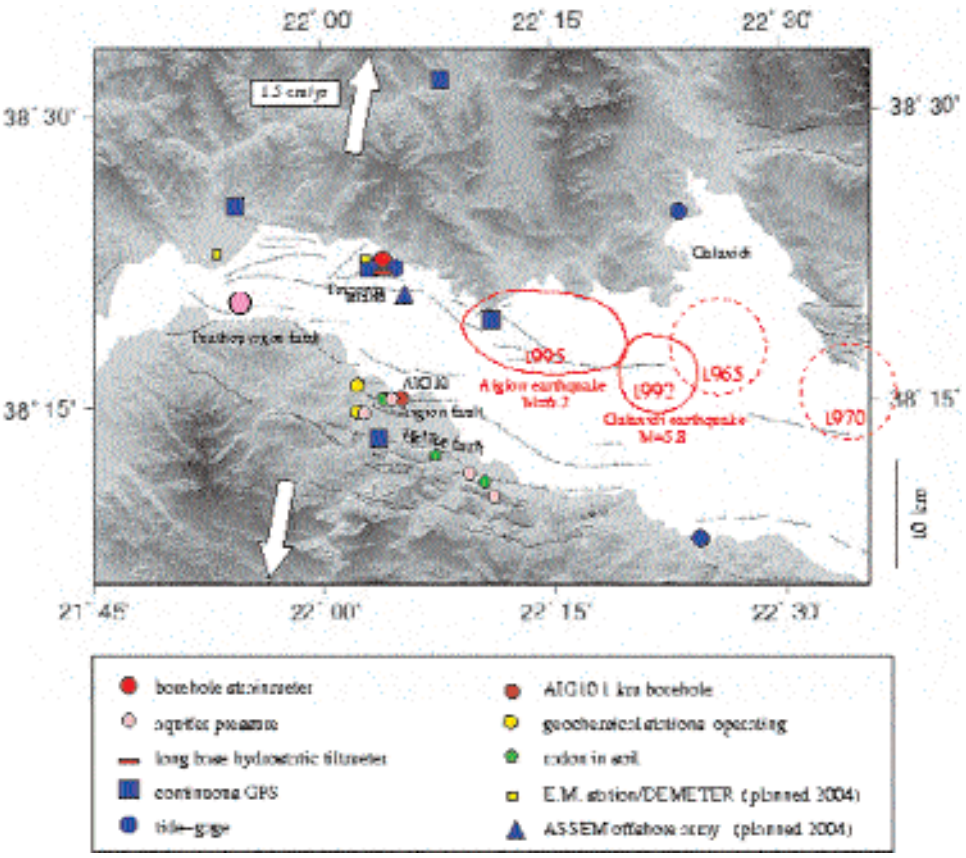

Fig. 2A. Strain monitoring arrays in the western rift of Corinth. The large red dot is the borehole strainmeter location on the trizonia island. The pink red dot is the location of the 3rd December 2002, M=3.7 earthquake (see Fig. 2B).

3rd December 2002 at about 11 p.m., with a regular compression increase, culminating at a level of 10^{-7} after half an hour with the record of a local earthquake. The strain then reversed sharply to dilatation within the S wave record of this earthquake, and then merged within the tidal wave. This earthquake occurred about 10 to 15 km west to the site, and had a magnitude 3.7 (orange dot in Fig. 2A). It happened to be the largest event of a swarm of about 20 earthquakes above magnitude 2 (catalogue of Patras University), which lasted 2 weeks. Its precise correlation in time with the peak of the slow strain event let us believe that both events are physically correlated. In this case, assuming them to be located within a few kilometres of each other, and assuming an aseismic slip on a fault, we estimate the equivalent moment magnitude of the slow event to be of the order of 5 ± 0.5.

As these slow events may be quite rare, a statistical approach of the coincidence between them and earthquakes may not prove to be very useful before many years to validate their correlation with earthquake activity. Instead, it seems necessary to increase the number of such sensitive instruments like strainmeters and tiltmeters, in order that slow transient deformation can be

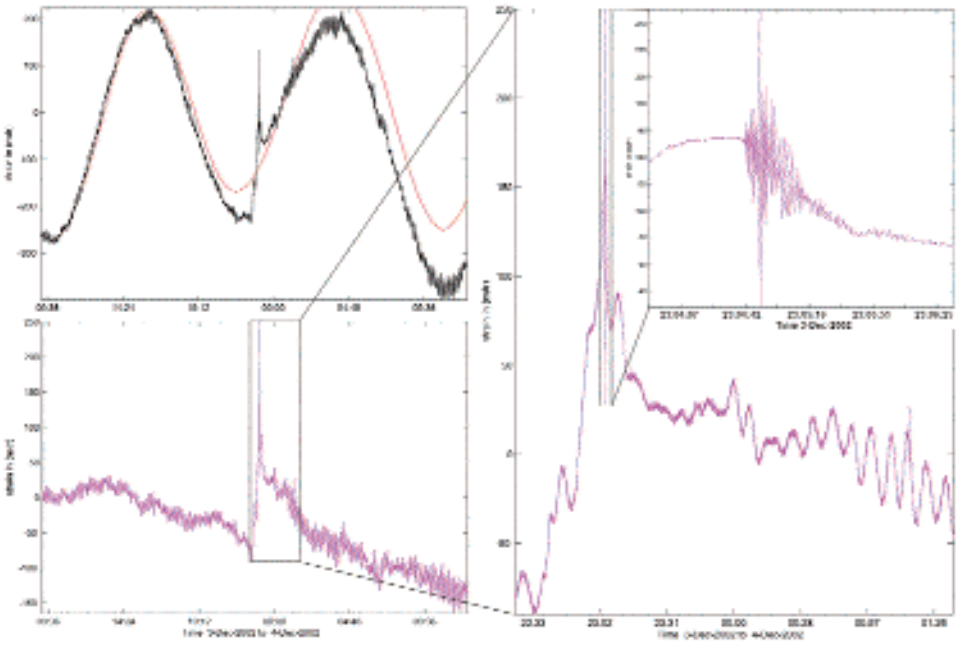

Fig. 2B. Trizonia dilatometer transient record. Top left: Record of the 3rd December 2002 compression transient (amplitude 1.5×10^{-7}) superimposed on tidal wave. Bottom left: residual when all tidal waves and air pressure removed. Right: zoom of the transient, also showing the free oscillations of the Gulf and seismic waves of a local M = 3.7 earthquake (top right insert), Compression is positive. Rapid extension occurs a few seconds after the arrival of the seismic waves.

recorded by several sensors simultaneously. This would unambiguously rule out the possibility of a local noise, close to the sensor, and overall allow to better constrain its main characteristics in term of moment tensor at the source.

Perspectives

The two examples above show that studying earthquake transients, and in particular the most frequent ones which are the seismic swarms, might be a clue to understand the nucleation process and the triggering of earthquakes, and to progress on the question of earthquake predictability. These studies require the continuous monitoring of crustal activity, not only through well designed, high-quality seismic arrays, allowing in particular the detection of multiplet sequences, but also with high-resolution borehole strainmeters. Rare observations of the coupling between transient strain and seismic activation (e.g., [17]), might then be more frequently reported, as the resolution level of strain or tiltmeters is at least one or two order of magnitude better than GPS. Finally, electromagnetic and geochemical monitoring, although much more difficult to interpret unambiguously as it is very sensitive to local heterogeneities, can also provide important clues to understand these processes.
From the modelling point of view, it is clear that the standard rate-and-state friction law models on faults have to go a step further than what is proposed by the standard slip (or slip velocity) strengthening and weakening. The former accounts for aseismic creep, the latter for seismic rupture nucleation and dynamics, respectively. Instead, fault surfaces allowing for both type of friction in neighbouring patches might be the requested models for those faults which exhibit coupled seismic and aseismic behaviour. These faults are of particular interest, as they are expected to be favourable areas to generate transient slip phenomena, and possibly precursory sequences for moderate to large earthquakes.

Acknowledgments

This work was partially supported by the CORSEIS E.C. project, contract EVG1-CT99-00002.

References

1. Kagan YY, Jackson DD. Probabilistic forecasting of earthquakes. *Geophys. J. Int.* 143:438-53, 2000.
2. Helmstetter A, Sornette D, Grasso J-R. Mainshocks are aftershocks of conditional foreshocks: how do foreshock statistical properties emerge from aftershock laws. *J. Geophys. Res.* 108:2046, 2003.

3. Papazachos B. Foreshocks and earthquake prediction. *Tectonophysics* 28:213-16, 1975.
4. Ziv A. Foreshocks, Aftershocks and remote triggering in quasi-static fault models. *J. Geophys. Res.* 108, 2003, in press.
5. Linde A, Gladwin TM, Johnston MJS, Gwyhter RL, Bilham RG. A slow earthquake sequence on the San Andreas fault. *Nature* 383:65-8, 1996.
6. Dragert H, Wang K, James TS. A silent slip event on the deeper Cascadia Subduction interface. *Science* 292:1525-8, 2001.
7. Lowry AR, Larson K, Kostoglodov V, Bilham R. Transient fault slip in Guerrero, southern Mexico. *Geophys. Res. Lett.* 28:3753-6, 2001.
8. Nature Debates. Is the Reliable prediction of individual earthquake a realistic scientific goal. *http://www.nature.com/nature/debates/earthquake/equake_frameset.html*, 1999.
9. Bernard P. From the search of precursors to the research on crustal transients. *Tectonophysics* 338:225-32, 2001.
10. Gaucher E. *Comportement hydromécanique d'un massif fracturé: apport de la microsismicité induite. Application au site géothermique de Soultz-sous-Forêts*. PhD thesis, Univ. Paris 7, 245 pp, March 1998.
11. Bourouis S, Bernard P, Cornet F. Triggered seismicity in the Hydraulic stimulation at Soultz (France): Evidence for the Control of the Multiplet Sequences by Major aseismic slip. *AGU fall meeting,* abstract, December 2003, San Francisco, 2003.
12. Dieterich JH. Modeling of rock friction, 1. Experimental results and constitutive equations. *J. Geophys. Res.* 84:2161-8, 1979.
13. Dieterich JH. A constitutive law for rate of earthquake production and its application to earthquake clustering. *J. Geophys. Res.* 99:2601-18, 1994.
14. Cornet FH, Bernard P, Moretti I. On the Corinth Rift problematic and the special Geoscience issue. *C.R. Ac. Sci. Geosciences* Special Issue (24 papers), March 2004.
15. Bernard P, Boudin F, Sacks S, Linde A, Blum P-A, Courteille C, Esnoult M-F, Castarède H, Felekis S, Billiris H. Continuous strain and tilt monitoring on the Trizonia island, Rift of Corinth, Greece. *C.R. Acad. Sci.* 2004, in press.
16. Sacks IS, Suyehiro S, Evertson DW, Yamagishi Y. Sacks-Evertson strainmeter, its installation in Japan and some preliminary results concerning strain steps. *Pap. Meteorol. Geophys.* 22:195-208, 1971.
17. Rogers G, Dragert H. Episodic tremor and slip on the Cascadia Subduction: The chatter of Silent slip. *Science* 300:1942-3, 2003.

Effect of focal mechanism in the probabilistic seismic hazard analysis

V. Convertito[a], A. Herrero[b]

[a]*Dipartimento di Fisica, Università degli Studi di Napoli "Federico II", Napoli, Italia*

[b]*Istituto Nazionale di Geofisica e Vulcanologia, Roma, Italia*

Introduction

A new formulation for the probabilistic seismic hazard analysis is proposed in order to introduce a-priori information about seismic source parameters. In particular, the focal mechanism may be taken into account with a theoretical corrective coefficient applied to the classical attenuation law. The new formulation is also compatible with the use of a de-aggregation technique and allows to extend the design earthquake to the focal mechanism. An application on the Southern Apennines, Italy is shown. The result of the analysis emphasizes the importance of strike-slip events in the seismic hazard context compared to main normal faulting seismic activity characterizing this region.

General formulation

In the classical approach to the probabilistic seismic hazard analysis (PSHA) proposed by Cornell [1], the hazard level at a site is obtained assessing the effects of a given seismic source zone through an attenuation law that, however, relate earthquake effects only with its magnitude and its distance to the site. Generally, the object of a PSHA is the estimation of a hazard curve that represents the probability of exceeding a range of ground motion amplitudes for a given time period. When a Poissonian earthquake recurrence model is adopted, the expression of the exceeding probability P_h for a strong ground motion parameter A and a set of N seismic source zones is as follows:

$$P_h(A \geq A_0, t) = 1 - e^{-\sum_{i=1}^{N} E_i(A \geq A_0) \cdot t} \tag{1}$$

where $E_i(A \geq A_0)$ for the i-th seismic source zone is the exceeding frequency of a given threshold A_0 and is expressed by the following formula:

$$E_i(A > A_0) \quad \alpha_i \int_R \int_M f_R(r) f_M(m) p_a | A(m,r) > A_0 | m, r | dm dr \tag{2}$$

The parameter α_i is the seismic activity rate, $f_M(m)$ and $f_R(r)$ are respectively the magnitude and distance probability density functions (pdfs) and p_a is the exceeding conditional probability for a given magnitude distance couple *(m, r)* deduced from the attenuation law.

We propose to generalize the hazard assessment also including the focal mechanism effect, through a correction of the ground motion parameter $A(m,r)$ estimated by the attenuation laws. In practice, attenuation laws account only for few parameters such as magnitude, distance and a simple discrete variable for site effect (e.g., [2]). On the other hand, the need for refining the estimation of strong ground motion parameters has led some authors to extend the attenuation law to a larger number of source parameters, such as the focal mechanism (e.g., [3]), the directivity effect (e.g., [4]) and the fault geometry (e.g., [5]). These approaches are generally based on the introduction of further coefficients inside the attenuation law formulation. However, they have to face with some inherent difficulties. Indeed, they require a complete and homogeneous catalogue and the implementation of an efficient regression technique. The method we present in this paper is aimed to overcome some of the previous limitations introducing the focal mechanism as a-priori information in the general formulation of the PSHA. The attenuation law is modified using a correction coefficient based on the theoretical formulation of the radiation pattern of a double-couple earthquake mechanism. In particular, if a focal mechanism is defined by its dip δ, rake λ and strike ϕ, the formulation of the correction coefficient c as a continuous function of the distance r, is expressed as follows:

$$c(r,\delta,\lambda) = \frac{|\overline{\Re}_{\phi}(r,\delta,\lambda)|}{|\overline{\Re}_{\phi r \delta \lambda}|} \tag{3}$$

In the equation (3), $|\overline{\Re}_{\phi r \delta \lambda}|$ is the absolute value of the radiation pattern averaged over all the possible ϕ, r, δ , λ values while $|\overline{\Re}_{\phi}(r,\delta,\lambda)|$ is the absolute value of the radiation pattern averaged over all the possible strike ϕ. The integration over the entire range of the strike allows to take into account for the dip and the rake effects disregarding the relative source-site orientation. The correction does not require any regression procedure and allows to take into account for a specific aspect of the seismic source, i.e. radiation pattern, avoiding problems related to the database completeness. Our proposal permits also to define a general double pdf $f_{\delta\lambda}(\delta,\lambda)$ which modify the formulation of the exceeding frequency reported in the equation (2). This further pdf allows to verify the effect of the focal mechanism directly on the hazard curve and can also be used in the "de-aggregation" technique. This technique has been introduced in the PSHA by McGuire [6] in order to associate a design earthquake at a given site, for a given hazard level.

Application to Southern Apennines (Italy)

In order to illustrate the new formulation, we applied it to a site located in the city of Naples, Italy. We first compute the exceeding probability curve for the horizontal PGA (peak ground acceleration) using the classical PSHA. The seismic source zones considered in the analysis are represented in Fig. 1 and the corresponding parameters are listed in the Tab. 1.
We use an attenuation law [2] obtained from an Italian strong ground motion database. The continuous line in Fig. 2 represents the result corresponding to the classical approach and the dashed line corresponds to the case in which the a-priori information is adopted. In order to introduce the "a-priori" information on focal mechanism, we define a specific double pdf $f_{\delta\lambda}(\delta,\lambda)$ composed by two Gaussian distributions and assume the presence in all the three zones of normal faults and strike-slip faults.

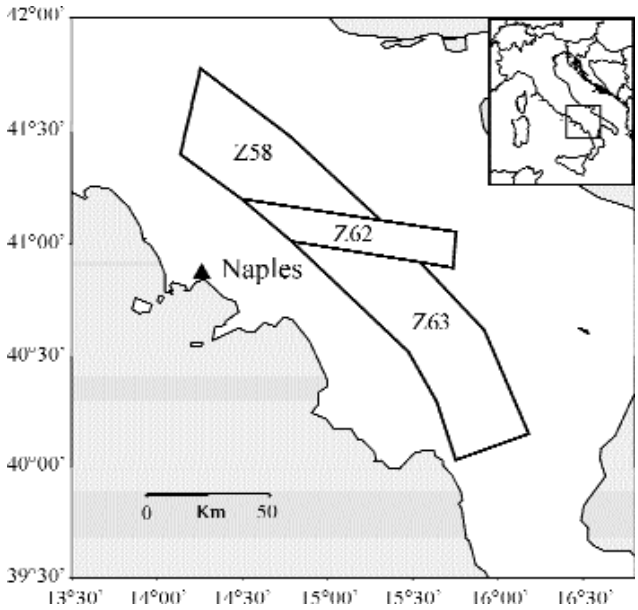

Fig. 1. Site location and configuration of the three seismic source zone used in the analysis.

Tab. 1. Seismic source zone parameters.

Zone	α (event/year)	b	M_{max}
Z58	0.088	0.5850	7.3
Z62	0.091	0.5722	6.7
Z63	0.315	0.6716	7.0

We de-aggregate the PGA values corresponding to a 10% of the exceeding probability and a return period of 475 years for the case without a-priori information and for the case in which the "a-priori" is used. The Fig. 3 shows the result of the de-aggregation. The bold lines represent the initial pdfs for all the variables. The marginal pdf on the rake clearly shows the two focal mechanisms with their relative weight (Fig. 3D). On the contrary, the marginal on the dip is unimodal due to the large width of the Gaussian we have assumed on the dip (Fig. 3C). The squares on Fig. 3 represent the retrieved pdfs after the de-aggregation for the no a-priori mechanism case. The de-aggregation for the distance is characterized by a uni-modal distribution while in the case of magnitude, the distribution is multi-modal with maxima close to each M_{max} listed in Tab. 1. The diamonds on the Fig. 3 show the result in the case in which the focal mechanism is introduced. It is interesting to note that the shape of the retrieved pdfs does not change for the magnitude and the distance in both cases (with and without a-priori). The variation in the PGA can then be attribute uniquely to the a-priori information.

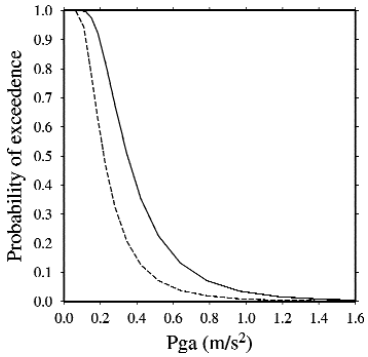

Fig. 2. Exceeding probability curves. The continuous line represent the result for the classical analysis. The introduction of a-priori focal mechanism information transforms the curve in the dashed one.

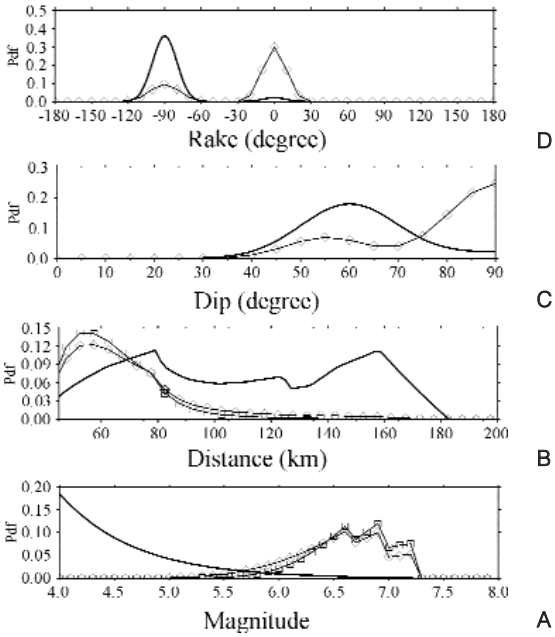

Fig. 3. Initial pdfs (bold lines) on the hazard variables [magnitude (A), distance (B), dip (C) and rake (D)] and marginal pdfs resulting form de-aggregation technique. The squares shows the result in the case in which no a-priori information on the focal mechanism is used. The diamonds shows the result in the case in which the information on the focal mechanism is introduced.

Discussion and conclusions

In this paper we investigate the possibility of refining the PSHA introducing the fault mechanism as an "a-priori" information. The originality of the proposed formulation is that it does not require any regression analysis on the database avoiding all the problems concerning completeness and homogeneity. The new formulation has been also used to extend the definition of the design earthquake deduced by the de-aggregation technique.
We present an application relative to a site located in the city of Naples, Italy. For a 10% of exceeding probability, the PSHA shows a pga decrease when the focal mechanism "a-priori" information is introduced. This is in agreement with observation where normal faults seems to generate smaller pga values than strike slip (e.g. [7, 8]).
The de-aggregation result shows that the design earthquake is most likely a strike slip. This may be explained by the type of radiation pattern used in our example. In fact, we use only the SH radiation pattern. Now, the site of Naples being far from the seismic source zones, its associated SH radiation pattern, integrated on the strike, is smaller for normal faults than strike slip faults.
The approach we have proposed may be seen as an alternative to introduce "a-priori" information in PSHA in the cases where the databases do not allow to realise a exhaustive statistical regression analysis. It also may be extended to other types of source parameters such as, for example, fault strike and focal depth.

References

1. Cornell CA. Engineering seismic risk analysis. *Bull. Seism. Soc. Am.* 58:1583-606, 1968.
2. Sabetta F, Pugliese A. Attenuation of peak horizontal acceleration and velocity from Italian strong-motion records. *Bull. Seism. Soc. Am.* 77:1491-513, 1987.
3. Abrahamson NA, Silva WJ. Empirical Response Spectral Attenuation Relations for Shallow Crustal Earthquakes. *Seism. Res. Lett.* 68:94-127, 1997.
4. Sommerville PG, Smith HF, Graves RW, Abrahamson NA. Modification of empirical strong ground motion attenuation relationship to include the amplitude and duration effects of rupture directivity. *Seism. Res. Lett.* 68(1):199-222, 1997.
5. Ohno S, Ohta T, Ikeura T, Takemura M. Revision of the attenuation formula considering the effect of fault size to evaluate strong ground motion spectra in near field. *Tectonophysics* 218:69-81, 1993.
6. McGuire RK. Probabilistic Seismic Hazard Analysis and Design Earthquakes: Closing the loop. *Bull. Seism. Soc. Am.* 85;1275-84, 1995.
7. Campbell KW. Near-source attenuation of peak horizontal acceleration. *Bull. Seism. Soc. Am.* 71:2039-65, 1981.
8. McGarr A. Scaling of ground motion parameters, state of stress and focal depth. *J. Geophys. Res.* 89:6969-79, 1984.
9. Anderson JG, Luco JE. Parametric study of near-field ground motions for oblique-slip and dip-slip dislocation models. *Bull. Seism. Soc. Am.* 73:45-57, 1983.
10. McGarr A. Upper bounds on near-source peak ground motion based on a model of inhomogeneous faulting. *Bull. Seism. Soc. Am.* 72:1825-41, 1982.

Quantitative seismic imaging of complex structures for seismic hazard estimation and for reservoir characterisation: a key strategy

J. Virieux[a], S. Operto[a], L. Improta[b], P. Dell'Aversana[c]
[a]*UMR Géosciences Azur – CNRS-UNSA-UPMC-IRD, Valbonne, France*
[b]*Istituto Nazionale di Geofisica e Vulcanologia, Roma, Italia*
[c]*Eni S.p.a., Milano, Italia*

Introduction

Seismic imaging of complex structures characterized by strong lateral variations in the velocity field remains a challenge, while sub-surface characterisation becomes a crucial challenge in our present society for safety, resources and wastes. Most of the time, the seismic imaging problem is applied to conventional surface-seismic multichannel reflection geometries which involve only near-vertical wave propagations (namely, short angle reflections). When applied to these geometries, the seismic imaging problem can be subdivided into two distinct tasks. Chronologically, the first one is the determination of a smooth background velocity model which describes the large-scale velocity distribution. The second task uses this background velocity model to image the short wavelength components of the structure (namely, discontinuities or interfaces) by prestack depth migration/inversion which is generally considered as a well-established procedure for imaging complex structures (see [1] for a review). By prestack depth migration/inversion, we define the prestack depth migration methods which are cast in the frame of inverse problem theory and return a quantitative estimate of the model parameters. Nevertheless, it is also well established that, in presence of complex media, estimation of a reliable velocity macromodel for migration/inversion is a very difficult task, if not impossible, when only conventional multichannel seismic reflection data are available. Moreover, the precise definition of a reliable macro-model for migration/inversion is still an open question which has been addressed only in a heuristic way (e.g., [2]). Indeed, conventional surface-seismic reflection geometries are not optimally designed for velocity estimation due to their limited aperture range. Refracted and post-critical reflected waves at large offsets are also sensitive to the smooth velocity distribution.
Surface wide-aperture geometries, generally referred as refraction geometries, are designed to yield sufficiently large source/receiver offsets in order to record waves refracted at the depths of investigation.

Smooth macro-velocity model can then be developed by first-arrival traveltime inversions (e.g., [3, 4]). If one can pick secondary arrival traveltimes consistently, simultaneous inversion of refraction and reflection traveltimes allows the derivation of interface geometries in addition to the background velocities (e.g, [5-8]).
Nevertheless, picking of secondary arrivals which requires a human intervention to identify and interpret reflected arrivals, is rarely a trivial task especially in the case of highly laterally heterogeneous media.
Compared to the conventional multichannel seismic reflection geometry, the main drawback of wide-aperture surveys is usually their poor fold due to the large spacing between receivers and shots. This precluded until recently application to this kind of data of wavefield propagation methods such as pre-stack depth migration/inversion or full wavefield inversion [9]. As a consequence, only the first step of the seismic imaging problem, namely, macromodel building by traveltime inversion, is generally applied to surface wide-aperture seismic data. However, the velocity models derived by this approach are usually poorly resolved since first-arrival traveltimes are only sensitive to the large-scale velocity distribution [10].
When a highly dense seismic acquisition system is available, global offset data could be simultaneously used for a full waveform linearized inversion with the deduced smooth traveltime model as the initial velocity structure.
The full waveform modeling and inversion are implemented in the frequency domain. The modeling part is solved with a finite difference method applied to the visco-acoustic wave equation. The inversion is based on a local gradient method. Only the P-wave velocity is involved in the inversion. The inversion is applied iteratively to discrete frequency components by proceeding from low to high frequencies. This defines a multi-scale imaging in the sense that high wavenumbers are progressively incorporated in images.

GEOLOGICAL SETTING

The seismic data processed in this paper have been collected in the axial zone of the Southern Apennines thrust-and-fold belt (Italy) by the Enterprise Oil Italiana (Fig. 1). The investigated area is characterized by a strongly heterogeneous crustal structure.
The geological setting consists of a tectonic stack of NE-verging sheets involving Jurassic rocks (cherty dolomites, cherts) and Cretaceous shales. These basinal units are overthrusted by a regional nappe, which consists of a tectonic melange of Paleocene clays and marly-limestones (Fig. 1). The shallower units include Pliocene soft sediments representing the infill of small basins. Main surface tectonic structures crossed by the seismic profile are a NW-trending synform, filled by soft Pliocene sediments, and broad nappe anticline, the latter responsible for a tectonic window where Mesozoic rocks outcrop.

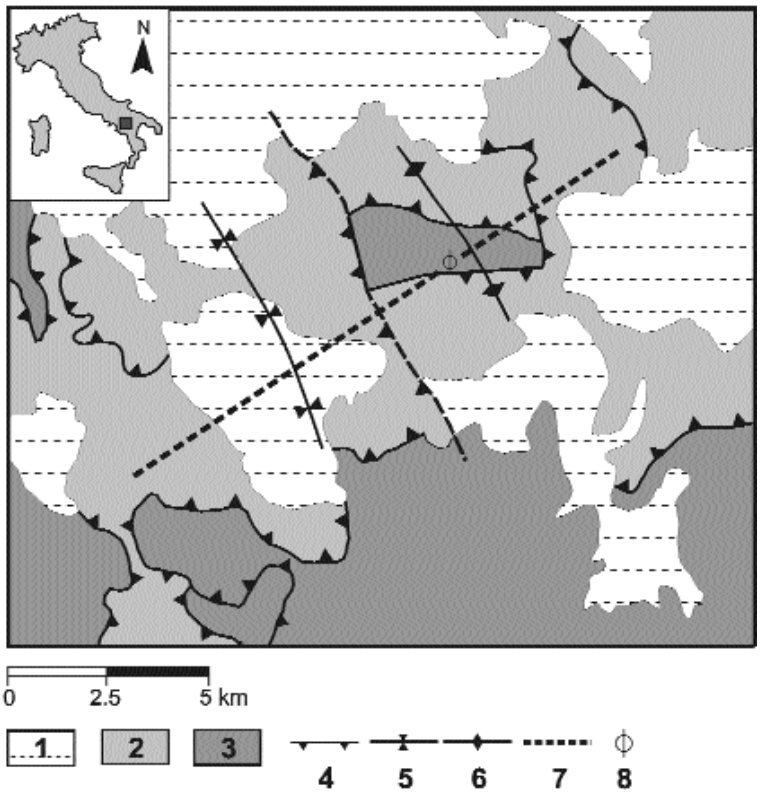

Fig. 1. Tectonic setting in the target area. (1) Plio-Pleistocene soft sediments, (2) Paleocene clayey and marly-calcareous tectonic melange, (3) Mesozoic basinal rocks, (4) thrust, (5) syncline, (6) anticline, (7) seismic profile, (8) well for oil exploration. b) Topography along the seismic profile. Position of the well along the profile is indicated.

Field experiment

The 2-D acquisition geometry consists of a SW-NE 14200m long line running above a synform and wide antiform. The profile strikes NE-SW and is almost perpendicular to the main thrust front and fold axes in the area. The profile is tied to a deep well drilled in the core of the antiform (Fig. 1). The topography along the profile is extremely rough. The maximum difference in altitude between sources reaches 700 m. The surface receiver array consists of 160 vertical geophones deployed along the 2-D line with 90 m interval. Two hundred thirty-three shots were fired with an average spacing of 60 m into the array by housing explosive charges in 30 m deep boreholes (for a detailed description of the experiment design see [11]). This acquisition geometry leads to a multifold wide-aperture acquisition with densely sampled source and receiver spacings amenable to wavefield propagation processings such as full waveform inversion and ray-based prestack depth migration (Fig. 2).

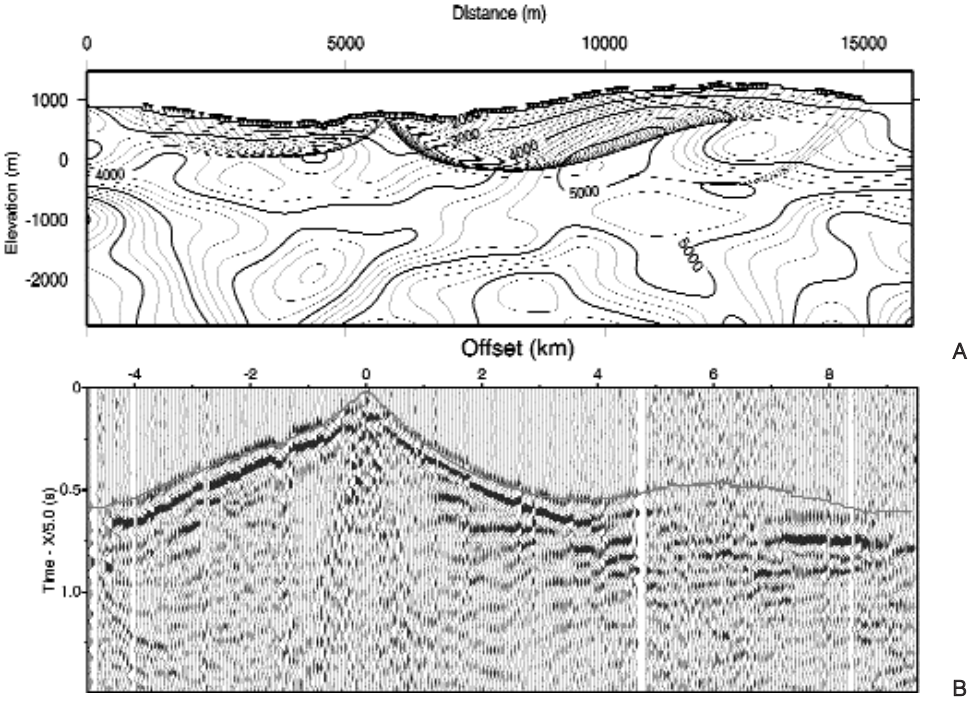

Fig. 2. A. Ray tracing in the final velocity model of Fig. 3 for estimating the ray sampling of the medium. Rays are traced from the receiver position given by x = 5.75 km. B. First-arrival traveltimes are superimposed on the associated common receiver gather (CRG).

After a specific pre-processing of the data, sixteen frequency components ranging between 5.6 Hz and 20 Hz were inverted. Ten iterations were computed per frequency components leading to 160 waveform inversion models. The waveform inversion successfully imaged SW-dipping structures previously identified as high-resistivity bodies. The relevance of the waveform inversion models is locally demonstrated by comparison of a velocity-depth function extracted from these models with a coincident Vertical Seismic Profiling (VSP) log available on the profile. Moreover, comparison between observed and synthetic seismograms computed in the (starting) traveltime and waveform inversion models demonstrates unambiguously that the waveform inversion successfully migrated wide-angle reflections from SW-dipping geological structures.

Due to the presence of clayey strata alternated with Mesozoic hard-rock sheets, and to a variable surface geology, strong lateral variations and velocity inversions are present at all depths. The heterogeneous velocity structure, along with a very rough topography hamper the collection of good-quality near-vertical reflection data, which are otherwise affected by strong diffractions, multiples, surface waves and static problems. In addition, in such a con-

text, standard velocity analysis is inadequate to estimate accurate background velocity models for prestack migration/inversion. As a consequence, multi-channel reflection seismic usually yields only poor-quality structural images in the investigated area. In order to address this problem, alternative geophysical exploration tools (multi-fold wide-angle seismic, well-logging, magnetotelluric and gravity) have been jointly used in the region [12].
The availability of a multi-fold wide-aperture seismic data set and supplementary information on the crustal structure make this area an optimal test site for assessing the feasibility of the full waveform inversion approach in the case of on-land exploration of complex structures.

Results

Application of the non-linear traveltime inversion to the data set used in this paper have already been presented in [6]. The velocity model used as a starting model for waveform inversion has been obtained by non-linear traveltime inversion by Improta et al. [6] and is displayed in Fig. 3. Over 6000 first-arrival traveltimes, from 32 receivers, have been inverted.
The small wavelength content of the velocity model resulting from the full waveform inversion and ray-Born prestack depth migration provides new insights into the structure of the upper crust and contributes to a better understanding of the internal geometry of the investigated thrust-and-fold system, which is instead only poorly imaged by conventional reflection seismic [12].
In the central part of the full waveform inversion velocity model, the most noticeable features are SW-dipping slices clearly delineated by sharp velocity contrasts between high-velocity bodies (5500-6500 m/s) and narrow low-velo-

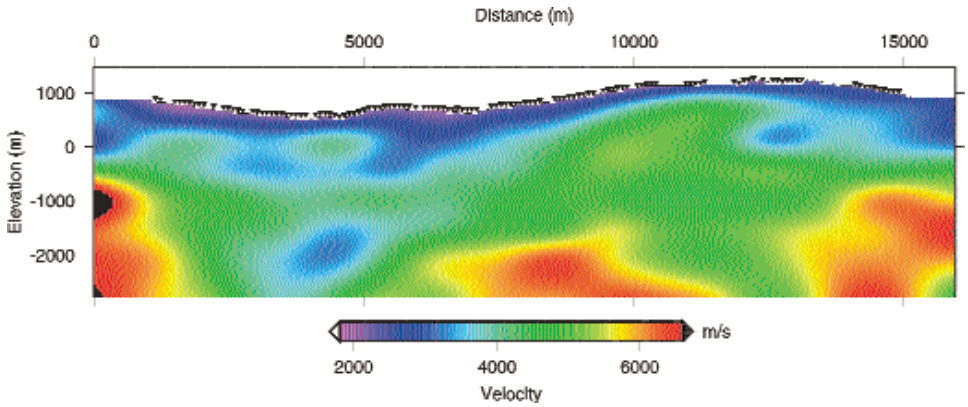

Fig. 3. Tomographic velocity model, as the initial model for full waveform inversion. The triangles label the position of the receivers that were involved in the full waveform inversion.

city regions (3500-4000 m/s) (Figs. 4A and 4B). In this region, the prestack depth migrated section shows between 5 and 7 km of distance clear antiformal structures which merge eastward with an evident near-surface high-velocity bumb. Beneath the western flank of the antiform, these slices are cross-cut by a sub-vertical body, with velocities ranging from 4500 to 5500 m/s, which merges upwards with an evident near-surface high velocity bump.
Both flanks of the antiform are characterized by near-surface low-velocity layers (2000-3000 m/s). The low-velocity layers reach a maximum thickness of about 1 km between 5 and 7 km of distance. On the western side of the profile, the shallow low-velocity layers overlay a region showing a quite chaotic succession of low amd intermediate-velocity layers, which make difficult the identification of major structures without the additional constraints provided by the prestack depth migrated section. Nevertheless, a low-velocity region (3500-4000 m/s) can be identified at about 4-5 km of distance in the 1-2.5 km depth range. On the western side of the profile, a noticeable feature of the prestack depth migrated section is the main west-dipping thrust delineated by truncated and tilted events.
Reliability of the full waveform inversion velocity model, which is locally proved by the good match found with the VSP log, has been further assessed by a comparison with a 2D resistivity model obtained by Dell'Aversana [12] inverting magnetotelluric data collected along the seismic profile (Fig. 4C).
We found a good agreement between velocity and resistivity images. The SW-dipping high-velocity bodies imaged at 1-2 km depth are consistent with two high-resistivity regions showing the same trend, while the high velocity bump imaged beneath the antiform matches quite well a high-resistivity shallow region. The near-surface low-velocity layers bounding the antiformmatch well strongly conductive bodies. In particular, note the pronounced thickening of the conductive body imaged between 5 and 7 km of distance that is cross-cut by a thin and flat high-resistivity layer. The latter matches well evident discontinuities showed by the prestack depth migrated image. Finally, the low-velocity region identified in the deeper part of the model at about 4-5 km of distance corresponds to a region of relatively low-resistivity values sandwiched between two high-resistivity bodies. Moreover, a weak arc-shaped reflector interprated on the migrated section at around 7.5 km of distance and at a depth of 1.5 km is consistent with a arc-shaped high-resistivity body.
A schematic geo-structural interpretation integrating the results of full waveform inversion, prestack depth migration, VSP log and resistivity imaging (Figs. 4A-4C) is shown in Fig. 4D. In addition, surface geological mapping (Fig. 1) facilitates the interpretation of the near-surface velocity structure.
We interpret the anticline explored by the well as a stack of two main SW-dipping sheets, which are in turn cross-cut by an out-of-sequence thrust. The out-of-sequence thrust, which we relate to the main discontinuity drilled at about 0.3 km depth, is responsible for a tectonic doubling, as well as for the formation of a wide nappe anticline in the shallow part of the crust. The internal

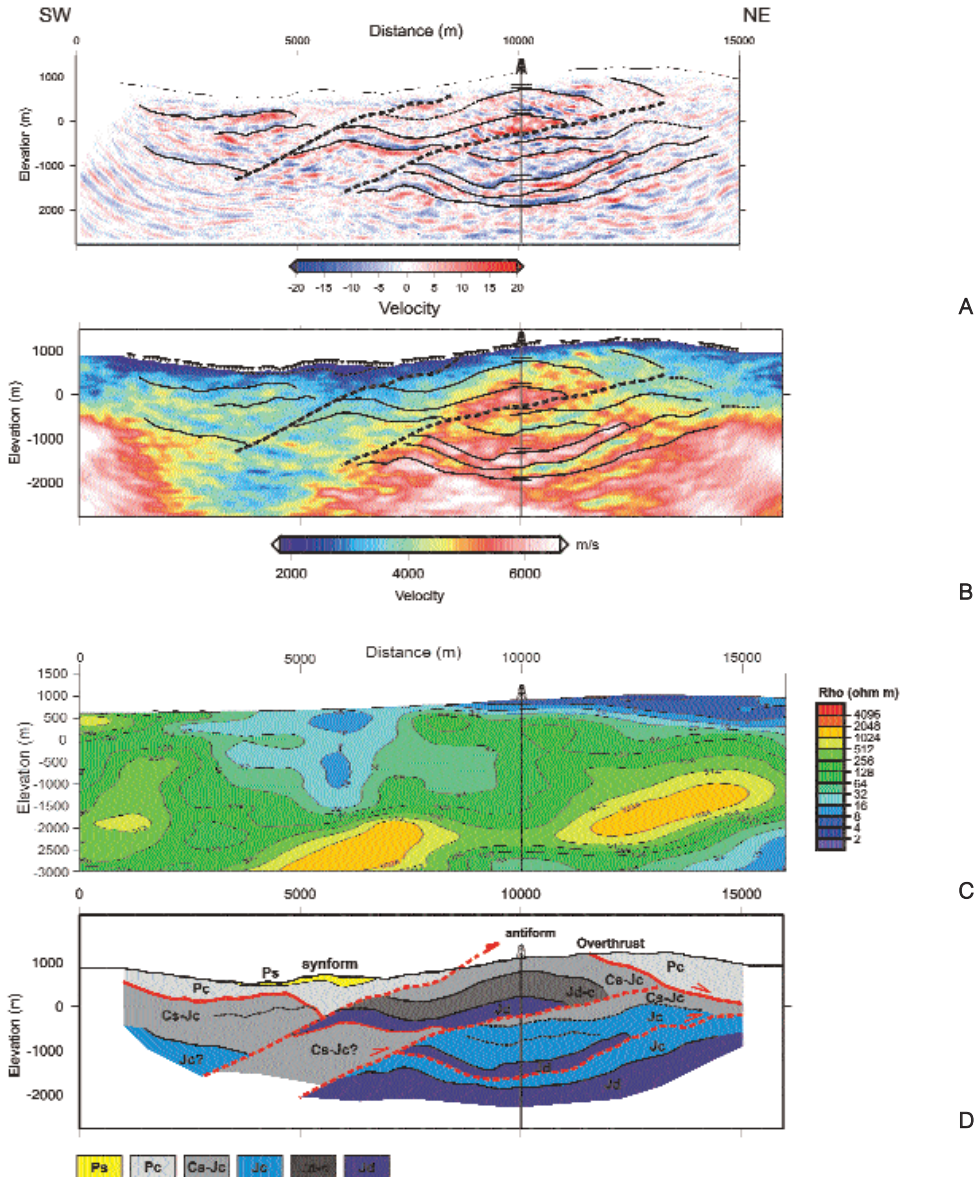

Fig. 4. Combined structural interpretation of the pre-stack depth migrated section (A) and full waveform inversion velocity model (B). The main discontinuities (e.g., velocity contrasts) identified on the model and used for the geological interpretation are indicated by black lines.
C. Two-dimensional resistivity model obtained by inverting magnetotelluric data collected along the profile. The resistivity model well delineates the large-scale structures of the waveform inversion velocity models. The high-velocity regions in the deep part of the model unambiguously correspond to two evident high-resistivity bodies in the MT section, while shallow low-velocity layer well match low-resistivity regions. D. Structural model. Ps: Pliocene clays and sands, Pc: Paleocene clayey sediments, Cs-Jc: Cretaceous shales and Jurassic cherts, Jc: Jurassic cherts, Jd-c: fractured Triassic dolomites and cherts, Jd: Triassic dolomites. The main thrusts are indicated by red lines. The central part of the model is constrained by subsurface data.

geometry of the anticline is well delineated by the high-velocity (5500-6500 m/s) and high-resistivity slices, which correspond to cherty dolomites (Fig. 4D), As inferred from the well, the bottom of the high-velocity slices delineates the main thrust planes. Intermediate-velocity bodies are associated with cherts and/or strongly fractured dolomites, while the regions showing a chaotic succession of low- and intermediate-velocity layers may be indicative of sequences lithologically dominated by Cretaceous shales. This hypothesis is based on surface and well data, and is further supported by the presence of low-resistivity regions (< 100 ohm.m), which suggests the presence of clayey materials. However, the low-velocity region identified at about 4-5 km of distance in the 1-2.5 km depth and interpreted as mainly Cretaceous clayey sequences, can also correspond to Triassic terrigenous deposits. This alternative interpretation is consistent with the well that penetrates Triassic sandstones and marly-calcareous deposits beneath the cherty limestones.
Finally, we relate the near-surface low-velocity and strongly conductive layers to the regional nappe mainly composed of Cenozoic clays, which overthrusts the Mesozoic terrains.

Conclusion

This study demonstrates that combining non linear first-arrival traveltime and frequency-domain full waveform inversions to dense wide-aperture seismic data is a promising approach to quantitatively image complex geological structures. Moreover, the velocity models derived from full waveform inversion of rather low frequency data components (20 Hz) can also be used as an improved velocity macromodel for less computationally expensive wavefield propagation methods such as asymptotic prestack depth migration. Extension of these seismic tools to 3D geometries will accomplish the critical reconstruction of a seismic velocity structure, a key parameter for seismic motion quantification once representative earthquake sources are described in a seismogenic zone. By chance, reservoir characterisation challenges follow same tracks and combined effort is advised for better performance. Passive and active seismic experiments will share same objectives reunifying two relatively disconnected research communauties.

References

1. Gray SH, Etgen J, Dellinger J, Whitmore D. Seismic migration problems and solutions. *Geophysics* 66:1622-40, 2001.
2. Operto S, Xu S, Lambaré G. Can we quantitatively image complex models with rays? *Geophysics* 65:1223-38, 2000.
3. Zelt C, Barton PJ. Three-dimensional seismic refraction tomography: a comparison of two methods applied to data from the Faeroe Basin. *J. Geophys. Res.* 103:7187-210, 1998.

4. Toomey DR, Solomon SC, Purdy GM. Tomographic imaging of the shallow crustal structure of the East Pacific Rise at 9deg.30'N. *J. Geophys. Res.* 99(24):135-24, 157, 1994.
5. Zelt C, Smith RB. Seismic traveltime inversion for 2-D crustal velocity structure. *Geophys. J. Int.* 108:16-34, 1992.
6. Improta L, Zollo A, Herrero A, Frattini R, Virieux J, Dell'Aversana P. Seismic imaging of complex structures by non-linear traveltime inversion of dense wide-angle data: application to a thrust belt. *Geophys. J. Int.* 151:264-78, 2002.
7. Hobbro JWD, Singh SC, Minshull TA. Three-dimensional tomographic inversion of combined reflection and refraction seismic traveltime data. *Geophys. J. Int.* 152:79-93, 2003.
8. Korenaga J, Holbrook WS, Kent GM, Kelemen PB, Detrick RS, Larsen HC, Hopper JR, Dahl-Jensen T. Crustal structure of the southeast Greenland margin from joint refraction and reflection seismic tomography. *Geophys. J. Int.* 105:21591-614, 2000.
9. Pratt RG, Song ZM, Warner M. Two-dimensional velocity models from wide-angle seismic data by wavefield inversion. *Geophys. J. Int.* 124:323-40, 1996.
10. Williamson PR, Worthington MH. Resolution limits in ray tomography due to wave behavior: Numerical experiments. *Geophysics* 58:727-35, 1993.
11. Dell'Aversana P, Ceragioli E, Morandi S, Zollo A. A simultaneous acquisition test of high-density "global offset" seismic in complex geological settings. *First Break* 18:87-96, 2000.
12. Dell'Aversana P. Integration of seismic, MT and gravity data in a thrust belt interpretation. *First Break* 19:335-41, 2001.

The "layered" seismicity of Irpinia (Southern Italy): important but incomplete lessons learned from the 23 November 1980 earthquake

U. Fracassi, G. Valensise

Istituto Nazionale di Geofisica e Vulcanologia, Roma, Italia

Introduction

Numerous studies following the large Irpinia earthquake of 1980 (among many others: [1-3]) shed light on the activity of the event's causative fault and of similar structures NW and SE of the epicentral area. The mechanism of earthquake generation in Southern Italy (Fig. 1) stemming from observations of the 1980 event is now rather firmly established [5-8]. This system is driven by a segmented belt of normal faults running near or on top of the Apennines regional divide [7, 9]. Nevertheless, several remarkable earthquakes in the southern portion of peninsular Italy (e.g. 1456, 1694, 1731, 1930, etc.) (Fig. 2) seem to contrast with the above model, especially on the ground of recently acquired field observations [10-12]. For instance, the mesoseismal areas of the 1694 (M_e 6.8) and 1980 (M_w 6.9) earthquakes (Fig. 3) are rather similar, yet the older earthquake did not cause slip along the fault responsible for the 1980 earthquake [13]. Furthermore, the 1-2 ky recurrence time estimated for 1980-like events [13] does not support the occurrence of two similar earthquakes within the very same region in a three century time span. We thus need to hypothesize the existence of a further set of large (and, to date, unknown) earthquake sources in Southern Italy. Such structures should conceivably form a system that is either independent from the above mentioned Apennines-top array, or somehow integrates it to the extents allowed by the present-day seismotectonic framework.

Dip-slip vs. strike-slip seismogenesis in Southern Italy

The recent Molise 2002 sequence [14, 15] and, previously, the 1990/91 Potenza (Fig. 4) earthquakes [11, 16], supplied a potential key for understanding such a dual system. These events and several minor ones bear indisputable instrumental evidence for the presence, the activity and the seismogenic potential of large deep faults roughly oriented E-W. These structures

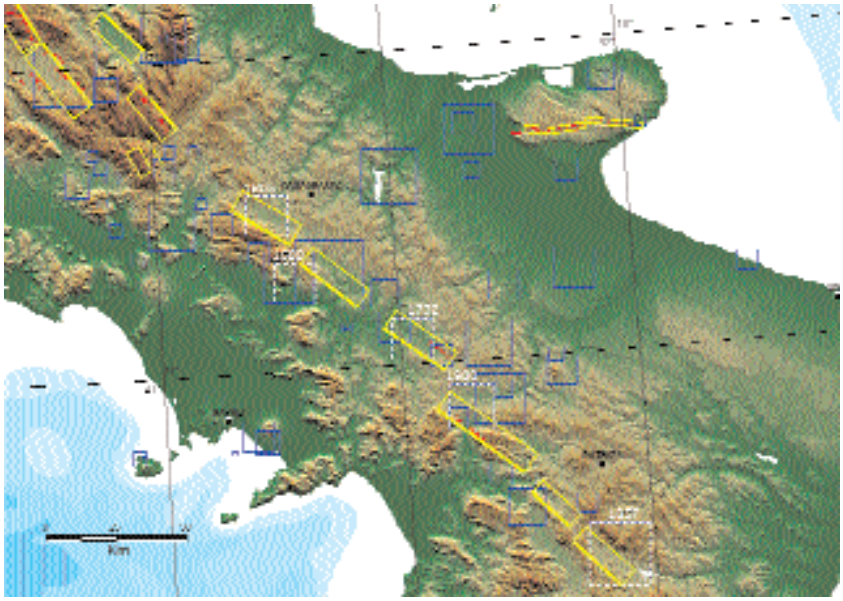

Fig. 1. Identified normal-faulting seismogenic sources in the Southern Apennines associated with major earthquakes and/or with activity indicators arising from surface and subsurface geology, geomorphology, trenching and geophysical investigations (based on [9]). The seismogenic sources, shown in yellow, are superimposed on historical earthquakes from the CFTI catalogue, shown in blue (from [4]).

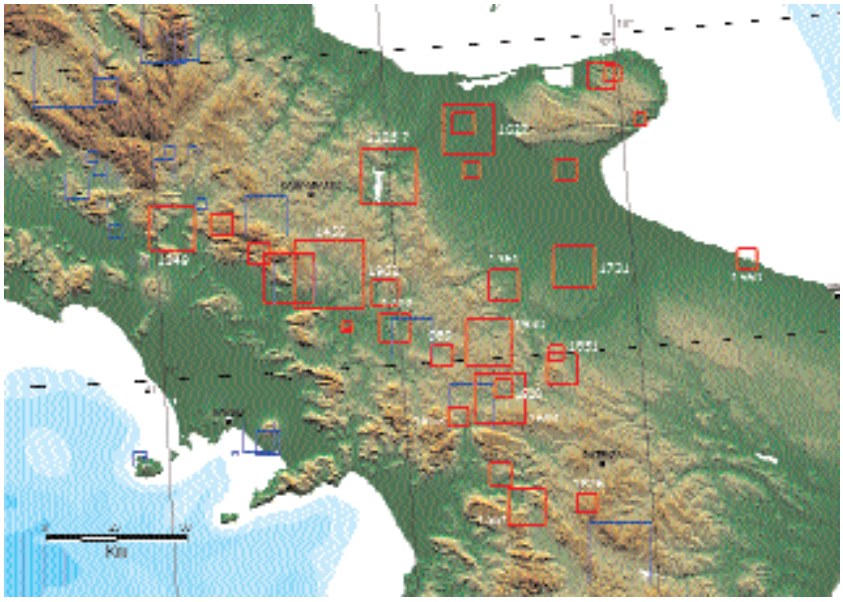

Fig. 2. Red squares show destructive historical earthquakes (M > 6.5) not yet associated with specific seismogenic sources. This circumstance is partly due to their incomplete or poorly known damage pattern and partly to the absence of a specific causative fault or of a plausibile seismotectonic scenario. Data source as in Fig. 1.

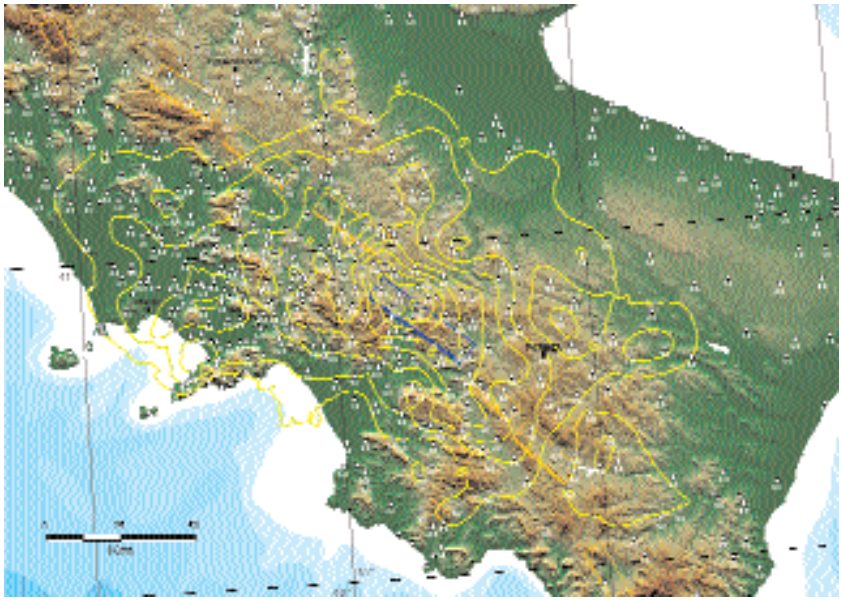

Fig. 3. Damage distribution and interpolated macroseismic field for the 23 November 1980, M_w 6.9 earthquake. Notice the elongation of isoseismals according to the Apennines-like normal structures. The earthquake ruptured down to a depth of 12-13 km and involved surface faulting. Data source as in Fig. 1.

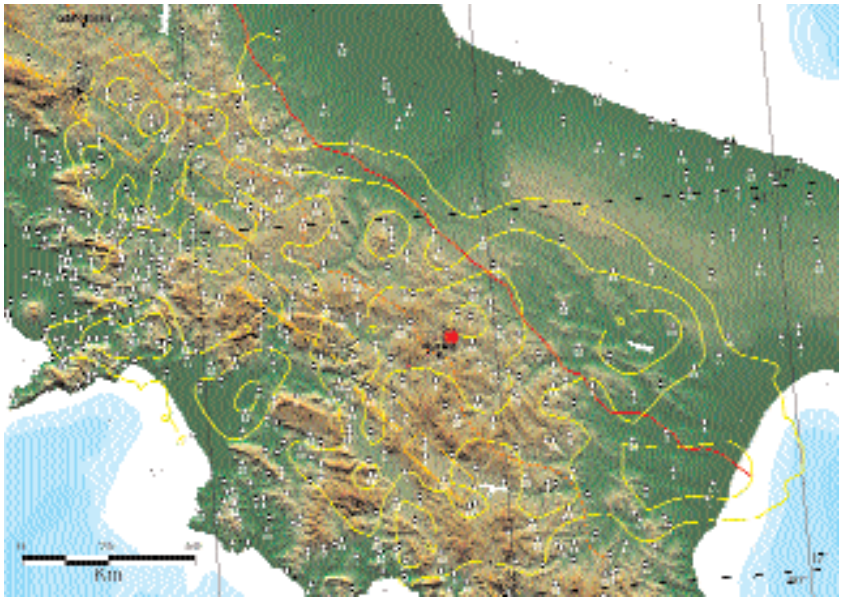

Fig. 4. Felt reports and interpolated macroseismic field of the 5 May 1990, M_w 5.2 earthquake. The red line separates the foreland (to the east) from the Apennines edifice (to the west) and marks the eastern boundary of allochtonous rocks. Notice that the damage pattern is rather irrespective of this regional geological boundary. Also notice the coexistence of NW-SE and E-W propagation trends. The earthquake ruptured between 15 and 18 km depth.

locate in the deep domain of the Apulian carbonate platform and the underlying Paleozoic basement (by terms of the Italian geology and geodynamics), which in their turn sit beneath a major portion of the Southern Apennines. These left-lateral strike-slip faults stem from the typical deformation style of the Meso-Paleozoic terrains subjected to NE-trending compression (e.g., [17, 18]). Such large structures were likely inherited during the thrust-belt build-up and extend across the entire width of the chain and beyond, that is to say, from the Adriatic to the Tyrrhenian coasts. These crustal discontinuities were often found to mark the boundaries of the known dip-slip seismogenic fault segments [9]. Localized seismic sequences occur along the same boundaries [6, 19], along with characteristic E-W-trending long-term geomorphic features and springs displaying anomalies in temperature, CO_2 content and $^3He/^4He$ ratio. The integration of these indicators into a coherent view suggests that the regional strike-slip system described above is being reactivated with reverse kinematics (right-lateral) within the current stress field, perhaps following a period of quiescence of tectonic deformation.

THE 1456 EARTHQUAKE: A LARGE "UNKNOWN" EVENT IN THE SOUTHERN APENNINES

As stated earlier, a large fraction of Southern Apennines seismicity sits within the Apennines thrust-belt. The majority of these destructive earthquakes are caused by faulting within the uppermost 10-12 km of the crust. With such structural framework in mind, we isolated several key events for which a "shallow" source could not be identified due to their peculiar location and damage pattern. Their macroseismic signature entails the possibility that their causative fault coincides with significant portions of the described E-W structures. This stimulating scenario may particularly fit the complex 1456 sequence (Fig. 5) in the Maiella, Sannio, Matese and upper Irpinia areas [21-23]. This earthquake was commonly believed to have ruptured across several normal faulting segments similar to those responsible for the typical Apennines-top earthquakes (shown in blue in Fig. 2). We are now proposing that 1456 and perhaps several other "off-belt" earthquakes (shown in red in Fig. 2) were generated by E-W strike-slip faults. The complexity of their damage pattern (Fig. 5) would be the result of (1) source multiplicity (i.e. combination of the shaking effects of faulting on two or more parallel E-W strands), (2) depth of the sources (10-15 km, calling for a strong regional propagation that emphasises the role of local anomalies), and (3) dynamic interaction with Apennines-like oriented surface tectonic structures and paleogeographic domains. Such challenging outlook is further substantiated by the peculiar damage signatures seen at the Abruzzi-Molise border and in the Benevento-Bari sectors.

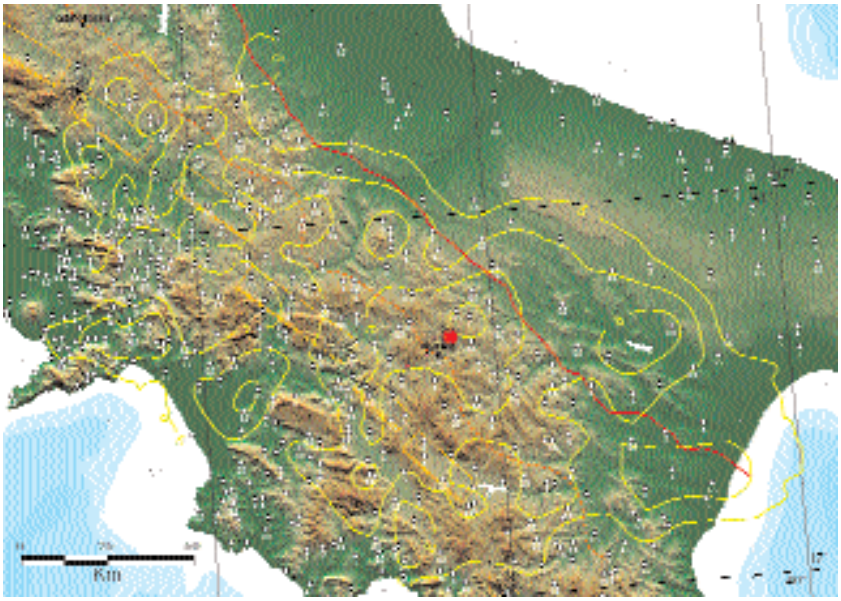

Fig. 5. Damage distribution and interpolated macroseismic field for the catastrophic 5 December 1456, M_w 6.6 and 7.0 earthquakes (reported as two independent shocks in the CPTI catalogue [20]). The earthquake was most likely composed of multiple M ~6.5 subevents. The felt reports include data from the entire seismic sequence. Notice how the damage pattern (the largest ever in Italian historical seismicity) spans from Abruzzi to the Molise/Bojano areas to Sannio/Benevento. Intensity XI can be found in all of these areas, thus suggesting the presence of at least 3 sub-events. However, both geographic and seismotectonic considerations suggest that the distance among their respective epicenters implies totally independent sources of unknown geometry and kinematics.

Concluding remarks

The above scenario represents a drastically alternative view of seismogenic patterns for Irpinia and peninsular Southern Italy. Given the coexistence of distinct earthquake sources at different depths and within different paleogeographic domains, we investigated in detail the deep morphostructural features of the Apulian platform. Based on (a) a major revision of the 1456 macroseismic pattern, (b) the identification of short- and long-wave landscape shifts and (c) further analyses of regional data (gravimetric, magnetic, lineament patterns, etc.), we are now extending the basic concepts of our hypothesis to the entire Southern Apennines. Nevertheless, both the depth and the expected kinematics of the investigated structures preclude a straightforward use of standard geological and geomorphological tools. We thus envisage an innovative and broadly multidisciplinary approach that will tackle the seismogenic capability of the E-W faults and ultimately help fine-tuning the seismic hazard portrait of Campania and surrounding regions.

REFERENCES

1. Pantosti D, Valensise G. Faulting mechanism and complexity of the 23 November, 1980, Campania-Lucania earthquake inferred form surface observations. *J. Geophys. Res.* 95(B10):15319-41, 1990.
2. Amato A, Selvaggi G. Aftershock location and P-velocity structure in the epicentral region of the 1980 Irpinia earthquake. *Annals of Geophysics* 36(1):3-15, 1993.
3. Ascione A, Cinque A, Improta L, Villani F. Late Quaternary faulting within the Southern Apennines seismic belt: new data from Mt. Marzano area (Southern Italy), *Quat. Intern.* 101-102:27-41, 2003.
4. Boschi E, Guidoboni E, Ferrari G, Mariotti D, Valensise G, Gasperini P. Catalogue of Strong Italian Earthquakes, 461 b.C. to 1997. *Annals of Geophysics* 43(4):609-868, 2000.
5. Scalera G, Favali P, Smriglio G, Frugoni F, Vinci L. Seismic hazard in Irpinia and considerations about the seismogenic area. *Annals of Geophysics* 36(1):337-43, 1993.
6. Milano G, Di Giovambattista R, Alessio G. Earthquake swarms in the Southern Apennines chain (Italy): the 1997 seismic sequence in the Sannio-Matese Mountains, *Tectonophysics* 306:57-78, 1999.
7. Valensise G, Pantosti D (eds.). Database of Potential Sources for Earthquakes Larger than M 5.5 in Italy. *Annali di Geofisica* 44(Suppl. 1), with CD-Rom, 2001.
8. Improta L, Bonagura M, Captano P, Iannaccone G. An integrated geophysical investigation of the upper crust in the epicentral area of the 1980, Ms=6.9, Irpinia earthquake (Southern Italy). *Tectonophysics* 361(1-2):139-69, 2003.
9. Valensise G, Pantosti D. The investigation of potential earthquake sources in peninsular Italy: A review. *Journal of Seismology* 5:287-306, 2001.
10. Azzara R, Basili A, Beranzoli L, Chiarabba C, Di Giovambattista R, Selvaggi G. La sequenza sismica del Maggio '90 nel Potentino. *Atti del IX Convegno Gruppo Nazionale di Geofisica della Terra Solida*, 13-15 novembre 1990, Roma, 209-220, 1992.
11. Ekström G. Teleseismic analysis of the 1990 and 1991 earthquakes near Potenza. *Annals of Geophysics* 37(6):1591-9,1994.
12. Galli P, Molin D, Galadini F, Giaccio B. Aspetti sismotettonici del terremoto Irpino del 1930. In *Il "terremoto del Vulture": 23 Luglio 1930, VIII anno dell'Era Fascista.* Servizio Sismico Nazionale, 349 pp, 2002.
13. Pantosti D, Schwartz DP, Valensise G. Paleoseismology along the 1980 Irpinia earthquake fault and implications for earthquake recurrence in the southern Apennines. *J. Geophys. Res.* 98:6561-77, 1993.
14. Di Bucci D, Mazzoli S. The October-November 2002 Molise seismic sequence (southern Italy): an expression of Adria intraplate deformation. *J. Geol. Soc. London* 160(4):503-6, 2003.
15. Valensise G, Pantosti D, Basili R. Seismology and Tectonic Setting of the Molise Earthquake Sequence of October 31-November 1, 2002. *Earthquake Spectra* 19(S1), 2003.
16. Tertulliani A, Anzidei M, Maramai A, Murru M, Riguzzi F. Macroseismic Study of the Potenza (Southern Italy) Earthquake of 5 May 1990. *Natural Hazards* 6:25-38, 1992.
17. Gambini R, Tozzi M. Tertiary geodynamic evolution of the Southern Adria microplate. *Terra Nova* 8:593-602, 1996.
18. Morelli D. Evoluzione tettonico-stratigrafica del Margine Adriatico compreso tra il Promontorio garganico e Brindisi. *Mem. Soc. Geol. It.* 57:343-53, 2002.
19. Milano G, Ventura G, Di Giovambattista R. Seismic evidence of longitudinal extension in the Southern Apennines chain (Italy): The 1997-1998 Sannio-Matese seismic sequence. *Geoph. Res. Lett.* 29(20), 2004, doi:10.1029/2002GL015188, 2002.

20 Gruppo di Lavoro CPTI. *Catalogo Parametrico dei Terremoti Italiani*. ING – GNDT – SGA – SSN, Bologna, 1999.
21. Magri G, Molin D. *Il terremoto del dicembre 1456 nell'Appennino centro-meridionale*. ENEA, RT/AMB 83/08, 180 pp, 1983.
22. Meletti C, Patacca E, Scandone P, Figliuolo B. Il Terremoto del 1456 e la sua interpretazione nel quadro sismotettonico dell'Appennino Meridionale. In Figliuolo B (ed.). *Il Terremoto del 1456*. Osservatorio Vesuviano, Storia e Scienze della Terra, Vol. I, 71-108 & Vol. II, 35-163, 1988.
23. SGA Storia Geofisica Ambiente. *A revision of the 1456 earthquake intensity data*. Unpublished report prepared for INGV, 2003.

The Irpinia fault system as a natural laboratory for earthquake fracture related studies

A. Zollo[a], G. Iannaccone[b], A. Emolo[a], M. Lancieri[a], E. Weber[b]

[a]*RISSC*, Dipartimento di Scienze Fisiche, Università degli Studi di Napoli "Federico II", Napoli, Italia*

[b]*RISSC, Osservatorio Vesuviano, Istituto Nazionale di Geofisica e Vulcanologia, Napoli, Italia*

Introduction

People who experienced the ground shaking produced by the November, 23 1980, Irpinia earthquake, consistently report of an intense, long lasting soil vibration. The area of maximum damages had a broad extension (Fig. 1), and the number of victims (about 3000) was anomalously high for a M = 6.9 event as compared to the earthquake losses observed worldwide for similar size events. Although the outdate manufacture of the building estate in the Irpinia region can have contributed to amplify the earthquake effects, the complex, segmented nature of the seismic source has likely been one of the major causes for damage intensity and widespreadness.

The 1980 Irpinia earthquake: a multiple fracture, normal faulting event

The 1980 Irpinia earthquake is one of the best documented event in the Mediterranean tectonic province. Due to a rather happy coincidence, sets of good quality seismic, geodetic and geological data have been made available to the scientific community few months after the event thus permitting the detailed investigation of the earthquake source characteristics. In particular, the analysis and modeling of the near-source strong motion records acquired by the permanent ENEL-ENEA network, provided a valuable contribution to the understanding of the complex rupture process [3, 4]. These studies revealed the segmentation of the primary faulting process, which produced three distinct rupture episodes (Fig. 2). In about 40 sec, the multiple ruptures activated different segments of a complex, sub-parallel fault system, generally oriented along the NW-SE direction of the Apenninic chain. The complexity

* The acronym "RISSC" stands for "RIcerca in Sismologia Sperimentale e Computazionale" and gives the name to the joint research group of DSF-UNINA and OV-INGV.

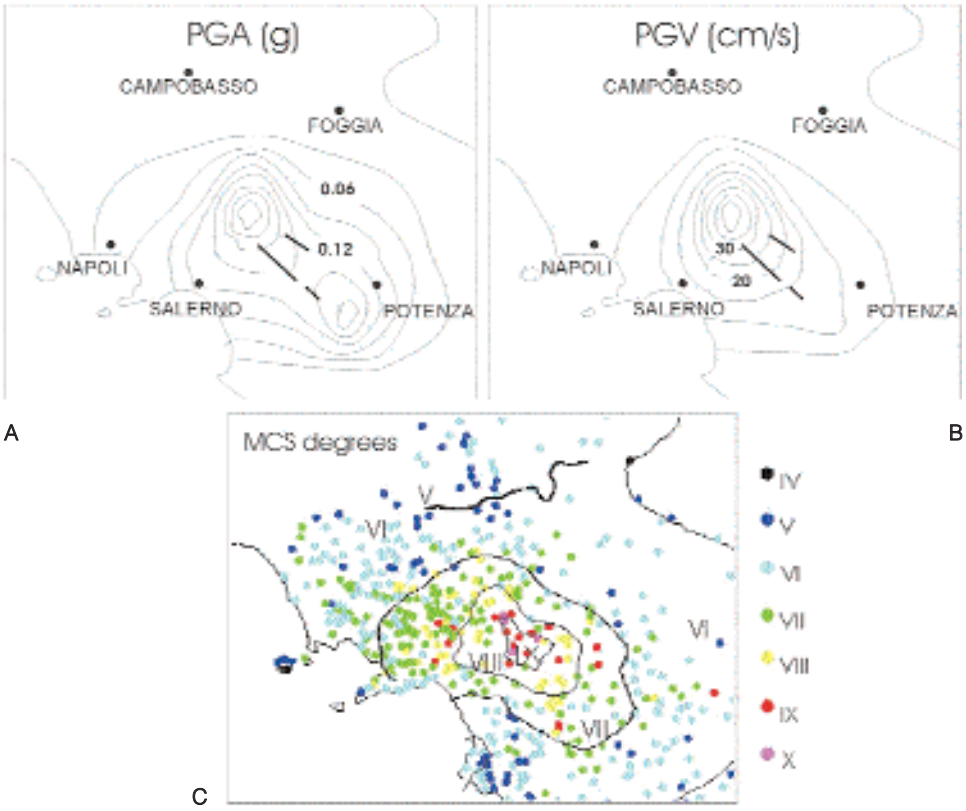

Fig. 1. A. Peak Ground Acceleration (PGA) distribution associated with the November 23, 1980, Irpinia earthquake. B. Peak Ground Velocity (PGV) associated with the November 23, 1980, Irpinia earthquake (modified after [1]). C. Macroseismic intensity according to the MCS scale associated with the November 23, 1980, Irpinia earthquake (modified after [2]).

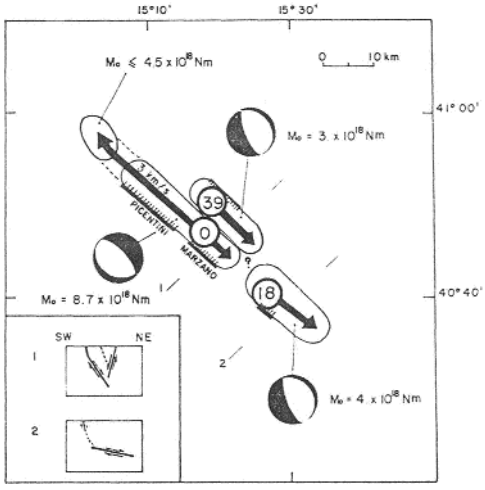

Fig. 2. The three fault segments activated during the November 23, 1980, Irpinia earthquake (after [4]).

of the causative faulting process reflects into the waveform shape of the recorded seismic radiation and into the anomalous ground shaking duration for a M = 6.9 seismic event.

However, seismic events which have ruptured multiple fault segments, during time intervals lasting from several seconds to days or months, are very common in Italy as testified by the recent past experience (e.g., Friuli, 1976; Irpinia, 1980, Abruzzo, 1984; Umbria-Marche, 1997; Molise, 2002) and by the historical earthquake record (e.g., Irpinia, 1456; Eastern Sicily, 1693). This peculiar characteristic of earthquake occurrence can produce unexpected amount of damages on building and infrastructures, due to the cumulative effect of repeated, long-lasting ground motion shaking.

Prior to the 1980 event, the Irpinia region was struck, by several destructive earthquakes (1456, 1688, 1930, etc.). According to paleo-seismological studies [5], the fault responsible for the 1980 earthquake has been active in the last 9000 years, producing four seismic events (paleo-earthquakes) of magnitude similar to the 1980 event, with a recurrence time interval of about 2000 years. The 1980' faulted area is currently interested by an intense background seismic activity at the low to moderate magnitude level, with about fifty events per year with magnitude greater than 2.5 (Fig. 3). Despite of the low accuracy of the epicenter determination (due to the poor spatial coverage of the INGV seismic

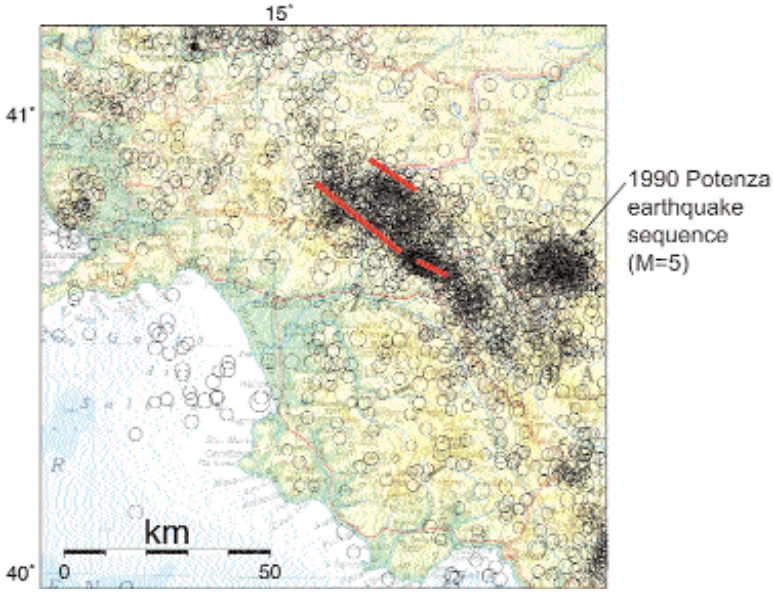

Fig. 3. Background seismicity in Irpinia in the period 1983-2002 from INGV catalogue. Events with magnitude greater than 2.5 are shown. The sequence relative to the 1990 Potenza earthquake (M = 5) is pointed out. The red lines represent the faults associated with the November 23, 1980, Irpinia earthquake.

network), the background seismic activity in the Irpinia region appears to be spatially correlated with the location and geometry of the fault segments activated during the 1980 event. In the recent past, moderate size events have also occurred within or at the closest border of the 1980' faulted area, namely the 1990,1991 Potenza (M 5.8) and the 1996 event (M 4.9) earthquake sequences.

The multi-component seismic network to monitor the background seismicity of the Irpinia fault system

Based on these grounds, the Irpinia fault zone can therefore be considered as a natural laboratory where to investigate the details of small to large scale seismic fractures (few hundred of m to several km) in Italy, occurring in and around an active fault system during an inter-seismic cycle. In particular it can provide betters insights on stress conditions under which seismic fractures initiates and propagates in the shallow crust. This would be of great seismological interest by addressing the issues of 1) how the background seismicity is spatially distributed and at which extent it is controlled by and linked to the primary fault system, 2) what are the mechanisms under which static stress distributes and releases along and around a complex active fault system, and 3) what is the relation between the small scale fracture properties with the geometry, mechanism and fracture characteristics of the primary faults.
The recordings of small to moderate size events located in the fault zone can also be very informative about the crustal and site transfer functions at local and regional distances, to be used for computing reliable deterministic and/or probabilistic strong ground motion scenarios for moderate to large magnitude events occurring along the southern Apenninic chain.
With these aims, the research unit "RISSC" (Ricerca in Sismologia Sperimentale e Computazionale) of the Department of Physics (University of Naples, "Federico II") and Osservatorio Vesuviano (Istituto Nazionale di Geofisica e Vulcanologia) is pursuing a project for installing and operating in the Irpinia region a very dense, wide-dynamic-range, multi-component seismic network (Fig. 4). The project is financially supported by the Center for Regional Competences AMRA (Analysis and Monitoring of Environmental Risks).
The network will be made up of 30 six-component digital seismographs and it will be deployed in area of 100x80 km^2 centred around the 1980' earthquake fault system with a station spacing less than 10 km in the fault area. Each seismograph will be equipped with a tri-axial accelerometer and short-period seismometer, with the exception of five stations, where the short-period geophone is replaced by a broad-band sensor. The seismic equipments and network geometry are designed to detect and record micro-earthquakes with a lower magnitude threshold of about 2, to span a wide recording frequency band (30s-200 Hz) and to get unsaturated waveforms at all the stations for M>4 events.

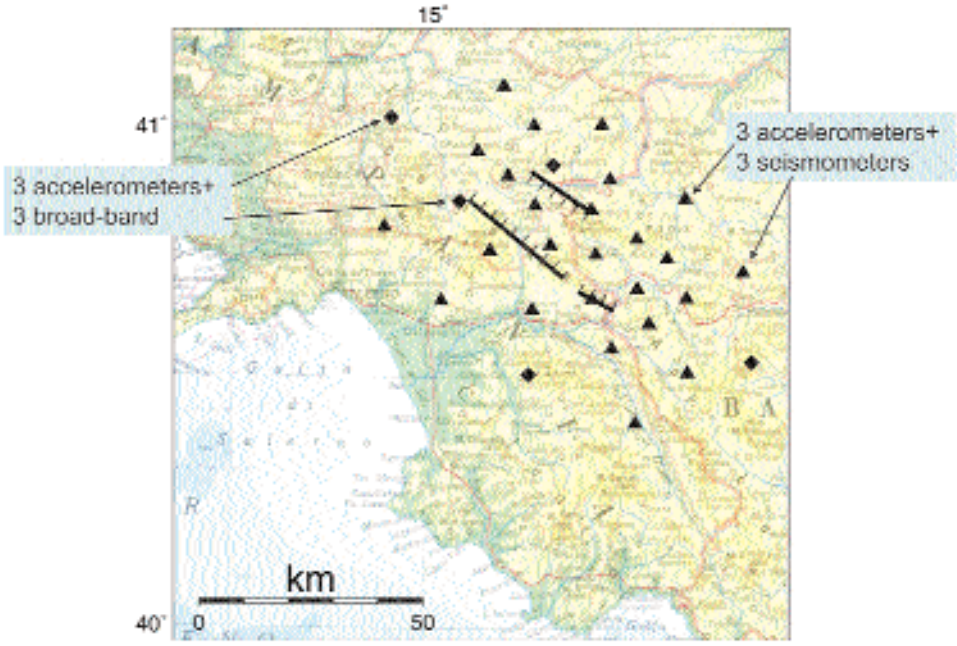

Fig. 4. Plan of seismic network to be installed in Irpinia. Triangles correspond to stations equipped with a 3C accelerometer and a 3C velocimeter. Squares correspond to stations equipped with a 3C accelerometer and a 3C broad-band sensor.

Each seismic station and its relative power supply system (batteries connected to solar panels) will be housed in a 2x2x2 m^3 well-engineered shelters. A continuous monitoring of environmental parameters (temperature, battery level, alarm for breaking and entering) will be ensured by a GSM remote control/maintenance system, with the periodic sending of the parameter string to the operations room.

The architecture of the data transmission system is based on the concept of station clusters (SCLU) communicating to a main server (HUB) through a wireless LAN radio bridge using the TCP/IP communication protocol (with throughput up to 54 Mbps) (Fig. 5).

The number of stations per SCLU depends on the shelter-to-HUB optic visibility and server capacity to manage the flux of information coming simultaneously from different stations. The SCLU will be composed of at least 5 stations, so that 6 HUBs will be needed for the entire coverage of the Irpinia network. HUBs sites have being selected in order to have direct connection to the electric, telephone and broadband digital lines, optimal visibility with the connected stations, easy access by car, safety and protected installation.

Through the ADSL connection to HUBs the network is managed and maintained by the regional main operations room placed in Naples, where the network data server will be installed. A secondary, local operations room will be

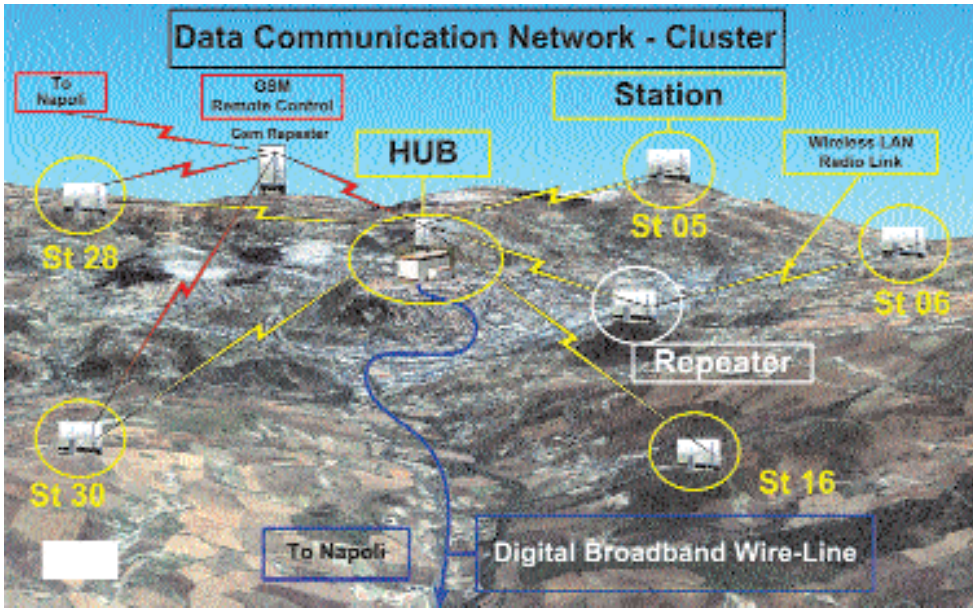

Fig. 5. The communication network between the stations and the data center in Naples is divided in two subnets. A local point-to-multipoint network between central site (HUB) and the seismic acquisition station. A second net which connects the HUBs to the monitoring and elaboration center in Naples through a high speed digital ADSL line or a dedicated point-to-point data line with guarantee of minimal bandwidth. Also shown is the GSM monitoring of environmental parameters system.

set up in the town of S. Angelo dei Lombardi, providing the local support for emergency and routine services and a back-up data server.
At its first stage, the network will operate in post-event delayed time mode. This means that information about seismic events (seismic wave arrival times and waveforms) will be available automatically or "on demand" through a post-event data retrieval procedure. Data are continuously recorded and stored by the data-logger at the station sites with a maximum storage capacity of about 30 days. A subnet of 10 stations is used for automatic local and regional event detection and for building the network catalogue. The download of waveforms is performed automatically overnight or, "on demand", in case of relevant earthquakes, by the data network servers in Naples.

An advanced seismic network to develop and experiment a prototype early-warning system in Campania region

An update of the network equipment and communication systems for operating in real-time mode is possible and it is programmed for the next future. With this perspective, the Irpinia seismic network can represent the laboratory for experimenting innovative technologies for seismic early-warning to be

tested on public infrastructures and buildings of strategic relevance (hospitals, gas pipelines, railways, railroads, etc.).
Considering a seismic warning window ranging from several tens of second before to several hundred of seconds after an earthquake, several strategic infrastructures and buildings are located in the Campania region, mostly at the periphery or within built-up areas. As an example of potential application of an early warning system in the Campania region based on the Irpinia network, the acceleration records generated by the 1980 event are simulated at sites located at an increasing distance from the epicentral area (Fig. 6). Assuming the initial time as the time of first P arrival at the closest station (20 km from the earthquake epicentre), the expected time delay to the first energetic S wave train varies between 7-9 sec at 35 km distance to 22-25 sec at 95 km. The latter distance corresponds to the location of the city of Naples, the largest built-up area of the region.
The effective "early warning" time window has to be further reduced if we consider the time needed for the seismic network to automatic detect the event and compute its location and magnitude.
Trying to minimize the time to be spent for event detection, location and magnitude estimate is a true technological challenge mostly depending on the storage and real-time computational capacities of data-loggers, on the efficiency and robustness of automatic algorithms and on the connectivity architecture of the seismic network.
Even considering such short time delays before the expected arrival of destructive seismic waves, a pre- and post-earthquake warning system can be experimented and realised in Campania region, based on Irpinia seismic network under construction. Infact few seconds may be sufficient to operate the automatic shut-down or disconnection of local plants controlling and protecting sensitive target infrastructures as gas pipelines, viaducts, railway network, operating rooms in hospital, high-risk industrial installations, relevant data-bank servers, etc.
Moreover, reliable predictions of most relevant ground motion parameters (peak values, spectral content, signal duration, etc.) can be obtained within a short post-event window (several hundred seconds) at the whole regional scale, based on direct measurements on the Irpinia network records in the source area integrated by simulations of seismic wave field at larger distances.

Conclusions

The implementation of an advanced multi-component seismic network in the 1980 Irpinia earthquake' source area opens new research perspectives either in basic seismology and seismic risk mitigation fields. The continuous, high resolution monitoring of small to moderate size seismicity will enable to investigate the details of fracture processes occurring during the inter-seismic period of an

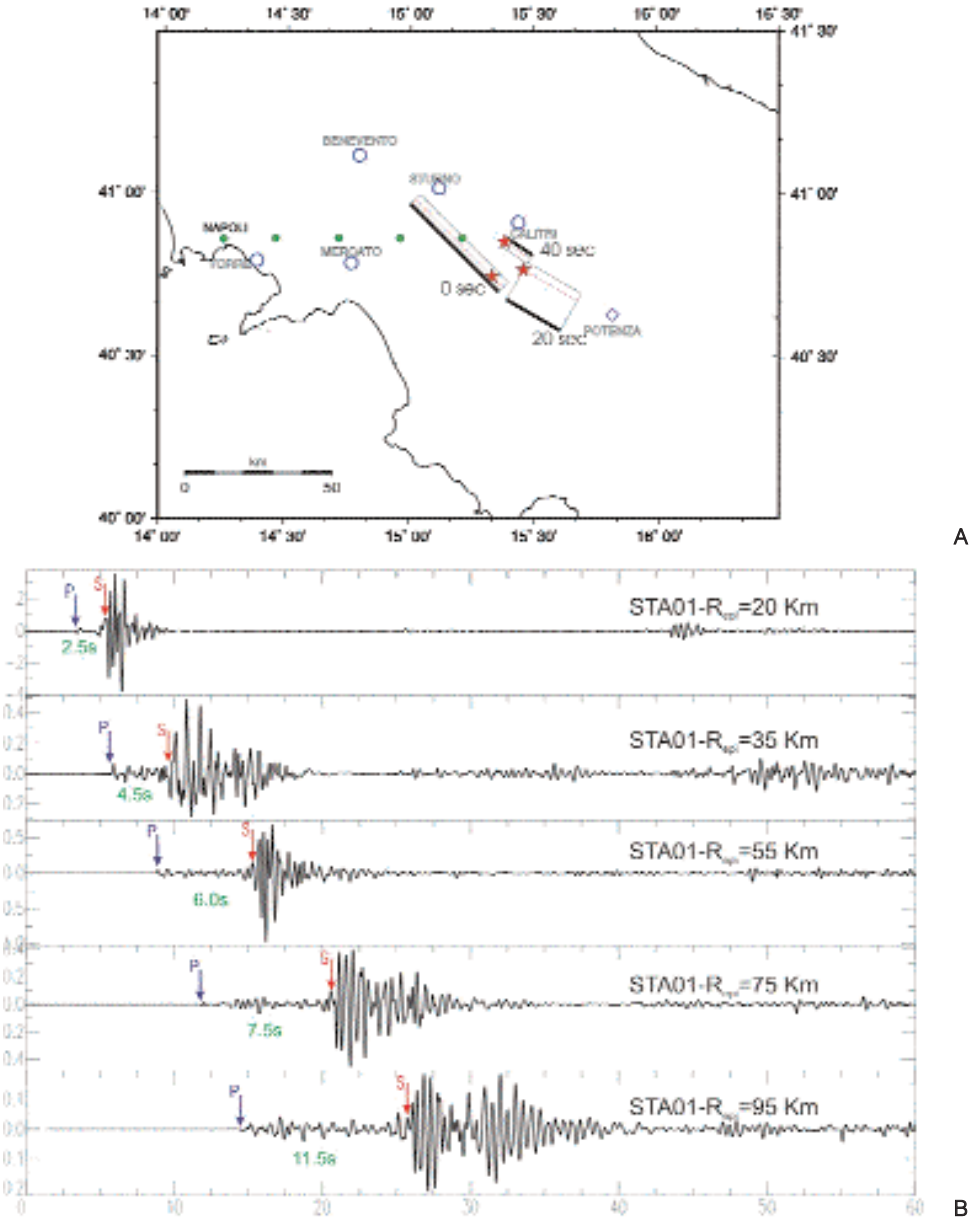

Fig. 6. Simulated accelerograms for the November 23, 1980, Irpinia earthquake using the kinematic fault model of Bernard and Zollo [4, 6]. **A.** The map shows the location and geometry the three segments rupturing at about 0,20 and 40 sec during the Irpinia event. Red stars indicate the epicenters of the nucleation point for the three sub-events. The sites at which synthetic waveform are computed are reported by green circles. **B.** Simulated accelerograms as a function of distance from the Irpinia fault area. Complete wave field synthetics are computed by the discrete wavenumber method [7, 8] assuming a multiple fracture model (3 sub-fault segments) and a 1D layered propagation medium. The predicted S-P times at each station are reported below seismograms.

active fault system of the southern Apenninic chain. The expected resolution of seismic observations in the space-magnitude-frequency domain will probably make the Irpinia fault system as a preferential site where to develop a multi-disciplinary observatory on physical, thermal and chemical conditions for earthquake generation processes, retracing the successful experiences carried out recently in Japan and USA along the Mozumi [9] and San Andreas faults [10].
The seismic network architecture and components (sensors, data loggers, transmission and remote control system) are conceived to be easily upgraded for real-time applications in the next future. Considering a warning window spanning from few seconds before to several hundred of sec after the arrival of potentially damaging seismic waves, a number of applications based on real-time processing of the Irpinia network records can be envisaged to protect strategic infrastructures during an earthquake emergency. The development and experimentation of a prototype earthquake warning system based on the multi-component Irpinia seismic network is one of the main objectives of an ongoing project in the frame of an agreement between the Center of Competences AMRA (Analysis and Monitoring of Environmental Risks) and Department of Civil Protection of the Regione Campania.

References

1. Cabanas L, Benito B, Chavez J, Goula X, Roca T, Sabetta F, Rinaldis D. Observaciones de Dano Correspondientes al Terremoto de Irpinia (Italia) de 1980. Parte I: Distribucion de Danos y Estudio de Parametros de Dano Potencial. *Proc. IX National Assembly on Geodesy and Geophysics*, February 1998.
2. De Rubeis V, Tosi P, Zenari A, Gasparini C. The anisotropic spatial character of macroseismic fileds in Italy. Poster at the *XXV Gen. Ass. ESC*, Reykjavik, 1996.
3. Westaway R, Jackson JA. Surface faulting in the southern Italian Campania-Basilicata earthquake of 23 November 1980. *Nature* 312:436-8, 1984.
4. Bernard P, Zollo A. The Irpinia (Italy) 1980 earthquake: detailed analysis of a complex normal fault. *J. Geophys. Res.* 94:1631-48, 1989.
5. Pantosti D, Valensise G. Faulting mechanism and complexity of the 23 November 1980, Campania-Lucania earthquake, inferred from surface observations. *J. Geophys. Res.* 95:15319-41, 1990.
6. Lancieri M, Zollo A. Deterministic scenario study for the 1980 Irpinia earthquake. *Geophysical Research Abstracts* 6, 04689, 2004, SRef-ID:1607-7962/gra/EGU04-A-04689.
7. Bouchon, M. A simple method to calculate Green's functions for elastic layered media. *Bull. Seism. Soc. Am.* 71:959-71, 1981.
8. Coutant O. Programme de simulation numerique AXITRA. *Res. Report LGIT*, Grenoble, 1989.
9. Takeuchi A, Ongirad H, Akimitsu T. Recurrence interval of big earthquakes along the Atotsugawa fault system, central Japan: Results of seismo-geological survey. *Geophys. Res. Lett.* 30(6):8011, doi:10.1029/2002GL014957, 2003.
10. Hickman S, Zoback M, Ellsworth W. Introduction to Special Issues: Preparing for the San Andreas Fault Observatory at Depth. *Geophys. Res. Lett.* 31:L12S01, doi:10.1029/2004GL0120688, in press.

Constraints on the source mechanism of the 1930 Irpinia (Southern Italy) earthquake from simulation of the kinematic rupture process

A. Emolo[a], A. Gorini[b], G. Iannaccone[c], A. Zollo[a]

[a]*Dipartimento di Scienze Fisiche, Università degli Studi di Napoli "Federico II", Napoli, Italia*

[b]*Servizio Sismico Nazionale, Dipartimento di Protezione Civile, Roma, Italia*

[c]*Osservatorio Vesuviano, Istituto Nazionale di Geofisica e Vulcanologia, Napoli, Italia*

Introduction

The 1930 Irpinia earthquake, with an epicentral intensity of X MCS, is one of the largest Italian event of the XX century. It struck the north-eastern part of the Irpinia region causing the loss of about 1500 lives.
The isoseismal curves (Fig. 1) trend NW-SE, such as most of largest historical earthquakes occurred in the Southern Apennines and show a weak concavity toward the SW.
Large uncertainties affect the source model proposed so far due to the poor quality of the available seismological records. In this study we propose a new source model for the 1930 Irpinia earthquake based on the comparison between simulated ground acceleration field and macroseismic intensity data.

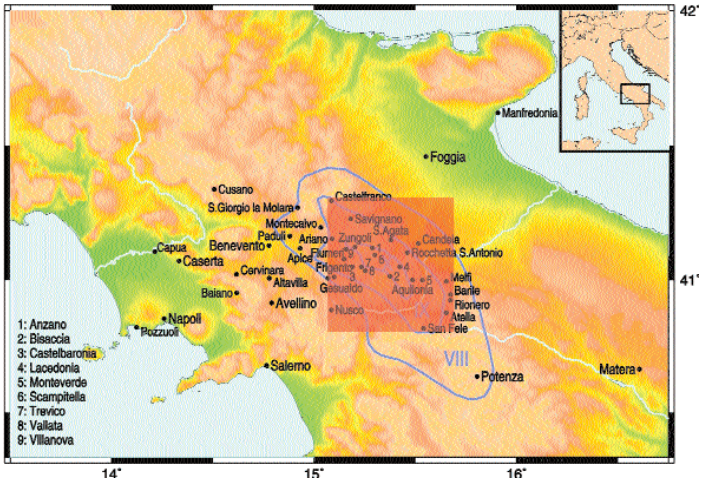

Fig. 1. Isoseismal curves for the 1930 Irpinia earthquake (After NT4.1 catalogue; [1]).

Previous studies

Earthquake location (Fig. 2, Tab. 1) was obtained by different authors using the first P wave arrival times at receivers located at distances between some tens and several thousands of kilometers. Most of proposed epicentral locations are near the eastern limit of the X MCS area. Fig. 2 also shows the fault segments responsible for the 1980 Campania-Lucania earthquake. Probably, the 1930 Irpinia earthquake fault is sub-parallel to the fault system activated in 1980 but shifted towards the north-eastern border of the Apenninic seismic belt. This confirms the complex geometry of fault systems responsible for the large earthquakes in Southern Apennines.

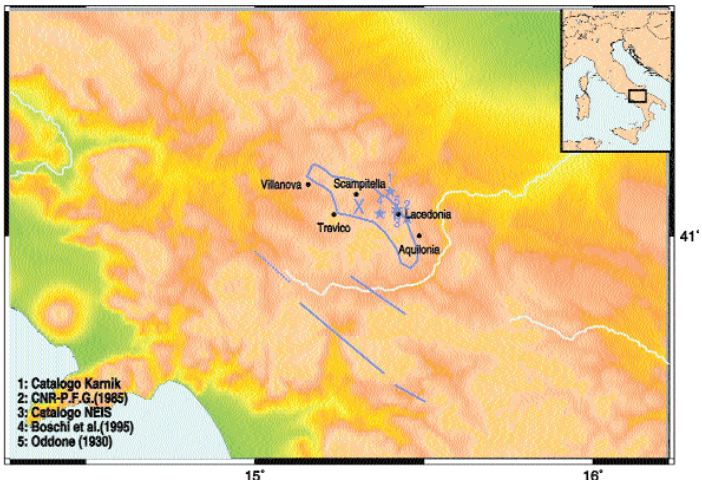

Fig. 2. 1930 Irpinia earthquake locations obtained by different authors.

Tab. 1. 1930 Irpinia earthquake locations.

Epicenter		Reference
Latitude north	Longitude east	
41°06’	15°24’	[2]
41.04°	15.45°	[3]
41.05°	15.42°	[4]
41.05°	15.37°	[5]
41°03’31”	15°25’15”	[6]

Tab. 2 reports the values of the earthquake magnitude and seismic moment obtained by different authors. In our simulation study we considered preliminarily the seismic moment determined by Jiménez [9] through the analysis of surface waves from the signals recorded at Jena station in Germany, since it was derived by a direct measurement on data.

Tab. 2. Magnitude and seismic moment for the 1930 Irpinia earthquake determined by different authors. In red the quantity really estimated. In blue the quantity computed by the Hanks and Kanamori relationship [7].

Magnitude	Seismic moment in Nm	Reference	Used data
6.5	7×10^{18}	[8]	After [2]
6.1	2×10^{18}	[9]	Surface waves (spectral analysis)
7.0	3.2×10^{18}	[10]	Maximum intensity value
6.3±0.2 (M_S)	3.5×10^{18}	[11]	Radii of greatest isoseismal areas
6.6±0.3 (M_S)	1×10^{19}	[12]	Amplitudes of surface waves from bulletins
6.7 (M_e)	1.1×10^{19}	[13]	Epicentral intensity and isoseismal areas

Fig. 3 reports some focal mechanisms for the 1930 seismic event available from literature. The solution by Martini and Scarpa [8] shows a normal fault mechanism with a moderate strike component, with nodal planes oriented in the WSW-ENE direction. On the contrary, Jiménez [9] determined a strike-slip mechanism. In this study we also determined the focal mechanism using the classical FPFIT computer program [14] and a probabilistic searching algorithm proposed by Zollo and Bernard [15]. The results are reported in Fig. 3. The found solutions are similar to the Martini and Scarpa [8] one and are consistent with the azimuthal value of 108° for the fault plane proposed by Gasperini et al. [13] after interpretation of macroseismic data.

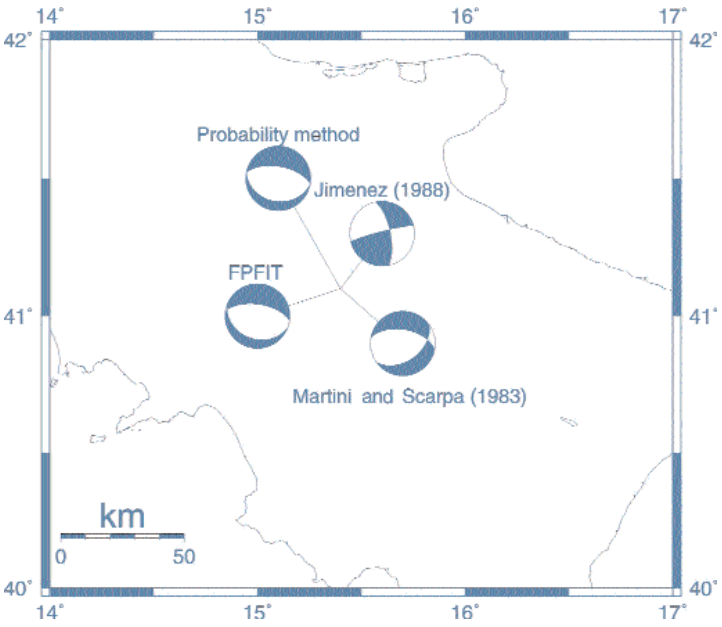

Fig. 3. Proposed fault plane solutions for the 1930 Irpinia earthquake.

A NEW SOURCE MODEL

In this study we use the simulation method proposed by Zollo et al. [16] to compute the PGA associated with the different source models proposed for the 1930 Irpinia earthquake. The simulated PGA maps are then qualitatively compared to the macroseismic map in order to validate the source model. The fault dimensions are determined starting from the magnitude of the earthquake by the Wells and Coppersmith [17] relationships. The source characteristics used in our simulation study are summarized in Tab. 3.

Tab. 3. Source parameters used in this simulation study.

	Length in km	Width in km	Max depth in km	Strike	Dip	Rake	Reference
Model A	14.5	9	13	290°	60°	-90°	This study
Model B	14.5	9	13	100°	30°	-90°	This study
Model C	32	14	15	108°	45°	-90°	[13]
Model D	14.5	9	13	280°	55°	-60°	[8]

For each source model we considered 100 different possible rupture processes described by different rupture nucleation point and final slip distribution (computed according to the k-square model; [18]). The idea behind this approach is that, in repeated rupture episodes along the same fault, some characteristics as fault geometry, source mechanism, and average slip, can be reasonably considered constant at a large time scale. However, the fracture process may not repeat the same style of nucleation, propagation and arrest in successive rupture events. For each rupture process we simulated the ground acceleration at a grid of 121 receivers located on an area of 60x60 km^2 corresponding to the shaded area of Fig. 1. The average PGA was computed at each receiver on the 100 rupture processes considered for each source model. The corresponding maps of mean PGA are shown in Fig. 4. The colour scale of Fig. 4 was created so the acceleration ranges for the yellow and red colours corresponds to macroseismic intensities in the range IX-X according to the relationship proposed by Trifunac and Brady [19].

The concave shape of the isoseismal areas is generally associated with a fault plane dipping in the direction of maximum concavity. The SW concavity observed for the isoseismal curves is retrieved in the PGA maps associated with the models B and C. Moreover, the NW-SE trend of isoseismal curves suggests a similar direction for the strike of the fault. On the other hand, the SW-NE extension of isoseismal curves seems to be well reproduced by the models A and D. Comparing the results from these models with the model B, this extension is associated with the dip of the fault. As a consequence we

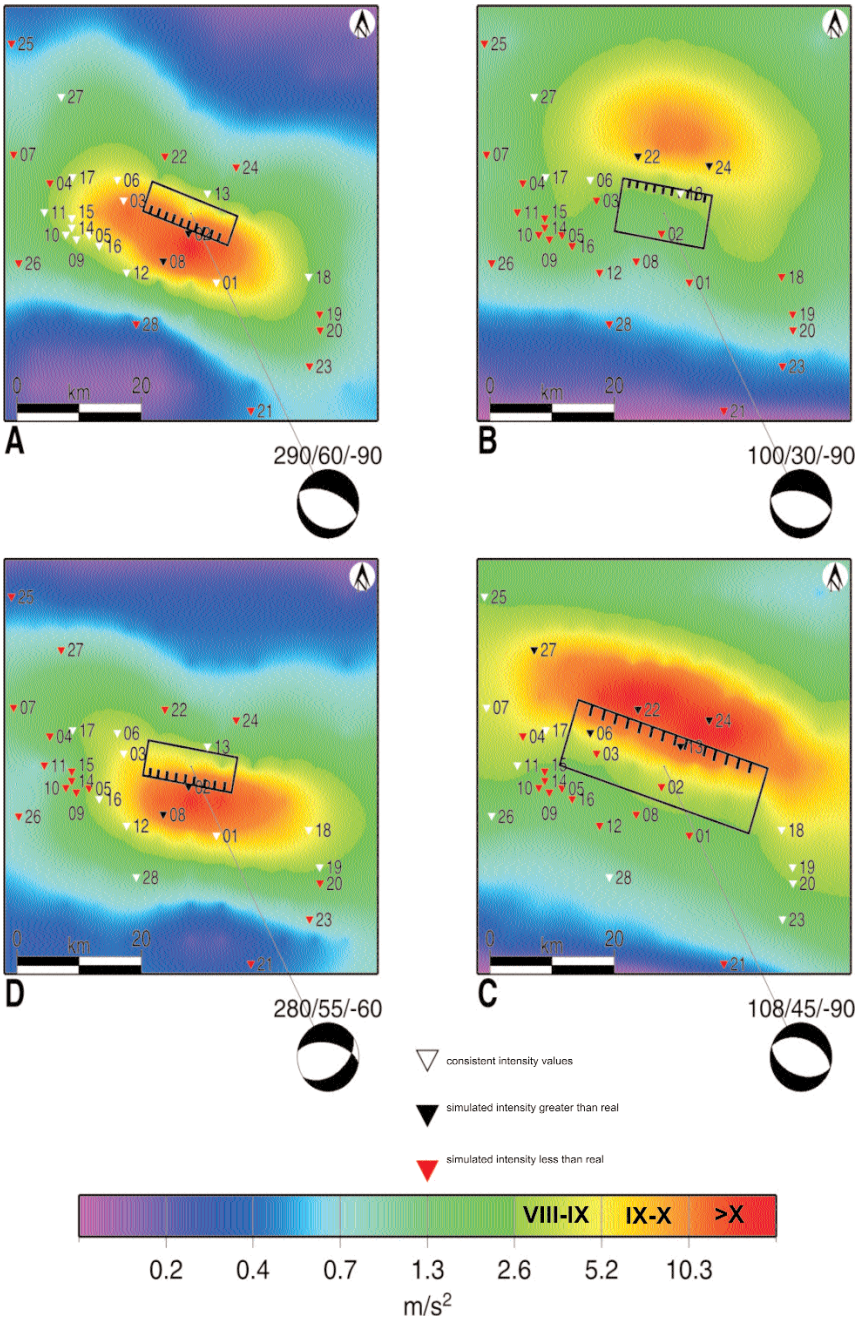

Fig. 4. PGA maps for the source models of Tab. 3. 01: Aquilonia; 02: Lacedonia; 03: Scampitella; 04: Villanova; 05: Trevico; 06: Anzano; 07: Ariano Irpino; 08: Bisaccia; 09: Carife; 10: Castel Baronia; 11: Flumeri; 12: Monteverde; 13: Rocchetta S. Antonio; 14: S. Nicola Baronia; 15: S. Sossio Baronia; 16: Vallata; 17: Zungoli; 18: Melfi; 19: Barile; 20: Rionero; 21: S. Fele; 22: S. Agata; 23: Atella; 24: Candela; 25: Castelfranco; 26: Frigento; 27: Savignano; 28: Andretta.

exclude the case of a sub-horizontal fault (model B) preferring a plane dipping between 40° and 70°. The NW-SE extension of the area of maximum PGA for the models A, B and D seems to under-estimate the analogous extension of the isoseismal curves while, it seems to be over-estimated by the model C. Based on these observations, we propose a source model for the 1930 Irpinia earthquake (Tab. 4). We computed the ground acceleration mean field for this model following the technique by Zollo et al. [16] (Fig. 5). After converting the PGA mean values in macroseismic intensities by the Trifunac and Brady relationship [19], we searched, by a trial-and-error approach, for the fault location able to minimizing the differences between estimated and observed macroseismic intensity data. On these basis, the centre of our proposed fault is moved to about 10 km in the SW direction (Fig. 5) compared to the epicentral area reported in Fig. 2. It results located in the central part of the Southern Apennines chain dipping in the west direction similarly to the eastern segment associated with the 1980 Irpinia earthquake.

Tab. 4. Source model for the 1930 Irpinia earthquake proposed in this study.

Length in km	25
Width in km	12
Max depth in km	15
Strike	110
Dip	55
Rake	-90
Seismic moment in Nm	5.6×10^{18}

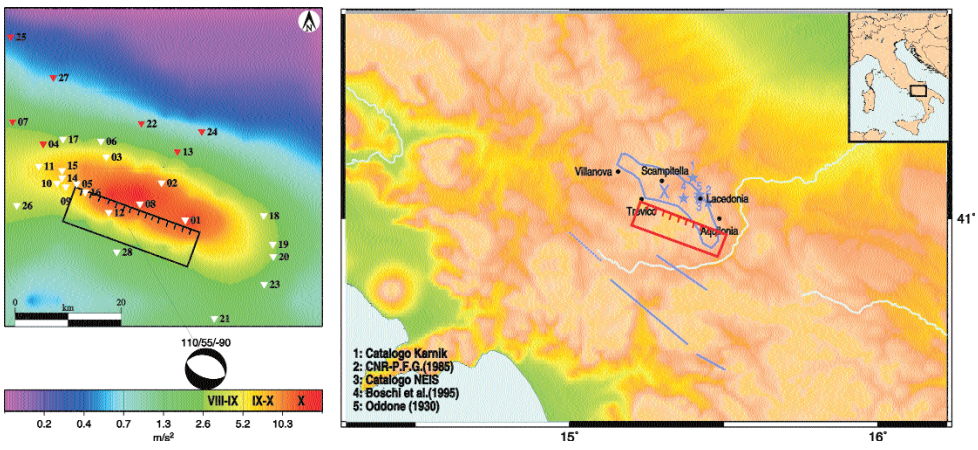

Fig. 5. Final sketch of the source for the 1930 Irpinia earthquake proposed in this work.

REFERENCES

1. Camassi R, Stucchi M. NT4.1, un catalogo parametrico di terremoti di area italiana al di sopra della soglia del danno. *http://emidius.itim.mi.cnr.it/NT/home.html*, 1998.
2. Karnik V. *Seismicity of the european area*. Kluwer, Dordrecht, 1969.
3. CNR-PFG. Atlas of isoseismal maps of italian earthquakes. *Quad. Ric. Scient.* 114, 1985.
4. NEIS Catalogue. National Earthquake Information Service of USGS. *http://neic.usgs.gov/neis*.
5. Boschi E, Ferrari G, Gasperini P, Guidoboni E, Smriglio G, Valensise G. *Catalogo dei forti terremoti in Italia dal 461 a.C. al 1980*. ING-SGA, Bologna, 1995.
6. Oddone E. Studio sul terremoto avvenuto il 23 luglio 1930 nell'Irpinia. Relazione a S.E. il Ministro dell'Agricoltura e Foreste. In *La meteorologia pratica*, Regio Ufficio centrale di Meteorologia e Geofisica, 1930.
7. Hanks TC, Kanamori H. A moment-magnitude scale. *J. Gephys. Res.* 84:2348-52, 1979.
8. Martini M, Scarpa R. Earthquakes in Italy in the last century. In Kanamori H, Boschi E (eds.) *Earthquakes: observation, theory and interpretation*. Scuola Italiana di Fisica "E. Fermi", 85th course, Bologna, pp. 479-492, 1983.
9. Jiménez E. *Etude des mécanismes au foyer à partir d'une station unique: application aux domaines Euro-Méditerranéen et Sud-Ouest Pacifique*. Ph.D. thesis, Université L. Pasteur, Stasbourg, 1988.
10. Postpischl D. Atlas of isoseismal maps of Italian earthquakes. *Quad. Ric. Scient.* 114(2A), 1985.
11. Westaway R. Seismic moment summation for historical earthquakes in Italy: tectonic implications. *J. Geophys. Res.* 97:415-37, 1992.
12. Margottini C, Ambraseys NA, Petrini V. *La magnitudo dei terremoti italiani del XX secolo*. Rapporto tecnico ENEA, 1993.
13. Gasperini P, Bernardini F, Valensise G, Boschi E. Defining seismogenic sources from historical earthquake felt report. *Bull. Seism. Soc. Am.* 89:94-110, 1999.
14. Oppenheimer DH, Reasenberg PA, Simpson RW. Fault plane solution for the 1984 Morgan Hill, California, earthquake sequence: evidence for the state of stress on the Calaveras fault. *J. Geophys. Res.* 93:9007-26, 1988.
15. Zollo A, Bernard P. Fault mechanism from near source data: joint inversion of S polarizations and P polarities. *Geophys. J. Int.* 104:441-51, 1991.
16. Zollo A, Bobbio A, Emolo A, Herrero A, De Natale G. Modelling of the ground acceleration in the near source range: the case of 1976 Friuli earthquake (M=6.5), Northern Italy. *J. Seism.* 1:305-19, 1997.
17. Wells DL, Coppersmith KJ. New empirical relationships among magnitude, rupture length, rupture width, rupture area, and surface displacement. *Bull. Seism. Soc. Am.* 84:974-1002, 1994.
18. Herrero A, Bernard P. A kinematic self-similar rupture process for earthquakes. *Bull. Seism. Soc. Am.* 84:1216-29, 1994.
19. Trifunac MD, Brady AG. On the correlation of seismic intensity data in California and western Nevada. *Bull. Seism. Soc. Am.* 65:1223-38, 1975.

Analyses of ambient noise recorded in the Colfiorito basin, Central Italy

R. Maresca[a], D. Galluzzo[b], F. Cara[c], G. Di Giulio[c], A. Rovelli[c]

[a]*Dipartimento di Studi Geologici e Ambientali, Università degli Studi del Sannio, Benevento, Italia*

[b]*Osservatorio Vesuviano, Istituto Nazionale di Geofisica e Vulcanologia, Napoli, Italia*

[c]*Istituto Nazionale di Geofisica e Vulcanologia, Roma, Italia*

Introduction

The amplification of earthquake motion by shallow sediments is an important parameter in determining seismic hazard. Furthermore, in presence of a complex subsurface structure, variation of ground motion can be significant over very short distance [1]. Nakamura [2] showed that, in the hypothesis that the noise mainly consists of Rayleigh waves, the single station spectral ratio between the horizontal and vertical components of noise is a reliable estimation of the site transfer function for S waves. Although this method has been largely applied and many authors agree in its effectiveness to estimate the resonance frequency of sediments, results are still debated, particularly in presence of strong perturbations by cultural noise, or if a high impedance contrast at depth is absent [3]. To better address the nature of the ambient noise wavefield, seismic arrays are a useful tool, allowing to determine wave types composing the noise, dispersion functions for surface waves, from which a velocity profile can be derived [4, 5]. In this work we analyse the ambient noise recorded in the Colfiorito Basin during two experiment carried out in May and July 2002. The Colfiorito Basin is a tectonic depression in the Southern part of the Northern Apennine Chain filled by Quaternary alluvial deposits. A joint approach using geophysical and geological data was adopted by Di Giulio et al. [6] to interpolate the interface between sediments and high-velocity basement within the Colfiorito basin. The structure of the basin results to be very irregular, with narrow and deep sags, the deepest one (up to 180 and 150 m) are located at the NW corner of the basin. A relatively flat and shallower (60-70 m) area occupies the centre of the basin. Previous studies performed in the Colfiorito basin have shown the role of the basin structure on the propagation of seismic waves [7]. Noise measurements were carried out in May 2002 along four profiles, investigating 45 different sites (Fig. 1) characterized by different sediment thickness over the basement. A reference-site (N2) was located on the outcropping rock-basement, at the South-Eastern border of the basin, recording continuously for all the time of the experiment. In July 2002

a second experiment was carried out in the Colfiorito Basin, installing 4 arrays in the sites shown by squares in the Fig. 1. This work is aimed at analysing the predominant frequency variations in the ambient noise recorded in the Colfiorito Basin, which could be correlated to the basin structure, through application of the Nakamura's method. The correlation method [8] applied to data collected by the B array allows to study the dispersive properties of the noise wavefield, from which a 1-D velocity model is derived.

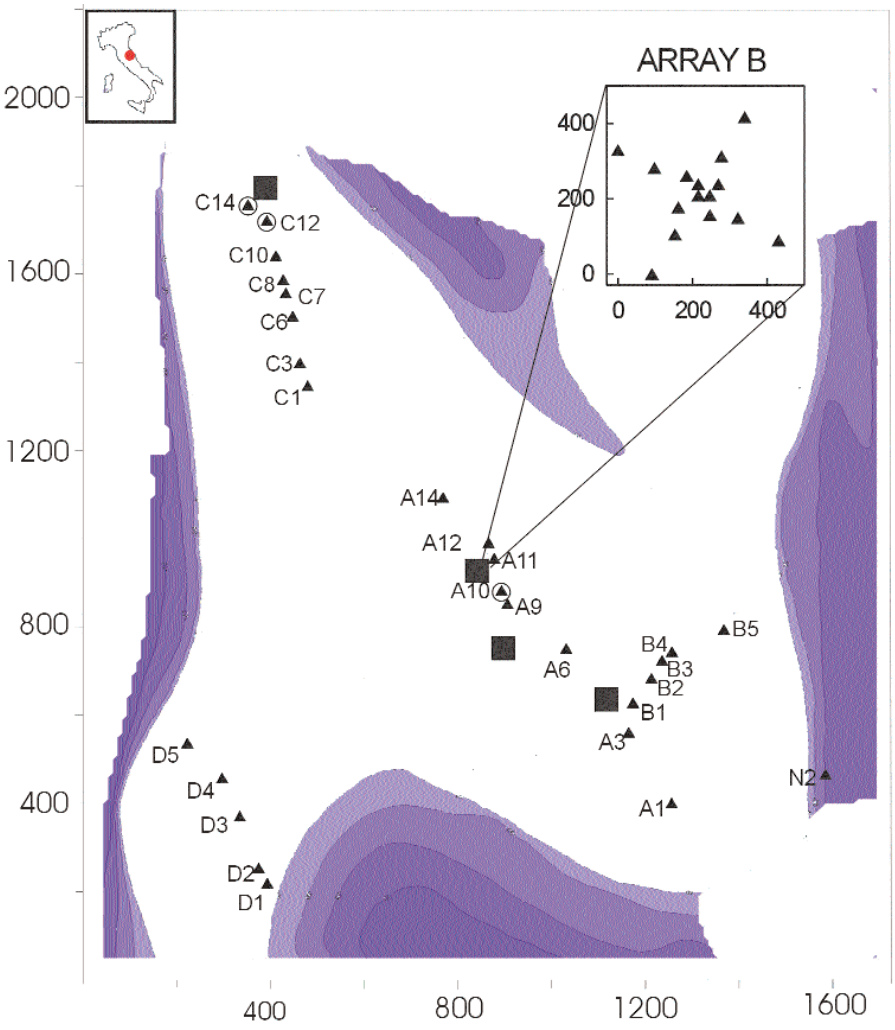

Fig. 1. Map of the Colfiorito Plain with recording sites (triangles) and array locations (squares). Axis-units are in metres. The open circles show the sites where an array-sensor was operating during the July experiment, within 20 metres. In the box the geometry of the B array is shown. The recording instruments consist of Lennarz MARSlite stations, equipped with LE-3D/5s sensors. The sample rate is 125 samples/s.

Instrumentation and spectral analysis

The recording instruments consist of Lennarz MARSlite stations, equipped with LE-3D/5s sensors. The sample rate is 125 samples/s. The instrument response is the same for all stations and flat in the frequency range of interest; for this reason we excluded to apply instrument correction to data. We start our analysis looking at the noise spectra computed at a reference-site located on rock (N2, Fig. 1).
This site operated continuously for all the time of the experiment, in this way we could check the time stability of the noise over long time intervals. It is possible to observe a good agreement among spectra related to different hours, so proving the time stationarity of the recorded noise, in the time interval of recording. A high spectral amplitude at low frequencies, more pronounced on the horizontal components, persists in the H/V spectra (Fig. 2).

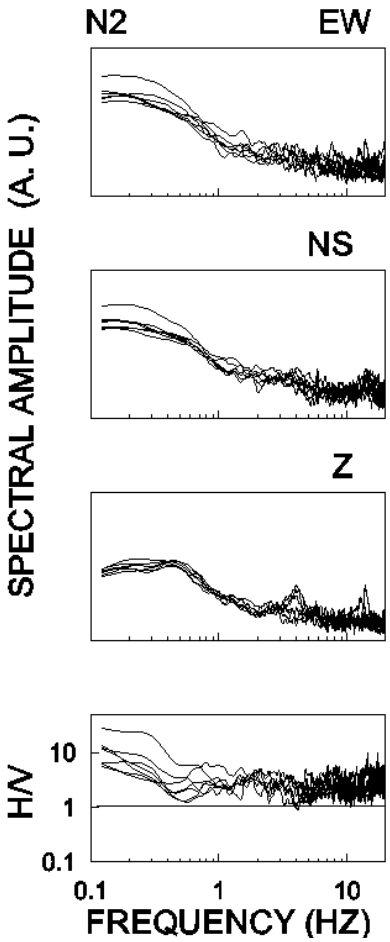

Fig. 2. Spectra for each component computed at the reference site N2 and H/V spectral ratios. Spectra were computed over seven selected 32-s-long windows collected at intervals of 1 h, since 9 a.m. to 16 p.m. Average-removing and 5% cosine tapering is applied to each window; then a smoothed spectrum, Konno-Ohmaki [9] logarithmic window, is computed. H/V spectral ratios are computed for each window, merging horizontal components through a quadratic mean; finally the geometrical mean over all the windows is estimated (SESAME code).

Then we computed the average H/V spectral ratios at all the sediment sites (Fig. 3). A high amplification level is observed at low frequencies (< 1.0 Hz), in some case appearing as a plateau extending up to 1-2 Hz (A3, B1, C7, D5). For three sites it was possible to compare the H/V spectral ratios to those related to the July experiment (dashed lines). The comparison at the A10 site shows a clear difference at low frequencies: the high spectral level observed during the May experiment is absent in the spectral ratio computed on the

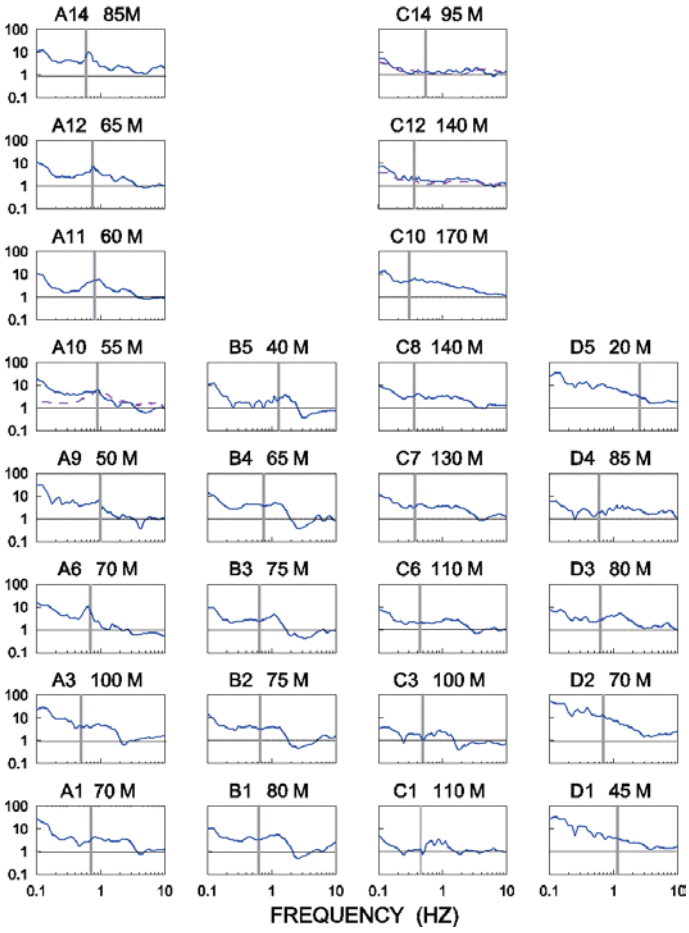

Fig. 3. Average H/V spectral ratios for the most representative sites in the plain. At the top of each panel the site code and the sediment thickness are shown. Dashed lines at a10, c12 and c14 sites show the average H/V spectral ratios computed on recordings performed in July, at one array-sensor located within 20 metres from the site. Spectral averages are computed over twenty-two 40-seconds-long time windows, selected in the signal through an antitrigger algorithm (0.01 < sta/lta < 2.0). The grey lines mark the fundamental resonance frequencies computed on the basis of the sediment thickness estimated by Di Giulio et al. [6] and taking a surface velocity of 200 m/s. Standard deviations are about 30% of values.

near site operating in July. In a previous study on the ambient noise recorded by broad-band stations in the middle of the plain [10] the authors observe a very high increase of the spectral amplitude at low frequencies, on the horizontal components, under disturbed weather conditions. Taking into account these observations, the high amplitude level observed in the spectra of noise recorded during the May experiment, could be attributed in some cases, as for the A10 site, to weather conditions, which were disturbed and rainy in May and calm in July. The comparison of the H/V spectral shapes with the computed fundamental resonance frequencies show that the sites located in the middle of the basin (A6, A9, A10, A11, A12, A14, B5) present a well-pronounced peak generally coincident with the computed resonance frequencies. The sites on the profiles C1-C14 and D1-D5 are situated in narrow sags of the basin; the profile C1-C14 is in the deepest part of the basin, along which the depth to the basement varies from 70 to 180 m. The H/V ratios computed along these profiles do not show significant peaks. A1-A5 and D1-D5 sites are located in correspondence of another 100-m-deep sag of the basin and also do not show evident spectral peaks.

Array analysis

In order to analyse the dispersive properties of the noise wave field, we applied the correlation technique designed by Aki [8] to the vertical ground velocity recorded by the B array (Fig. 1). The array configuration is shown in the box of Fig. 1, the black triangles show the station used in this analysis. This method is based on a statistical investigation of the stationarity in time and space of the noise signal. Based on these assumptions, it can be shown that the azimuthal average of correlation coefficients $\rho(r,\omega)$ calculated for pair of vertically-polarized signals, would have predictable patterns as a function of angular frequency ω and station spacing r as:

$$\rho(r,\omega) \quad J_o(r\omega/c(\omega)) \tag{1}$$

in which J_o represents a Bessel function of order zero, and $c(\omega)$ is the phase velocity dispersive function. Computing the azimuthal average of the correlation coefficients at different frequencies and at a fixed distance, it is possible to get an experimental correlogram $\rho(r,\omega)$, from which the dispersive function $c(\omega)$ can be calculated. We first calculated the spacing among all the possible station pairs and then selected those belonging to the most represented classes of spacing, for which the range of azimuths was sufficiently wide. Eight 4-minute-long time windows have been selected in the signal, filtered in a narrow frequency band, in the range 0.5-6 Hz with a 0.5 Hz step; for the middle value of each frequency band the spatial correlation coefficients and their azimuthal averages were computed for the selected classes of distance (Fig. 4).

Then we derived phase velocities by reading of zero-crossings, maxima and minima of the correlation functions. The lower bound of the frequency band for which phase velocities have been computed is controlled by station spacing. In order to extend this limit to lower frequencies, we calculated the correlation coefficients among all the possible station pairs. Then assuming that the dispersion relationship in equation (1) may be expressed through a simple analytical expression of the form:

$$c(f) = A \cdot f^{\,b} \tag{2}$$

where f is the frequency in Hz and A and b are constants, it was possible to derive the best values for A and b (sought over a grid of values varying from 0 to 2, with a grid spacing of 0.02) which minimized the sum of square residuals [differences between experimental correlation coefficients and theoretical values expressed by the relation (1), in which the dispersive function assumes the analytical form given by the relation (2)]. The computed dispersion function is shown in Fig. 5A together with the velocity values derived from the correlograms of Fig. 4. The obtained dispersion curve is then inverted for the corresponding 1-D velocity structure, assuming that this dispersion represents the fundamental mode of Rayleigh waves. The velocity model producing the theoretical dispersion curve which best fits the experimental one is depicted in Fig. 5B. To test if the estimated velocity model can reproduce the characteristics of the sediments transfer function, we use a simple 1D approach to estimate the amplification function of sediment layers, when excited by SH waves

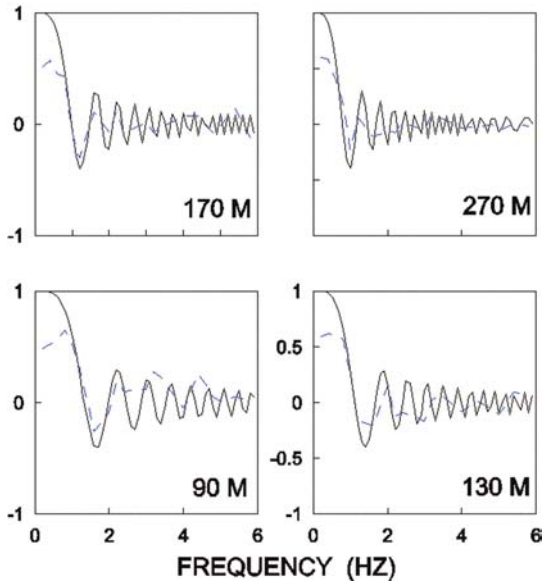

Fig. 4. Correlation curves as a function of frequency for groups of array stations separated by the same range of distance. The solid line represents the 0^{th} order Bessel function derived from substitution of the dispersion relationship expressed through equation (2) to the phase-velocity term at the right-hand site of equation (1).

vertically incident [11]. Different authors [9, 12] pointed out that the frequency of occurrence of the highest amplification peak in the H/V ratios is correlated with the S-wave amplification function, at least for simple structures. The array-average H/V spectral ratio is compared to the computed amplification curve in Fig. 6: the experimental H/V spectral ratio is peaked at frequency around 0.9 Hz, in agreement with the transfer function computed on the basis of the 1D velocity model inferred from the dispersion function.

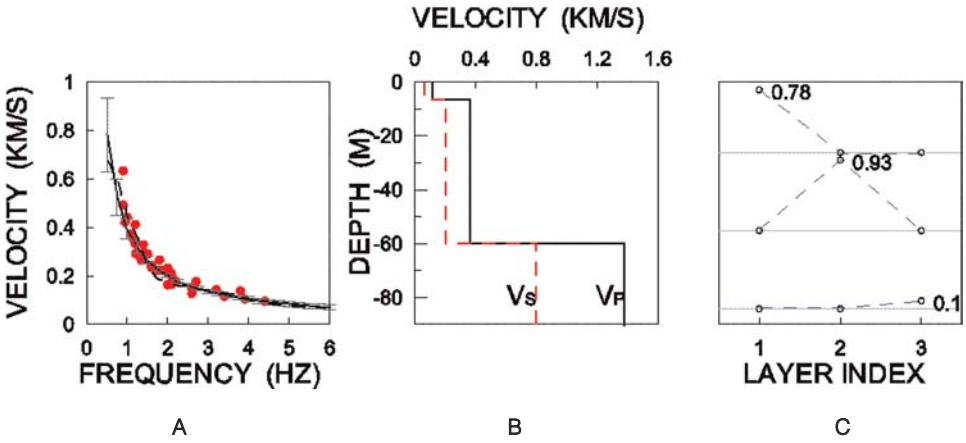

Fig. 5. A. Dispersion function for Rayleigh waves derived from the B array data. The thick line represents the analytical function (2) for which the differences between the experimental and computed correlation functions are minimized. Error estimates (+/- 1σ) are shown. The solid circles represent the phase-velocity values inferred from the experimental correlation curves. The dashed curve corresponds to the Rayleigh wave dispersion curve which best fits the experimental one. B. P and S velocity model derived from inversion of the dispersion data depicted in A. C. Resolution matrix for the velocity model shown in B.

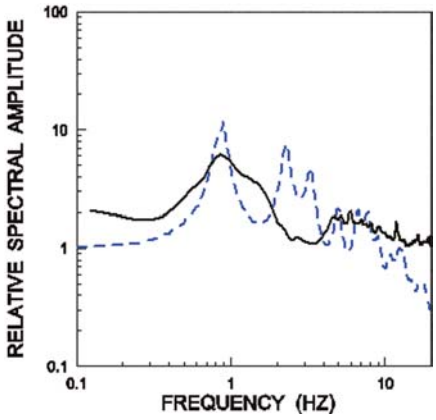

Fig. 6. Array-average H/V spectral ratio (continuous line) compared to the S-wave amplification spectrum (dashed line) computed on the basis of the S-wave velocity model depicted in Fig. 5B.

Conclusions

In this paper we analysed the ambient noise recorded in the Colfiorito plain during two experiment in 2002. During the first experiment noise measurement were carried out in the basin along four profiles, in order to evaluate the influence of the basin structure on the predominant frequencies of the recorded noise. During the second experiment four dense arrays were deployed in the area, in order to get insights into the noise wavefield composition. Here we present the first results obtained applying the noise correlation method to the data collected by the B array, in terms of Rayleigh waves dispersive curve, and relevant 1-D velocity structure. The main results are:

1. A high amplification level is generally evident in the horizontal components of noise spectra at low frequencies, clearly evident in the H/V spectral ratios. This feature is common to most of the sites, included the reference one, and is observed in the noise spectrum even by other authors [3]. The weather disturbances which characterize the noise measurements of the May experiment, could affect the spectral shapes, generating amplifications at low frequencies.
2. The sites located in the middle of the basin, where the topography of the substratum is relatively flat, are characterized by H/V ratios with an evident resonance peak. Results are more ambiguous where strong lateral variations of sediments thickness are present.
3. The correlation method applied to the noise recorded by a dense array in the basin allows to evaluate the phase velocity of Rayleigh waves in the 0.5-6 Hz frequency band. The dispersion curve is than used to infer a shallow velocity profile for beneath the array. The site transfer function for S waves computed on the basis of the inferred velocity model, well predicts the fundamental resonance frequency in the experimental H/V spectral ratio. The computed higher modes of resonance in the 2-4 Hz frequency band, are not observed in the experimental H/V ratio.

Acknowledgments

We are grateful to P.Y. Bard, coordinator of the SESAME Project (EVG1-CT-2000-0026), who provided us with the HVROC0_1 Code. We are grateful to P. Moczo, M. Ohrnberger and F. Scherbaum, who kindly make available the data set collected during the experiments.

References

1. Riepl J, Bard PY, Hatzfeld D, Papaioannou C, Nechtschin S. Detailed Evaluation of Site-Response Estimation Methods across and along the Sedimentary Valley of Volvi (EURO-SEISTEST). *Bull. Seism. Soc. Am.* 88(2):488-502, 1998.

2. Nakamura Y. A method for dynamic characteristics estimation od subsurface using microtremor on the ground surface. *Q. Rept. Railway Tech. Res. Inst.* 30(1), 25-33, 1989.
3. Bard PY. Microtremor measurements: A tool for site effect estimation? *Proc of the 2nd Int. Symp. On Effects of Surface Geology on Seismic Motion*, 1-3 December, Yokohama, Japan, 3:1251-82, 1999.
4. Saccorotti G, Maresca R, Del Pezzo E. Array Analyses of Seismic Noise at Mt. Vesuvius Volcano, Italy. *Journ. Volc. Geotherm. Res.* 110(1-2):79-100, 2001.
5. Cornou C, Bard PY, Dietrich M. Contribution of Dense Array Analysis to the Identification and Quantification of Basin-Edge-Induced Waves, Part II: Application to Grenoble Basin (French Alps). *Bull. Seism. Soc. Am.* 93(6):2624-48, 2003.
6. Di Giulio G, Rovelli A, Cara F, Azzara RM, Basili R, Caserta A. Long-duration, asynchronous ground motions in the Colfiorito Plain, Central Italy, observed on a two-dimensional dense array. *J. Geophys. Res.* 108, NO.B10,2486, doi:10.1029/2002JB002367, 2003.
7. Rovelli A, Scognamiglio L, Marra F, Caserta A. Edge-diffracted 1-s surface waves observed in a small-size intramountain basin. *Bull. Seism. Soc. Am.* 91:1851-66, 2001.
8. Aki K. Space and time spectra of stationary stochastic waves, with special reference to microtremors. *Bull. Earthq. Res. Inst.* 35(Part 3):415-56, 1957.
9. Konno K, Ohmachi T. Ground-motion characteristics estimated from spectral ratio between horizontal and vertical components of microtremors. *Bull. Seism. Soc. Am.* 88:228-41, 1998.
10. Cara F, Di Giulio G, Rovelli A. A study on seismic noise variations at Colfiorito, Central Italy: implications for the use of H/V spectral ratios. *Geophys. Res. Lett.* 30, 18, 1972, doi:10.1029/2003GL017807, 2003.
11. Idriss IM, Sun JI. *User's Manual for SHAKE91*. Department of Civil & Environmental Engineering, University of California, Davis, California, 1992.
12. Lermo J, Chavez-Garcia FJ. Are microtremors useful in site response evaluation? *Bull. Seism. Soc. Am.* 84(5):1350-64, 1994.
13. Tertulliani A. Qualitative effects of local geology on damage pattern. *Bull. Seism. Soc. Am.* 90:1543-8, 2000.

The EduSeis project in Italy: a tool for training and awareness on the seismic risk

A. Bobbio[a], L. Cantore[b], F. Di Martino[c], N. Miranda[d], M. Simini[e], A. Zollo[b]

[a]*Osservatorio Vesuviano, Istituto Nazionale di Geofisica e Vulcanologia, Napoli, Italia*

[b]*Dipartimento di Scienze Fisiche, Università degli Studi di Napoli "Federico II", Napoli, Italia*

[c]*Fondazione IDIS, Città della Scienza, Napoli, Italia*

[d]*ITIS "E. Majorana", Somma Vesuviana, Napoli, Italia*

[e]*ITIS "E. Elia", Castellamare di Stabia, Napoli, Italia*

Introduction

EduSeis (The Educational Seismological Project), is a scientific and educational project involving research centres, Universities, scientific museums and high schools with the aim to acquire a new teaching method in scientific divulgation. Teachers and students have been involved in the maintenance of seismic stations and the experimentation of didactic activities. The purpose of this network is to make advanced research-level instruments and data analysis tools available to schools and to increase the students attention to observations of earth phenomena and earth science in general.

In a region characterized by an elevated seismic and volcanic risk, the EduSeis project has a remarkable impact on the prevention of the seismic risk through a strong effect on awakening and involvement of students and teachers in the schools and of general public in museums.

The project has several educational, scientific and social aims. The main educational objectives are to expose and teach students and teachers to internet-based networking and data transfer as well as the acquisition, analysis and interpretation of seismological data. An important task is to develop, upgrade and test educational modules and activities on seismology and other disciplines (electronics, physics, informatics) using informatics and web-oriented tools.

The main scientific objective is the development and testing of hardware and software components of an advanced, but low-cost seismic acquisition system, according to the general requirements of the best quality/cost ratio as constrained by school budgets. In additional, the best quality data corresponding to relevant events selected by the EduSeis operators, set up a school-based earthquake waveform database available on the EduSeis web site. In short the main social objective is to establish a direct link between the scientific community, schools and general public to contribute actively to the diffu-

sion of the information related to seismic risk and to mitigate the social effect of earthquakes.
Products from the project are available to the schools hosting the EduSeis seismograph, the Science Centre's visitors and to the general public via an Internet web site (http://eduseis.na.infn.it) (Fig. 1).
The web site, designed in a synthetic and efficient style, provides the information about seismology, therefore many section are available: *The EduSeis Project*, *EduSeis Network*, *Data Base*, *Teaching*, *News* and *Links*; each section allows to choose more options.

The EduSeis network

A network of digital seismographs has been installed in a number of high schools in Central and Southern Italy (Fig. 2). The school seismic stations are installed inside the building. The sensor is preferably deployed at a ground or underground level while the acquisition PC is hosted in the informatics lab.

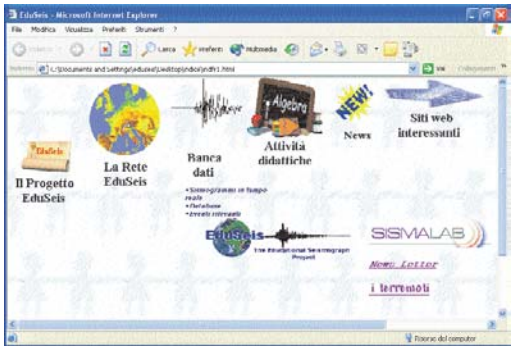

Fig. 1. The EduSeis web site (http://eduseis.na.infn.it).

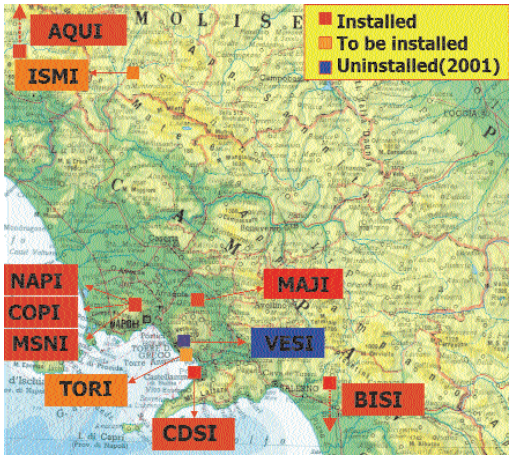

Fig. 2. EduSeis Network.

All the elements of the seismic station are especially designed for educational purposes and can be operated independently by the students and teachers themselves. The EduSeis network is made up of seismic stations that can record local, regional and world seismic events. Some stations are equipped with PMD Scientific sensors broad-band (20s-20Hz) and others are equipped with MARK L-28LB sensor (4.5 Hz).
Special software applications have been conceived to make it easy for pupils to work on seismological data. Seismic recordings can be visualized and analysed with the Java Applet called *SeisGram* that was developed by A. Lomax; this applet allows students and teachers to study recent seismic signals as well as older recordings. The seismic signals from several other stations can be zoomed and displayed, in addition, the different seismic waves arrival times can be picked and different band-pass filters are available to improve the seismogram analysis.

Remote control & Data retrieval

An important step was reached in 2002 concerning software and hardware development for the seismic acquisition system. Since the EduSeis project started, standard phone connections had been used to allow data extraction from the stations to central PC From the beginning of 2002, a new generation of seismic acquisition system (compact hardware system to be connected to a computer) and data communication system (to be run in the dedicated computer), has been developed in collaboration with the French "Agecodagis Company". This Internet Remote Acquisition System (IRAE) (Fig. 3) allows us to get information and data from very far stations, quickly and securely. IRAE is a software suite acting as a distributed TCP/IP oriented acquisition

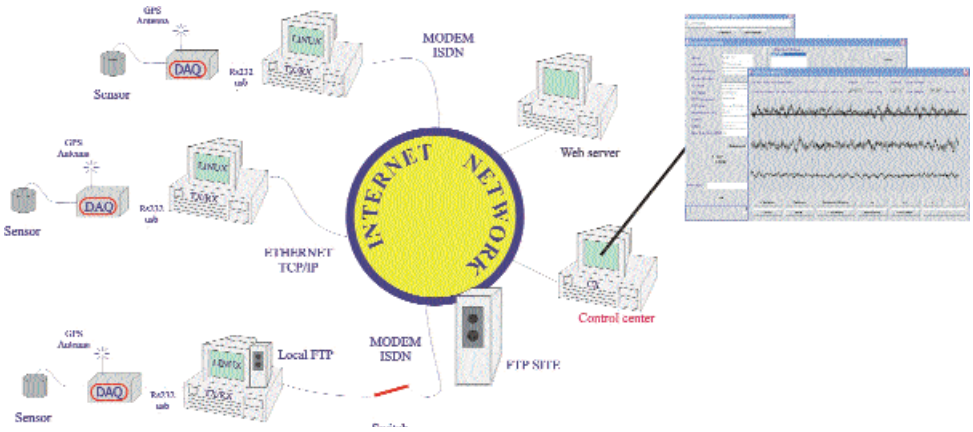

Fig. 3. Remote control & Data retrieval.

system and completely written in Java, the IRAE components can thus be installed on any system supported by the Java-platform: Linux, Windows for instance. Contrary to the "traditional" acquisition system, the whole recorded data can be extracted from the station by Internet connection, and stocked on a dedicated FTP server. The daily communications between stations and the FTP site are cheaper and stations could be installed in some areas where no research centres are located. The IRAE software consist of 3 parts: IRAE-SENDER (TX), IRAE-RECEIVER (RX) and IRAE-CONTROL (CX). TX runs on a PC connected to the seismological data logger; over the internet, it's possible to connect to a RX station using IRAE-CONTROL (CX) code. Any TX attached to the RX station, build and send data requests, or even plot the real time data stream. Subsequently all the data are sent on FTP SITE and removed from RX.

The school' role in the EduSeis Project

The fundamental educational aim of the EduSeis Project is the development and the implementation of the current practice of scientific data acquisition and management in Earth Science for high school students. The basic idea is that seismology can be a vehicle to train the active use of modern technologies, learn about the dynamics and evolution of the Earth and create public awareness about the seismic activity and risk. The innovative method developed in this project offers students and teachers, the opportunity to have access to the data and tools of advanced technology. The educational activity is organized at different levels for teachers, students and the general public, with the aim to experiment the practicability, the contents and the didactic valence. For this reason, have been developed activities dedicated to the seismological practice and information of seismic risk. This educational material is available on the EduSeis web site in the section "*Didactic Modules and Didactic Activities*", with the aim to diffuse the didactic experiences.
Each activity has a valuation card for the teachers, this card allows them to verify the efficiency of the activity. The activities include several sections, for each one, the learning goals are described and a list of the necessary materials is provided. Some activities involve the graphic display of seismic records, the reading of principal seismic phases arrival times, the earthquake location and so on. Analogical and software tools have been created and used for the activities with students, for example the activity "Simulation of body wave propagation", can be performed by using either an analogical device that illustrate the wave excitation and propagation through a five slinky model or by a java applet that simulate the analogical instrument (Fig. 4).
Some experiences of training and awakening to the seismic risk based on EduSeis, have been realized by the Science Centre of "Città della Scienza". In March 2003, the *SismaLab*, a seismology laboratory, has been open (Fig. 5).

The SismaLab is an interactive lab where students, teachers and visitor can play and make experiments with earthquakes and seismology. This SismaLab is an information point about earthquakes and an educational centre about seismic risk.
Moreover another two activities have been produced:

1. "Terremoti: Come, dove, quando, perché…" by Aldo Zollo and Luciana Cantore, Ten information schedules for SismaLab to learn about earthquakes.
2. Bimestrial Newsletter to inform the users about the EduSeis project and about the divulgation initiative.

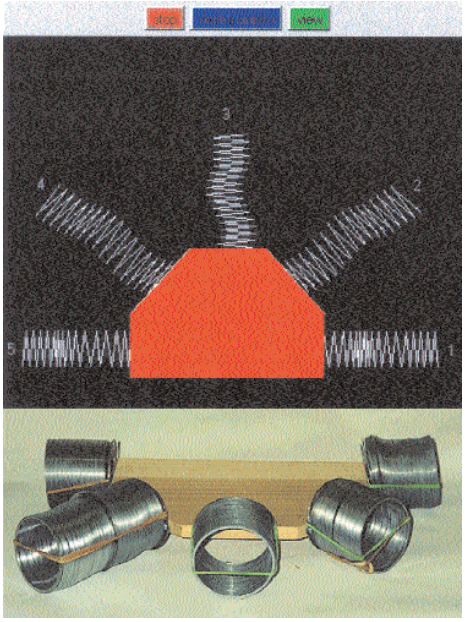

Fig. 4. Analogical and software tools used for the didactic activities.

Fig. 5. Science Centre's SismaLab. A seismology laboratory for learning about earthquakes.

Conclusion and perspectives

The fundamental aims of EduSeis project is to involve students, teachers and general public in the experimentation of the social and educational activities, based on innovative methodologies and on the use of new technologies, with the aim to propagate the knowledge about seismic phenomena and seismic hazard. This effect is achieved in two ways: by involving students, teachers and their families in schools and by using museum to educate the general public.

Although there is a risk of strong earthquakes in the Mediterranean area, the amount of information and awakening to the seismic prevention are insufficient by comparison with analogous initiatives undertaken in other seismic regions in the world.
The seismic stations in the schools and all related educational activities represent an important vehicle for increasing the people awareness about environmental risks, by stimulating students (and indirectly their own family) to maintain a continuous attention and observation on earth phenomena.
Through regional and teleseismic earthquake data processing, the students take an active part in monitoring of the territory, and the recordings of strong events, which allows them to understand the dynamic evolution of the Earth and to have a direct knowledge of the seismic hazard of the regions where they live.

REFERENCES

Virieux J. EDUSEIS, An EDUcational SEISmological European Network. *Orfeus Electronic Newsletter* 1:13, 1999.

Bobbio A, Zollo A. The educational broadband seismic network at Naples (Southern Italy). *Orfeus, Electronic Newsletter* 2:3, 2000.

Virieux J. Educational Seismological project: EDUSEIS. *Seismological Research Letters* 71:530-5, 2000.

Lomax A. QuakeExplorer-Earthquake Internet Browser and Analysis Tool. *Orfeus Electronic Newsletter* 3:1, 2001.

Cantore L, Bobbio A, De Martino F, Petrillo A, Simini M, Zollo A. The EduSeis project in Italy: a tool for training and awareness on the seismic risk. *Seismological Research Letter* 74(5), 2003.

Michelson interferometer system for seismic noise measurement

F. Acernese[a,b], F. Barone[b,c], R. De Rosa[a,b], L. Milano[a,b], K. Qipiani[b]

[a]*Dipartimento di Scienze Fisiche, Università degli Studi di Napoli "Federico II", Napoli, Italia*

[b]*Istituto Nazionale di Fisica Nucleare, sezione di Napoli, Napoli, Italia*

[c]*Dipartimento di Scienze Farmaceutiche, Università degli Studi di Salerno, Fisciano, Salerno, Italia*

Introduction

Laser Optical Interferometry has been introduced in different fields of research for applications requiring very high precision displacement measurements [1], so that a large number of optical configurations are today available both for absolute and relative displacements measurement. Therefore, the application of this technique also for seismic waves detection and measurement is therefore straightforward [2].
Following this line, we have applied the optical interferometry for solving the problem of measurement of the amplitude and direction of surface seismic waves. For this task we have developed a laser interferometric sensor, with band and sensitivity satisfying the requirements.
Actually, band and sensitivity were not the only parameters we took into account in the design of the optical system: portability, simplicity of configuration and management were other relevant parameters.

Michelson interferometer

The optical configuration that easily satisfies all these requirements and typology of measurement is the Michelson interferometer (Fig. 1), a classical dual-wave optical interferometer characterized by a very simple configuration. According to this configuration, a laser beam is split into two beams by a beam splitter. The two beams, are then first reflected by end mirrors and then recombined again by same the beam splitter, producing an output signal acquired through a photodiode. Assuming a plane wave beam, then the Michelson interferometer output *I(t)*, can be generally expressed as a combination of the error signals of all displacements and tilts of its mirrors as

$$I(t) \quad I_{min} + \frac{I_{max} \quad I_{min}}{2}\left[1 + cos\left(\frac{4\pi n}{\lambda}\left\{|l_2(t) \quad l_1(t)| \sum_{i=1}^{2}|l_i(t) + d| \sum_{i=1}^{2}\theta_{i,j}^{2}(t)\right\}\right)\right] \quad (1)$$

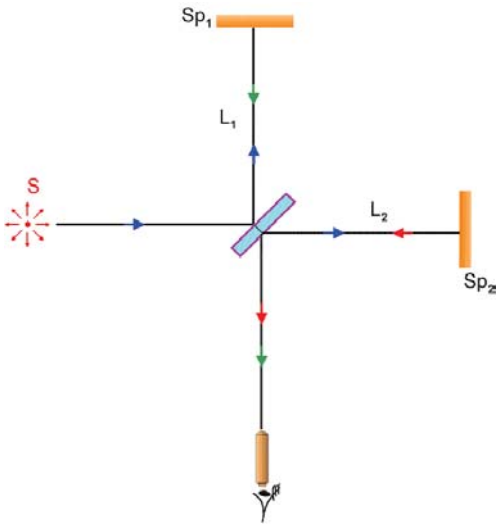

Fig. 1.

where I_{max} and I_{min} are the maximum and the minimum output intensities, λ is the laser beam wavelength, n is the spatial mean refraction index, $li(t)$ is the i^{th} arm-length, d is the distance of the beam-splitter from the output photodiode, and $\theta_{i,j}$ is the j^{th} tilt of the mirror in the i^{th} arm.
Then, since techniques exists for an alignment control of the optics completely independent from the longitudinal control, then the hypothesis of a perfectly aligned system is perfectly acceptable and the output intensity can be written as

$$I(t) \quad I_{min} \mid \frac{I_{max}}{2} \quad \frac{I_{min}}{2} \mid 1 \mid cos(\phi(t)) \mid \quad I_{min} \mid \frac{I_{max}}{2} \quad \frac{I_{min}}{2} \left[1 \mid cos\left(\frac{4\pi n}{\lambda} l_{eq}(t) \right) \right] \quad (2)$$

where $l_{eq}(t)$ is the longitudinal motion. Finally, in order to extract the arm-length change due to the presence of a seismic wave, then it is necessary to choose one arm as reference and therefore to fix and protect it from refraction index changes. The other arm, the measurement arm, is instead allowed to change in length in presence of a seismic wave.
A further approximation must be done if we do not consider the refraction index constant and equal for both arms. Yet, for optical and infrared wavelengths the refraction index change of the atmosphere can be expressed as [3]

$$\begin{aligned} \Delta n(R,t) = & -1.17 \cdot 10^{-9} \lambda^{-3} \frac{P(R,t)}{T(R,t)} \Delta\lambda + \\ & + 77.6 \cdot 10^{-6} (1 + 7.52 \cdot 10^{-3} \lambda^{-2}) \frac{\Delta P(R,t)}{T(R,t)} - \frac{\Delta T(R,t)}{T^2(R,t)} \end{aligned} \quad (3)$$

where $\boldsymbol{R}$ is a point in the space, λ is the optical wavelength in μm, P is the pressure in *mBar*, and T is the temperature in Kelvin. As can be seen, the refrac-

tion index change is small for laser emitting in the optical and near infrared bands.
Since we have theoretically and experimentally demonstrated the possibility of measuring in real-time the interferometer arm length change with respect to an arbitrary initial arm length using the non linear error signal extraction techniques [4], then the next step is to calculate the transfer function of this kind of interferometric seismic sensor. For this task we consider that the seismic wave $s(t)$ whose propagation vector $\boldsymbol{k}$ is in the plane in which the sensitive arm $l_2(t)$ of the interferometer is located. Therefore, the arrival of a seismic wave along the plane of the interferometer is generally sensed first by one mirror and then, with a delay time t_0 that depends on the direction of the seismic wave with respect to the optical axis of its sensitive arm.
Let α the angle between the wave vector $\boldsymbol{k}$ and the line optical axes $l_2(t)$, L_1 the reference arms length, and v_s the wave group velocity of signal $s(t)$. Note that the length of the arm L_1 containing the reference mirror is quite constant, apart from small residual displacement due to the oscillations of the optical holders induced by ground motion. These oscillations are anyway at frequencies enough high to be attenuated by the low pass anti-aliasing filters located before the ADCs, so that the phase difference depends only on the length of the measurement arm. Then it is possible to write

$$t_0 = \frac{[L_2 + g_2(t)]\cos(\alpha) - L_1 \sin(\alpha)}{v_s} \tag{4}$$

where $g_2(t)$ is the residual ground displacement of free mirror due to local micro-seismic waves that is the limiting background noise and represent the sensitivity limit of the instrument. For $t>t_0$ the wave front moves both the mirrors and, using $L_2(t)=L_2+g_2(t)$, the phase change becomes

$$\phi(t) \quad \frac{4\pi n}{\lambda} |L_2 \quad L_1 + g_2(t) + (s(t) \quad a_s s(t \quad t_0))\cos\alpha| \tag{5}$$

where a_s is the attenuation factor expressing the different amplitude of the seismic wave when reaches the two mirrors due to the different path lengths. Neglecting the length change in absence of signal, if there is no signal $s(t)$, the interferometer response is proportional to seismic noise that it can be measured inverting the equation 2. Otherwise the transfer function that links the input seismic signal $s(t)$ and with the output phase change $\phi(t)$ can be written as

$$H(s) = \frac{\Phi(s)}{S(s)} = \frac{4\pi n}{\lambda}(1 - a_s e^{\quad t_0 s})\cos(\alpha) \tag{6}$$

In the case of short arms interferometer, the delay time t_0 becomes small, the attenuation factor is equal to one and, expanding the transfer function in Taylor series, it is possible to consider the interferometer response at the first order.

In this case, the relationship between the input signal *s(t)* and the phase change is

$$\phi(t) = \frac{4\pi n}{\lambda} t_0 \cos(\alpha) \left(U(t - t_0) \frac{ds(t)}{dt} \right) \tag{7}$$

This means that the phase of interferometer is dependent on the derivatives of the input signal, and, therefore, the Michelson interferometer behaves at the first order like a velocimeter.
To calculate the directional diagram to determine the angular dependence of instrument sensitivity, we can use the harmonic response and the explicit form of t_0:

$$H(\omega) = \frac{4\pi n}{\lambda v_s} \cos(\alpha) [L_2(\omega)\cos(\alpha) - L_1 \sin(\alpha)] i\omega \tag{8}$$

From this equation is can be seen four directions exist where the sensitivity is zero *($\alpha = \pi/2$, $\omega = 3\pi/2$, $\omega = atan(L_2(\omega)/L_1(\omega))$, $\alpha = atan(L_2(\omega)/L_1)+\pi$).*

Experimental results

The experimental apparatus used as prototype for a laser interferometry based seismic sensor consists mainly of a Michelson interferometer in air, an accelerometer for comparison, a digital acquisition system to get data from these instruments and to store them in an electronic archive (Fig. 2). All the optical elements of the interferometer are fixed to an optical bench. A triaxial episensor (model FBA ES-T, from Kinemetrics) is located close to the first mirror to monitor the acceleration in that point. A picture of the experimental setup is shown in Fig. 3.
The data coming from the photodiodes and from the episensor are collected by an acquisition system. This is composed by an analog pre-processing board followed by the analog to digital converter (ADC) board. The analog pre-processing consists in amplifying the signals to fit their amplitude to the ADC converters dynamics and in filtering them with suitable anti-aliasing filters. The sampling frequency was fixed at 1 kHz for the tests, in order to guarantee very good performances of the anti alias filters. By applying the signal analysis procedure described in the previous section to the data provided by the interferometer and comparing the results with the data coming from the episensor.
To determine the sensitivity of the interferometric sensor, we acquired 900s of data during the night to reduce the noise generated by human activity.
In Fig. 4 the power spectral density of the output of the accelerometer and of the derivative of the output of the interferometer are shown. It is possible to see the very good agreement of the output of the acceleration in the band 1-100 Hz of the two instruments. The main results that it is possible to extract from this figure is the fact that since the acceleration is obtained as derivative of the output of the interferometer, it is clear that it behaves as a velocimeter at least in the band 1-100 Hz, validating in this way the model we presented in the previous paragraph.

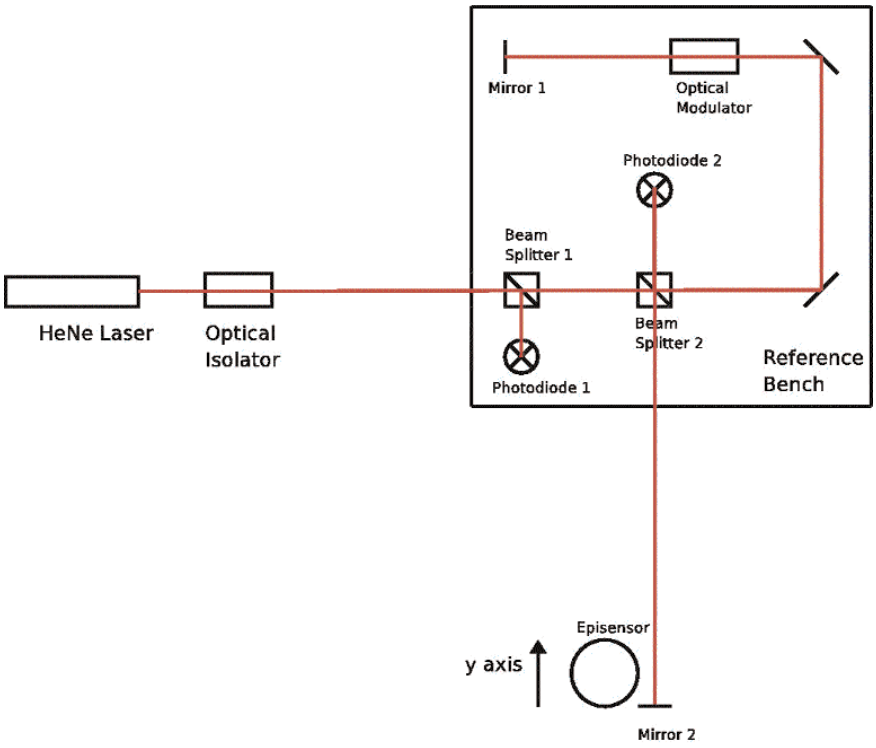
Mirror 1
Optical Modulator
Photodiode 2
Beam Splitter 1
HeNe Laser
Optical Isolator
Beam Splitter 2
Reference Bench
Photodiode 1
Episensor
y axis
Mirror 2

Fig. 2.

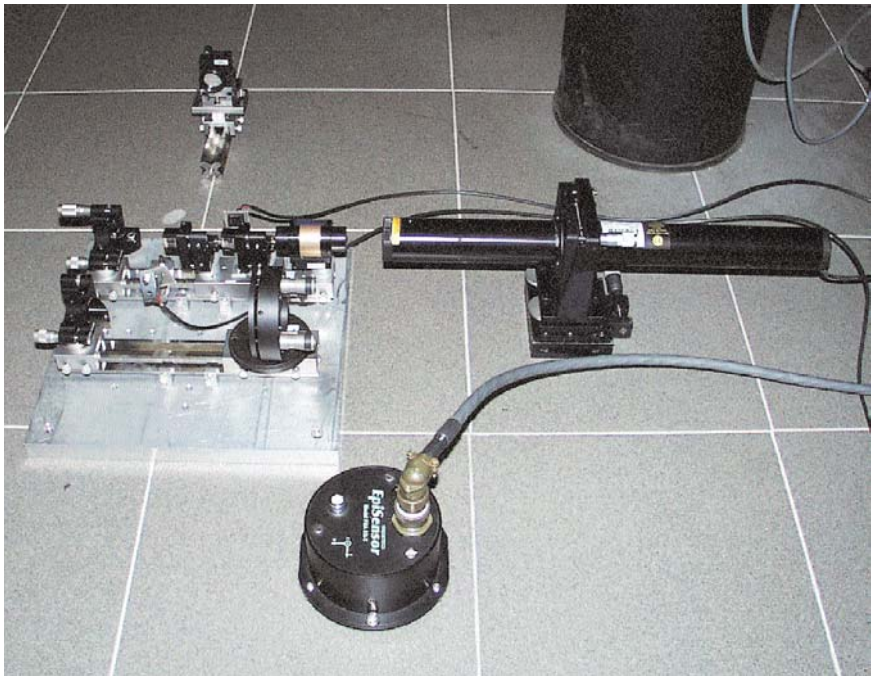

Fig. 3.

Conclusions and future research

We demonstrated that a very Michelson interferometers can be used as an effective seismic sensor. The sensitivity of such device should be limited only by the environmental parameters like temperature and pressure, whereas the laser intensity can be continuously monitored in order to take into account its variations. The interferometer output is proportional to the velocity of seismic waves. A preliminary experimental test on this technique, using a single Michelson interferometer, confirms the theoretical results, allowing for an interferometric measurements of the ground speed that is in good agreement with the measure provided by a standard accelerometer for seismic applications.

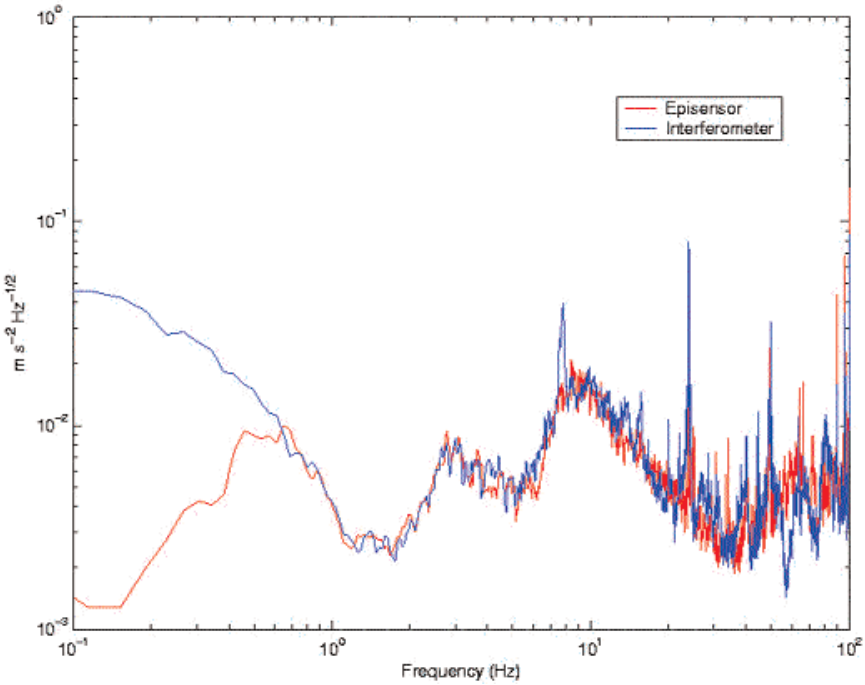

Fig. 4.

References

1. Levine J. Laser distance-measuring techniques. *Ann. Rev. Earth Planet Sci.* 5:357, 1977.
2. Crescentini L, Amoruso A, Fiocco G, Visconti G. Installation of a high-sensitivity laser strainmeter in a tunnel in central Italy. *Rev. Sci. Instrum.* 68:3206-10, 1997.
3. Born M, Wolf E. *Principles of Optics*. Pergamon Press, Oxford, 1964.
4. Barone F, Calloni E, Di Fiore L, Grado A, Milano L, Russo G. Digital Error Signal Extraction Technique for Real-Time Automatic Control of Optical Interferometers. *Applied Optics* 34:8100-5, 1994.

Seismic engineering

Innovative techniques for the seismic protection of structures: theory, applications and experimental tests in Italy

M. Dolce, D. Cardone, F.C. Ponzo

Dipartimento di Strutture, Geotecnica, Geologia Applicata all'Ingegneria, Università della Basilicata, Potenza, Italia

Introduction

Conventional seismic design practice considers structural damage acceptable under strong earthquakes, provided that the structure is "ductile" enough to undergo large plastic deformations without collapsing. The inelastic demand is generally intended to concentrate in specially detailed critical zones, e.g. at the ends of beams in framed structures. The inelastic behaviour of such regions, however, while increasing flexibility and energy dissipation of the structural system, results in significant damage to structural elements. Moreover, the interstorey drifts occurring under severe earthquakes cause extensive damage and collapse of non-structural elements, such as infill masonry walls, partitions, etc., implying important economic losses.

Alternative design strategies commonly referred to as "passive control" techniques [1] have been developed in the last thirty years. They are aimed at eliminating – or at least considerably reducing – damage in structures under strong earthquakes, by exploiting the favourable behaviour of special devices introduced into the structural system. The concept behind passive protection techniques is similar to that of conventional seismic protection techniques, but flexibility and energy dissipation capacity is provided by purposely designed devices and systems. Current applications are mainly based on (i) seismic isolation [2] or (ii) energy dissipation techniques [3].

To realize seismic isolation, the structure is vertically divided in two parts, separated by the isolation system: the sub-structure, rigidly fixed to ground, and the super-structure. Basically, the isolation system is made up of bearing devices, allowing for large horizontal displacements (200-400 mm) with low stiffness or low friction. It works like a filter which reduces the transfer of seismic energy from ground to superstructure, thus limiting seismic forces within the elastic capacity of structural members. In order to limit its displacements during (and at the end of) an earthquake, the isolation system must be provided with energy dissipation and/or re-centering capabilities, by either using

isolators having these properties intrinsically, or embodying additional dissipating and/or re-centering elements, or even providing separate dissipating and/or re-centering devices.
To realise energy dissipation, different parts of a structure, moving relatively during an earthquake, are connected through special devices, purposely made to absorb and dissipate large amounts of energy with a stable cyclic behaviour. In this case, the energy entering into the structure remains practically the same, but most of it is dissipated by the special devices. As a result, the damage in primary gravity load-resisting structural members is drastically reduced.
The number of passive seismic protection applications is rapidly increasing all over the world, and several different devices have been proposed [4, 5]. Basically, four types of isolation devices are used nowadays: (i) Rubber isolators, (ii) Sliding isolators, (iii) Rolling isolators and (iv) Isolators of the above types with added dissipation, as well as four types of energy dissipating devices: (i) Visco-elastic devices, (ii) Elasto-plastic hysteretic devices, (iii) Friction devices and (iv) Viscous devices. More recently new devices, exploiting the properties of advanced materials, such as Shape Memory Alloys (SMA) [6] have been developed.

Applications in Italy and seismic regulations

Several applications of seismic isolation have been made in Italy, in the eighties and early ninenties, especially on several important bridges and viaducts, while the first buildings have been isolated in the early nineties. At that time Italy was the country where the applications of seismic isolations to bridges were more numerous and important. In the second half of the nineties up to one year ago, very few applications of passive control have been made, essentially due to the long time required to get the approval of the competent authority, lacking a specific seismic isolation regulation. In Figs. 1 and 2 there are shown two applications, one is the seismic isolation of two important buildings of the University of Basilicata [7], the other is the seismic retrofit of a school in Potenza, using energy dissipating bracing system [8].
It is supposed that the number of applications in Italy will increase considerably in the next years, as the new Seismic Code (Ordinanza 3274) [9], which follows the general criteria of EC8 [10], includes two chapters devoted to seismic isolation of buildings and bridges, while the general design and analysis criteria can be consistently applied to energy dissipation techniques.
According to the criteria and rules given for the seismic isolation of buildings, it can be shown that in many cases there can be considerable savings in the costs of the superstructure (the part above the isolation interface), which can even overcome the additional costs of the devices and the additional works at the isolation level [11]. In some cases an isolated building, besides being considerably safer than a similar fixed-base one, can even result less expensive.

Fig. 1. Seismically isolated building of the University of Basilicata.

Fig. 2. School building retrofitted with energy dissipating braces.

Experimental tests

A large number of tests on R/C and steel models equipped with passive control devices, have been carried out all over the world, in order to evaluate the effectiveness of the passive control strategies to reduce drastically the effects of earthquakes, as well as to compare different types of devices for seismic isolation and energy dissipation.

In the last ten years the writers and the Laboratory of Structure of the University of Basilicata have been deeply involved in several experimental investigations on reinforced concrete (R/C) models seismically protected with different types of devices for seismic isolation or energy dissipating and re-centering bracing systems. These investigations were part of European or National research project.
Tests have been carried out on R/C and steel structural models at different scales, 1:4, 1:3.3, 1:2.5, real structure, in 4 laboratories all over Europe, University of Bristol (UK), Laboratorio Nacional de Engenharia Civil (LNEC) of Lisbon (PT), Technical University of Athens (GR), University of Basilicata (IT). Different types of testing techniques have been used, namely shaking table, pseudodynamic and release test. The shaking table tests have been carried out using 1 or 2 components of natural and artificial accelerograms. Device technologies based on the use of different materials, such as Rubber, Steel, Shape Memory Alloys, PTFE with stainless steel, have been employed and compared. Most of the investigations were aimed at evaluating the capabilities of passive control to retrofit existing structures designed for gravity loads only.
In Figs. 3 to 9 there are reported the main information relevant to some of the following experimental investigations: ECOEST I [12], ECOEST II [13], MANSIDE [14], SICURO [15], POP-SSN [16].

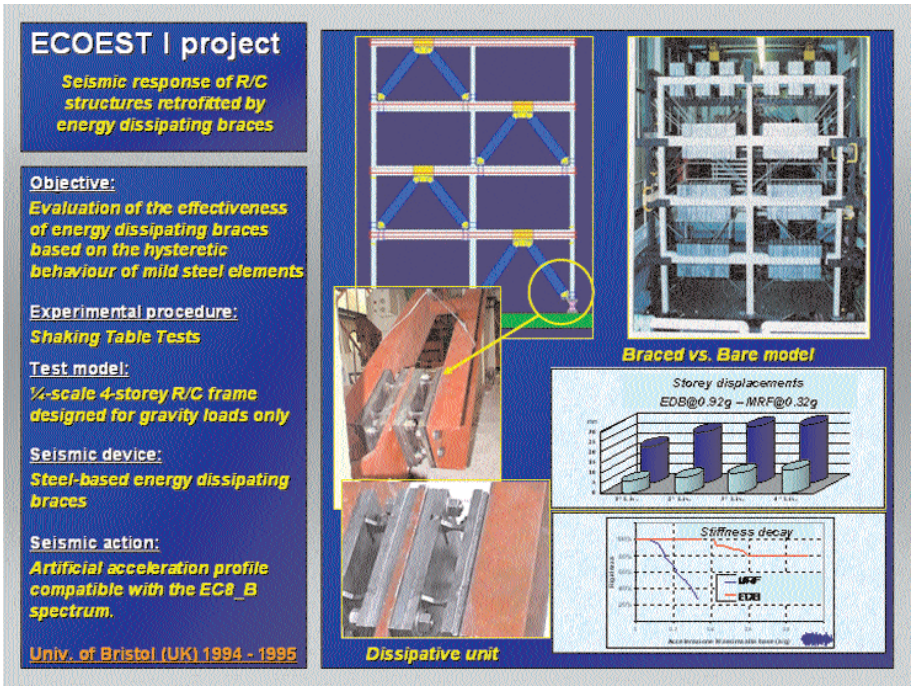

Fig. 3. Summary of the ECOEST I project.

Fig. 4. Summary of the ECOEST II project.

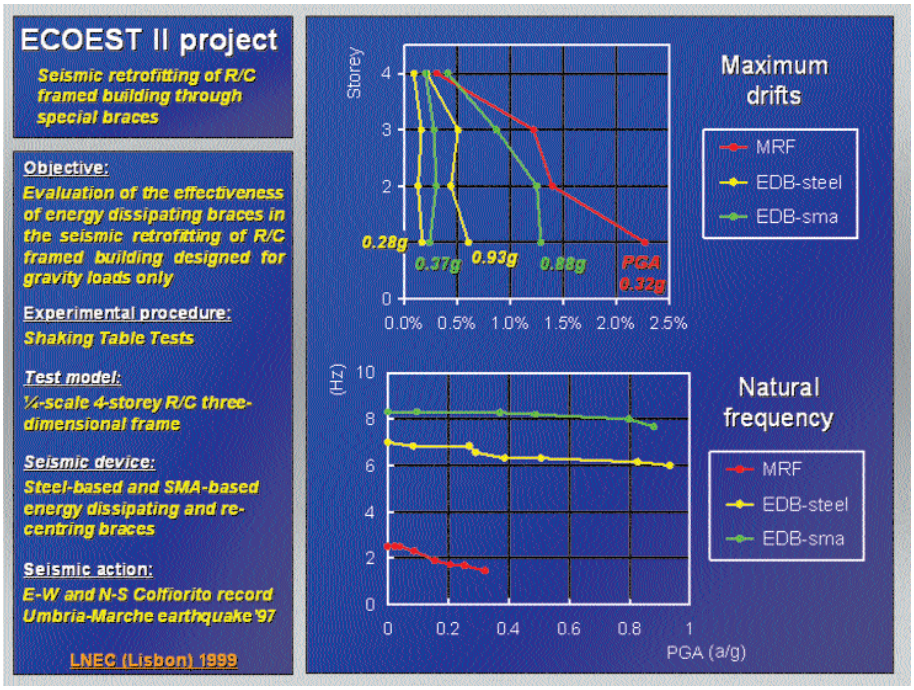

Fig. 5. Summary of the ECOEST II project (results).

Fig. 6. Summary of the MANSIDE project.

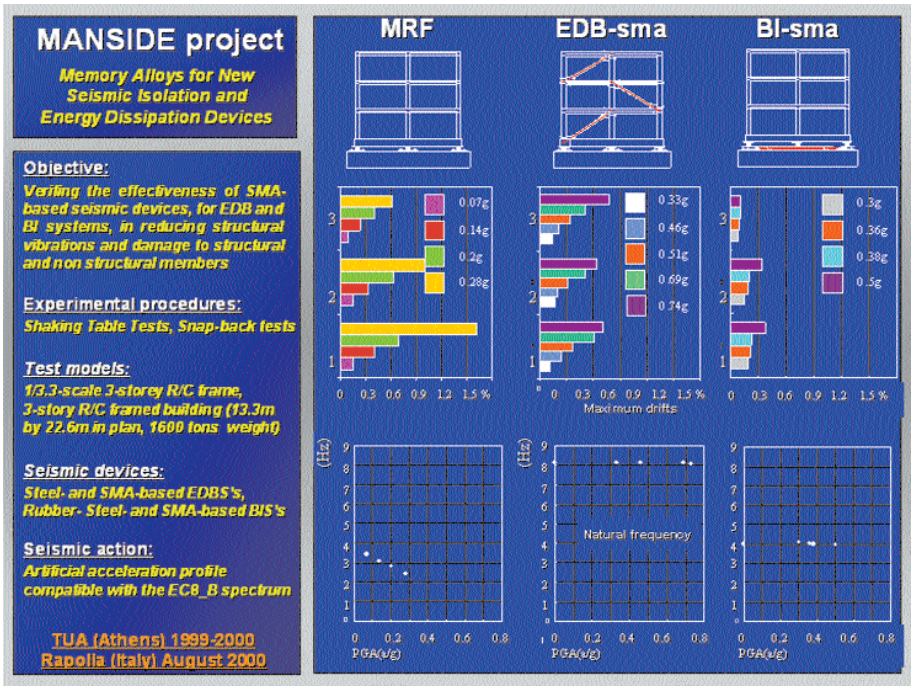

Fig. 7. Summary of the MANSIDE project (results).

Fig. 8. Summary of the SICURO project.

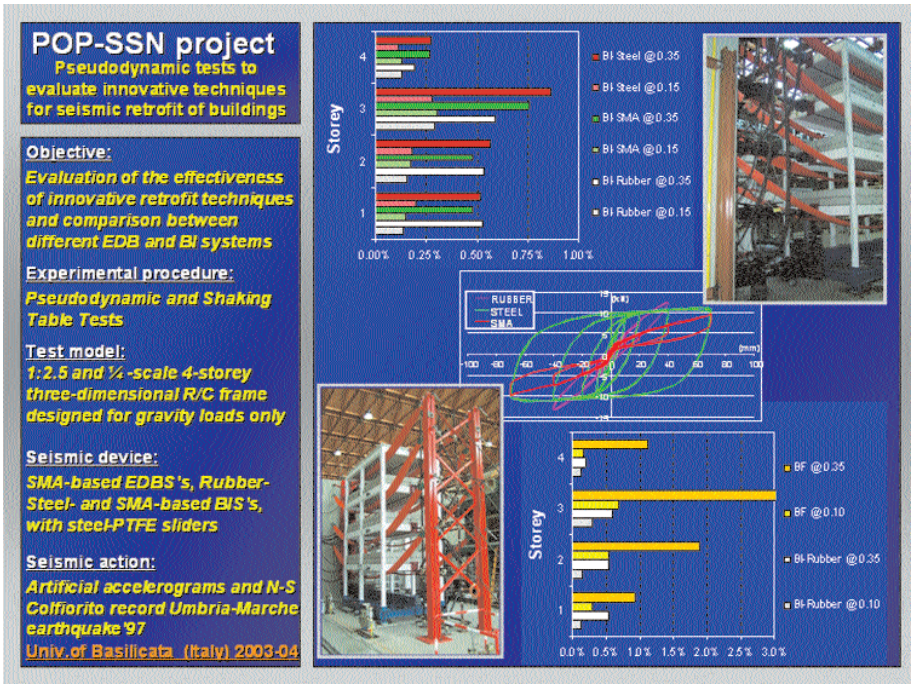

Fig. 9. Summary of the POP-SSN project.

As can be seen, the common result of all the tests, as drawn from the few diagrams that are shown in the figures, is that both strategies (seismic isolation and energy dissipation), as well as all the type of isolation and energy dissipation devices and systems, are highly effective in reducing the seismic response of the structure. A reduction of one order of magnitude of the interstorey drift can be easily detected by comparing the response of conventional structural model and the model protected with passive control, for either seismic isolation or energy dissipation systems. This means that for the earthquake intensity which normally causes heavy damage or collapse of a normal building (interstorey drift of the order of 2-3% for 0.30-0.35g PGA earthquake), practically no damage occurs to a similar passively controlled building (interstorey drift of the order of 0.1-0.3%). Moreover, even for earthquakes several times stronger than the usual design earthquake, no or slight damage occurs to structural and non structural elements (interstorey drift of the order of 0.5-1% for up to 1g PGA earthquake and even more), as the slight changes of natural frequency also demonstrate. In no experimental test it was possible to reach the collapse condition of the model. The experimental tests also show the great effectiveness in the retrofit of existing buildings designed for gravity loads only. Finally some tests on real structures, carried out by moving (up to 17 cm) and releasing them suddenly, demonstrate the practical applicability of these techniques [17, 18].

Conclusion

Ten years of tests on different structural models with different testing techniques, different seismic actions have shown the full reliability of advanced techniques of seismic isolation and of energy dissipating and/or recentring braces for the seismic retrofit of existing R/C buildings designed for gravity loads only.
Device technologies using rubber, steel, Shape Memory Alloys, steel-PTFE or rubber isolators can provide comparable performances, when the retrofit intervention is suitably designed. The performance level achievable is considerably higher, even using simplified design procedures, than conventional seismically designed structures, conditioned upon the care of the details in the design as well as in the execution.

References

1. Dolce M. Passive Control of Structure. *Proc. 10th European Conference on Earthquake Engineering*, Vienna, 1994.
2. Naeim F, Kelly JM. *Design of seismic isolated structures*. John Wiley & Sons Ltd, 1999.
3. Constantinou MC, Soong TT, Dargush GF. *Passive energy dissipation systems for structural design and retrofit*. MCEER, State University of New York at Buffalo, 1998.

4. Housner GW et al. Structural control: past, present and future. *ASCE, Journal of Engineering Mechanics* 123(9):897-971.
5. Hanson RD et al. State of the art and state of the practice in seismic energy dissipation. *Proc. of the ATC-17-1 Seminar*, San Francisco, California, 1993.
6. Duerig TW, Melton KN, Stoeckel D, Wayman CM (eds.). *Engineering aspects of shape memory alloys*. Butterworth-Heinemann Ltd, London, 1990.
7. Braga F, Dolce M. The Isolated Buildings of the University of Basilicata at Potenza – Italy. *Proc. of International Post SMiRT Conference Seminar on Seismic Isolation, Passive Energy Dissipation and Active Control of Vibrations of Structures*, August 1997, Taormina.
8. Dolce M, Marnetto R. Energy Dissipating Coverplates for Steel Brace Joints. *Proc. of 5th World Congress on Joints, Bearings and Seismic Systems for Concrete Structures*, October 2001, Rome.
9. Ordinanza n. 3274 del Presidente del Consiglio dei Ministri 20/03/2003 "Primi elementi in materia di criteri generali per la classificazione sismica del territorio nazionale e normative tecniche per le costruzioni in zona sismica". *G.U.* 08.05.03.
10. CEN, European Committee for Standardisation. *Eurocode 8: Design Provisions for Earthquake Resistance of Structures, Part 1.1: General rules, seismic actions and rules for buildings*. ENV1998-1-1.
11. Dolce M, Santarsiero G. Progress on Development of Design Rules for Seismic Vibrations Control Techniques of Civil Structures in The European Union. *8th World Seminar on Seismic Isolation, Energy Dissipation and Active Vibration Control of Structures*, October 6-10, 2003, Yerevan, Armenia.
12. Braga F, Crewe A, D'Anzi P, Dolce M, Ponzo FC. Experimental and Numerical Behaviour of R/C Building Frames Upgraded with Energy Dissipating Braces. *European Earthquake Engineering Journal* 1, 2002.
13. Cardone D, Coelho E, Dolce M, Ponzo FC. Experimental behaviour of R/C frames retrofitted with dissipating and re-centring braces. To appear on *International Journal of Earthquake Engineering*.
14. Valente C, Cardone D, Dolce M, Ponzo FC. MANSIDE: Shaking Table Tests of R/C Frames with various Passive Control Systems. *Proc. of 12th World Conference on Earthquake Engineering*, January 2000, Auckland, New Zealand.
15. Cardone D, De Canio G, Dolce M, Marnetto R, Moroni C, Nicoletti M, Nigro D, Pizzari A, Ponzo FC, Renzi E, Santarsiero G, Spina D. Comparison of Different Passive Control Techniques through Shaking Table Tests. *8th World Seminar on Seismic Isolation, Energy Dissipation and Active Vibration Control of Structures*, October 6-10, 2003, Yerevan, Armenia.
16. Dolce M, Cardone D, Moroni C, Nigro D, Ponzo FC, Nicoletti M. Pseudodynamic Tests on a Large Scale Base-Isolated Model. *8th World Seminar on Seismic Isolation, Energy Dissipation and Active Vibration Control of Structures*, October 6-10, 2003, Yerevan, Armenia.
17. Bixio AR, Braga F, Dolce M, Nicoletti M, Nigro D, Ponzo FC. Repeatable dynamic release tests on a base-isolated building. *International Journal of Earthquake Engineering* 5(3), 2001. *Atti del DiSGG* n. 1/2000.
18. Dolce M, Cardone D, Ponzo FC, Bixio AR, Nigro D. The Behaviour of SMA Isolation Systems during the Full-Scale Release Tests of the Rapolla's Building. *Proc. of 5th World Congress on Joints, Bearings and Seismic Systems for Concrete Structures*, October 2001, Rome.

Shaking tables for seismic simulation overview of the CRdC-AMRA project

G. Fabbrocino, E. Cosenza

Dipartimento di Analisi e Progettazione Strutturale, Università degli Studi di Napoli "Federico II", Napoli, Italia

Introduction

Research in the field of earthquake engineering and mitigation of seismic risk needs complex experimental facilities. Depending on the specific topic of interest, earthquake research can need large and stiff reaction walls, strong floors or dynamic testing equipments. Dynamic performances of structures can be evaluated via field experimentation and monitoring at real scale or using shaking tables able to simulate earthquake ground motions with high levels of fidelity; the latter can be used both for structural and geotechnical tests, even if centrifuges are widely used for geotechnical problems. In the present paper, an overview of the CRdC-AMRA project concerning shaking tables for seismic simulation is briefly reported.

Experimental facilities for earthquake engineering

A review of major existing facilities for seismic simulation can be carried out referring to data collected in the frame of a research issued by U.S. National Science Foundation's George E. Brown, Jr. Network for Earthquake Engineering Simulation (NEES) (2001). The work updated former data published by Earthquake Engineering Research Institute (EERI) in the document Assessment of Earthquake Engineering Research and Testing Capabilities in the United States (1995).
Tab. 1 gives a very interesting view of academic and industrial strategies in the field of seismic experimental assessment of structures and constructional solutions. It is easy to recognise that a large number of facilities are located in Japan (19 of 39) (Fig. 1A); they represent, in conjunction with similar equipments installed in Asia, about 60% of available facilities (Fig. 1B). If the shaking table properties are concerned, it is worth noting that 1 and 2 DOF are less common than 3 and 6 DOF (Fig. 1C), even if torsional input generally is not used and the corresponding DOFs are employed to ensure the equilibrium of the table and avoid vertical and rotational motions. Referring to Fig.

Tab. 1. The major world seismic simulation facilities.

	Institution	Payload (tons)	Area (m^2)	DOF
1.	Aichi Institute of Technology (Japan)	136.1	11.0x6.0	1
2.	Ansaldo Meccanica Nucleare (Italy)	6.3	3.5x3.5	3
3.	Building Research Institute (Japan)	18.13	3.0x4.0	3
4.	CEA (France)	90.72	6.0x6.0	3
5.	ENEA (Italy)	9.07	4.0x4.0	6
6.	Fujita Corporation (Japan)	25	4.0x4.0	1
7.	Hazama Corp Ltd. (Japan)	80.0	6.0x4.0	3
8.	Hitachi Engineering Corp (Japan)	20.0	4.0x4.0	1
9.	Hydroproject Research Institute (Russia)	45.36	6.0x6.0	3
10.	Enel. Hydro S.p.A.; busines unit ISMES (Italy)	15	4.0x4.0	6
11.	Kajima Corp Ltd. (Japan)	45.5	5.0x5.0	6
12.	KFA Juelich (Germany)	22.7	5.0x5.0	3
13.	Korea Institute of Machinery and Metals, (Korea)	27.22	4.0x4.0	6
14.	Kumagai-Gumi Corp Ltd (Japan)	63.50	5.0x5.0	6
15.	Kyoto University (Japan)	13.6	5.0x3.0	6
16.	Laboratorio Nacional de Engenharia Civil (Portugal)	36.29	5.6x5.6	3
17.	NASA (Alabama)	0.907	3.0x4.5	6
18.	National Research Institute of Agriculture Eng. (Japan)	45.4	6.0x4.0	3
19.	National Research Institute for Earth Science and Disaster Prevention (Japan)	1088	6.0x6.0	3
20.	National Technical University (Athens, Greece)	9.07	4.0x4.0	6
21.	National Center for Res. in Earthquake Eng. (Taiwan)	27.21	5.0x5.0	6
22.	Nishimatsu Construction Corp (Japan)	NA	5.5x5.5	6
23.	Nuclear Power Engineering Corporation (Japan)	907.18	15.0x15.0	2
24.	NYK Corporation (Japan)	20	2.6x2.6	6
25.	Obayashi-Gumi Corporation (Japan)	45.35	5.0x5.0	3
26.	Public Works Research Institute (Japan)	272.15	8.0x8.0	6
27.	Sanryo Heavy Industries Corporation (Japan)	90.7	6.0x6.0	3
28.	Shimizu Corporation (Japan)	20	4.0x4.0	3
29.	Taisei Corp Ltd (Japan)	20	4.0x4.0	2
30.	Tobishima Corp Ltd (Japan)	20	4.0x4.0	3
31.	Tonji University (China)	13.6	4.0x4.0	2
32.	University at Buffalo (USA)	50	3.6x3.6	5
33.	University of California at Berkeley (USA)	45.36	6.1x6.1	6
34.	University of California at San Diego (two tables) (USA)	32.66	3.0x4.9	1
35.	University of Nevada at Reno (two tables) (USA)	45.36	4.3x4.5	2
36.	University of Illinois at Urbana-Champaign (USA)	4.5	3.7x3.7	1
37.	University of St. Cyril and Methodius (Macedonia)	36.28	5.0x5.0	3
38.	U.S. Army Civil Engineering Research Lab (USA)	45.36	3.6x3.6	3
39.	Wyle Laboratories (USA)	27	6.1x6.1	2

1D, the distribution of specimen masses can be considered; data show that commonly specimen mass of about 20-30 ton are assumed as satisfactory, even if a more recent trend, especially in Japan, leads to enlarge the specimen mass up to 1000 tons. However, the system E-Defense under development at Kobe National Research Institute for Earth Science and Disaster Prevention is a 6 DOF with a very large number of actuators that can ensure high levels

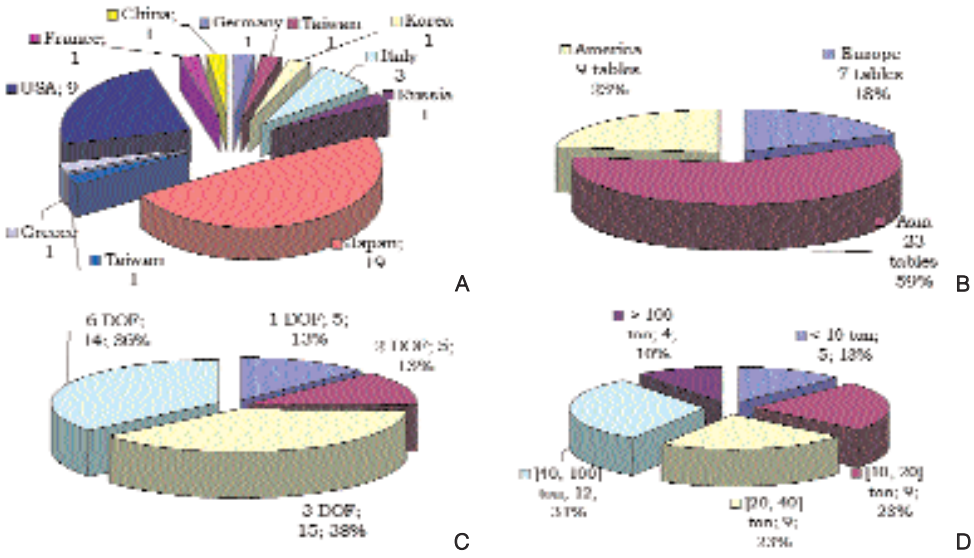

Fig. 1. Review of major world seismic simulation facilities.

of overturning moments. Conversely, limited is the specimen mass when 2 or 3 DOF systems are concerned, since reaction force act on mechanical or special restraints, that can become too expensive and complex when very high reaction forces have to be managed. European data, finally, do not reflect scientific interest and social relevance of seismic risk problem, due to the limited number of installations and the lack of integration.

The AMRA project for shaking table seismic lab

The AMRA project of the shaking tables seismic simulation Lab starts from this background and is based on some clear and simple concepts: modularity; maintainability; innovation and safety; transportability and integration. The main feature of the system is avoiding the disadvantages of some existing shaking table facilities with medium specimen mass (20-30 ton): large reduction factors for specimens and inability to simulate long span infrastructures and buildings with specific reference to asynchronous ground motions.
This is why a multiple biaxial shaking table system, analogous to the University of Reno – Nevada US (Fig. 2A), has been chosen and principles of flexibility and modularity common to other NEES project sites, i.e. Multi-Axial Subassemblage Testing (MAST) Laboratory at University of Minnesota, Fig. 2B, have been adopted. The system fits the requirements of National integration of facilities (Fig. 3) and is relocatable and reconfigurable. The two tables can be set to produce a single biaxial table shaking in the two horizontal directions

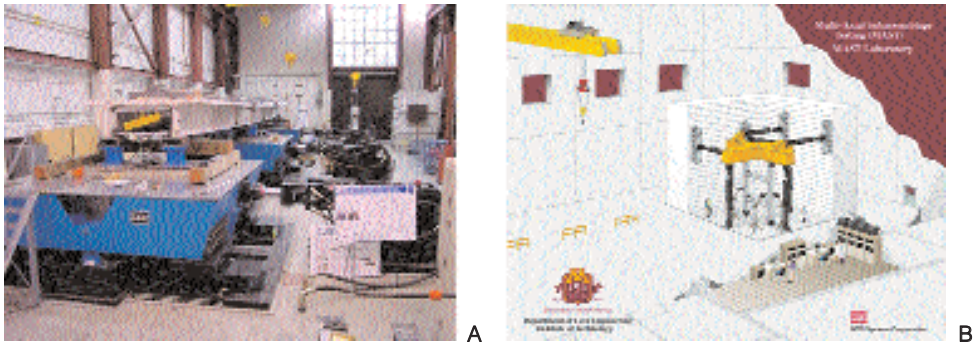

A B

Fig. 2. US NEES facilities under development: shaking tables at University at Reno, Nevada [1] (A) and Multi-Axial Subassemblages Testing (MAST) [3] (B).

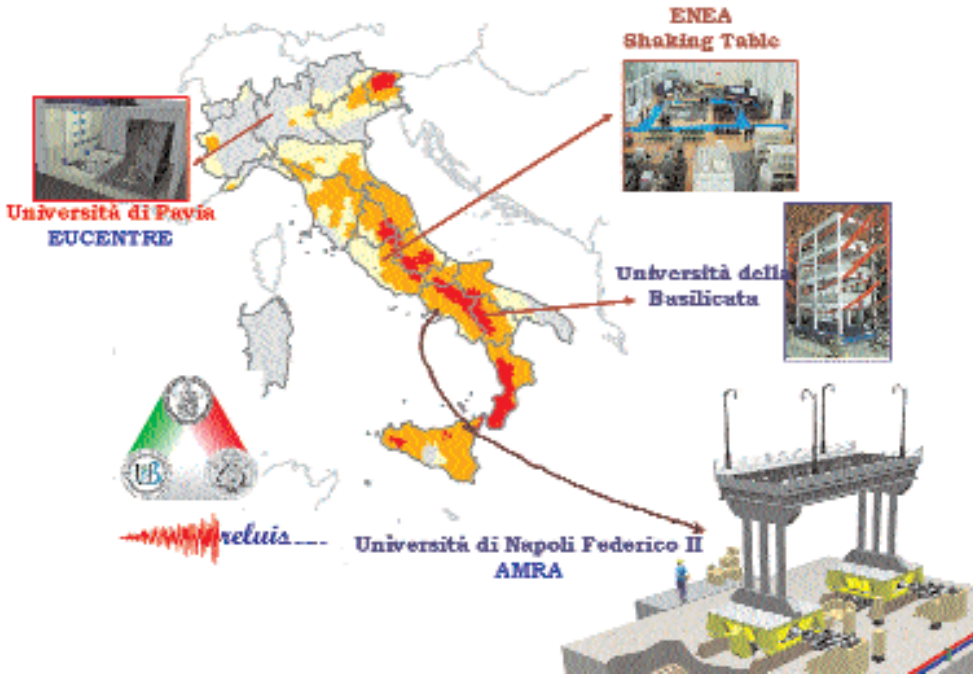

Fig. 3. AMRA shaking table program and National facilities integration.

or to reproduce asynchronous seismic inputs controlling each table separately. They can be constrained to act together as a single large table, or can be operated individually with independent motions. The maximum specimen mass will be around about 20 ton and the tables 3 meters by 3 meters wide. This equipment will also operate in the frame of Reluis consortium, that is schematically described in Fig. 3. It consists of the Network of Academic Seismic

Engineering Laboratories and has been funded by University of Naples "Federico II", University of Pavia, University of Basilicata, Potenza and promoted by Italian Emergency Management Department. Its mission is to manage activities of Seismic Labs giving scientific, technical, administrative and financial support and promoting the participation of members to scientific and technological activities related to Seismic Engineering, in compliance with national and international research programs. Its experimental facilities will cover both pseudodynamic, static and dynamic testing capabilities. AMRA shaking tables will be furthermore integrated with ENEA Casaccia and EUCENTRE (Pavia) ones; the latter will be designed to bear large masses and reach high values of velocity and is a SDOF system (base shear greater than 2000 kN, velocity 1.5 m/sec).

REFERENCES

1. University of Nevada Reno, Bridge Research and Information Center: *http://bric.ce.unr.edu*
2. NEES Consortium Inc.: *www.nees.org*
3. University of Minnesota, MAST: *http://nees.umn.edu*
4. Earthquake Engineering Research Institute, EERI: *www.eeri.org*
5. National Research Institute for Earth Science and Disaster Prevention, E-Defense program: *www.bosai.go.jp/sougou/sanjigen/index.htm*
6. French CW, Schultz AE, Hajjar JF, Shield CK, Ernie DW, Dexter RJ, Du DH-C, Bergson PM. A System for Multi-Axial Subassemblage Testing (MAST): Design Concepts and Capabilities. Paper No. NS-1a. *Proc. of the 7th National Conference on Earthquake Engineering*, Boston, 2002.
7. Crewe AJ, Severn RT. The European collaborative programme on evaluating the performance of shaking tables. *Phi.l Trans. R. Soc. Lond. A.* 359:1671-96, 2001.

SPACE project: shaking table tests on a steel building prototype equipped with magnetorheological dampers

M. Spizzuoco, A. Occhiuzzi, G. Serino

Dipartimento di Analisi e Progettazione Strutturale, Università degli Studi di Napoli "Federico II", Napoli, Italia

Introduction

The implementation of semi-active control systems to protect building and bridge structures subjected to strong external excitations such as large earthquakes [1, 2], is the object of several research efforts both from theoretical and experimental perspective. A semi-active control device is obtained by providing to a passive device the ability to be "smart", i.e. to self-adjust its own mechanical properties in real time according to properly selected control algorithms. The latters represent the operational logic driving the device's instantaneous behaviour according to the structural response and/or the external dynamic excitation. The modification of the device's parameters allows a semi-active control system to produce a temporary variation of the stiffness and/or damping characteristics of the structure in order to maximize the dissipated energy and eliminate the possibility of resonance. The available scientific literature has not yet given answers on some fundamental questions: the type and complexity of the equipment to be adopted in the experimental tests, the practical things still to be made to bring a semi-active control system outside of a lab for real-life applications, and the effective improvement in the reduction of the structural response associated to semi-active control systems compared to their passive counterparts. To the aim to contribute to the solution of the above questions, this paper describes the experimental campaign designed so as to verify the efficacy of a properly manufactured semi-active control system based on magnetorheological (MR) dampers for a steel structure. In the general view of the recently investigated semi-active devices, MR dampers can effectively materialize the concept of time-varying damping device: they are characterized by the possibility of continuously varying the intensity of the magnetic field inside its body by using low-power electrical currents, so that a wide range of physical behaviours can be commanded to the device.

Experimental set-up of tested structure and analysis of experimental results

The experimental campaign performed on a steel frame mock-up equipped with a semi-active bracings system (Fig. 1A), has been one of the main objects of the EU funded SPACE (Semi-active and PAssive Control of the dynamic behaviour of structures subjected to Earthquakes, wind and vibrations) research project (5th FP, 1998-2002). It has been carried out by using the 6-DOF Multi Axes Shaking Table for Earthquake Reproduction located at the Structural Dynamics Testing Laboratory of ENEL.Hydro – ISMES (Bergamo, Italy).
The semi-active "smart" bracings system has demonstrated to be quite effective to help such a kind of structure to resist lateral forces [3]. It is made up by three parts: an elastic brace, a semi-active device representing the time-varying damping element linking the brace to the hosting structure, and a control algorithm [4]. In the framework of the SPACE research project, the semi-active MR dampers (Fig. 1A) have been designed and manufactured by the German firm Maurer Söhne (Munich), and experimentally tested to characterize their passive and semi-active operation [5]. The shaking table, used for the experimental tests on the controlled MISS structure, has been driven only along the transversal direction X of the frame (Fig. 1B). Two different data acquisition systems have been utilized for the acquisition of the structural response and for the control system. The scheme in Fig. 1B shows the experimental set-up of the building, i.e. the position of the most significant transducers on the shaking table and on the structure, whereas Tabs. 1 and 2 list, respectively for the structural response and the control system, the channels acquired during the experiments, the instrumentation used and the measured

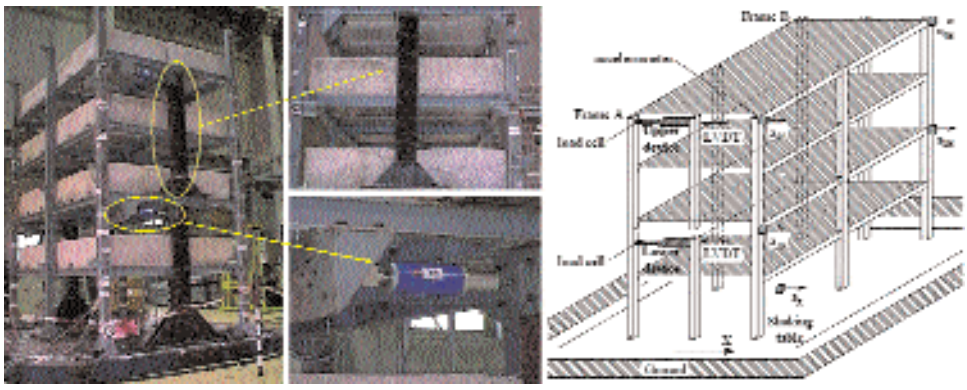

Fig. 1. Tested structure. A. Elastic brace and MR damper. B. Experimental set-up.

Tab. 1. Sensors for the response acquisition: acquisition channels, transducers and measured physical quantities.

Channel	Transducer	Physical quantity acquired
ATx, ATy, ATz	Accelerometer	Accelerations of shaking table
A1÷A12	Accelerometer	Accelerations of the floors (X and Y directions)
R1x	LVDT	2nd floor displacement relative to the shaking table
P1, P2	Voltage transd.	Voltage commanding the upper and lower devices
C1÷C4	Current transd.	Current supplied to the devices
LD1÷LD4	LVDT	Relative displacement in the dampers
FD1÷FD4	Load cell	Axial force on dampers piston

Tab. 2. Sensors for the control system: acquisition channels, transducers and measured physical quantities.

Channel	Transducer	Physical quantity acquired
AT	Accelerometer	Acceleration of shaking table
AC1÷AC4	Accelerometer	Accelerations of the floors (X direction)
LD1÷LD4	LVDT	Relative displacement in the dampers
FD1÷FD4	Load cell	Axial force on dampers piston

physical quantities. A specific electronic hardware and software (Fig. 2A) has been acquired for the semi-active operation of the MR dampers. They consist of a real time National Instruments CPU (Pentium III, 850 MHz), two digital acquisition boards (DAQ boards) with a total of 16 inputs and 4 outputs (16 bits resolutions and 333 kHz sampling rate), the environment Labview Real-Time, and four operational power supplies (model BOP 50-4M) from Kepco Inc. (New York, USA). Four different structural configurations have been investigated for the seismic tests: an uncontrolled, or unbraced, configuration (i.e. without MR dampers), a "passive off" control configuration (i.e. no control signal provided to MR dampers), a "passive on" (rigid link) control configuration (i.e. a constant 2.5 A current provided to MR dampers), and a semi-active control configuration (i.e. a time-varying current input signal feeds the MR dampers according to the algorithm). Fig. 3, relative to the second (N-S) component (Northridge) recorded in 1994 at Sylmar County Hospital parking lot (California), show the experimental results, in terms of peak 2nd floor relative displacement and peak 4th floor absolute acceleration, for all the control configurations and the input levels. First of all, for any given earthquake and amplitude level, both displacements and accelerations in the "passive off" configuration are reduced with respect to the uncontrolled case, not shown in the Fig. 3. Comparing "passive off" and "passive on" cases, the latter condition corresponds to a more rigid structure, resulting in higher accelerations

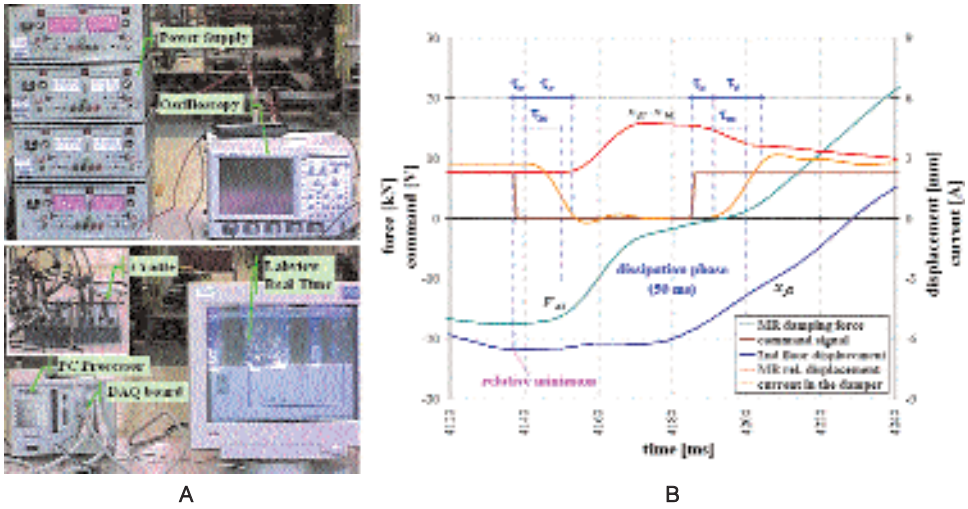

Fig. 2. Electronics for semi-active tests and semi-active operation in test under Northridge -6 dB.

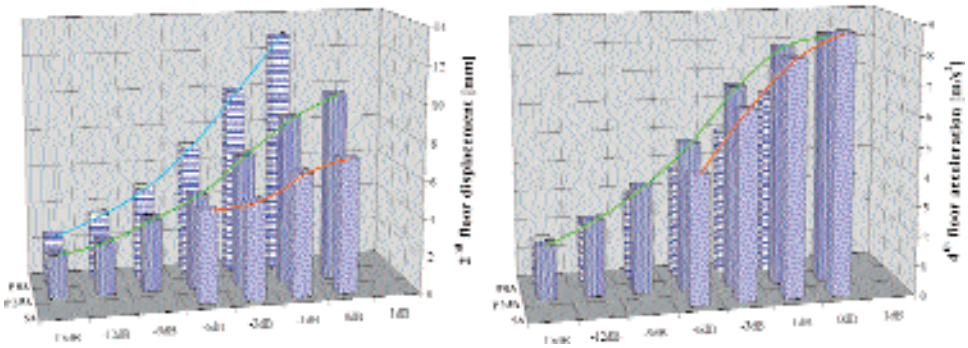

Fig. 3. Tolmezzo: relative displacement of the 2nd floor and absolute acceleration of the 4th floor.

and lower displacements. However, in the semi-active configuration, the recorded displacements are recognized to be reduced of about 30% ÷ 40% with respect to the "passive on" case, whereas the maximum accelerations appear very close to those recorded in the rigid link configuration [6]. The time delays characterizing the control sequence (acquisition-processing-actuation) of the semi-active bracing system can be described as follows: a time delay of the control electronics τ_e, including, consecutively, the time intervals associated to signal acquisition, to acquired signal processing through the control logic and to operations of the power supply; a time delay of the damper's electromagnetic τ_e, i.e. the time interval starting when the current (in input to the device) begins to change and ending when the current reaches the commanded

nominal value within a ± 5% tolerance; a time delay of the mechanical part of the damper τ_m, i.e. the time interval between the instant when the current (in input to the device) begins to change and the instant when the damper begins to adjust its mechanical behaviour. Fig. 2B shows the promptness of the semi-active MR device through a magnification of some time histories recorded during the seismic test performed under Northridge -6 dB earthquake. The delay τ_c of the control electronics is within 6 ms, the delay τ_e of the electromagnetic circuit is within 13 ms, and the mechanical delay τ_m is within 10 ms, i.e. shorter than the electric delay.

REFERENCES

1. Kobori T. Past, present and future in seismic response control of civil engineering structures. *Proc. of the 3rd World Conf. on Structural Control*, Como, Italy. Wiley, United Kingdom, vol. 1, pp. 9-14, 2002.
2. Nishitani A, Inoue Y. Overview of the application of active/semiactive control to building structures in Japan. *Earth. Eng. and Struct. Dyn.* 30:1565-74, 2001.
3. Serino G, Occhiuzzi A, Spizzuoco M, Seiler C, Fischer O. Semi-active control via MR dampers: algorithms, numerical modeling and prediction of the resulting response of structures. *Proc. of the 3rd World Conf. on Structural Control*, Como, Italy. Wiley, United Kingdom, vol. 2, pp. 1113-8, 2002.
4. Occhiuzzi A, Serino G. Control strategies for semi-active structural control devices. *Proc. of the 3rd World Conf. on Structural Control*, Como, Italy. Wiley, United Kingdom, vol. 3, pp. 641-7, 2002.
5. Occhiuzzi A, Spizzuoco M, Serino G. Experimental analysis of magnetorheological dampers for structural control. *Smart Materials and Structures* 12(5):703-11.G, 2003.
6. Renzi E, Serino G. Testing and modeling a semi-actively controlled steel frame structure equipped with MR dampers. *Structural Control and Health Monitoring* 11, 2004.

Multilevel analysis of existing RC buildings seismic capacity

E. Cosenza, G. Manfredi, M. Polese, G.M. Verderame

Dipartimento di Analisi e Progettazione Strutturale, Università degli Studi di Napoli "Federico II", Napoli, Italia

Introduction

A rational mechanistic based approach for the seismic capacity assessment of classes of buildings is presented and capacity curves in terms of ultimate strength and deformation capacities are derived. The proposed procedure allows to choose the main parameters (morphologic and geometric configuration, mechanical properties, etc.) for response and to evaluate their relative influence on capacity of reinforced concrete (RC) buildings. This evaluation is useful, since it permits, in the framework of vulnerability assessment at a regional or sub-regional scale, to have a measure of results error that is related to the amount of the information available. Consequently, depending on the relative influence of parameters on response, but also considering the different type of parameters and related availability (by public databases for *low order* parameters, or by field survey for *high order* ones), a multilevel building class specialisation in function of input variables is proposed.

Assessment procedure

The steps listed below are summarised in Fig. 1.
1st step is aimed at the evaluation of seismic capacity of buildings R_{LS}. In order to achieve this in the framework of a mechanistic based approach, it is necessary to implement a building "*generation*" process that allow to reproduce a dataset significant for building morphology and structural system. To this end, the choice of a set of representative parameters $\mathbf{X}=(X_1,\ldots X_n)$ is the first step for generation process; secondly the implementation of a simplified mechanistic model, that depends on such X_i,. enables the calculation of $R_{LS}(\mathbf{X})$ for any given LS.
2nd step in the procedure is aimed at the identification of building classes: a building class is identified in function of those parameters **X** that have, on the basis of an engineering judgement, a major effect on mean structural capacity, either in terms of strength or deformation supplies, and are contemporarily

easily obtained by a rapid survey of buildings (i.e. morphologic parameters) or by existing databases (i.e. construction age). Parameters *order* is defined first of all by their *availability level* (external survey, integration with engineering judgement, detailed investigation) and also considering the *relative influence* of input parameters on building response.

3rd step is the particularisation of the input parameters for the *territorial area considered*. It is necessary, in fact, to account for real distributions of parameters X_i on the territorial area studied in order to estimate in a reliable way, using mechanical model implemented in step 1, the capacity $R_{LS}(X)$ for the existing building stock. The consequent definition of different response surfaces of the seismic capacity in function of the input parameters sets, allows the determination of the major or minor influence of parameters on response. This back-analysis permits to check and/or integrate the definition of parameters *order*, formerly introduced in step 2.

4th step is the calculation of capacity curves for building classes evaluating the probability of attaining fixed levels of strength or displacement capacity. This calculation can be performed adopting a Montecarlo simulation technique or other equivalent methods.

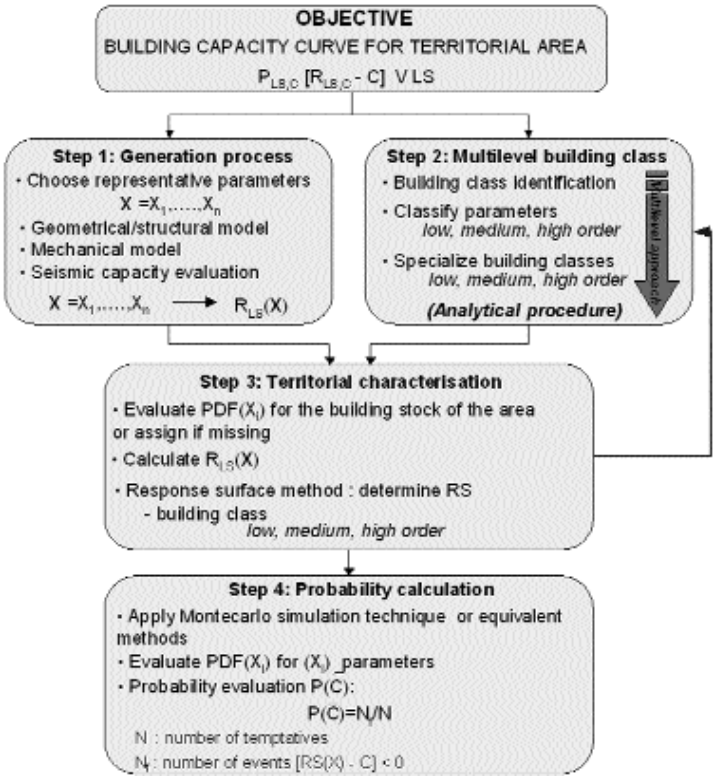

Fig. 1. Assessment procedure.

Building generation

The generation process of a building model follow the steps listed below:

1. *Definition of geometric/structural model.* Structural model identification depends on the choice of a number of parameters that allow the clear definition of morphology, dimensions and structural mesh-grid of the building. In Fig. 2 such process is summarised. In fact, starting from base footprint and linear measures of the base plant and the height of the building, morphology (rectangular shape, L shape, etc.) and dimensions (Lx, Ly and Lz for a rectangular shape) are established (morphology definition in Fig. 2). Adopting a three-dimensional mesh in the tree main directions x, y and z (height), then, it is possible to explicitly locate the number of bays in x and y direction (n_x and n_y for a rectangular shaped building), and the number of floors in elevation n_z (three-dimensional mesh definition in Fig. 2). Number and location of beam/column elements are determined intersecting the three-dimensional mesh joints with the existing plane frames in both directions; moreover, thanks to the explicit introduction of mesh module amplitude in both horizontal directions, it is possible to associate to each element a suitably defined influence area for gravity loads.
2. *Elements design.* In order to proceed with elements design, i.e. to determine elements transverse section and steel reinforcement, a number of rules affecting the entire design process have to be established, as illustrated in Tab. 1.

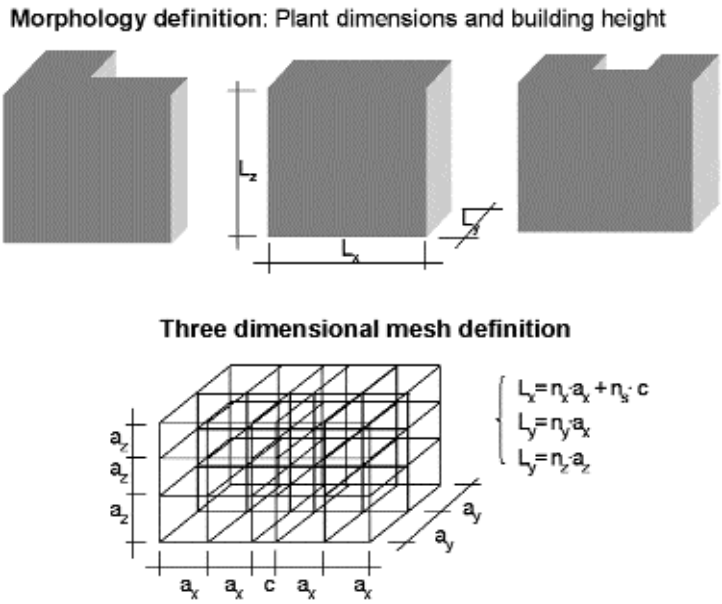

Fig. 2. Definition of geometric/structural model.

Tab. 1. Design rules.

MODEL BUILDING (localization, year, codes)	Gravity load design	Seismic design
loads	- accidental loads - elevation distribution - etc.	- seismic loads value - elevation distribution - etc.
models	Columns *axial load (influence area)* Beams *continuous beam*	Shear type frames Beams *(bending moment)* Columns *(bending moment under axial load)*
codes	- material: allowable strength - minimum reinforcement - detailing based on codes of practice	- material: allowable strength - minimum reinforcement - detailing based on codes of practice

EVALUATION OF SEISMIC CAPACITY

Once the building model derived from the geometric/structural generation process is defined it is possible to proceed with its mechanical characterization; in particular three main steps are developed:

1. mechanical characterisation of the structural elements;
2. establishment of a number of pre-defined collapse mechanisms;
3. calculation of the capacity parameters representative of global seismic behaviour.

Flexural element's behaviour is determined for yielding and ultimate limit states; hence it is defined by a bilinear representation of bending moment-curvature, M-ϕ, relationship (Cosenza et al., 2004).
Adopting a number of predefined collapse mechanisms for the building model it is possible to determine corresponding bending moment distribution for the elements that are in the inelastic range, and to evaluate, by simple equilibrium rules, global seismic capacity for fixed limit states.
The definition of a prefixed collapse mechanism and the knowledge of yielding and ultimate curvatures allow to evaluate yielding θ_y and ultimate θ_u rotation for the elements:

$$\theta_y = \frac{\phi_y \cdot L}{6}; \quad \theta_u = \theta_y + \theta_p = \theta_y + l_p \cdot (\phi_u - \phi_y); \quad l_p \quad 0.5\left(\begin{matrix} M_u & M_y \\ & M_u \end{matrix}\right) L$$

where ϕ_y and ϕ_u are yielding and ultimate curvatures of the element's transverse section, L is the element's length and l_p is the linear dimension of the plastic region within the element.

In particular three different typologies of collapse mechanism of frames under horizontal forces are considered, as shown in Fig. 3. This way capacity parameters are easily determined; as example, for mechanism 1 (the first to the left in Fig. 3) base shear and top displacement, and the relative base shear coefficient and top displacement are:

$$V_{b,1} \quad \frac{\sum M_c^k + \sum_k^n \sum M_b}{\sum_k^n H_i \cdot (H_i \quad H_{k-1})} \quad ; \quad \sum_1^n H_i \quad \Delta_{n,1} \quad \theta_n \cdot (H_n \quad H_k) + \gamma_1$$

Starting from base shear and top displacement the base shear coefficient and global drift can be determined for each considered i-th mechanism:

$$C_{b,i} = \frac{V_{b,i}}{W} \qquad (drift)i \quad \frac{\Delta_{n,i}}{H_n}$$

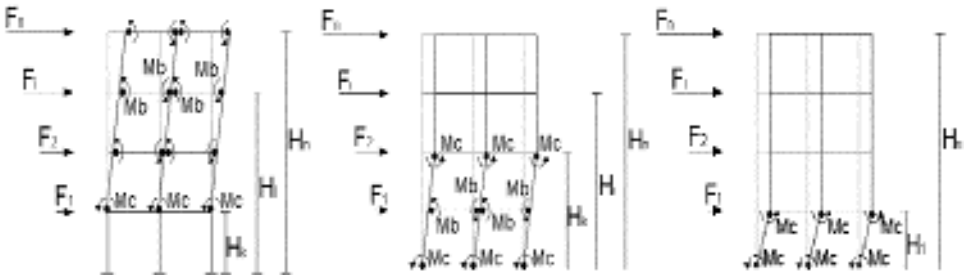

Fig. 3. The pre-defined collapse mechanisms.

The multilevel analysis

Following the generation process of the building dataset, the relative availability of model parameters is easily determined (Tab. 2).

In order to evaluate the relative influence of parameters on response, a possible way to proceed is to find an interpolation response surface RS(**X**) in function of **X** and to study the variation of predictive capability in function of the input variables; this sensitivity analysis allows to specialise building classes in different order levels, as explained in the flowchart of Fig. 4.

The sensitivity analysis performed considering the macro class of moment resisting frames, rectangular shaped, non seismically designed buildings (GLD constructions) shows that the most important parameter to define a class is the number of storeys and that the parameters availability has a good correspondence with the relative influence on capacity; hence low medium and high order class specialization is obtained.

Tab. 2. Parameters and relative availability.

MODEL PARAMETERS		AVAILABILITY	
geometric	*Morphology* *Global dimensions (Lx - Ly - Lz)*	*- Plano-volumetric survey* SURVEY FORM	Low order
structural	nx, ny = *number of modules (X, Y)* nz = *number of modules (Z)* Nv = *number of stairs* Nt = *number of resisting frames*	SURVEY FORM	Medium order
mechanic	*Minimum reinforcement* *Detailing* *Materials*	*- Codes* *- Manuals* *- Mechanical characteristics* DATABASE	High order

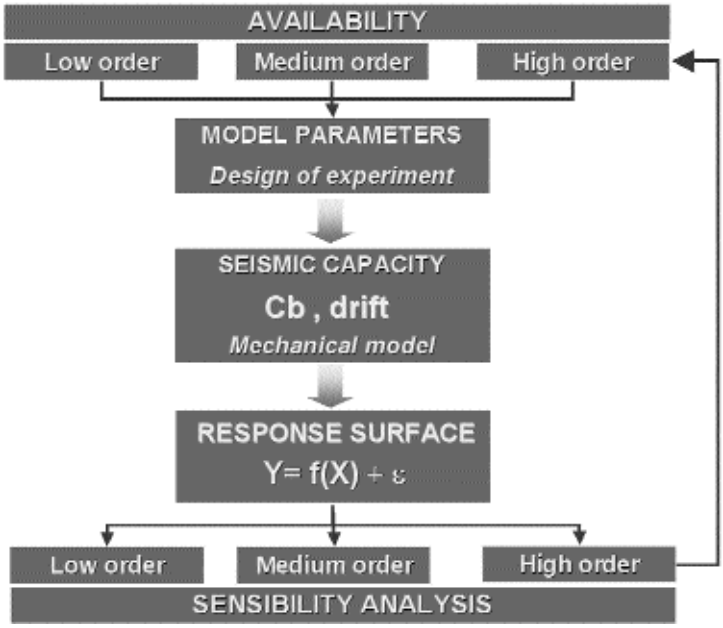

Fig. 4. Multilevel analysis procedure: sensibility analysis for low, medium, high order parameters.

Adopting the response surface derived for each class of buildings, capacity curve for such class may be found. In Fig. 5 the capacity curves (median and median ± the average error) in terms of C_b and $drift_u$ for 3 storey building class are shown. In particular, the three levels of class specialization (low, medium and high) are considered, showing the variation of results (error reduction) depending on the knowledge level of the built environment. Analogous results are shown in Fig. 6 for 6 storey building class.

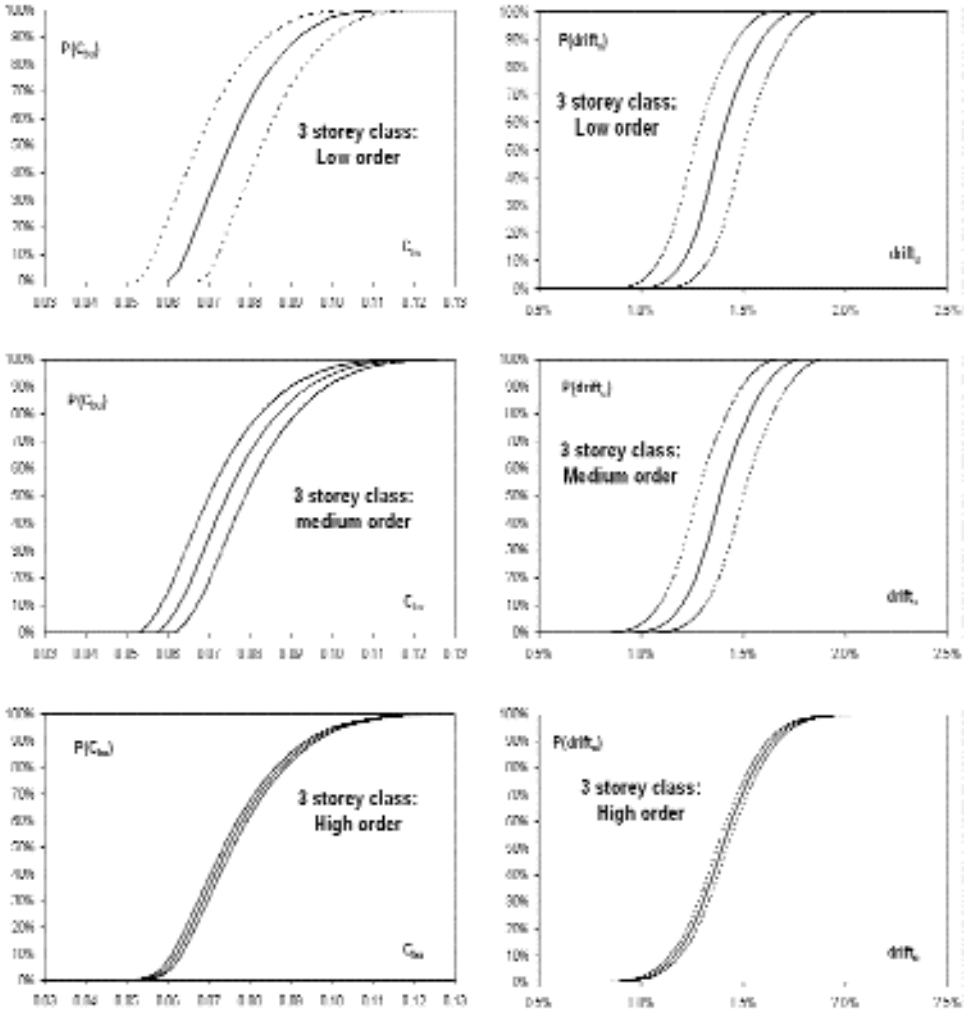

Fig. 5. Three storeys building class capacity curves in terms of C_{bu} and $drift_u$ for low, medium and high order parameters specification; in each graph curve corresponding to determined *RS* and to RS±μ RMSE are shown.

REFERENCES

Calvi GM. A displacement based approach for vulnerability evaluation of classes of buildings. *Journal of Earthquake Engineering* 3(3):411-38, 1999.

Cosenza E, Manfredi G, Polese M, Verderame GM. A multilevel approach to the capacity assessment of existing r.c. buildings. Submitted to *Journal of earthquake engineering*, 2004.

Fib. *Displacement based seismic design of reinforced concrete buildings*. Bulletin n. 25, State of art report prepared by Task Group 7.2, 2003.

Fib. *Seismic assessment and retrofit of reinforced concrete buildings*. Bulletin n. 24, State of art report prepared by Task Group 7.1, 2003.

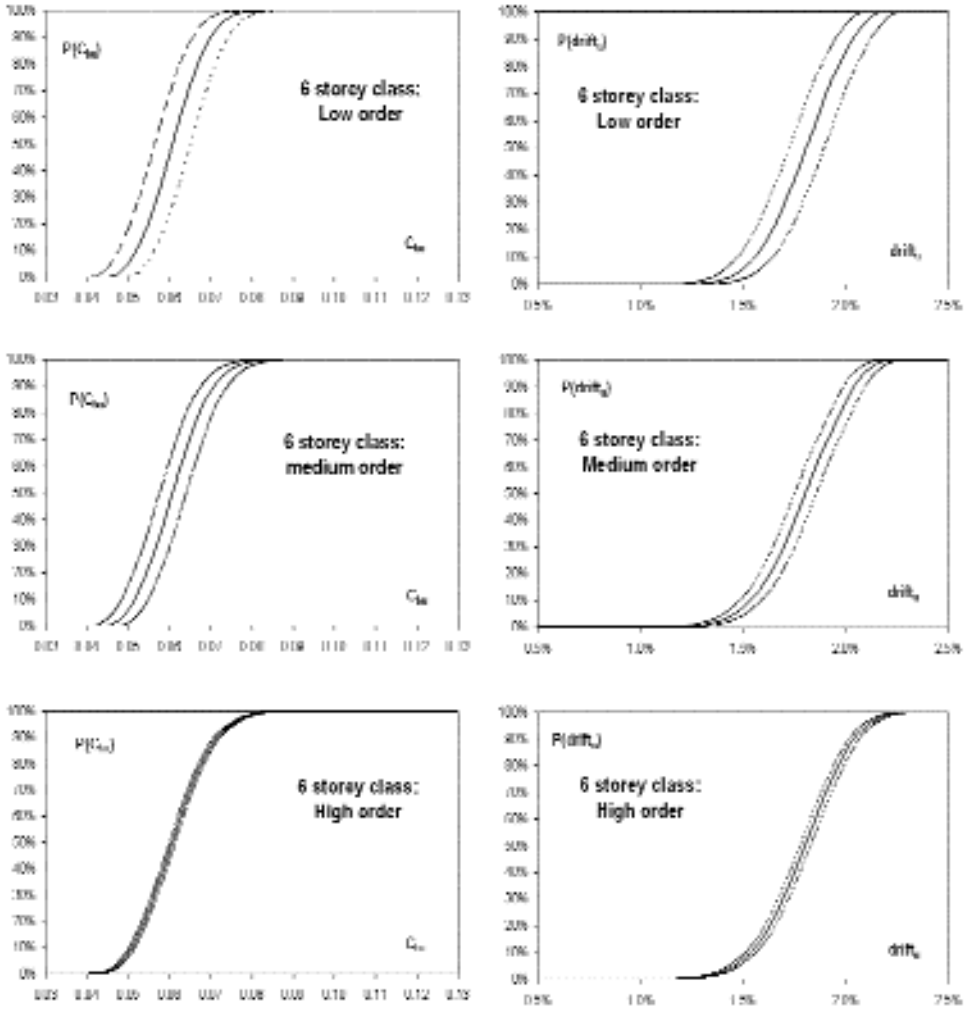

Fig. 6. Six storeys building class capacity curves in terms of C_{bu} and $drift_u$ for low, medium and high order parameters specification; in each graph curve corresponding to *RS* and to *RS*±μ *RMSE* are shown.

Ordinanza n. 3274 del Presidente del Consiglio dei Ministri 20/03/2003 "Primi elementi in materia di criteri generali per la classificazione sismica del territorio nazionale e normative tecniche per le costruzioni in zona sismica". *G.U.* 08.05.03.

Polese M, Verderame GM, Manfredi G, Cosenza E. Simplified models for vulnerability analyses of r.c. buildings at a territorial scale. *XI National Italian conference on earthquake engineering*, 2004, Genova, 2004 (in Italian).

Verderame GM, Stella A, Cosenza E. Le proprietà meccaniche degli acciai impiegati nelle strutture in c.a. realizzate negli anni '60. *X Convegno Nazionale "L'Ingegneria Sismica in Italia"*, 9-13 settembre 2001, Potenza e Matera, 2001.

Verderame GM, Manfredi G, Frunzio G. Le proprietà meccaniche dei calcestruzzi impiegati nelle strutture in cemento armato realizzate negli anni '60. *X Convegno Nazionale "L'Ingegneria Sismica in Italia"*, 9-13 settembre 2001, Potenza e Matera, 2001.

Seismic assessment of existing buildings made of precast members

G. Magliulo, G. Fabbrocino, G. Manfredi, E. Cosenza
Dipartimento di Analisi e Progettazione Strutturale, Università degli Studi di Napoli "Federico II", Napoli, Italia

Introduction

Rehabilitation and seismic upgrading concerns a large number of existing precast structures: many constructions are located in areas recognised to be exposed to seismic risk after erection. Development of specific procedures for the estimation of seismic vulnerability of existing precast structures represents a key step not only when relevant structures are concerned, but also when rehabilitation and functional re-planning of large urban areas have to be carried out. The related problems are:
1. definition of mechanical and geometrical properties of the members;
2. assessment of reinforcement;
3. review of available data;
4. development of refined structural analyses.

Existing industrial precast structures: data collection, structural systems and connections

A review of existing data has been carried out in order to define mechanical and geometrical properties of the members, type and characteristics of reinforcement and devices used for connections and mutual restraints of components. To this aim a large number of companies that operate from a long time all over Italian country have been interviewed for data acquisition; they are listed in Tab. 1. Common structural solutions and techniques have been identified, so that a group of structures that can be addressed as representative of classes of industrial buildings has been collected in Tab. 2.
A classification of the existing precast structures can be based on the layout of the main horizontal members: full web main beam (I, Y, W, T shapes with constant or variable depth), reticular main beam, arch (1. arch with tie, pin connected to the columns; 2. rigid frame, with arch shaped beam; 3. arch without tie, fixed restrained) (Fig. 1). The adopted structural systems were: straight elements, frames parts (1. frames with 3 hinges, 2. "lambda" system) and one piece frames

Tab. 1. Interviewed companies.

Company	Precast Structures manufacturer	Reinforcement manufacturer	Design Engineering / Consultancy Office	Location
Aquila Prefabbricati	■			Torre Annunziata (Naples)
BARACLIT	■			Arezzo
Consorzio Generale Cantieri "Varese"	■			Milan
DLC			■	Milan
DYWIDAG		■		Milan
Edilgon	■			Orte (Viterbo)
FREYSSINET		■		Milan
Galasso Prefabbricati	■			Pisa
GECOFIN	■			Verona
Gianese	■			Rome
IMEC	■			Sorrento (Naples)
Magnetti Larco Building (Larco Astori)	■			Bergamo
Manini Prefabbricati	■			Assisi (Perugia)
Pizzuti Prefabbricati	■			Crotone
Pomi			■	Milan
Pre.Mer.	■			Capua (Caserta)
RDB	■			Piacenza and Bellona (Caserta)
SINTEC	■			Bari
Truzzi Prefabbricati	■			Mantova
Zecca Prefabbricati	■			Sondrio e Teramo

Tab. 2. Some of the analysed existing industrial precast structures.

Location	Year	Column net [m]	Beam	Roof element	Connection
Marcianise (Caserta)	1973	24x5	Reticular beam (Fig. 3)	Tiles	
Terni	1988	18x6	Arch beam	Hollow flat blocks	
Torni	after 1976	17,45x7	Constant cross-section beam	Tiles	Neoprene bearing
Aversa (Caserta)	1973	12x12	Constant cross-section	Sheds	Neoprene bearing + pin (Fig. 4)
Caserta	1973	10x5,5	Reticular beam	Sheds	Double layer of ternobit
Ronchi dei Legionari (Gorizia)	1968	16x16	Ω beam (Fig. 5)	Sheds	Neoprene bearing
Ronchi dei Legionari (Gorizia)	1988	16x5	Double slope beam	Curved roof panels	Neoprene bearing

(span < 12 m) (Fig. 2). Concerning the materials the steel is characterised by seven wire strands and high strength bar (fsy > 700 MPa) and the concrete by fck > 35 MPa. The mild reinforcement has fsy > 320 MPa and the concrete fck > 25 MPa. The column-foundation connections are characterised by pin connections, which emulate the solutions adopted for steel constructions or by precast socket footings for fixed connections, which are currently used. The beam-roof elements

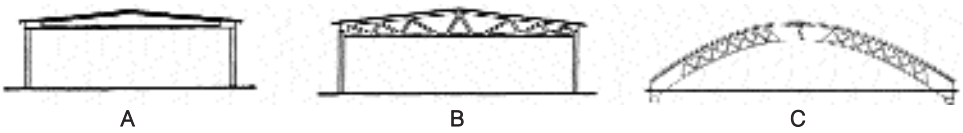

Fig. 1. Full web main beam (A), reticular main beam (B), arch (C).

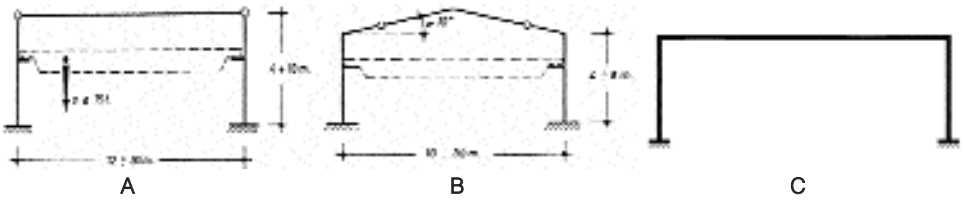

Fig. 2. Structural systems: straight elements (A), frame parts (B), one piece frame (C).

connections are strongly dependent by the structure used for the roof. In the case of flat or double slope roofs, they are characterised by bolted L shaped metallic plates; in the case of shed elements, by pins jutting out of the beam or tongues coming out of the shed. The beam-column connections (Fig. 3) can be classified on the base of the support elements (when used): 1. reinforced mortar bearing (thickness > 1.5-2.0 cm), 2. rubber or synthetic resin bearing, 3. two metallic plates anchored in the concrete, 4. hard lead plate between two metallic sheets.

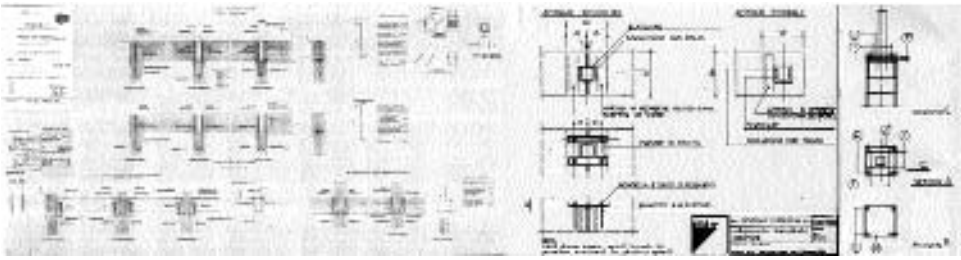

Fig. 3. Beam-column connections made by IMEC.

Case studies: buildings characteristics and vulnerability evaluation

Some precast industrial buildings, properly identified as representative of class of structures built in the reference period, are analysed. Elastic analyses are carried out by SAP2000 program in order to estimate the building internal forces and the modal shapes, using a space model of each building (Fig. 4). On the same buil-

dings non linear "push over" analyses are performed in order to determine the bi-linear capacity curves; such curves are calculated considering the same energy at the mechanism point (Fig. 5). In Tab. 3 the evaluation by spectral analysis of the reference buildings vulnerability is reported. In the first column is cited the refe-

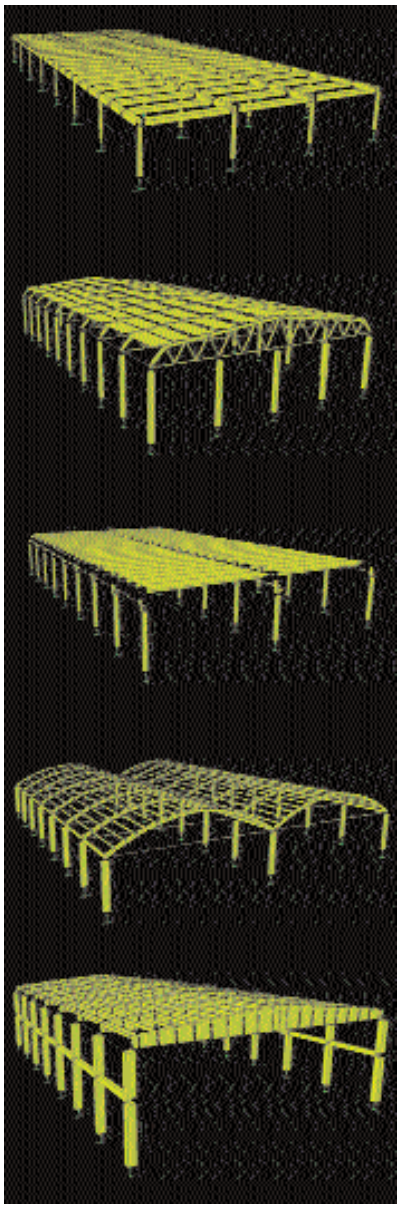

Fig. 4. Reference build: A, B, C, D, E.

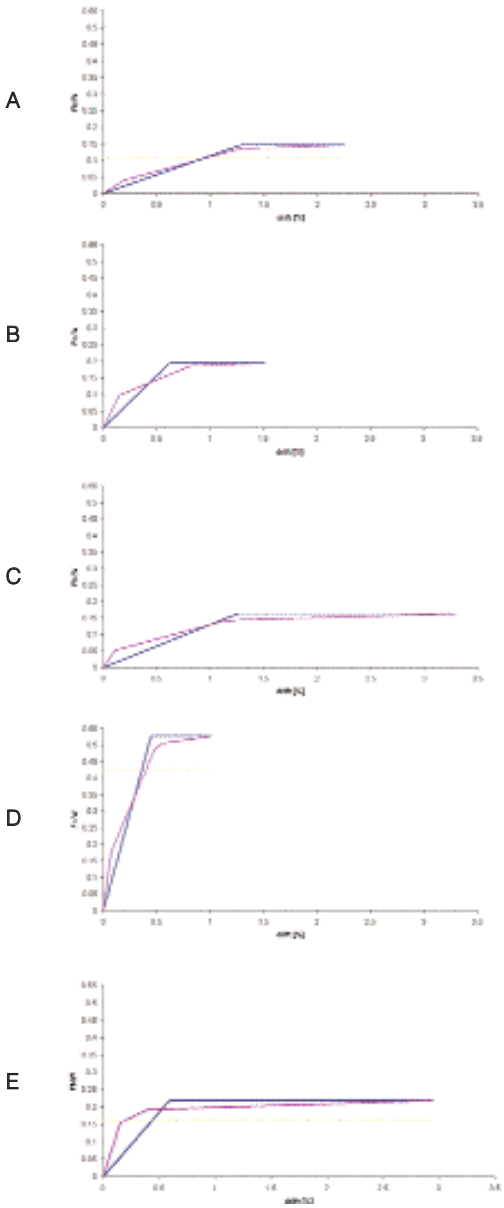

Fig. 5. "Push-over" and bi-linear capacity curves of reference buildings as ordered in Fig. 4.

Tab. 3. Spectral analyses results.

	T [sec]	Sae(T) [g]	Capacity [g]	ρ	Duc. dem.	Av. duc.	Collapse?
A	1.74	0.21	0.15	1.42	1.42	1.76	NO
B	1.00	0.35	0.19	1.80	1.80	2.43	NO
C	1.59	0.23	0.19	1.18	1.18	2.61	NO
D	0.45	0.60	0.53	1.15	1.16	2.24	NO
E	0.89	0.41	0.22	1.88	1.88	4.97	NO

rence structure, in the second the period of the equivalent system, which is the one characterised by an elastic – perfectly plastic relationship computed as already said. In this vulnerability evaluation, the demand is represented by the elastic EC8 spectrum for a soil having medium mechanical characteristics (C type) and peak ground acceleration PGA = 0.21, which, as aforesaid, is determined on the base of a fixed probability to be overpass in the reference site: in the third column the ordinate of this spectrum corresponding to the equivalent system period is shown. The ratio between this and the capacity of the equivalent system, reported in the following columns, gives the parameter ρ, which by relations depending on the period of the equivalent system, allows to compute the demanded ductility. The available ductility is assumed as ratio between the maximum displacement and the yielding one of the equivalent bilinear curve: it is observed that in the examined cases, for the assumed level of the seismic and action if the effectiveness of connections can be assured, the availability is always larger than the demand.

References

1. CENSIS. *33° "Rapporto sulla situazione sociale del paese 1999", Territorio e Reti*. CENSIS Centro Studi Investimenti Sociali, pp. 347-448, 2000 (in Italian).
2. Koncz T. *Manuale della prefabbricazione*. Tecniche Bauverlag, Milano, 1962 (in Italian).
3. *Il laterizio – Bollettino tecnico RDB*. Piacenza, years 1956, 1959, 1962, 1965, 1968, 1971-74 (in Italian).
4. Cestelli Guidi G. *Cemento armato precompresso: teoria, esperienze, realizzazioni*. Hoepli, Milano, 1970 (in Italian).
5. Marioni A. *Apparecchi d'appoggio per ponti e strutture*. ITEC Editrice, 1968 (in Italian).
6. Prakash V, Powell GH, Campbell S. *DRAIN-2DX, base program description and user guide*, Nov. 1993.
7. Cosenza E, Manfredi G, Verderame GM. Seismic assessment of gravity load designed r.c. frames: critical issues in structural modeling. *Journal of Earthquake Engineering* Vol. 6 Special Issue 1, 2002.
8. European Committee for Standardisation. *Eurocode 8: "Design of structures for earthquake resistance"*. Draft version, May 2002.
9. Pampanin S. Seismic design of precast concrete buildings. *Elite* 3, 2001.
10. Posada M, Wood SL. Seismic performance of precast industrial buildings in Turkey. *7th National Conference on Earthquake Engineering (7NCEE)*, Boston, 2002.
11. Scawthorn C. (ed.). *MCEER, The Marmara, Turkey earthquake of August 17, 1999: Reconnaissance report*. University of Buffalo, New York, 2000.

Studies on the seismic zonation of the city of Benevento

F. Santucci de Magistris, A. d'Onofrio, S. Sica
Dipartimento di Ingegneria Geotecnica, Università degli Studi di Napoli "Federico II", Napoli, Italia

Introduction

The "Benevento Seismic Risk Project" (BSRP), financed by the European Union, was developed at the beginning of the '90s by a group of geophysicists, geologists and geotechnical engineers to detect the seismic hazard of the city of Benevento in Southern Italy. In the BSRP a preliminary geological and geotechnical structure of the city was determined and a first seismic zonation map was developed on the basis of an assumed seismic scenario [1, 2]. In the late '90s, two further projects (Traiano Project and RSV7 Project) were financed by the GNDT (National Group of Defence against Earthquake) and the Italian Ministry of University through the European Union support. Both projects are aimed at defining a damage scenario for the city of Benevento improving the analyses performed in the past and integrating information from geophysical, geological, geotechnical, urban planning and structural engineering research teams. The operative units cooperate through a Geographic Information System (GIS), which allows the storage of the specific databases and of the synthetic results provided by each task unit. This paper accounts for the progress made in evaluating the seismic hazard of the city of Benevento from the geotechnical engineering viewpoint, focusing the attention on the role of the surface soils in modifying seismic motion propagating from bedrock to ground level.

Site description and soil characterization

The city of Benevento rises on a hill dominating the confluence of the Calore and Sabato rivers. The city subsoil is essentially made of a Pliocenic clay formation covered by coarse alluvial mixed to fluvial clayey deposits (the so-called Ariano unit). The Pliocenic clay formation, whose top ranges from tens of meters (Sabato river valley) to hundreds of meters below the ground level (Calore river valley and the Benevento hill) was often assumed as a bedrock in the site response analyses described in the reminder of the paper. The city historic centre lies on a hill made of a Pleistocenic (Rissian) conglomeratic formation,

overlying the pliocenic clay. Towards the S-E side of the hill, fluvio-lacustrine deposits (the so-called Cretarossa unit) overlay the conglomerate formation. The Cretarossa succession consists of silty and clayey layers with polygenic and heterometric clasts in a sandy matrix. Debris and colluvial deposits deriving from the disintegration of the rissian conglomerates and/or remoulding of Phlegrean and Vesiuvian pyroclastic materials, are finally present along the hill slopes of the city. In the Sabato and Calore river valleys terraced alluvia are present. The alluvial materials of the Sabato river are found along the western marginal areas of the hill, where they overlay the Rissian conglomerates.
Throughout the whole urban territory, man-made grounds, including large masonry blocks and archaeological ruins, are present. As it will be underlined later, these materials might strongly influence the seismic response of the studied area.
The geotechnical characterization of the soils in the urban area was achieved integrating data published in the BSRP with new information provided by recent literature and local administrations.
236 boreholes were carefully analyzed and relevant geotechnical data properly stored in the GIS. Quantitative definition of all soil parameters needed for detailed seismic response analyses was obtained in 19 verticals only. In such verticals, any soil layer was characterized by its total unit weight, shear stiffness and damping ratio, including their initial value (G_0 and D_0) and their variation with the shear strain level ($G(\gamma)$ and $D(\gamma)$). The decay of the stiffness with shear level was summarised through a modified Ramberg-Osgood (R-O) model as reported in Santucci de Magistris et al. (2004). A summary of geotechnical soil properties for the lithological units found in the city of Benevento, not including the shear wave velocity, is given in Tab. 1.

Simplified seismic zonation

It is well-known that zonation of ground motion can be achieved using a three-level approach that varies according to the scale of the problem in hand [3]. Grade 1 zonation, that is a general zonation, can be achieved collecting information available in literature and in historical documentation. This approach is the simplest and the lowest-cost and it is suitable for studying very large areas. Grade 2 zonation is that adopted by the Italian building code (OPCM 3274, 20.03.2003) and the Eurocode 8 that is now in preparation [4]. Please notice that such codes are aimed at detecting seismic forces on building rather than giving 2 zonation, that is a detailed zonation, improving the previous approach, increasing the amount and typology of information without significantly increasing the costs. Finally, Grade 3 is a rigorous zonation that is performed in the range of 1:25.000 to 1:5.000, using specific site investigations that are usually incorporated into computer codes.
The first attempt in zonation of the city of Benevento was performed following a grade 2 approach, that was carried out using correlations between shear

Tab. 1. Geotechnical characterization of materials constituting the Benevento subsoil.

Soil type		D_s (%)	λ_s (%)	γ_r (%)	Non linear parameters	
					C	R
Man-made ground	Shallow MG-s	5	0.001	0.01	403407	2.38
	Deep MG-d	4	0.003	0.03	51877	2.38
	Masonry MG-m	0.5	0.01	0.1	8794	2.38
Debris colluvium	Fine DC-f	5	0.0029	0.0971	562510	2.61
	Coarse DC-c	7.5	0.0005	0.0017	3290207	3.00
Pyroclastites PI		1	0.001	0.01	67810	2.38
Recent alluvium RA		2	0.001	0.01	403407	2.38
Terraced alluvium	Dense TA-d	1	0.002	0.02	16/956	2.38
	Cemented TA-c	0.5	0.01	0.1	8794	2.38
Fine fluvio lacustrine	Shallow FL-f	5	0.005	0.05	4/955	2.38
	Intermediate FL-i	4	0.005	0.05	47510	2.38
	Deep FL-f	3	0.005	0.05	4/955	2.38
Coarse fluvio lacustrine	Shallow FL-c	1	0.007	0.07	107970	2.38
	Intermediate FL-c	1	0.002	0.02	16/956	2.38
	Deep FL-c	1	0.007	0.07	107970	2.38
Ilissian conglomerate	Weathered IC-w	1	0.005	0.042	32508	2.60
	Cemented IC-c	0.5	0.02	0.2	7041	2.38
Pliocenic clay	Shallow AP-s	3	0.01	0.1	38271	2.38
	Deep AP-d	2	0.01	0.1	8794	2.38

wave velocity profiles and response spectra at the ground level under free-field condition. This approach is included in several national building codes, counting the recent indication on methods for seismic zonation. Referring here to Eurocode 8, shear wave velocity profiles can be summarized by the equivalent $v_{s,30}$ value that is defined as:

$$v_{s,30} = \frac{30}{\sum_{i=1}^{N} \frac{h_i}{v_i}} \tag{1}$$

where h_i and v_i denote respectively the thickness and the shear wave velocity of the i-th formation or layer existing in the top 30 meters. A single vertical can be classified into one of the five EC8 categories according to the $v_{s,30}$ value; a normalized response spectrum is associated to each category. The horizontal elastic spectrum can be obtained once the design acceleration on a stiff ground a_g is established. Such acceleration for the city of Benevento was established by the OPCM 3274 to be equal to 0.25 g.

Fig. 1 shows a map of the city of Benevento. In this map each dot corresponds to the location of the before mentioned 19 verticals; numbers represent the $v_{s,30}$ values and labels indicate site category according to the EC8. It can be observed that $v_{s,30}$ spans from 333 m/s to 853 m/s but it is mostly concentrated around 500 m/s. The majority of the sites belongs to the class B, only one to class A and three to C category. We can conclude that in the whole

urban area of Benevento, site effects are not relevant, since an almost homogeneous distribution of acceleration response spectra was obtained. This statement was not confirmed from subsequent detailed zonation analyses.

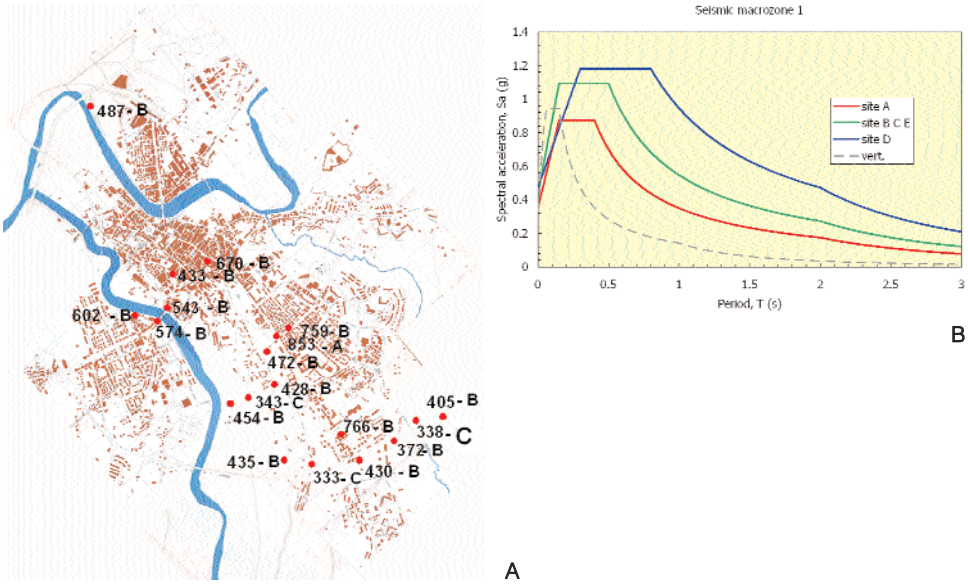

Fig. 1. A. Distribution of $v_{s,30}$ (in m/s) and site classification according to EC8 for the city of Benevento. B. Response spectra for the different site class.

Detailed zonation

Detailed zonation of the seismic response for the city of Benevento was obtained using the EERA code [5]. This code operates in the frequency domain and assumes that soil behaves as a continuous 1-phase equivalent linear material. This code uses the same algorithm employed in the well-known Shake program. Geotechnical soil properties are those reported in the previous paragraph. A single earthquake scenario was employed for the zonation, that is the 1688 Sannio earthquake.

Input motion

According to the Catalogue of Strong Italian Earthquakes [6], 1688 Sannio earthquake had maximum intensity I_{max} = XI, magnitude M = 6.72 with the epicentre located about 40 km NNE of Benevento. This earthquake was simulated by the seismological team trough three set of 150 synthetic seismograms

for the three components of the motion. Synthetic seismograms are assumed to be representative of the input motion at the bedrock level. NS component, that has a slightly larger average PGA value, was employed in the subsequent analyses. Fig. 2A shows the acceleration response spectra for the all seismograms, while Fig. 2B, and 2C respectively show the values of the PGA and the Arias intensity together with their average values and the standard deviation.

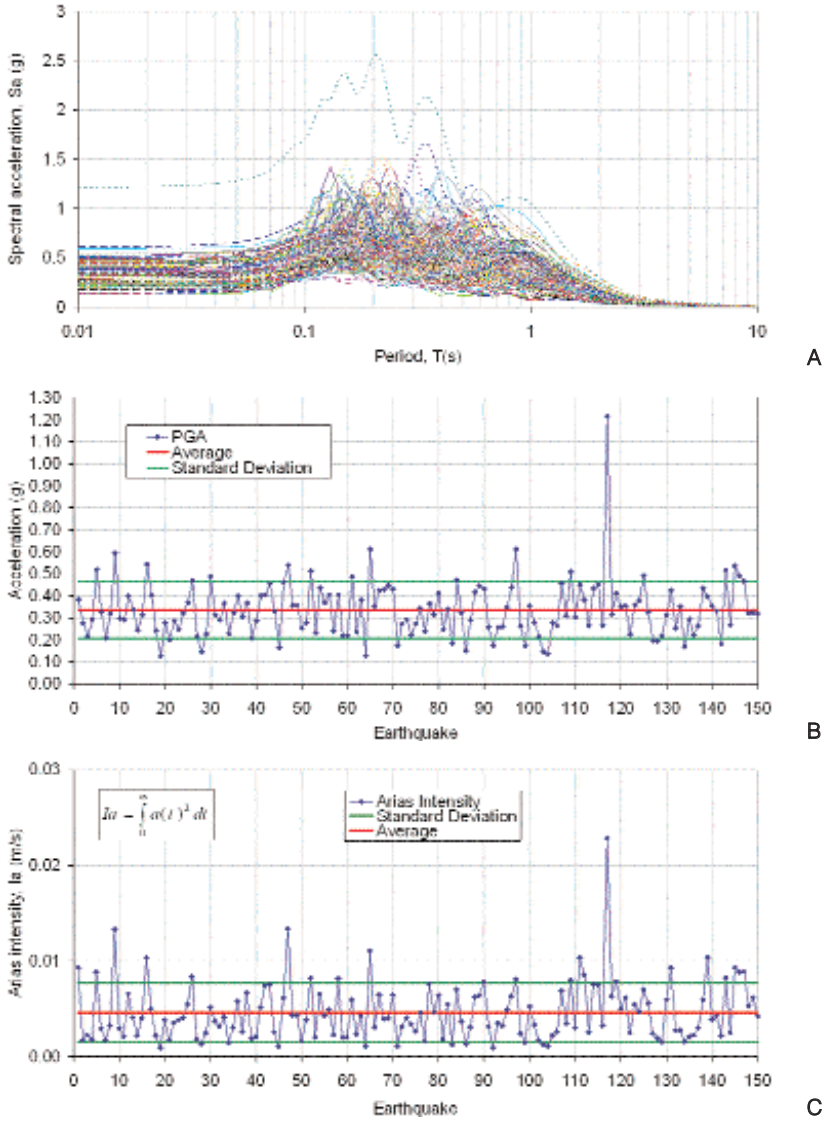

Fig. 2. Response spectra, Peak Ground Acceleration and Arias intensity for the synthetic seismograms representative of the 1688 Sannio earthquake.

Tab. 2 summarises average and standard deviation values for some parameters relevant for the NS component of the synthetic seismograms. Readers can refer to Kramer [7] or Cosenza and Manfredi [8] for the meaning of the parameters.

Tab. 2. Numerical parameters from the NS component of synthetic seismograms.

Ground Motion Parameter	Input sismico Nord-Sud	
	Media	Dev ST
Maximum acceleration PGA (g)	0,33590	0,12899
Maximum relative velocity PGV (m/s)	0,00549	0,00211
Maximum relative displacement PGD (m)	0,000499	0,000182
Arias intesity (m/s)	0,0046	0,0031
aRMS (g)	0,1270	0,0518
Trifunac duration (sec)	1,581	0,390
Characteristic intensity	0,0573	0,0301
Maximum Spectral Acceleration (g)	0,889	0,300
Maximum Spectral Velocity (cm/s)	69,798	27,464
Spectral acceleration at 0,3 s (g)	0,594	0,248
Spectral acceleration at 1 s (g)	0,376	0,175
Fattore di Cosenza e Manfredi ID	15,311	4,379
PGA PGV	61,222	0,141

Analyses results

To reduce computation time, a criteria was established to avoid performing 150 seismograms times 19 vertical analyses to get seismic response for the city of Benevento. It was first noticed that representative numerical parameters extracted from synthetic seismograms (i.e., PGA, PGV or Arias intensity) are distributed according to a Gaussian law. Then, from the whole set of 150 seismograms, a sample of 15 elements was extracted, keeping average and standard deviation values of its representative numerical parameters close of those pertaining to the whole set of data. χ^2 and adaptability tests confirmed the validity of the extracted sample. Finally, numerical analyses were performed in six verticals to obtain seismic motion at the ground level staring from the whole and the reduced set of earthquake bedrock input motion. It was shown that the distribution of the representative numerical parameters and the response spectra obtained in the two cases are very close, thus further confirming the choice.
Figs. 3-5 show distribution in the city of Benevento of the average and the standard deviation values of the PGA, the amplification factor and the Arias intensity as obtained by using the reduced set of input motion, while Fig. 6 shows the average acceleration response spectra. Relevant variation in the seismic motion can be noticed in different part of the city. At least four different

zones can be drawn (Santucci de Magistris et al., 2004) grouping together areas having similar seismic response both in terms of response spectra or representative numerical parameters.

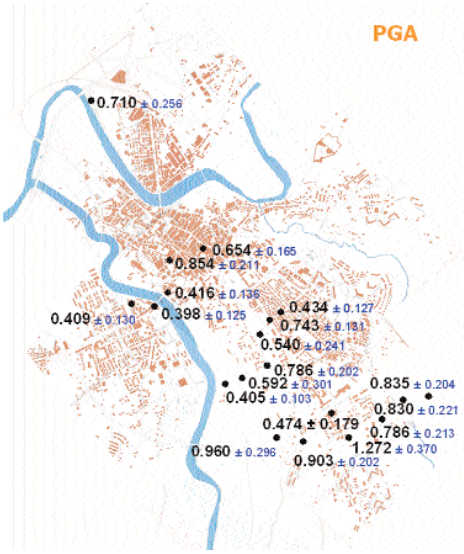

Fig. 3. Distribution of average and standard deviation of the PGA.

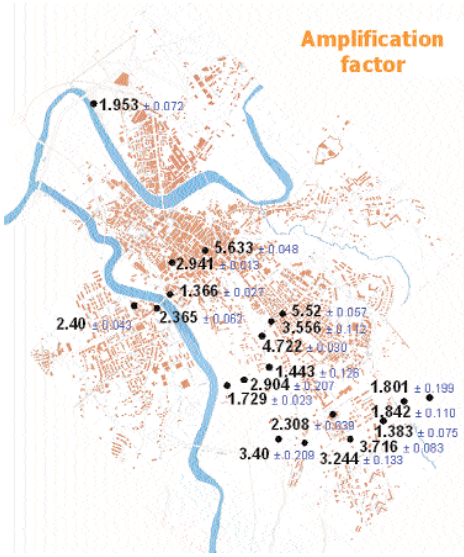

Fig. 4. Distribution of average and standard deviation of the amplification factor.

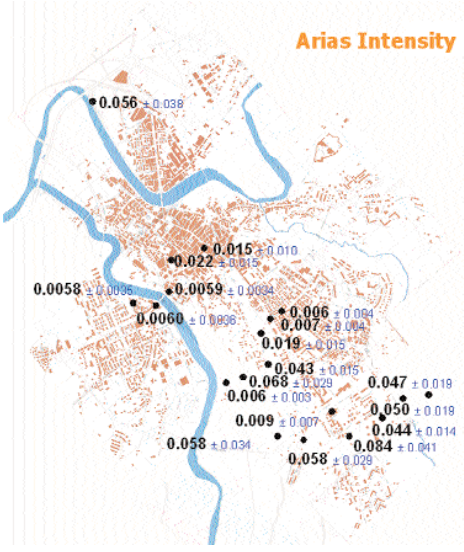

Fig. 5. Distribution of average and standard deviation of the Arias intensity.

A

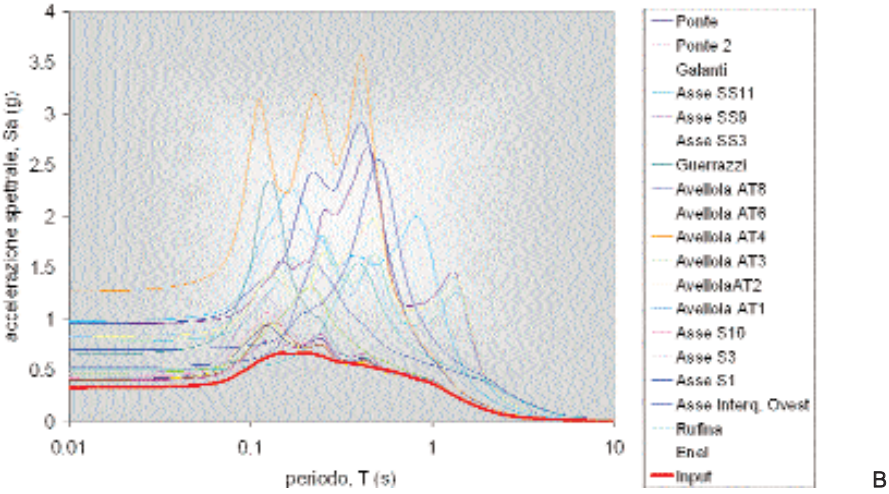

B

Fig. 6. Distribution of response spectra from numerical analyses simulating 1688 Sannio earthquake.

References

1. Marcellini A et al. The Benevento Seismic Risk Project: I – Seismotectonic and geotechnical background. *Proc. V Int. Conf. on Seismic Zonation*, Nice, France, 1995.
2. Marcellini A et al. The Benevento Seismic Risk Project: II – The microzonation. *Proc. V Int. Conf. on Seismic Zonation*, Nice, France, 1995.
3. ISSMGE, TC4. *Manual for Zonation of Seismic Geotechnical Hazards*. Revised Version), The Japanese Geotechnical Society, 1999.

4. CEN. *Eurocode 8: Design of structures for earthquake resistance. Part 1. General rules, seismic actions and rules for buildings*. Draft n. 6, 2003.
5. Bardet JP, Ichii K, Lin CH. *EERA A Computer Program for Equivalent-linear Earthquake site Response Analyses of Layered Soil Deposits*. University of South California, 2000.
6. Boschi E et al. Catalogo parametrico dei terremoti italiani. Available at *www.emidius.mi.ingv.it/CPTI*, 1999.
7. Kramer SL. *Geotechnical Earthquake Engineering*. Prentice Hall Inc., Upper Saddle River, New Jersey, 1996.
8. Cosenza E, Manfredi G. *Index and damage measurement in the seismic design*. National Group of Defence against Earthquakes, Roma, 2000 (in Italian).

Seismic vulnerability aspects of RC buildings in Benevento

M. Pecce[a], M. Polese[b], G.M. Verderame[b]

[a]*Dipartimento di Ingegneria, Università degli Studi del Sannio, Benevento, Italia*

[b]*Dipartimento di Analisi e Progettazione Strutturale, Università degli Studi di Napoli "Federico II", Napoli, Italia*

Introduction

This study is performed in the framework of 2000-2002 GNDT project "Traiano – project for the assessment and the reduction of vulnerability of urban areas". The paper presents some aspects of vulnerability investigation for RC buildings in Benevento town and the preliminary results of the push-over analysis for a single representative building.

Choice of a sample urban area and field survey

In order to perform seismic vulnerability assessment of a building stock it is necessary to have a measure of the quantitative and qualitative characteristics of the built environment. The scope of a field survey is to integrate basic information on buildings made disposable from public databases (Istat data, Census data, etc.), and to collect data on constructions that are necessary to perform the analysis at different levels of detail. Data collected in the field survey are referred to the sample area investigated but are extendible to other areas if there is sufficient homogeneity among them.
The analysis of building stock's characteristics enables a building class identification and the individuation of representative buildings for the class (Fig. 1). Whether for the analysis of the entire class it is necessary to rely on simplified models, the study of single representative buildings can be done using more detailed models; results of detailed analyses for representative buildings are validation and integration for simplified analyses of the building class.
Survey forms are an essential part of field survey since they are a guide and the basic support for the building identification. In Fig. 2 (A, B, C) the form for rectangular shaped buildings is shown. In the viewpoint of a multilevel approach they are organised in a 'multilevel' format; basic information to have a geometric-morphologic identification are contained in the first section (low level section); to collect such kind of information it is sufficient a rapid scree-

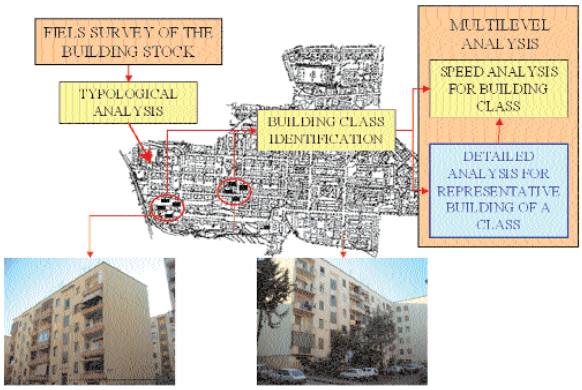

Fig. 1.

Construction age *(changes in Italian seismic code)*	Year ___; period: ante '35 □; '36-'37 □; '38-'62 □; '63-'74 □; '75-'81 □; post '82 □
Plant dimensions	L_y=__ ; L_x=___
Metric data	floor number *n* (total, in and out ground) __; mean inter-story high [m] __; n° of floors with equal inter-story high ____;
Stair structure	r.c. ascending slab □; r.c. beam + cantilever steps □
Elevation irregularity	Soft story No □ Yes□; floor/s if present _____
	Small length columns: Absent □; Present □; Cause if present ____
Use	Total units ___; n° main residence ___; n° secondary resid. __; n° production activity__

Fig. 2A. Survey forms: low level section.

Bay number in x and y direction	n_x=___; n_y=___;
Frame number in x and y direction (stairs excluded)	t_x=___; t_y=___;
Infill position and type	Position: 4 external sides □; 3 external sides □ 2 external sides □; 1 external side □ concrete blocks □; natural blocks □; filled bricks □ bricks with holes □; other ___
Stairs and elevator group	Resisting stairs and elevator group: yes □; no □ Stair number ____; Position (sign on the plant)

Fig. 2B. Survey forms: medium level section.

Min and max bay length [*m*] for x and y frames (first floor)	a_{mn}=__; a_{mx}=__; b_{mn}=__; b_{mx}=__;
First floor column dimensions [*cm*], for at least one x or y frame (or both, if existing) blackening main direction for such frame	blacken main direction and write dimensions
Infill thickness [*cm*]	

Fig. 2C. Survey forms: high level section.

ning from exterior. More details on structural system are in the medium level section, where number of bays in both directions, position of the stairs, etc. are needed; this second section requires a relatively speed inspection from the interior, but allows a structural identification of the system. Third part of the form goes into more details, asking the number and position of plane frames, columns orientations and elements dimensions; it goes towards detailed analysis of a building.

Building typological characterization and sample building identification

The sample area chosen in Benevento is Rione Libertà, the south-east part of which is nearly entirely constituted by RC popular buildings. Benevento town was classified seismically in 1935, thus all RC buildings are designed according to seismic codes. However since that date seismic provisions have been changing several times up to nowadays and the construction rules are funded on an obsolete conception of the structural system; in order to know which codes have been applied for the buildings it is necessary to date back the construction age and frame it in appropriate temporal windows. In Tab. 1 main seismic codes from 1935 to 1975 are represented; note that triangular horizontal distribution was introduced only in 1975 and that from 1937 to 1962, that is a large time window in which most of the buildings in Rione Libertà were built, the horizontal forces were just 5% of the vertical load. In Tab. 2 some results of the building typological analysis are resumed; moreover in Fig. 3 longitudinal and transverse dimensions of rectangular R shaped buildings are plotted, together with the identification of the most frequent dimensional ranges of this morphologic typology. As it can be seen, the data on base plant dimensions of rectangular buildings allow to identify two frequent ranges of variation for transversal and longitudinal dimensions ($B \in [8,12]$; $D \in [14,24]$ and $B \in [8,12]$; $D \in [33,43]$), and representative building should be chosen considering these values. Note that second range ($D>33$) may contain buildings that have a structural connection that cannot be seen from the exterior.

Detailed analysis of representative building

Representative building was chosen based on base plant dimension; the building has 4 storeys in elevation and 2 storeys under ground level. Original project was available, thus material adopted in design, elements dimensions and reinforcement are known (Fig. 4). The building was designed in 1958 according to seismic codes of the time. Regularity of structural system and rigid floor plans allow to model real system with 2D plane frame. Non linear static push-over analysis is performed with program DRAIN 2dx; such analysis

Tab. 1. seismic codes evolution from 1935 to 1975.

	R.D.L. 25 marzo 1935 n°640		L. 22 novembre 1937 n°2202		L. 25 novembre 1962 n°1684		D.M. 3 marzo 1975
	1st category	2nd category	1st category	2nd category	1st category	2nd category	
vertical loads	1,40(g+q)	1,25(g+q)	1,40(g+q/3) if 1,40(g+q/3)>(g+q) otherwise (g+q)	1,25(g+q/3) if 1,40(g+q/3)>(g+q) otherwise (g+q)	1(g+q)	1(g+q)	Static analysis allowed for buildings regular in plant and elevation
horizontal loads	0,10(g+q/3) if (g+q/3)>(g+q)2/3 otherwise 0,10(g+q)2/3	0,07(g+q/3) if (g+q/3)>(g+q)2/3 otherwise 0,07(g+q)2/3	0,10(g+q/3)	0,05(g+q/3)	0,10(g+q/3)	0,07(g+q/3)	
	Constant in elevation						Triangular

Tab. 2. Some results of the building typological analysis.

Investigated parameter	Percentage range
Construction age	60% ante 1962; 37% 1962-1975; 3% post 1975
Plant shape	78% rectangular; 15% L shape; 2% T shape; 5% other
Number of storeys	%-nr. floors: 4%-1; 2%-2; 11%-3; 46%-4; 33%-5; 5%-6
Inter-storey high	1% <3m; 90% 3m; 6% 3-4m; 4%>4m
Mean bay length	11% 3.0-3.9; 53% 4.0-4.9; 31% 5.0-5.9; 4% 6.0-6.9; 1% >6.9

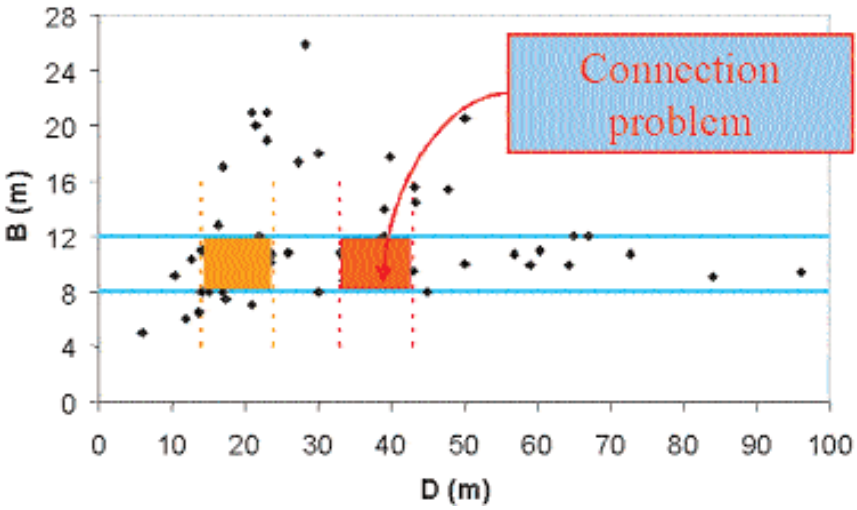

Fig. 3. Dimensional ranges for rectangular shape buildings.

gives reliable results if the structures vibrates essentially in the 1st mode. Structural collapse corresponds to the ultimate rotation of an element of the 3rd floor in elevation. Preliminary assessment is performed applying a modified version of the Capacity Spectrum method CSM, as suggested in (Fajfar 1999). In CSM the capacity spectrum is obtained converting base shear forces and roof displacement of the push-over curve relative to the Multi Degree Of Freedom (MDOF) system, to spectral accelerations and spectral displacements of an equivalent Single Degree Of Freedom (SDOF) system; SDOF capacity is then compared to earthquake demand expressed in acceleration displacement response spectra (ADRS), suitably reduced to account for inelastic

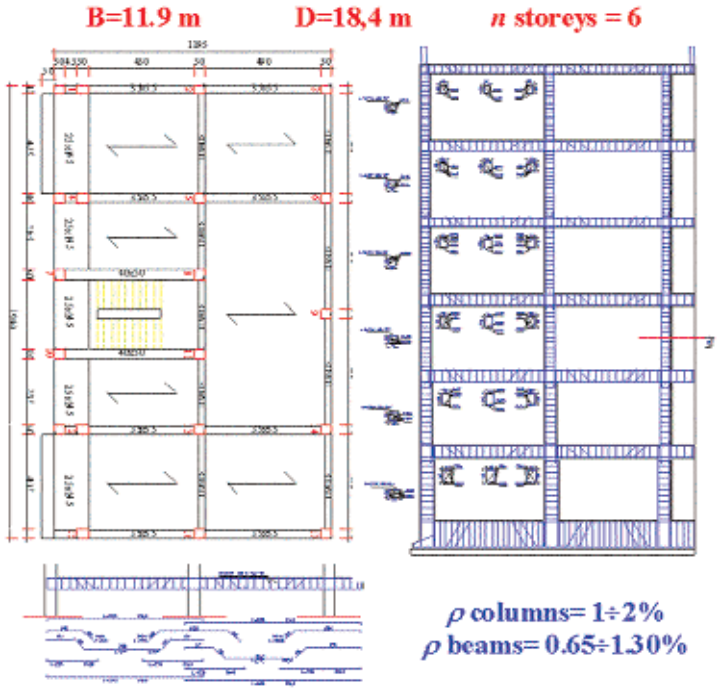

Fig. 4. Sample building: base plant and reinforcement details.

system's behavior. Seismic demand, in particular, is derived starting from a tentative synthetic seismogram derived in the Traiano Project for rock site (PGA= 0.39 g). An ideal elasto-plastic behaviour of the system is considered and the elastic spectrum is scaled on the base of the reduction factor R_μ (eq. (1)) that is found as the ratio of elastic to inelastic strength (Fig. 5).

$$R_\mu = 1 + (\mu - 1)\frac{T^*}{T_C} \tag{1}$$

where μ is ductility demand and T_C represents the threshold period from constant acceleration to constant velocity spectral range. Structural limit state LS thresholds, on the other hand, are evaluated considering a modified version of Park & Ang damage index DM_i for the single structural elements (eq. (2)) (Fajfar et al. 1996) and computing a global weighted value (eq. (3)) for the entire structure.

$$DM_i = \frac{\Theta}{\Theta_u}\left(1 + \beta\gamma^2 \frac{\mu^2}{\mu - 1}\frac{\Theta - \Theta_y}{\Theta}\right) \tag{2}$$

$$DM = \sum_i \frac{M_{yi}(\Theta_i - \Theta_{yi})}{\sum_i M_{yi}(\Theta_i - \Theta_{yi})} DM_i \tag{3}$$

In eq. (2) Θ is the element rotation and Θ_y is the rotation at yield; β is the coefficient of the classic Park & Ang damage functional and γ is a coefficient that represents a normalised form of hysteretic energy (Fajfar 1992). In eq. (3) *i* index refers to the generic i-th structural element, so that Θ_{yi} and M_{yi} are the yielding rotation and moment of the i-th structural element, Θ_i is the current rotation and DM_i its damage index.
In particular three LS are considered: DM<0.2 no damage; 0.2<DM<0.5 repairable damage; DM>1.0 collapse (Cosenza et al 2004b). As it can be seen (Fig. 5), the structure performs at a serviceability limit state for the considered earthquake; a significant role in the system's bearing capacity is played by the high percentage of reinforcements in the vertical and horizontal elements, that appear to be dimensioned and detailed with large margins for safety. However, more investigations are needed before these results may be accepted, especially considering the possible variation in material characteristics.

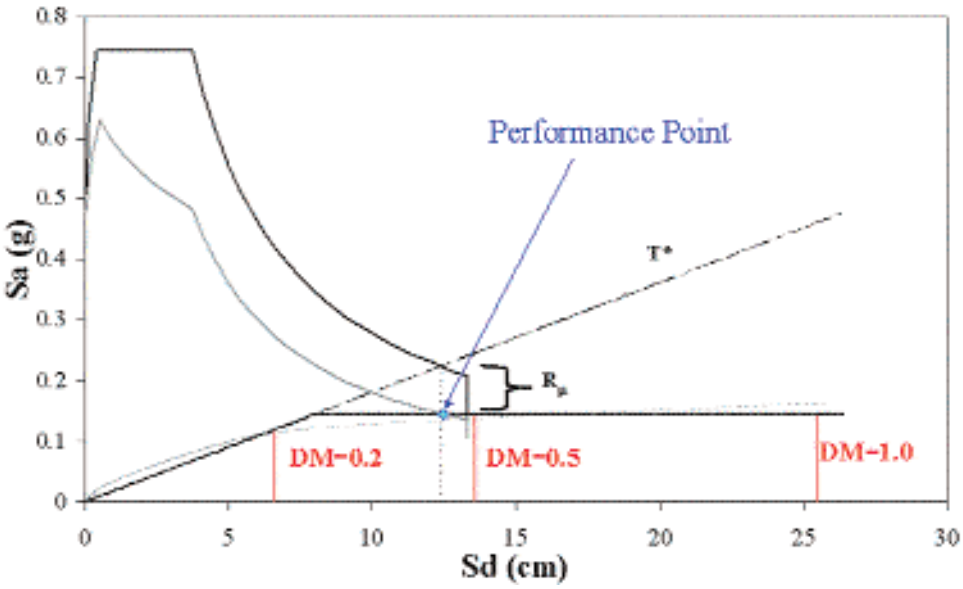

Fig. 5. Capacity Spectrum Method: assessment of structural behaviour for the given elastic spectrum.

References

Cosenza E, Manfredi G, Polese M, Verderame GM. A multilevel approach to the capacity assessment of existing r.c. buildings. Submitted to *Journal of earthquake engineering*, 2003.
Cosenza E, Manfredi G, Polese M. Damage models in the push-over analysis of existing buildings. *XI National Italian conference on earthquake engineering*, Genova, 2004 (in Italian).

Cosenza E, Manfredi G, Polese M. Seismic performance assessment of existing buildings including cumulative damage. Submitted to *Journal of Structural Engineering, ASCE*, 2004.

Fajfar P. Equivalent ductility factors taking into account low cycle fatigue. *Earthquake Engineering and Structural Dynamics* 21:837-48, 1992.

Fajfar P, Gaspersic P. The N2 Method for the Seismic Analysis of RC buildings. *Earthquake Engineering and Structural Dynamics* 25:31-46, 1996.

Fajfar P. Capacity spectrum method based on inelastic demand spectra. *Earthquake Engineering and Structural Dynamics* 28:979-93, 1999.

FEMA 356. *Prestandard and commentary for the seismic rehabilitation of buildings*. Federal Emergency Management Agency, Washington D.C., November 2000.

Fib. *Displacement based seismic design of reinforced concrete buildings*. Bulletin n. 25, State of art report prepared by Task Group 7.2, 2003.

Fib. *Seismic assessment and retrofit of reinforced concrete buildings*. Bulletin n. 24, State of art report prepared by Task Group 7.1, 2003.

Ordinanza n. 3274 del Presidente del Consiglio dei Ministri 20/03/2003 "Primi elementi in materia di criteri generali per la classificazione sismica del territorio nazionale e normative tecniche per le costruzioni in zona sismica". *G.U.* 08.05.03.

Polese M, Verderame GM, Manfredi G, Cosenza E. Simplified models for vulnerability analyses of r.c. buildings at a territorial scale. *XI National Italian conference on earthquake engineering*, 2004, Genova, 2004 (in Italian).

Verderame GM, Stella A, Cosenza E. Le proprietà meccaniche degli acciai impiegati nelle strutture in c.a. realizzate negli anni '60. *X Convegno Nazionale "L'Ingegneria Sismica in Italia"*, 9-13 settembre 2001, Potenza e Matera, 2001.

Verderame GM, Manfredi G, Frunzio G. Le proprietà meccaniche dei calcestruzzi impiegati nelle strutture in cemento armato realizzate negli anni '60. *X Convegno Nazionale "L'Ingegneria Sismica in Italia"*, 9-13 settembre 2001, Potenza e Matera, 2001.

Amplification effects of a site in the city of Salerno

A.L. Simonelli[a], F. Santucci de Magistris[b]

[a]*Dipartimento di Ingegneria, Università degli Studi del Sannio, Benevento, Italia*

[b]*Dipartimento di Ingegneria Geotecnica, Università degli Studi di Napoli "Federico II", Napoli, Italia*

Introduction

Microzonation studies can be typically grouped in three different categories:

1. microzonation of very large areas (regional or urban territories), for which the features of existing or designed buildings are neglected and the site response at the free-field surface is evaluated;
2. local site effect studies in limited area, relevant to buildings under design, for which the structural features of the buildings, and the potential types of foundations, should be taken into account;
3. local site effect for a specific building, already designed or even realized, for which the complete interaction analysis involves the seismic motion at bedrock, the subsoil and the structure.

Depending on the relation between the time of the study and the time of the building construction, the three approaches can be respectively defined as: "*a priori*" microzonation, "*in itinere*" microzonation and "*a posteriori*" analysis. The case studied here is a typical example of the "*in intinere*" microzonation, and put in evidence the important role that such a kind of geotechnical analysis can play in defining the seismic actions on a building structure.

Case under study

In the eastern area of the city of Salerno (Campania region, 50 Km South of Napoli) the New Law Court Buildings are going to be constructed (Fig. 1). It consists of 6 buildings, which have from 6 to 15 floors in elevation, and 2 underground floors; hence the foundation levels lies at -7 m from the ground surface. The project involves a large area, whose subsoil was thoroughly investigated by means of conventional tests, with the aim to characterise the mechanical properties of the soils and individuate the proper foundation typology. The design of the structures was then carried out in the years 2000-2001, computing the seismic forces according to the indications of the current natio-

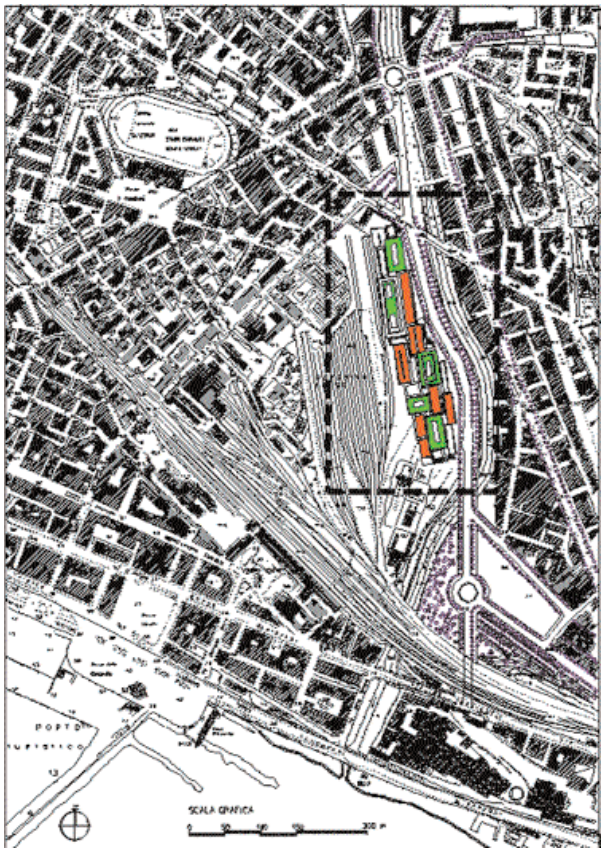

Fig. 1. Location of the New Court Buildings in the city of Salerno.

nal code, which takes into account the subsoil amplification role by means of an oversimplified approach. In particular the Italian Code (D.M. 16.01.1996) provides a foundation coefficient which increases seismic action (coefficient $\varepsilon \geq 1$) when local soil amplification effects are expected. Nevertheless, the application is quite crude, since it is normally assumed ε equal to 1 but for the case of "alluvial deposits (5 to 20 m thick) overlying a stiff soil formation", in which the value 1.3 is assumed.

After the earthquake which struck Molise region (Southern Italy) on November 1st, 2002, the Regional Government has updated Campania seismic classification. According to the new classification of the city of Salerno, seismic forces acting on the Law Court Buildings would seriously increase, and the designed structures would result largely under-dimensioned. Hence, a specific geotechnical study was requested, with the aim to better investigate on the local seismic effects at the design site, and to accurately determine the seismic forces acting on the structures.

Subsoil geotechnical characterization

In the design area a geotechnical investigation had been performed: boreholes, SPT and CPT tests, groundwater measurements, and Down Hole (DH) tests in situ, and usual laboratory tests on undisturbed and partially disturbed soil samples. The stratigraphy (Fig. 2) and the mechanical characterization of the single soil layers was achieved. In particular the shear modulus G_o of the soils at low strain levels was determined through the shear wave velocity values, obtained by DH tests performed from the surface down to a depth of about 30 m, inside the more rigid base formation of Argille Varicolori (Fig. 2). The decay laws of shear modulus G and damping D with strain level were defined on the basis of the results of numerous laboratory tests performed on the same soils.

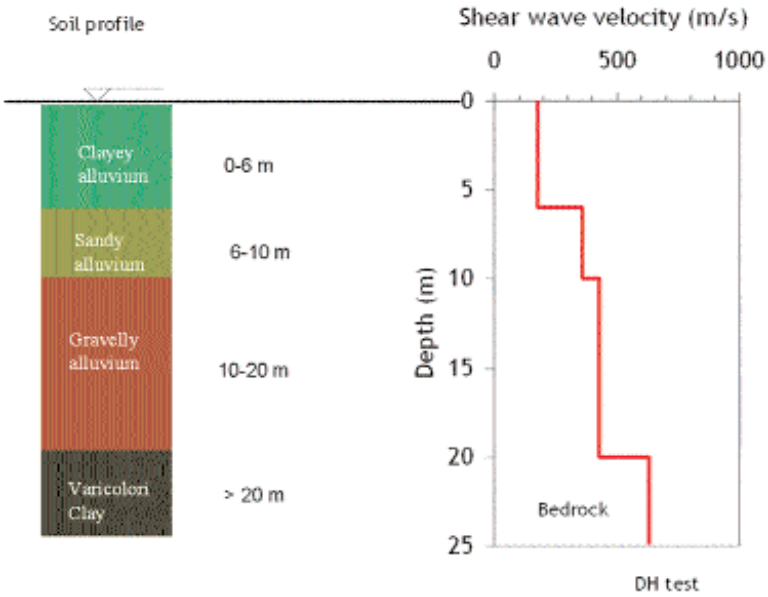

Fig. 2. Main geotechnical units and shear wave velocity profile for the New Court Building site.

Local soil effect analyses

Dynamic analyses of the subsoil behaviour have been performed, with the aim to investigate the local soil effect and eventually validate the simplified approaches proposed by National Building code. The analysis was performed using the EERA code [1], which operates in the frequency domain and assumes that

soil behaves as a continuous 1-phase equivalent linear material. This code uses the same algorithm employed in the well-known Shake code [2], and therefore has its advantages and limits but it has a more convenient user-interface.
The accelerometric time history recorded at Mercato San Severino during the Irpinia 1980 earthquake (Ms=6.9) has been utilised as input motion at the outcropping bedrock. The 1980 event should have a returning period of about 375 years, as evaluated by combining the historical seismicity records for the Irpinia-Lucania area with a recurrence law; as well-known, this earthquake produced considerable effects in Salerno area. The choice of Mercato San Severino seismic motion is mainly due to the fact that this town is located at the same distance of the city of Salerno from the Irpinia 1980 epicenter, as can be seen from Fig. 3. In the same figure the recorded horizontal time-history (NS component), which has the peak acceleration equal to 0.145 g, is also plotted. It is remarkable the long duration of the motion (about 80 s), due to the fact that the earthquake was characterized by three distinct sub-events occurring along different faults, starting at different times. Since Mercato S. Severino recording station is not located above a stiff soil, some site-specific amplification certainly affected the motion coming from the bedrock. Nevertheless the time history recorded at the surface has been utilised as outcropping bedrock motion, such assuming a more severe input. In the first step the seismic motion at a depth of 20 m has been derived by the downward propagation analysis; in the second step this signal has been utilised as the accelerogram at the top of the base formation (Argille Varicolori).

Fig. 3. Seismic input motion utilised for this study.

The seismic wave propagation along depth has been investigated. In particular Fig. 4 illustrates the acceleration time history at the bedrock level (-20 m from the ground surface), at the foundation level (-7 m) and at the ground surface. The amplification of the seismic motion moving from the bottom to the top of the site is clearly shown by this figure, in which the variation of the maximum horizontal acceleration (PGA) with the depth is also plotted. It can be seen that the signal amplification mainly concentrate in the top subsoil layer (about 6 m in thickness), that is characterized by very low shear wave velocity values. The same conclusion can be derived by the analysis of the signal propagation in the frequency domain, comparing the Fourier spectrum of the acceleration time history at the bedrock outcrop, with those at level -7 m and at the ground surface. Moving from the stiff base to the ground, the seismic signal is practically unmodified for frequencies lower than 3 Hz. As regards larger frequencies, at the foundation level the signal is slightly amplified only between 3 and 4 Hz, while for frequencies larger than 4.5 Hz it even de-amplifies. On the contrary at the ground level the signal amplification is not negligible for frequencies larger than 3 Hz; actually the dominant frequency is about 3.8 Hz. This behaviour is summarised by the spectral amplification ratios plotted in Fig. 5: at the ground surface some amplification factors larger than 2 are measured in a frequency range spanning from 3 to 6 Hz, while the amplifications are lower outside such frequency range (the peak amplification value is 2.4 for the frequency component 4.6 Hz); at the foundation level the amplification is negligible up to 4 Hz, and becomes even negative between 4 and 8 Hz.

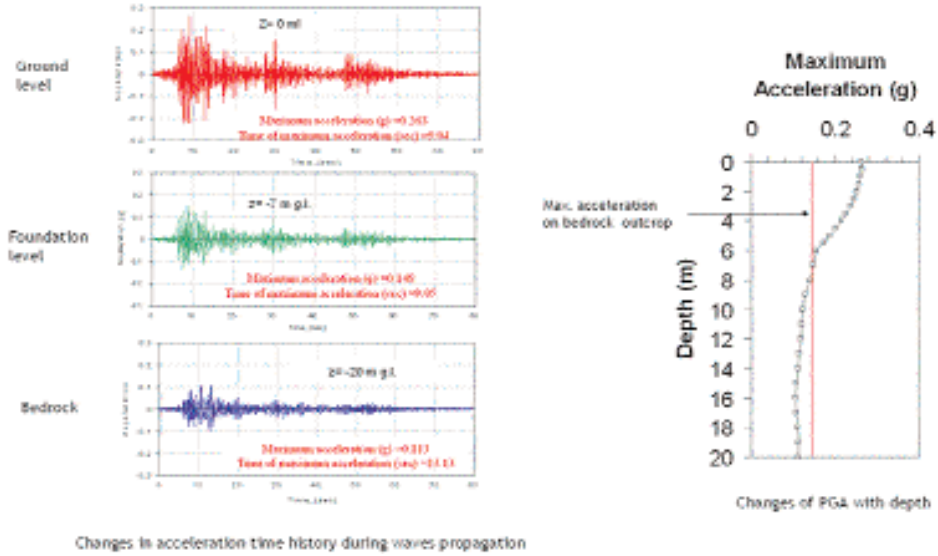

Fig. 4. Changes in acceleration time histories and peak ground acceleration with depth for the New Court Buildings site.

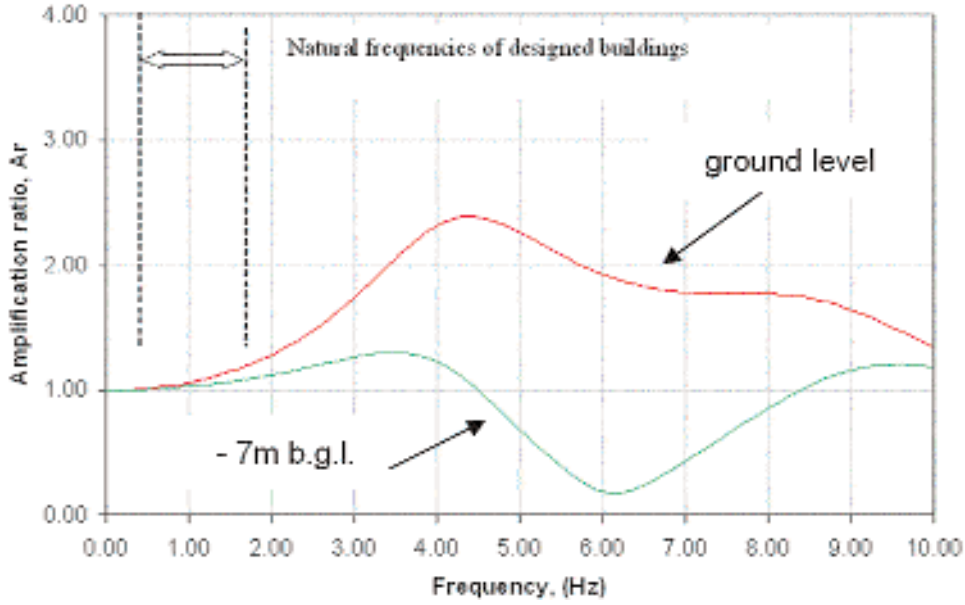

Fig. 5. Amplification functions bedrock // ground level and bedrock //-7 m b.g.l.

Engineering consequences

The analysis results presented above suggest that no relevant seismic amplification of the seismic motion deriving from local soil conditions has to be considered in the design of the buildings of the New Law Court. In particular Fig. 5 indicates that, in the range of the main frequencies of the buildings, amplification ratios about 1 have been computed; in other words the seismic motion remains unchanged moving from the bedrock to the building foundations, which lie at -7 m from the ground surface. As a consequence, in the application of the design procedure suggested by the traditional national code, a value of the foundation coefficient ε equal to 1 has to be adopted, in order to achieve a reliable evaluation of the seismic actions on the New Law Court Buildings.

Further, this study confirm that seismic motion highly modifies generally within the top soil layers; therefore the actual seismic actions which structures undergo strongly depends on the depth of the foundation level. Hence it must be observed that a conventional microzonation study, which gives the site response just at the ground surface, could be not reliable from an engineering point of view.

It can be concluded that, even for "*a priori*" microzonation studies, the site seismic response should be defined at various depths from the ground surface, selected according to the stratigraphy and the mechanical properties of the

soils which control the choice of the foundation level. The results of such a kind of multiple analyses would give rise to "multilevel" microzonation maps, which could be drawn and effectively represented by means of GIS tools.

References

1. Bardet JP, Ichii K, Lin CH. *EERA A Computer Program for Equivalent-linear Earthquake site Response Analyses of Layered Soil Deposits*. University of South California, Los Angeles, 2000.
2. Schnabel PB, Lysmer J, Seed HB. *SHAKE: A Computer Program for Earthquake Response Analysis of Horizontally Layered Sites*. Report No. UCB/EERC-72/12, Earthquake Engineering Research Center, University of California, Berkeley, 1972.

Diagnostic and monitoring of structures by innovative methods

Detection and localization of reinforcement bars in concrete via microwave imaging

R. Pierri, J. Romano, A. Liseno

Dipartimento di Ingegneria dell'Informazione, Seconda Università di Napoli, Aversa, Italia

Introduction

In this paper, we face the problem of determining the number and the locations of unknown thin cylinders from the knowledge of their scattered far field. The number and the locations of the unknown cylinders are described in terms of support of δ-functions. Neglecting the mutual interactions between the scatterers leads to a linear inverse problem which is solved by means of the Singular Value Decomposition approach. This problem is of interest in Ground Penetrating Radar and in civil engineering, where, for example, the problem arises of determining the number and the positions of reinforcement bars in concrete.

Linear distributional approach to the problem

We consider the inverse problem [1] of determining the number and the positions of perfectly conducting infinitely long "thin" cylinders with axis parallel to the z axis from the knowledge of the electric field scattered in the far zone under plane wave incidence. We suppose that the scatterers are located in free space and that the illuminating plane waves have TM polarization (i.e. the electric field has only one component along the direction of the axis of the cylinders), fixed angle of incidence and varying frequency ranging from f_{min} to f_{max}. The cylinders are assumed to have circular cross section with radius a. By representing the scattered far field in terms of cylindrical harmonics and by supposing $a<<\lambda_{min}$, where λ_{min} is the minimum exploited wavelength, the scattered electric far field can be written as[1]:

$$E_s(\rho,\phi) \simeq \sum_{i=1}^{N} c_i e^{j\beta\rho_i' \cos(\phi_i'-\phi)} \qquad (1)$$

[1] The hypothesis $a<<\lambda_{min}$ allows to keep only the cylindrical harmonic of zero order within the expansion.

where (ρ,ϕ) denotes the polar coordinates of the measurement point, (ρ_i',ϕ_i') denotes the polar coordinates of the axis of the i-th cylinder, $\beta=2\pi/\lambda$ is the free space wavenumber, λ is the impinging wavelength, c_i is the coefficient of the cylindrical harmonic for the i-th cylinder and N is the total number of scatterers. The coefficients c_i can be determined, by forcing the boundary conditions on the surface of each cylinder, as the solution of the following linear system

$$\underline{\underline{A}} \cdot \underline{c} = \underline{b} \tag{2}$$

where $\underline{\underline{A}}$ is the NxN coefficients matrix, $\underline{b}$ is the known terms vector and $\underline{c}$ is the unknown coefficients vector, both of dimension $Nx1$. Note that the terms A_{ij} of $\underline{\underline{A}}$, with $i \neq j$, represent the mutual interactions between the scatterers.
If we assume that the spacing between the cylinders is sufficiently large as compared to the impinging wavelength, then the mutual interactions between the scatterers can be neglected. This means that, from a point of view of the electromagnetic scattering, we can consider each cylinder as it were scattering alone in the free space. According to this, eq. (1) rewrites, after normalization to non-essential factors, as

$$E_s(\rho,\phi) \simeq \sum_{i=1}^{N} e^{-j\beta\rho_i'[\cos(\phi_i' - \phi_0) - \cos(\phi_i' - \phi)]} \tag{3}$$

In eq. (3), E_s represents the data of the problem, whereas the number of cylinders and the cylinders' centers (ρ_i',ϕ_i') are the unknowns. However, by representing the unknown cylinders' positions (ρ_i',ϕ_i') as the support of δ-functions [2], a linear relationship between the "new unknowns" (that is, the δ-functions) and the data is obtained as

$$E_s(u,v) = \int\int_D C(\underline{r}') e^{-jux'} e^{-jvy'} d\underline{r}' \tag{4}$$

where $u=\beta(\cos\phi_0-\cos\phi)$, $v=\beta(\sin\phi_0-\sin\phi)$, $\underline{r}=(x',y')$, D is the *investigation domain*, that is a domain we a priori know that contains the cylinders' cross section, representing the region within which we search for the presence and the locations of the scatterers, $C(\underline{r}') = \sum_{i=1}^{N} \delta(\underline{r}'-\underline{r}_i')$ and $\underline{r}_i'$ denotes the cartesian coordinates of the axis of the i-th cylinder.
According to eqs. (3-5), we face the problem of determining the location of the cylinders from the knowledge of E_s as a two step procedure. In the first step, the distribution C is reconstructed by means of a Singular Value Decomposition (SVD) approach. Note that in [3], an extention of the SVD approach to the inversion of linear operators acting on distribution spaces has been given. In the second one, the total number of the scatterers and their unknown locations are determined as the locus of points where the retrieved distribution C achieves its maxima [2].

As far as the second step is concerned, we underline that the incompleteness of the data along with the presence of the noise entails that, during the regularization procedure, the unknown distribution undergoes a filtering which is band-pass for the spatial variations along the direction of incidence and low-pass for the spatial variations along the direction orthogonal to that of incidence [3]. This makes sidelobes appear in the reconstruction besides the main peaks corresponding to the positions of the scatterers [4]. Also, in presence of additive noise the Truncated SVD (TSVD) algorithm filters from the data the projections of the noise on the right singular functions corresponding to the cut-off singular values, but the reconstruction remains affected by the projection of the noise on the right singular functions retained within the TSVD expansion. Therefore, in this paper we cut the reconstructed images by a threshold, according to the criteria worked out in [4], to mitigate the presence of artifacts due to the sidelobes and to the presence of the noise.

NUMERICAL RESULTS

We now present numerical examples in which the scattered field is gathered over the angular sector $\phi \in (\pi-\phi_M, \pi+\phi_M)$ of the far zone circular observation curve $(\rho\cos\phi, \rho\sin\phi)$. In particular, we consider a square investigation domain $D=[-x_M, x_M]\times[-y_M, y_M]$ with $x_M=y_M=4\lambda_c$, where λ_c is the wavelength referring to the frequency $(f_{max}+f_{min})/2$, and a measurement configuration with $\phi_M=70°$ and $[f_{min}, f_{max}]=[300MHz, 750MHz]$. The reconstructions are performed on noisy data with a Signal to Noise Ratio equal to *10 dB*. Also, the data are affected by model error defined as:

$$e = \frac{\|E_s - E_{s_0}\|}{\|E_s\|}$$

where E_s is the "exact" scattered far field (eq. (1)) and is the approximated one (eq. (3)).

The images in Figs. 1A and 1B refer to the reconstruction of two cylinders located at $\rho_1=(0.1\lambda_c, 135°)$ and $\rho_2=(0.1\lambda_c, 315°)$ and at $\rho_1=(0.5\lambda_c, 135°)$ and $\rho_2=(0.5\lambda_c, 315°)$, respectively. For the second configuration, the model error e equals 0.3. A significant interference between the two objects is observed in Fig. 1A, where the reciprocal distance is $0.2\lambda_c$. The coupling decreases with the increase of the distance as shown in Fig. 1B. When the objects are spaced by more than λ_c, they can be resolved as shown in Fig. 1B [4].

Finally, we present the reconstruction of five cylinders located as shown in Fig. 2. In Fig. 3A, the reciprocal distance d is $\lambda_c/2$, whereas in Fig. 3B is λ_c. As it can be seen, also in this case, the localization is possible when d is greater than λ_c.

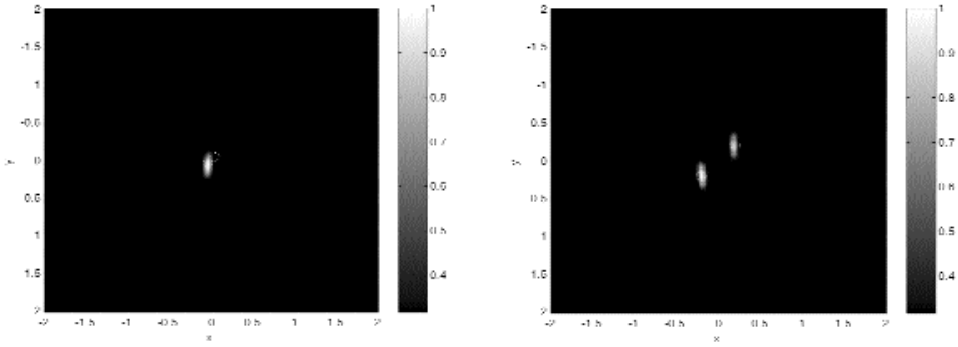

Fig. 1. Reconstruction of two thin metal cylinders. **A** (left): the reciprocal distance is $0.2\lambda_c$. **B** (right): the reciprocal distance is $1\lambda_c$.

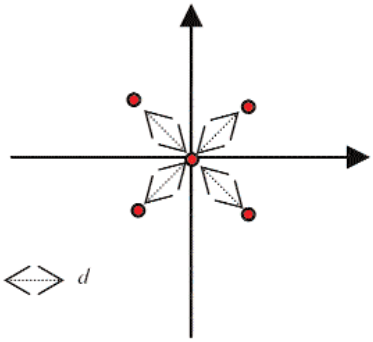

Fig. 2. Location of the cylinders for the reconstructions in Figs. 3A and 3B.

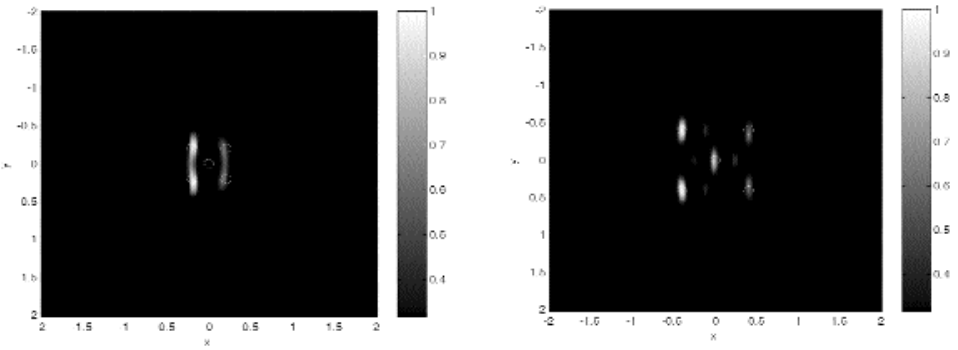

Fig. 3. Reconstructions of the cylinders for the configuration depicted in Fig. 2. **A** (left): $d=\lambda_c/2$. **B** (right): $d=\lambda_c$.

REFERENCES

1. Bertero M, Boccacci P. *Introduction to inverse problems in imaging*. Institute of Physics, Bristol, 1998.
2. Pierri R, Liseno A, Soldovieri F. Shape reconstruction from PO multifrequency scattered fields via the singular value decomposition approach. *IEEE Trans. Antennas Prop.* 49:1333-43, 2001.
3. Liseno A, Pierri R. Imaging perfectly conducting objects as support of induced currents: Kirchhoff approximation and frequency diversity. *J. Opt. Soc. Am. A.* 19:1308-18, 2002.
4. Liseno A, Soldovieri F, Pierri R. Improving a shape reconstruction algorithm with thresholds and multi-view data. In print on *Int. J. Electron. Commun. (AEÜ)*, 58, 2004.

Structural monitoring by means of distributed fiber-optic sensors

L. Zeni[a], R. Bernini[b], A. Minardo[a], F. Soldovieri[b], R. Pierri[a]
[a]*Dipartimento di Ingegneria dell'Informazione, Seconda Università di Napoli, Aversa, Italia*
[b]*Istituto per il Rilevamento Elettromagnetico dell'Ambiente, CNR, Napoli, Italia*

Introduction

It is well known that fiber optic sensors show some definite advantages with respect to traditional sensors such as low weight, small size, electromagnetic interference immunity and the possibility of being embedded in the structures under test (smart structures).
The capability for long-range distributed sensing is unique to optical-fiber technology. A distributed sensor returns a value of the measurand of interest as a function of linear position along the fiber length. These sensors are particularly advantageous for use in monitoring the structural integrity and the temperature of large structures.
Stimulated Brillouin scattering (SBS) allows the distributed sensing of temperature and strain, employing as the sensing element a standard silica-based single-mode communication fiber. It is based on the interaction between an acoustic wave, a pump wave and a Stokes wave [1-3]. The pump wave and the Stokes wave counter-propagate in the fiber creating a moving interference pattern that induces an acoustic wave via the electrostriction effect. The acoustic wave causes a transfer of power from the pump to the Stokes wave, provided that their frequency offset falls within the Brillouin gain spectrum of the fiber itself. Such spectrum is centred at the so-called Brillouin frequency shift, that is in the 10 GHz range. This latter is linearly dependent on temperature and strain, so that any change in the measurand of interest can be detected by measuring the resulting Brillouin frequency shift change.

Brillouin frequency shift profile reconstruction

Distributed measurements of Brillouin frequency shift are generally achieved by employing an optical time-domain reflectometry (OTDR)-based configuration: one of the two lightwaves is pulsed, while recording the temporal changes induced on the received CW wave intensity as the pulse propagates along the fiber [4]. The temporal coordinate is related to the spatial position along

the fiber via the pulse time-of-flight. By recording the Brillouin signals for a range of frequency offsets between the two beams, the Brillouin gain spectrum at each fiber section can be retrieved. Brillouin frequency shift can be obtained by fitting the Brillouin gain spectrum, at each section along the fiber, to a spectral shape (typically a Lorentzian curve [1]). The peak frequency of the fitting curve provides the value of the local Brillouin shift. This latter can be then translated in a temperature or strain value by multiplication with a suitable scale factor. The above described signal processing is illustrated in Fig. 1.

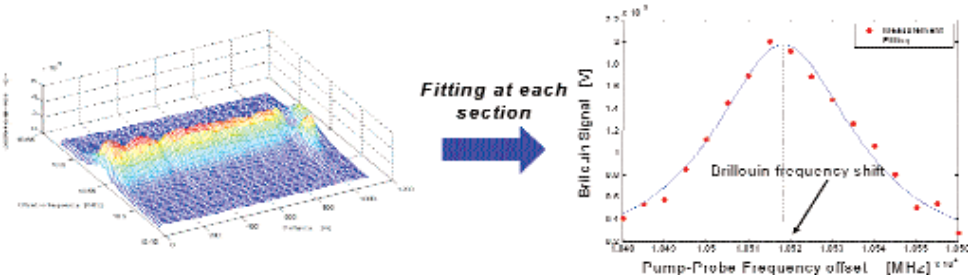

Fig. 1. Brillouin frequency shift profile reconstruction by local fitting of Brillouin gain spectra.

Experimental measurements

The experimental configuration shown in Fig. 2 was employed. The semiconductor laser was a pigtailed DFB module emitting at 1.550 μm with an output power of about 25 mW. The output light was first split by a fiber-fused coupler, which directed the 95% of the power to an acousto-optic modulator (AOM) for optical pulse generation, whereas the remaining 5% was launched into an external electro-optic modulator (EOM). This latter was employed for the generation of a CW light having an opportune frequency offset (around 10 GHz), by means of the sideband technique described in [5].
The main difference between the present configuration and the one described in [3] stems from the use of an AOM for pulse generation. In fact, our AOM provided optical pulses frequency-shifted of a fixed amount of 300 MHz with respect to the input optical frequency. This shift allowed to restrict the Brillouin interaction at only one of the CW sidebands generated by the EOM, making unnecessary the use of any optical bandpass filter in front of the detector. The system was then totally immune to any drift on the source wavelength, allowing very stable and accurate SBS measurements.
A polyvinyl chloride (PVC) buffered single-mode fiber was attached along a 3m-long plastic beam using epoxy-based structural adhesive (Fig. 3).

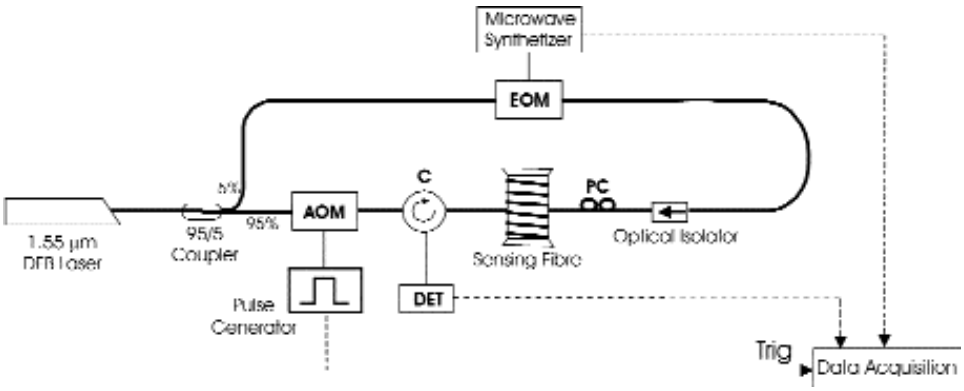

Fig. 2. Experimental setup for distributed temperature measurements using an electro-optic modulator (EOM) to generate the interaction waves and an acusto-optic modulator (AOM) to generate frequency-shifted pulses (PC = polarization controller, C = optical circulator, DET = detector).

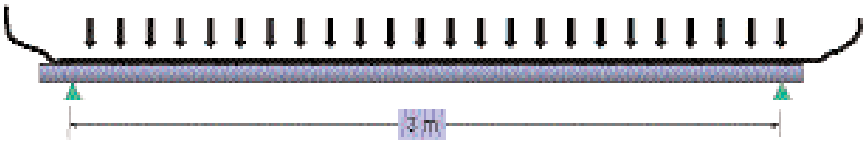

Fig. 3. The sensing fiber is attached at the top of the plastic beam.

The deformation of the plastic beam is induced by its own weight. Tensile strain is measured when the fiber is located at the top of the beam, whereas compressive strain is measured by rotating the beam so that the fiber is located at the bottom of the beam. The spatial resolution is 1 m, and the strain resolution is 20 με (= 20 μm/m). Fig. 4 shows the strain profile obtained by

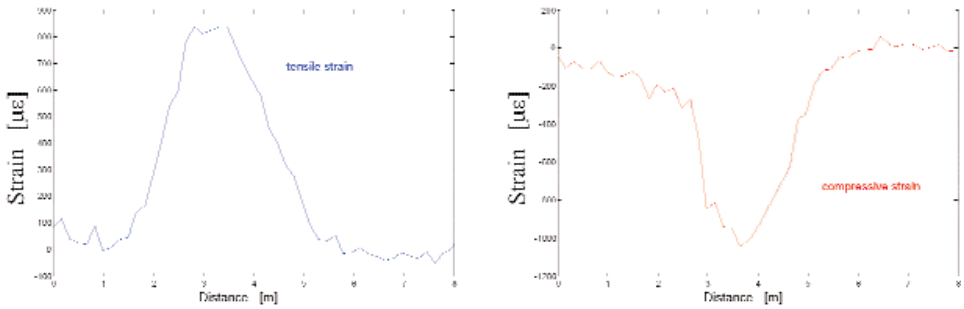

Fig. 4. Strain profile reconstruction along the 8-m long fiber attached along a 3m-long plastic beam subjected to tensile/compressive strain.

processing the signals by applying the technique described in the previous Section. Measured peak tensile strain is about 850 με, whereas measured peak compressive strain is about -1000 με. The behavior shown in Fig. 3 is in good agreement with the theoretical strain profile exhibited by an elastic beam which is fixed at two opposite ends and subjected to its own weight.

Conclusions

An experimental setup for structural health monitoring applications, based on Brillouin scattering measurements, has been demonstrated. It allows distributed strain measurements along a single-mode optical fiber, which can be easily bonded to the structure to be monitored. Both tensile strain and compressive strain can be measured, with about one meter spatial resolution and high accuracy.

References

1. Agrawal GP. *Nonlinear Fiber Optics*. Academic Press, Boston, p. 372, 1989.
2. Bernini R, Minardo A, Zeni L. Reconstruction technique for stimulated Brillouin scattering distributed fiber optic sensors. *Optical Engineering* 41(9):2186-94, 2002.
3. Bernini R, Minardo A, Zeni L. A reconstruction technique for Stimulated Brillouin Scattering fiber-optic sensors for simultaneous measurement of temperature and strain. *IEEE-Sensors 2002*, Orlando, Florida, June 2002.
4. Horiguchi T, Shimizu K, Kurashima T, Tateda M, Koyamada Y. Development of a distributed sensing technique using Brillouin scattering. *J. Lightwave Technol.* 13:1296-302, 1995.
5. Nikles M, Thevenaz L, Robert PA. Brillouin gain spectrum characterization in single-mode optical-fibers. *J. Lightwave Technol.* 15(10):1842-51, 1997.

Electromagnetic characterization of tuff via microwaves

A. Brancaccio[a], D. Sglavo[a], R. Pierri[a], F. Soldovieri[b], G. Leone[c]

[a]*Dipartimento di Ingegneria dell'Informazione, Seconda Università di Napoli, Aversa, Italia*

[b]*Istituto per il Rilevamento Elettromagnetico dell'Ambiente, CNR, Napoli, Italia*

[c]*Dipartimento di Informatica, Matematica, Elettronica e Trasporti, Università di Reggio Calabria, Reggio Calabria, Italia*

Introduction

An important topic in civil engineering and construction industry is the material properties evaluation. Different techniques can be exploited for evaluating the physical and mechanical properties of materials. It is worth noting that one of the main interests is in the compression strength of the material: the common testing procedure for its evaluation consists in drilling out a cylindrical core from the structure and then testing it in the laboratory. However, this method is destructive, time-consuming, costly and operator skill dependent. Moreover, it only provides information about the specific location from which the core is drilled out.

Some of the above limitations can be overcome by resorting to electromagnetic techniques based on the measurement of the electromagnetic field at microwave frequency [1-3]. In fact, microwave signal can penetrate into a dielectric medium and interacts with its inside. The parameters affecting this interaction are the dielectric permittivity and the conductivity, that can be related to properties of the structure under test, such as humidity, compression strength, presence of voids and so on, which are of ultimate interest. It is possible to perform an indirect measurement of the dielectric permittivity and conductivity starting from the free-space measurement of the electromagnetic field reflected and/or transmitted by the structure. Once the estimation of the parameters is achieved, it is possible to monitor the material; as an example, the time-behavior in the curing process of the concrete.

An accurate determination of the above mentioned parameters needs of three steps.

The first one is the set-up of proper microwave measurement set-up and technique. The second one is the development of models of the electromagnetic scattering phenomenon, which must satisfy the requirements of simplicity and accuracy. The third one involves the development of solution algorithms able to give reliable and accurate estimate of the dielectric permittivity and of the conductivity starting from the measurements of the electromagnetic field.

In this paper, we afford the electromagnetic characterization with reference to tuff masonry, which has been very largely employed in the ancient buildings of Southern Italy; the diagnostics of such masonry is of interest for historical and safety purposes.
Tuff characterization fits in a broad range project, whose main objective is the research of innovative technologies and materials for preserving historical and monumental buildings.
It must be noted that the electromagnetic characterization of tuff masonry is rarely dealt with in the literature. In addition, different kinds of tuff, ranging from very porous zeolite rich (for instance the Neapolitan yellow tuff) to the very compact varieties (such as the piperno facies of the campanian grey tuff or the peperino variety of the romasn volcanoes) are present in nature. Furthermore, the material can present variable characteristics in dependence on the site and on local humidity conditions. So, laboratory measurements on samples are not exhaustive an on-site non invasive procedure is needed [4]. In this paper we refer to the Neapolitan yellow tuff.

The measurement campaign

Measurements were collected at the Applied Electromagnetics Laboratory of the Information Engineering Department of the Second University of Naples. The measurement system is depicted in Fig. 1. A pyramidal horn antenna is connected to a vectorial network analyzer (VNA) (ANRITSU, model 37225B) by means of coaxial cables and adapters, needed in order to set-up the measurement chain. The VNA is driven by a Personal Computer that also controls a positioning system moving the antenna into different zones of the masonry. The antenna is located in contact with the masonry, which in turn is backed by a conducting plate.
Data acquisitions have been performed in a reflection mode monostatic configuration; the choice of this configuration is due to the fact that the signal measured in a bistatic configuration is too low (less than -90 dB). The frequency range is 8.2 ÷ 12.4 GHz, depending on the operational range of the employed antennas.
Once the measurements have been acquired and calibrated in module and phase [4], they have been processed according to a solution algorithm that searches for the unknown dielectric permittivity and conductivity as the global minimum of an error function, accounting for the squared distance between the measured data and the ones simulated on the basis of a theoretical model [4].
An extensive measurement campaign was performed for a masonry made up of Neapolitan yellow tuff bricks (Fig. 2). The first aim of the campaign was to investigate the homogeneity of the masonry by exploiting measurements in its different zones. Fig. 3 shows a scheme of the different locations of the dry masonry where the measurements were performed, while Tab. 1 shows the

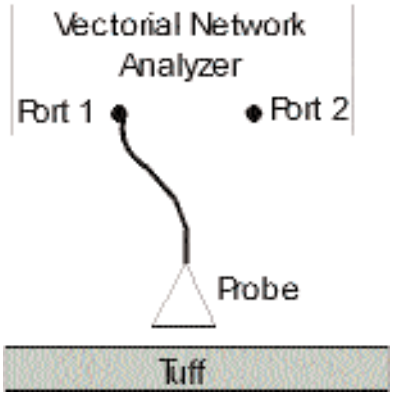

Fig. 1.

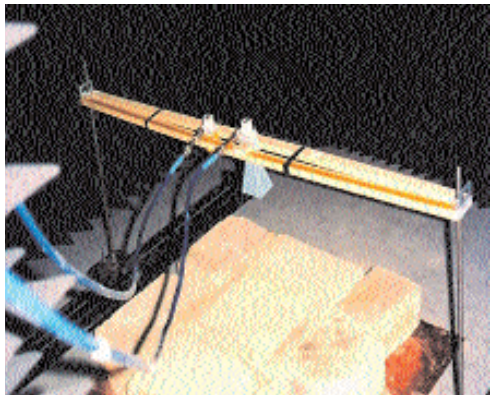

Fig. 2.

estimated values of relative dielectric permittivity and conductivity for the corresponding measurement. Since the estimated values are not really different, we can state the good homogeneity of the masonry. We obtained for the relative dielectric permittivity and for the conductivity a mean value of about 3 and 0.15 S/m respectively. It is worth noting that such values, estimated in the case of dry masonry, have been confirmed by measurement of the field performed under a transmission mode configuration, where a horn antennas acts as a transmitter and a receiving horn located at the opposite side of the masonry acts as a receiver.

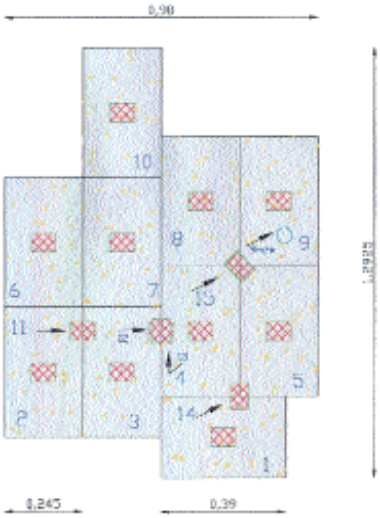

Fig. 3.

Single bricks plan

Position	ε	σ(S/m)
1	2,7	0,15
2	2,8	0,16
3	2,8	0,14
4	3,3	0,14
5	2,7	0,14
6	2,2	0,12
7	2,7	0,14
8	2,4	0,24
9	2,7	0,14
10	2,8	0,14
11	1,6	0,10

Tab. 1.

A further step has been the investigation of the dependence of the electromagnetic behaviour of tuff on different humidity conditions. To this end, we dipped a tuff brick into water for 72h (during this time three litres of water were absorbed). Then, we monitored drying of the brick. The estimated values of the conductivity and of the dielectric permittivity (Figs. 4 and 5, respectively) allow us to state their strong dependence on the moisture content.

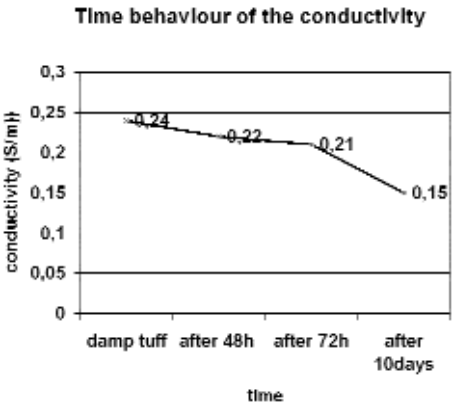

Fig. 4.

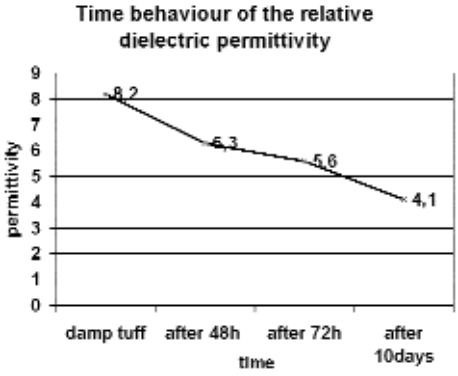

Fig. 5.

Conclusions

Results on tuff characterization have been presented, and the feasibility of characterization by means of a relatively simple measurement instrumentation and by a simple estimation algorithm has been shown. The strong dependence of the electromagnetic parameters by the water content of the material has also been shown.
As regards the estimated value of the permittivity, it agrees with that found in the literature ([5] and ref. therein). However, careful attention should be paid on a possible dependence on the frequency, which would result in a dispersive behavior of the material. Such a question deserves deeper investigation in future work.

References

1. Muqaibel AH, Safaai-jazi A. A new formulation for characterization of materials based on measured insertion transfer function. *IEEE Trans. Microwave Theory and Techniques*, 51:1946-51, 2003.

2. Peer S, Case JT, Gallaher E, Kurtis KE, Zoughi R. Microwave reflection and dielectric properties of mortar subject to compression force and cyclically exposed to water and sodium chloride solution. *IEEE Trans. Instrumentation and Measurements* 52:111-7, 2003.
3. Kharkovsky SN, Akay MF, Hasar UC, Atis CD. Measurement and monitoring of microwave reflection and transmission properties of cement based specimens. *IEEE Trans. Instrumentation and Measurements* 51:1210-8, 2002.
4. Brancaccio A, Sglavo D, Leone G, Soldovieri F, Pierri R. In situ dielectric characterization of tuff for masonry microwave tomography. *Proc. of PIERS 2004*, March 2004, Pisa, Italy.
5. Adams R, Perger WF, Rose W, Kostinski A. Measurements of the Complex Dielectric Constant of Volcanic Ash from 4 to 19 GHz. *J. Geological Research* 101:8175-85, 1996.

Forward models for simulations in electromagnetic diagnostics applications

G. Leone[a], R. Persico[b], R. Solimene[c], R. Tamburrino[c], R. Pierri[c]

[a]*Dipartimento di Informatica, Matematica, Elettronica e Trasporti, Università di Reggio Calabria, Reggio Calabria, Italia*

[b]*Istituto per il Rilevamento Elettromagnetico dell'Ambiente, CNR, Napoli, Italia*

[c]*Dipartimento di Ingegneria dell'Informazione, Seconda Università di Napoli, Aversa, Italia*

Introduction

Localization and determination of the dielectric properties of objects embedded in a layered scenario is of interest for many applications, such as GPR monitoring in civil engineering (masonry diagnostics), subsurface prospecting, industrial process tomography, material diagnostics [1]. In order to pursue this goal, an inverse scattering algorithm can be set out. However, any reconstruction algorithm should be tested properly before being applied to experimental data and, therefore, it is timely to settle simulation codes able to provide sinthetic data. In this way, burdening and likely expensive preliminar experimental tests can be avoided and, above all, the limits of the adopted models can be understood. In fact, often, inversion algorithms involve some approximations on the mathematical model [2, 3] (especially if the investigation domain is electrically large) and some regularization procedure. These steps are needed in order to perform the reconstruction in an acceptable time and in order to avoid some mathematical difficulties inherent to the inverse problem (such as instability of the solution). Accordingly it is particularly important to understand the range of validity of the adopted model. Approximate modeling, moreover, can be a valuable guideline for the choice of the parameters of the measurement configuration to be adopted in realistic conditions. Some tradeoffs between the accuracy of the result and the required computational time can be investigated. This is particularly relevant in inverse scattering problems for two reasons, related to the fact that the ill-position makes essentially finite the available amount information. This makes it useless to reduce the spatial and/or frequency step of the data beyond a certain finite limit.

For these reasons, in this contribution we are concerned with direct modeling of scattered field data for diagnostics applications in half-space geometry and introduce a new method for the field computation based on the modal expansion. We test its reliability by comparison with an algorithm based on the exact solution of integral equations of scattering based on the method of moments

(MoM) [4]. The relevance is twofold. First, the modal expansion can provide a very fast method for the generation of data. Second, it allows to test inversion algoritms (based on the MoM) with data generated in a completely independent way. Finally, let us outline that to have at one's disposal different simulation codes can be helpful for their different scopes.

Modal method

Consider a TM polarized plane wave impinging on the interface between two media (e.g. air and soil). A circular cylinder of radius a is buried at a depth d (denoting the depth of the center) (Fig. 1). The cylinder is of infinite extent and invariant along the z-axis. The difficulty of this geometry is to account for its inhomogeneity. In fact, when the transmitted plane wave impinges on the cylinder, the scattered field is reflected by the plane air-soil interface, and this generates multiple interactions between the interface and the cylinder. The modal method evaluates the electric scattered field using modal expansion by an iterative procedure, computing the electric field as the sum of successive contributions and evaluating it at the planar interface. Plane and cylindrical wave expansions are joined by use of explicit expressions relating cylindrical and plane waves. In this way, it has been observed that the subsequent iterations take into account the different contributions to the scattered field as a result of different interactions between the object and the planar interface.
At the first step the field in air is provided by a contribution E_{s0} due to the reflection of the incident wave E_{inc} at the air-soil interface.
Secondly both the field scattered by the embedded object and the transmitted field E_t are expressed by cylindrical waves in order to enforce the appropriate boundary conditions on the surface of the cylinder (for a penetrable cylinder the field inside the object is also expressed under a modal expansion). In this way the scattered field inside the soil is approximated in closed form.

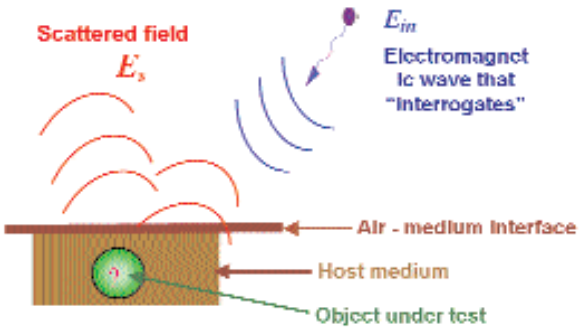

Fig. 1. The scattering phenomenon.

Next in order to evaluate this first contribution in air, the plane wave spectra representations are exploited (to be efficiently computed by making use of a Fast Fourier Transform (FFT) algorithm) so obtaining "transmitted" field in air $\tau\hat{E}_s$ by multiplication of the appropriate Fresnel coefficient and, finally, the scattered field E_{s1} is available by an Inverse Fast Fourier Transform (IFFT).
In turn the part $\Gamma\hat{E}_s$ of the scattered field E_{s1} reflected by the interface inside the soil impinges on the cylinder (it is evaluated by IFFT of the reflected spectrum of $\hat{E}_{s1}$) and provides the incidence for a second contribution to the scattered field, E_{s2}, also to be expressed by modal expansion. Again, the coefficients of the expansion are calculated imposing the boundary conditions on the surface of the cylinder.
The procedure iterates for a further refinement by following the same steps and by taking into account the fact that at each iteration the incident field impinging on the object is equal to the field scattered by the object at the previous step and the one reflected at the soil-air inteface (Fig. 2).

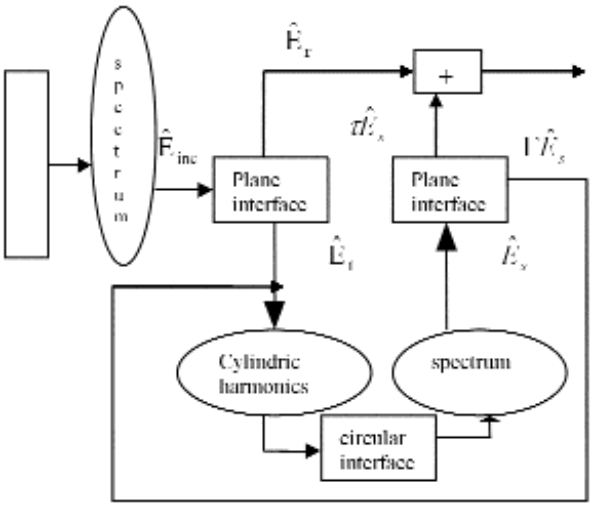

Fig. 2. Iterative algorithm.

The accuracy of the result will depend on number of iterations considered.
As far as the "theory of small reflections" remains valid (in particular, when the object is not too close to the interface, its size is not too large with respect to the wavelenght in the soil, the relative permittivity of the soil is not too high and the host medium is lossy) only a few contributions are relevant.
Let us point out that this method can be applied both to dielectric and conducting objects, can be extended also to the case of more than one object and

to filamentary current excitation. For the TM case, according to configuration shown in Fig. 3, a comparison between the present approach and the method of moments for a perfect electric conducting cylinder with circular cross section is shown in Fig. 4. In Fig. 4 the first three terms of the modal expansion have been taken into account. Finally, according the configuration depicted in Fig. 5, in Fig. 6 a result for the case of two void objects is shown. In this last reconstruction, however, only the first contribution is accounted for.

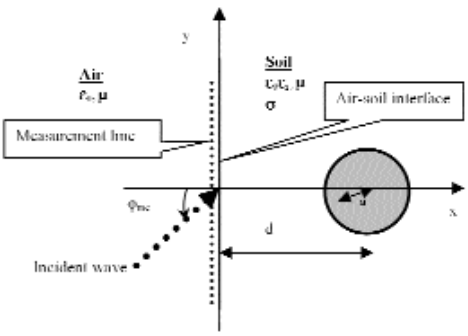

Fig. 3. Measurement configuration.

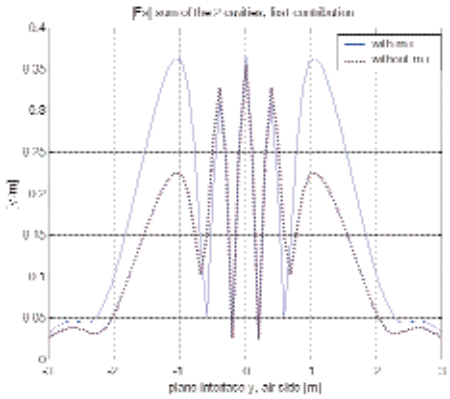

Fig. 4. A comparison between the iterative method and method of moments (c.e.p) (φ_{inc}= 0, ε_r=16, sigma = 0.01 Siemens/m, d= 0.3 m, a=0.125 m).

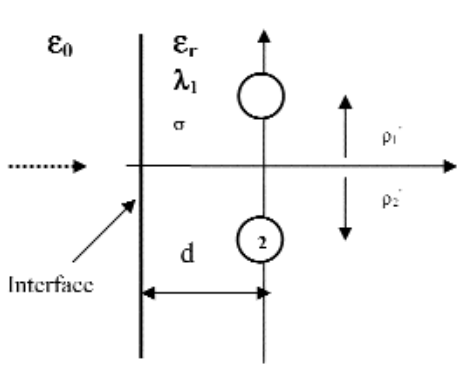

Fig. 5. Configuration for the case of two objects.

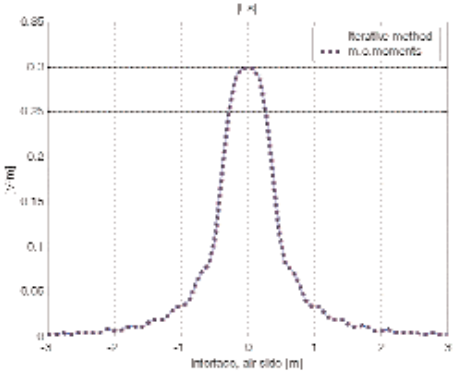

Fig. 6. Two cavities. Comparison: mutual interaction and without m.i.

Conclusions

In this contribution, we have shown that an accurate modelling of the electromagnetic scattering gives an answer to various requirements. In particular, it allows the selection of parameters of the measurement configuration in realistic conditions. It allows to investigate the limits of validity of approximate models necessary to obtain reliable and efficient inversion algorithms. It provides the synthetic data which are the basis for testing and evaluating the reconstruction performances of any inversion algorithms.

References

1. Daniels DJ. *Surface-penetrating radar*. The Institution of Electrical Engineers, London, 1996.
2. Leone G, Persico R, Solimene R. A Quadratic Model for Electromagnetic Subsurface Prospecting. *AEÜ, Int. J. of Electron. and Comm.* 57(1):33-46, 2003.
3. Pierri R, Leone G, Persico R, Soldovieri F. Electromagnetic inversion for subsurface applications under the distorted Born approximation. *Nuovo Cimento* 24C(2):245-61, 2001.
4. Sadiku M. *Numerical techniques in electromagnetics*. CRC Press, U.S.A., 1992.

Microwave tomographic sensing of voids and cavities in mansory structures

A. Liseno[a], F. Soldovieri[b], M. Torellini[a], R. Pierri[a]

[a]*Dipartimento di Ingegneria dell'Informazione, Seconda Università di Napoli, Aversa, Italia*

[b]*Istituto per il Rilevamento Elettromagnetico dell'Ambiente, CNR, Napoli, Italia*

Introduction

In a region as Campania characterized by extended zones with high seismic risk, it is very important to have efficient instrumentations for monitoring and controlling buildings and cultural heritages. The development of non-destructive testing techniques is an interesting alternative to traditional (destructive) methods of survey and those employing electromagnetic waves are between the most promising ones. Indeed, the capability of the electromagnetic waves to propagate across the bodies and to be sensitive to their chemical and physical characteristics makes it possible to recover information about the internal features of objects in a non-destructive way, starting from the knowledge of the scattered field. At present, electromagnetic diagnostics allows, in civil engineering, to inspect for example walls or pillars in order to decide the correct actions for restoration and to verify their effectiveness.

In the "tool-bag" of electromagnetic diagnostics, the equipment employing electromagnetic waves in the frequency band of microwaves is called *Ground Penetrating Radar* (or GPR for short). Present GPRs work by emitting an electromagnetic "pulse" into the ground and by recording above the air-soil interface the echo reflected back by the buried objects. By changing the location of the radar and determining the echo delay-time at each radar position, a two-dimensional plot (*radargram*) is obtained in which the echo delay-time (corresponding to depth) is drawn versus the radar location. This simple and fast operating mode presents however some drawbacks. First of all, GPRs are not capable to determine the shape as well as the material composition of the targets. Furthermore, the interpretation of the radargrams to detect and localize multiple targets is a challenge encompassing the ability and the experience of the user and this unavoidably gives a character of subjectivity to the prospections.

A methodology to process georadar data that overcomes the limitation of the present GPRs' operating modality is the tomographic approach which consists into determining an image of the spatial features of the objects. This allows to make the prospections more objective, namely to detect and localize the

objects and to retrieve information about their shape, dielectric permittivity and conductivity.

Shape reconstruction of voids

In this paper, the tomographic approach has been adopted to reconstruct the shape of embedded voids or cavities.
The geometry of the problem is two-dimensional and consists of two half-spaces, one with dielectric permittivity equal to that of the free-space ε_0 that represents the air, and the other with dielectric permittivity equal to $\varepsilon_b\varepsilon_0$ and conductivity σ_b that represents the medium in which the voids are embedded (Fig. 1). The two media are separated by a plane interface, the voids are represented by dielectric cylinders, infinite along the y axis, having dielectric permittivity equal to ε_0, and both, the cylinders and the host medium, have a magnetic permeability equal to that of the free-space μ_0 (Fig. 1). It is assumed, as an *a priori information*, that the voids are contained in the investigation region $\Omega = [z_{min}, z_{min} + 2b]\times[-a, a]$ and that the scattered field is collected along the air-soil interface over the segment of the x-axis $\Sigma = [-X_M, X_M]$, as depicted in Fig. 1.
The reconstruction algorithm is based on a linear approximation of the electromagnetic scattering, namely physical optics, and consists of a "regularized" inversion (based on the Truncated Singular Value Decomposition - TSVD) of the integral equation that relates the unknown (that is, the shape of the voids)

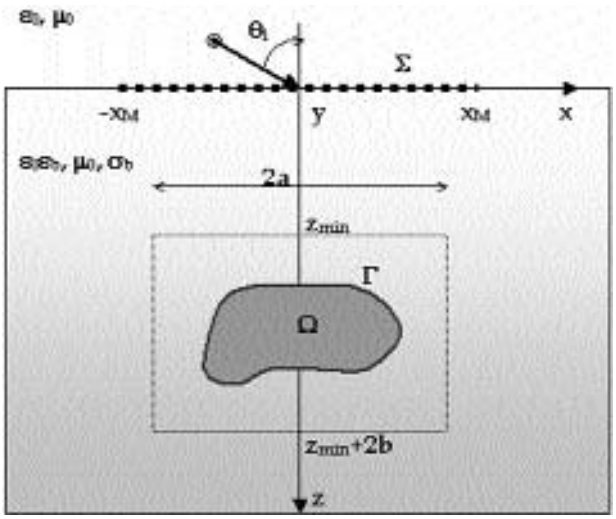

Fig. 1. Geometry of the problem.

to the data (that is, the scattered electric field) [1]. The physical optics approximation can be adopted under the hypothesis that the voids can be considered as strong scatterers and this happens when the dielectric permittivity of the soil is greater than that of the voids [1]. In these circumstances, only the upper side of the voids can be reconstructed, as it can be seen in the following examples.

The reconstructions are performed on synthetic data obtained by a numerical code that computes the exact field scattered by embedded circular voids.

Fig. 2 shows the reconstruction of a circular void with radius 0.3m, supposed to reside within the investigation domain $\Omega = [-0.6, 0.6]\times[-0.01, 1]m^2$, located at a depth equal to 0.45m, and illuminated by an infinitely long electric current distribution located at a distance equal to 0.3m from the interface. The half-space has $\varepsilon_b = 4\varepsilon_0$ and $\sigma_b = 0.001\ S/m$. The impinging field has frequency varying within [300, 1000]MHz, and the only y-component of the scattered field is collected over the segment [-1, 1]m at the air-soil interface in a single-view/multi-static/multi-frequency configuration.

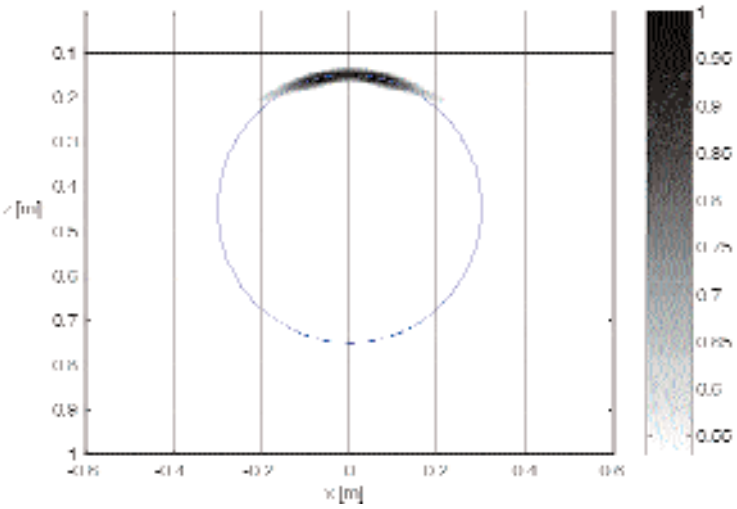

Fig. 2. First reconstruction of a circular void.

Fig. 3 shows the reconstruction of two circular voids having radius equal to 0.3m, residing within $\Omega = [-1.3, 1.3]\times[-0.01, 1.5]m^2$ and located at a depth equal to 0.6m and lm, respectively, when the same measurement configuration of Fig. 2 is exploited.

Fig. 4 shows the reconstruction of a circular void supposed again to reside within the investigation domain $\Omega = [-0.6, 0.6]\times[-0.01, 1]m^2$ at a depth equal

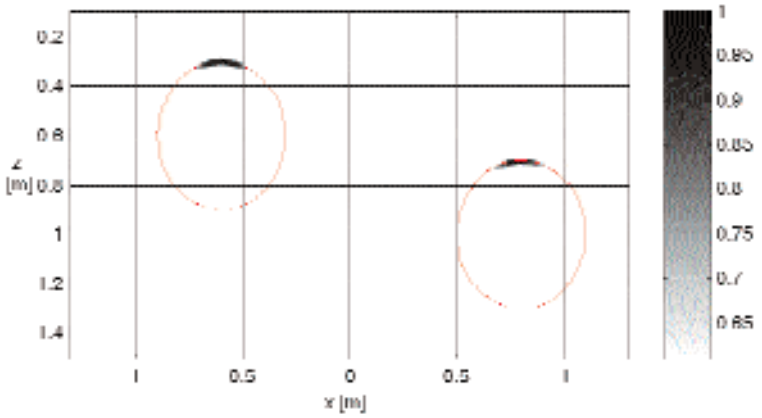

Fig. 3. Reconstruction of two circular voids.

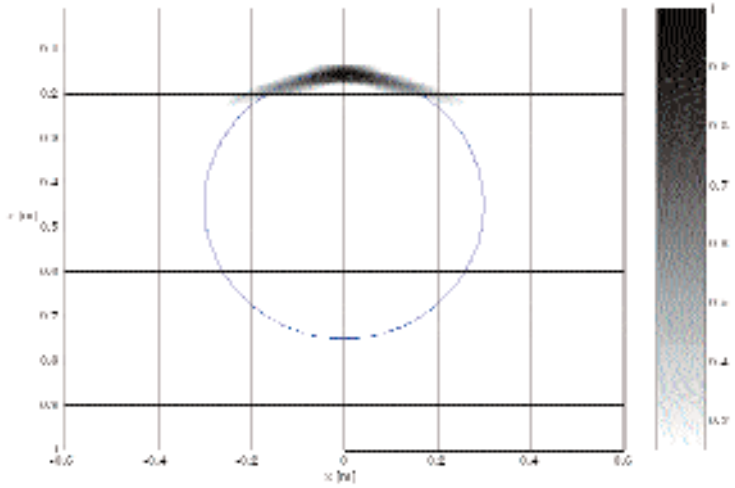

Fig. 4. Second reconstruction of a circular void.

to 0.45*m*, but in this case the half-space has $\varepsilon_b = 4\varepsilon_0$ and $\sigma_b = 0.03\ S/m$. The measurement configuration is multi-frequency (the frequency varies within [300, 1000]*MHz*), multi-static/multi-view, collecting the scattered field over the segment [-1, 1]*m* at the air-soil interface for each position of the transmitter. The adopted choice of the conductivity makes the inversion conditions closer to a realistic one.

For each of the presented results, noisy data (SNR = 10dB) have been considered and, within the TSVD expansion, terms corresponding to singular values smaller than -10dB with respect to the maximum one have been cut-

out. The reconstructions have been improved by using a thresholding procedure [2] that allows to eliminate unwanted artifacts in the retrieved unknown.

Conclusion

A method to reconstruct the shape of voids buried in a homogeneous half space with a planar air-soil interface has been presented in this paper for a two-dimensional geometry. The algorithm exploits the physical optics approximation which holds when the hosting half-space has a dielectric permittivity much different from that of the free-space [1]. Under these circumstances, the presented numerical reconstructions have demonstrated that the inversion scheme is capable to localize and reconstruct the illuminated part of the buried voids.

References

1 Liseno A, Pierri R. Imaging of voids via a PO-based shape reconstruction. In print on the *Journal of Optical Society of America*, part A.
2 Liseno A, Soldovieri F, Pierri R. Improving a shape reconstruction algorithm with thresholds and multi-view data. In print on *Int. J. Electron. Commun. (AEÜ)* 58, 2004.

Management of urban systems in sesmic areas

GIS and seismic risk

R. Fistola[a], R. Papa[b], C. Pascale[c]

[a]*Dipartimento di Ingegneria, Università degli Studi del Sannio, Benevento, Italia*

[b]*Dipartimento di Pianificazione e Scienza del Territorio, Università degli Studi di Napoli "Federico II", Napoli, Italia*

[c]*Consorzio TRE, Napoli, Italia*

Introduction

Geographical Information Systems are revolutionizing the way of studying the territory and the management system of the urban transformations. Thanks to the contribution of researchers to different disciplinary fields, a new discipline is born: the Geographical Information Science (GISc). Many European and world university centers academic courses have been activated in order to promote the birth of new professional profile; these profiles will operate considering the GIS like a development environment of new urban knowledge. The use of GIS is finding an increasing number of application in the field of the assessment of the natural risk, in order to drive efficiently the actions of damage mitigation within the city. A very interesting experience in this field, with a multidisciplinary approach to seismic risk, it is actually being developed by a multidisciplinary staff of scientists cooperating at the TRAIANO Project.

The TRAIANO Project

The TRAIANO Project is a research project for the evaluation and reduction of seismic vulnerability in urban environments. It involves research units operating in different fields (structural engineering, geology, geotechnics, geophysics, urban planning) for a common final purpose: to envisage the seismic risk in urban areas.

A particular attention has been given to the development of a Geographycal Information System that is being structured and built by the Department of Town and Country Planning of the University of Naples. The GIS has been developed considering three roles that the system has to play inside the project:

1. GIS as a common groundwork for data exchange among scientists;
2. GIS as a development environment to get the project objectives;
3. GIS as a deliverable product for municipalities and disaster managers.

The first role that has to be highlighted is that the GIS has been considered an environment for the exchange of information between the different research units. The "position" of phenomena as been used as a common information for all the disciplinary units. Georeferenced data, show to structure different information levels for each research unit, in order to establish relationships between data (based on their position).
Basically, it has been built a main information level for each research unit. Some of these levels, based on polygonal topologies, are populated through direct input. Other levels are populated through interpolation from auxiliary point topology which are stored the field data.
The project involves different disciplines: geophysic, geology, geotechnic, structural engineering urban planning. For this reason it has been decided to use different polygonal grids to connect the data. The first level, based on a 5 square km grid, stores geophysical information and in particular is used by the system to acquire data on the bedrock acceleration. The second topological level, based on a 50 m square grid, stores both data from the geology unit and the geotechnic unit. In particular, this level is populated through data connected to the bore-hole positions (Fig. 1).
The data connected to the buildings, such as the construction materials and techniques or the actual conditions of the building, have been organized on a dedicated polygonal topology representing every single building of the study area (Fig. 2). A last polygonal topology is used to store urban data, such as population and land use, and it has been built on the census tract of the study area.
The database connected to each topology is directed to store synthetic data that will define relational algorithms between different levels, and also to define hotlinks between the single research unit work. This solution enables the system to be sufficiently fast in evaluating the queries, but at the same time, does not avoid a full control on the whole set of the data.
Furthermore, the GIS has an important role in supporting the research work, as a matter of facts, it has been conceived as a development area where to apply existent procedures or integrate new ones (with spatial analysis tools owned by the GIS software).
One of the main goals of the project is to set up a full package of algorithms that allow the system to establish connections between the different data layers. Basically, the aim is to determine, for the specific site, the relations between a certain value of the bedrock accelerations and the peak ground accelerations. This allows to compare these values with the state of the analyzed structures and to define the produced damage.
In other words, the project wants to develop a number of procedures based on GIS spatial analysis tools, that will enable the user to map the seismic risk in the analyzed area.
There are two interactions that must be underlined: the first one is between the geophysical data (stored on the 5 km grid) and the ground level (repre-

Managing data on different information levels:

– Polygonal Topology – Grid (5 km) – Input for bedrock accelerations

– Polygonal Topology – Grid (50 m) – Geological and geotechnical definition

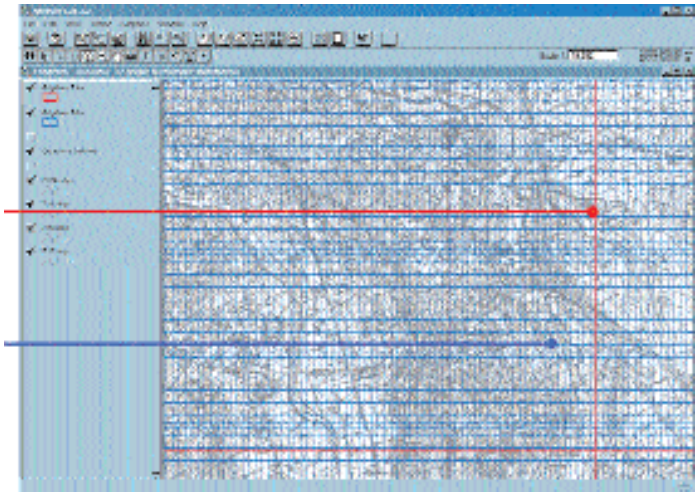

Fig. 1. The different polygonal grids.

Managing data on different information levels:

– Polygonal Topology – Buildings in the study areas

– Point Topology – Measurement stations

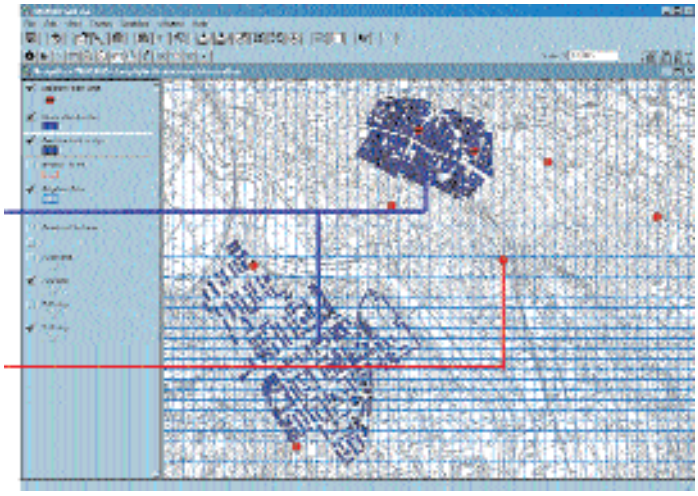

Fig. 2. The building topology and seismic station sites (points).

sented through the 50 m grid), that necessarily involves a study of geological and geotechnical properties of the site. The second one it is between the ground level and the structural properties of the single building that will lead to the evaluation of the seismic risk. The interaction with social data (stored on the topological level defined by the census tract), will have great influence on the evaluation of the total exposure connected with the intrinsic risk due to the structural conditions (Fig. 3).

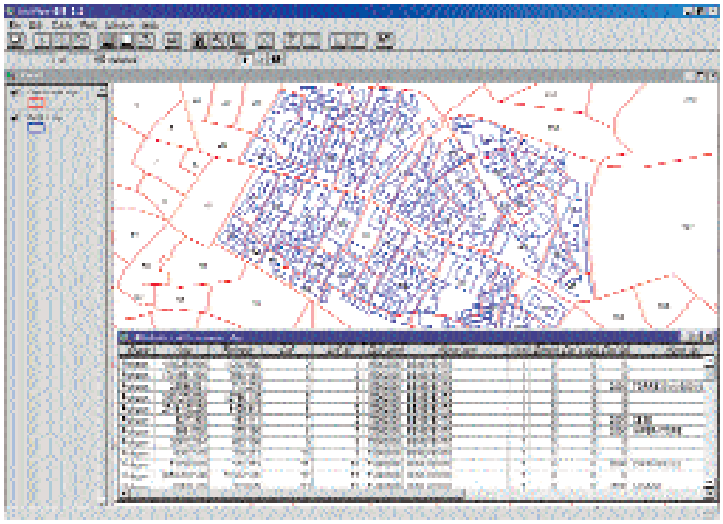

Fig. 3. The census tract topology.

The last role of the GIS in the TRAIANO project is to define a Decision Support System that will enable, once implemented, the political or technical decision maker to have an immediate view of the scenario connected with a predefined seismic event. The DSS cannot be customized for a particular user. Therefore it is important to have a completely defined structure to drive the end user in the data input, in order to update the system correctly (Fig. 4).

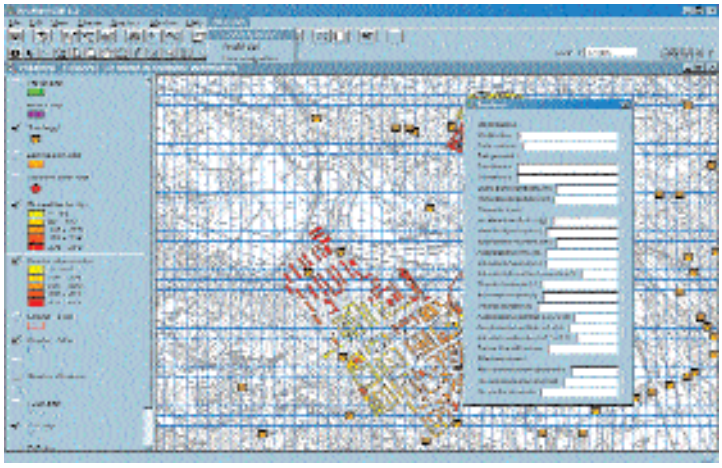

Fig. 4. The data input mask.

At the same time, one of the goals of the project is to define an analysis of the scenario based on previous events. This will enable to have a comparison (considering the different structural materials and maintenance conditions), between the actual expected damage and the reported damage of the historical events (Fig. 5).
Data input user interface has a great value (specially for the building connected data) in order to have a 3D structure that will enable the end user to better identify the single building (Fig. 6).
At the moment it is in progress the work on the definition of relational algorithms for the damage envisage. The last part of the research work will be focused on the development of the final user interface and on the 3D urban model.

Fig. 5. An historical view of the inner city life of Benevento after 1688 earthquake.

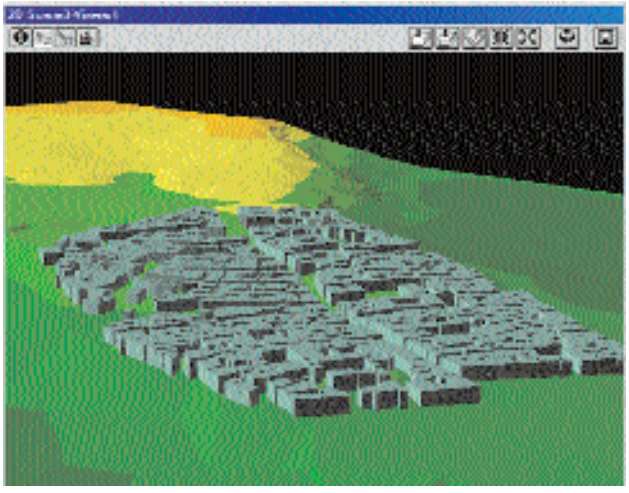

Fig. 6. The 3D urban model.

References

Batty M. Using GIS for visual simulation modelling. *GIS World* 7, 1994.

Biallo G. Introduzione ai sistemi informativi geografici. *Quaderni di Mondo GIS*, 2002.

Fistola R, Pugliese G. Nuove dimensioni del rischio per l'ambiente antropizzato: l'inquinamento elettromagnetico. Un piano urbanistico per la compatibilità territoriale. *XII Conferenza AISRE*, 10-12 ottobre 2001, Venezia, 2001.

Fistola R, Pascale C. GIS e mobilità: ipotesi d'uso dei sistemi informativi territoriali per l'analisi e l'interpretazione della rete cinematica della città. In *Atti del convegno "GIS: strumenti avanzati ed applicazioni per la gestione ed il controllo del territorio"*, Università degli Studi del Sannio, novembre 2001.

Fistola R. Nuovi strumenti per il governo delle trasformazioni urbane e territoriali: i GIS. In Papa R. *Lezioni di Urbanistica*. Di.Pi.S.T., Napoli, 2000.

Longley PA, Goodchild MF, Maguire DJ, Rhind DW. *Geographical Information Systems*. John Wiley & Sons, 1999.

Papa R, Fistola R. Urbanistica e città digitale. Il governo del sistema funzionale nella città del XXI secolo: il caso Napoli. *XIX Conferenza Italiana di Scienze Regionali: Le regioni interne d'Europa: strategie e strumenti per l'integrazione*, 7-9 ottobre 1998, L'Aquila, 1998.

Poletti A. (ed.). *GIS metodi e strumenti per un nuovo governo della città e del territorio*. Maggioli, 2001.

Spagnoletti E. (ed.). *Atti della IV conferenza di Mondo GIS: "In rete con la comunicazione geografica"*. MondoGIS s.r.l., Roma, 2002.

Safeguarding of urban and landscape identity in post-earthquake reconstructions in Italy. Methodology of the analysis and first results

D. Mazzoleni[a], M. Sepe[b]

[a]*Dipartimento di Progettazione Urbana, Università degli Studi di Napoli "Federico II", Napoli, Italia*
[b]*CNR, Dipartimento di Progettazione Urbana, Università degli Studi di Napoli "Federico II", Napoli, Italia*

Introduction

The loss of identity for places and landscapes represents an important cultural component of environmental hazards. Experiences such as the recent post-earthquake reconstruction in Irpinia show how the damage to the identity of places, far from being repaired, can actually be worsened if the reconstruction processes are not based on a solid architectonic and environmental culture and a well established repertoire of intervention methodologies and know-how.
In order to ensure truly sustainable development, the Council of Europe recently called for a common denominator for widely endorsed interventions which can nonetheless be implemented in a variety of geographical and cultural situations. This key concept is "landscape", which in a broad multi-disciplinary context is defined as "an area, as perceived by people, whose character is the result of the action and interaction of natural and/or human factors". In this sense landscape is considered "a key element of individual and social well-being", "basic component of the European natural and cultural heritage", and the "human well-being and consolidation of the European identity" (European Landscape Convention, Firenze, 20th October 2000). The common aim must be to work at "landscape protection" and "landscape planning".
These statements underline the importance of safeguarding the urban and landscape identity of a place to ensure cultural, sociological and environmental values. Yet most studies relating to earthquakes and subsequent reconstruction work in Italy tend to focus above all on the technical data of the episode and fail to pay any attention to the identity of the sites. This is probably due to the difficulty of obtaining objective results.
Starting from these considerations, the research project "Development of innovative methodologies for the safeguard of the urban and landscape identity in the areas subjected to the environmental risks" overseen by the Operative Unit "Architecture of towns and landscapes" of the Regional

Centre of Competence AMRA, Section for Territorial Policies and Technological Transfers, sets out to identify the issues involved in linking earthquake risk and loss of urban and landscape identity in experiences of post-earthquake reconstruction in Italy to date[1]. We had a dual objective: to establish the strong and weak elements in such reconstructions and match these against the reconstruction carried out in Irpinia and other reconstructions chosen as benchmark experiences. Below we give a summary of the research carried out, the methodology adopted and the first results obtained.

Description of research project

Method and Phases

Observation of the current reality, both locally and globally, shows that landscape identity is at risk from two types of agent:

a) chronic: processes of cultural homologation. The progressive disappearance of traditional construction cultures, on one hand, and the lack of a comprehensive awareness of modernity, on the other, play no little part in environmental hazards, in both material and immaterial terms;
b) sporadic: natural and/or artificial catastrophes. Just as catastrophic events may impart a strong impulse for architectural renovation in cities and landscapes, so they may also provide an alibi for allowing processes of cultural degradation to set in. Particularly during the emergency situation immediately following a catastrophe, the processes of homologation can be drastically accelerated.

The method adopted to research phenomena of post-earthquake reconstruction in Irpinia was to compare experiences of reconstruction in Italy, paying particular attention to the safeguarding of the urban and landscape identity, which were analogous for the period of the event and the typology of damage caused.
The means adopted was the setting up of a data bank containing information on the earthquake events and the subsequent reconstructions as criteria for comparison.
The project was carried out in three phases. In the first phase we collected data on earthquakes and reconstructions in Italy and selected the benchmark

[1] The workgroup which has produced this study is made up of Prof. Arch. Donatella Mazzoleni (Full Professor DPU Università di Napoli Federico II), coordinator of the Operative Unit "Architecture of towns and landscapes", and the Architects: Marichela Sepe (coordination, researcher C.N.R. – DPU Università di Napoli Federico II), Emilia d'Amelio (PhD student in History of Architecture, DSR Università di Napoli Federico II), Biagio Costato, Roberta Esposito, Fabrizio Mirarchi (Post-graduate students in Architectonic Design DPU Università di Napoli Federico II).

events. In the second phase we drew up systematic records of the benchmark reconstructions to insert in the data bank. In the third phase we proceeded to elaborate the data and produce the first results.

First results obtained and observations

During the first phase we began by collecting data about the most recent earthquake in Irpinia, in 1980, and went on to review the benchmark earthquakes from other regions in Italy. This involved investigating the existing bibliography on the topic, via internet and through contacts with Local Authorities responsible for reconstruction in the chosen regions.
The earthquakes selected as benchmark episodes were: *Belice, 1968*; *Friuli, 1976*; *Irpinia, 1980*; *Umbria, 1997*. These episodes were selected on the basis of the criteria outlined above – period of the event and typology of damage – and because all four appeared emblematic of post-earthquake reconstruction in Italy.
The second phase was crucial in our research because it involved deciding which elements to focus on. The parameters used to measure data concerning the urban and landscape identity of a place are highly relative, and establishing these parameters is all-important.
A concise record of each event was drawn up using data on the earthquake and the subsequent reconstruction. Taken individually the details register the entity of the event, while both their comparison and the degree of difficulty we found in obtaining the data lead to considerations concerning our objective. The data for the earthquakes served to identify: where, when, magnitude and duration of the main shock(s), area affected, towns damaged, population affected, number of homeless; also the localisation of the earthquake with the area affected and the epicentre. The information on the reconstruction involved: period, cost, legislation for the reconstruction, with the year of start and finish, the cost of the reconstruction, the main laws used; in addition significant images of the reconstruction, notably of before and after; also data concerning the evaluation and monitoring of the reconstruction, meaning the results achieved, the existence of an observatory with indications about who set it up and its brief, and the consensus of opinion about the reconstruction in question.
In the third and final phase, the assembled data was examined and compared with the reconstruction in Irpinia, leading to some preliminary considerations. An earthquake will never reverse a trend in course; it can merely accentuate current tendencies, whether of development or crisis. Economic growth will be furthered, while an economic crisis will deepen. The damage linked with the loss of identity is more evident where the catastrophes, and the problems existing prior to the event, were greater.
The Belice earthquake devastated the urban and landscape identity, with whole cities being duplicated and rebuilt elsewhere. In Gibellina, for example, the

buildings that collapsed were simply buried under tons of cement. At Santa Margherita many of the churches damaged by the earthquake were demolished to make way for motorway spurs, roads and new buildings.
The reconstruction in Friuli was able to some extent to learn from the mistakes made in Belice, and is the only example of work seen through to its conclusion. The criterion adopted was *"where it stood, as it stood"*, so that the historical centres were rebuilt on the original sites, paying particular attention to conserving the historical and cultural identity. In this case the territory was already in a phase of development and the post-earthquake reconstruction in fact represented not a handicap but, on the contrary, an incentive and a significant boost for economic growth.
In Irpinia the earthquake produced extensive damage, eliminating almost entirely the "crib-style" villages (in italian: "paesi-presepe") perched picturesquely on rocky outcrops, typical of this region. They were replaced by other urban typologies and new landscape morphologies, which more often than not the local population still finds alien. The consensus of opinion is that although the reconstruction has favoured the building of infrastructures needed to link the various localities in Irpinia, it was nonetheless a missed opportunity for the area's development. There is a widespread feeling of alienation and rejection on the part of the population vis à vis the new constructions, and the whole experience has left quite severe psychological scars. In Umbria the earthquake

Fig. 1. Venzone, Friuli. Town Hall, before the reconstruction [From: Segreteria Generale Straordinaria per la ricostruzione del Friuli, Direzione Generale dell'Istruzione, della Formazione Professionale delle Attività e Beni Culturali (eds) (1988) *"Friuli ricostruzione. 1976 – 1986"* Udine, Arti grafiche Friulane].

Fig. 2. Venzone, Friuli. Town hall, after the reconstruction [From: Segreteria Generale Straordinaria per la ricostruzione del Friuli, Direzione Generale dell'Istruzione, della Formazione Professionale delle Attività e Beni Culturali (eds) (1988) *"Friuli ricostruzione. 1976 – 1986"* Udine, Arti grafiche Friulane].

Fig. 3. Conza, Irpinia. Town, before the reconstruction.

Fig. 4. Conza, Irpinia. The town re-built in another place.

caused fewer casualties and homeless than elsewhere. The ensuing problems were above all in terms of economic growth. The most significant damage concerned the historical and architectonic patrimony, one of the region's prime sources of prosperity in view of the importance of tourism. Thus questions related to loss of identity were assimilated above all to the problem of recuperating traditional images in the form that had been more or less artificially formulated and commercialised for the tourist trade.
Some regions such as Irpinia and Umbria set up observatories to monitor the achievements of reconstruction. The documentation accumulated by these institutions is very useful for the conservation of a historical memory and the possibility of evaluating the events and processes of the reconstruction.
The goals of the observatory in Irpinia were set out as follows: "to provide for permanent mechanisms for the conservation of the memory of places and

Fig. 5. Montella, Irpinia. The new Town Hall.

Fig. 6. Sellano, Umbria. Before the reconstruction (From: www.regione.umbria.it, *Relazione di Monitoraggio dell'accordo di Programma Quadro riguardante l'Azione di ricostruzione a seguito degli eventi sismici del 1997*).

Fig. 7. Sellano, Umbria. After the reconstruction (From: www.regione.umbria.it, *Relazione di Monitoraggio dell'accordo di Programma Quadro riguardante l'Azione di ricostruzione a seguito degli eventi sismici del 1997*).

the event; to comprehend and document the transformations induced by means of scientific research and on site investigations". In Umbria, the observatory was set up to: "monitor the reconstruction process, elaborate and diffuse data and information on the state of advancement; coordinate the various sources of funding and oversee expenditure and the financial requirements; monitor the more general socio-economic effects produced by the reconstruction".

The difference in the aims of the two observatories points to the different experiences of earthquake and reconstruction in the two regions.

The Regional Administration of Friuli was the first to adopt a law on protection of the territory (which pre-dated national legislation). To safeguard its architectonic patrimony in view of earthquake risk it set up a Centre of Documentation on Earthquake and Cultural Assets. This Centre drew on the documentation and systematic analysis of the various phases of the earthquake event. For us it was very significant that in Friuli the National Disasters Centre was set up and the new discipline of sociology of disasters came into being.

In the light of these experiences, the "reconstruction" in Belice appears all the more distressing. Certainly the historical and political climate of 1968 ruled out an adequate preparation in the face of such an event, and there were no previous experiences to learn from. Nonetheless, the lack of systematic documentation and the impossibility, nearly 40 years on, of obtaining complete and unequivocal information make it particularly difficult to quantify, qualify and above all monitor on the basis of precise data the reconstruction as it happened there.

Conclusions and notes for further analysis

The research project implemented in the context of the project "Development of innovative methodologies for safeguarding urban and landscape identity in environments at risk" by the Operative Unit "Architecture of towns and landscapes" of the Regional Centre of Competence AMRA, Section for Territorial Policies and Technological Transfers set out to identify the issues involved in linking earthquake risk and loss of urban and landscape identity in experiences of post-earthquake reconstruction in Italy. The dual objective was to establish the strong and weak elements in such reconstructions and match these against the reconstruction carried out in Irpinia and other reconstructions chosen as benchmark experiences. The first results show the peculiar features of the post-earthquake reconstructions of 1968 in Belice, 1976 in Friuli, 1980 in Irpinia, and 1997 in Umbria. In Irpinia, in particular, the earthquake caused extensive damage to urban and landscape identity, with the obliteration of almost all the characteristic "crib villages", replaced by new urban developments which are still alien to the local population.

The consensus of opinion is that although the reconstruction has favoured the building of infrastructures needed to link the various localities in Irpinia, it was nonetheless a missed opportunity for the area's development.
We intend to pursue our research in order to be able to quantify "loss of identity" (urban and landscape) as a factor in the calculation of the level of risk for a certain area, so as to facilitate:

a) the comprehensibility and transmitability of the humanistic "values" of identity in a technical and scientific context; and hence
b) an elaboration largely endorsed by the whole scientific community of a suitable interdisciplinary approach to the safeguarding of identity in the event of an earthquake.

We also intend to establish guidelines for planning the safeguarding of urban and landscape identity in Irpinia, by applying the results obtained and focusing on the reconstruction in this region. We are convinced that new construction cultures must be forged using a thoroughly multidisciplinary approach. On one hand these new cultures will capitalise on the traditional know-how present on the territory, strengthening local identity, and on the other they will facilitate the insertion of this identity in the networks of global relations which characterise the contemporary world.
Finally we would like to identify areas of Irpinia distinguished by the greater or lesser concentration of such elements in order to study the different methods for operating safeguards in the event of earthquake hazards. In this perspective we are elaborating a methodology of analysis which will permit us to identify, highlight and represent such components for the territory. Such analysis requires bi- and tri-dimensional mapping on various levels, to be carried out during multi-focal surveys in Irpinia and the other benchmark areas, producing maps of urban and landscape identity.

References

AA.VV. *La città, letture interdisciplinari*. Guida, Napoli, 1970.
AA.VV. *Friuli: la prova terremoto*. Franco Angeli, Milano, 1978.
AA.VV. *Per una simbolica dell'ambiente*. Marsilio, Padova, 1978.
AA.VV. *Proposte per la ricostruzione*. Gallina, Napoli, 1981.
AA.VV. *Atlas of Isoseismal maps of Italian earthquakes, C.N.R. "Progetto Finalizzato Geodinamica" – Sottoprogetto Rischio sismico e ingegneria sismica*. Bologna, 1985.
Blowers A. Ecological and political modernisation: the challenge for planning. *Town Planning Review* 71(4)371-93, 2000.
Boeri S, Lanzani A, Marini E. *Il territorio che cambia*. Sagesta, Milano, 1993.
Boschi E, Ferrari G, Gasperini P, Guidoboni E, Smiriglio G, Valensise G. Catalogo dei forti terremoti in Italia dal 461 a.C. al 1980. Istituto Nazionale di Geofisica, Roma, and SGA – Storia Geofisica Ambientale, Bologna, 1995.
Bramerini F, Di Pasquale G, Orsini G, Pugliese A, Romeo R, Sabetta F. Rischio sismico del territorio italiano. Proposta di una metodologia e risultati preliminari. Sintesi del

Rapporto tecnico SSN/RT/95/1. *Proc. of "7° Convegno Nazionale di Ingegneria Sismica"*, 25-28 September 1995, Siena, Italy, 1995.
Canevari A, Palazzi D. *Paesaggio e territorio*. Franco Angeli, Milano, 2001.
Carter E, Donald J, Squires J (eds.). *Space & Place. Theories of Identity and Place*. Lawrence & Wishart, London, 1993.
Chierici G. *I monumenti dell'Alta Irpinia e il terremoto del 1930*. Collana di studi regionali nella Società storica irpina, Tip. Pergola, Avellino, 1932.
Cullen G. *Il paesaggio urbano*. Calderini, Bologna, 1976.
Farinella R. La città tra urbanistica e paesaggio. *Paesaggio urbano* 5-6:8-13, 2000.
Koolhaas R, Boeri S, Kwinter S. *Mutations*. Actar, New York, 2001.
Landrove S (ed.). *Nuevos territorios Nuevos Paisajes*. MACBA, Barcellona, 1997.
Mazzoleni D (ed.). *La città e l'immaginario*. Officina, Roma, 1985.
Mazzoleni D (ed.). *Spazi della vita collettiva*. CUEN, Napoli, 1989.
Mazzoleni D. *Natura Architettura Diversità/Nature Architecture Diversity*. Electa Napoli, Napoli, 1998.
Mazzoleni D, Anzani G. *Cilento antico. I luoghi e l'immaginario*. Electa Napoli, Napoli, 1993.
Ministero per i beni culturali ed ambientali – Soprintendenza generale agli interventi post-sismici in Campania e Basilicata. *Dopo la polvere*. Rilevazione degli interventi di recupero post-sismico del patrimonio archeologico, architettonico ed artistico delle regioni Campania e Basilicata danneggiato dal terremoto del 23 novembre 1980 e del 14 febbraio 1981 (Anni 1985-89), voll. I-V, Istituto Poligrafico e Zecca dello Stato, Roma, 1994.
Nigro G, Sartorio Francesca S (eds.). *Ricostruire la complessità*. Alinea Editrice, Firenze, 2002.
Nijkamp P, Perrels AH. *Sustainable Cities in Europe*. Earthscan, London, 1994.
Piroddi E et al. (eds.). *I futuri della città. Mutamenti, nuovi soggetti e progetti*. Franco Angeli, Milano, 2000.
Relazione di Monitoraggio dell'accordo di Programma Quadro riguardante l'Azione di ricostruzione a seguito degli eventi sismici del 1997 (art. 16, comma 1, Lg 61/98). 30 Giugno 2003.
Sbordone L. *Città e territorio fra sostenibilità e globalizzazione*. Franco Angeli, Milano, 2001.
Segreteria Generale Straordinaria per la ricostruzione del Friuli, Direzione Generale dell'Istruzione, della Formazione Professionale delle Attività e Beni Culturali (eds.). *Friuli ricostruzione. 1976-1986*. Arti Grafiche Friulane, Udine, 1988.
Shama S. *Paesaggio e memoria*. Mondadori, Milano, 1997.
Sepe M. The "sensitive relief" and urban planning: a cultural approach to the sustainable city construction. *Proc. of "Sustainable city 2002"*, WIT Press, Southampton, 2002.
Sepe M. Green architecture and city transformation: the "sensitive relief" for a cultural approach to the sustainability. *Proc. of "Sustainable Building 2002"*, EcoBuild, Oslo, 2002.
Sepe M. Il Distretto Culturale forma innovativa di integrazione per lo sviluppo. In: Moccia FD, Sepe M (eds.). *Progetti integrati territoriali. Esperienze avanzate in Campania*. Graffiti, Napoli, 2003.
Wright FL. *La città vivente*. Einaudi, Torino, 1991.
Zanini A, Ladini U. *Scenari in mutazione Per un lessico postfordista*. Feltrinelli, Milano, 2000.
Zardini M (ed.). *Paesaggi ibridi. Un viaggio nella città contemporanea*. Skira Editore, Milano, 1996.